AUTOMATED OPTIMUM DESIGN OF AXIAL FLOW GAS TURBINE STAGE

By

RAM SAJIWAN GUPTA

DEPARTMENT OF MECHANICAL ENGINEERING
INDIAN INSTITUTE OF TECHNOLOGY, KANPUR
AUGUST, 1977

AUTOMATED OPTIMUM DESIGN OF AXIAL FLOW GAS TURBINE STAGE

A Thesis Submitted
In Partial Fulfilment of the Requirements
for the degree of
DOCTOR OF PHILOSOPHY

By
RAM SAJIWAN GUPTA

to the
DEPARTMENT OF MECHANICAL ENGINEERING
INDIAN INSTITUTE OF TECHNOLOGY, KANPUR
AUGUST, 1977

TO

MY GRANDMOTHER

CERTIFICATE

This is to certify that the thesis entitled AUTOMATED OPTIMUM DESIGN OF AXIAL FLOW GAS TURBINE STAGE by Ram Sajiwan Gupta for the award of the degree of Doctor of Philosophy is a record of bonafide research work carried out by him under my supervision, and has not been submitted elsewhere for a degree.

SSRao

AUGUST, 1977.

(Dr. S.S. Rao)
Assistant Professor
Department of Mechanical Engineering
Indian Institute of Technology
Kanpur

ACKNOWLEDGEMENTS

The author expresses his appreciation and gratitude to:

His advisor, Dr. S.S. Rao, whose continuous encouragement, guidance and enthusiasm were vital to the success of this effort,

Dr. S. Prasad and Dr. V.P. Vasandani for their encouragement during the work,

Dr. R. Singh and Dr. R.K. Sullerey for their valuable discussions in the area of turbomachines,

Prof. D. Yadav and Prof. B.D. Gupta for their help in computations and extending ever helping attitude,

H.B. Technological Institute, Kanpur for sponsoring for Ph.D. programme at I.I.T. Kanpur,

Punjab Engineering College, Chandigarh and Chandigarh Administration for providing financial help,

Computer Centre, I.I.T. Kanpur and Delhi University for computational facilities,

Sri R.N. Srivastava for typing of the manuscript,

His family for understanding, patience and encouragement.

Ram Sajiwan Gupta

CONTENTS

LIST OF TABLES

LIST OF FIGURES

LIST OF SYMBOLS

$a_1, a_2 \ldots a_5$	:	Function of end dimensions of beam
A	:	Cross sectional area
A_1, A_2, A_3	:	Area for flow at stations 1, 2 and 3
A_N, A_R	:	Area of nozzle and rotor blade section
A_{root}	:	Area of cross section of blade at root
$[A_i]$	:	Matrix
b, b_1, b_2	:	Breadth of beam
$b_1, b_2 \ldots b_5$	:	Coefficient of polynomial
b_{eq}	:	Equivalent breadth of rectangular section
B	:	Constant for clearance space
$[B_i]$	:	Matrix
c_1, c_2, c_3	:	Function of end dimensions of beam
$c_1, c_2 \ldots c_5$	:	Coefficient of polynomial
c_N, c_R	:	Chord of the nozzle and rotor blade
c_p	:	Specific heat at constant pressure
C_1, C_2, C_3	:	Absolute velocity at stations 1, 2 and 3
C_a	:	Axial velocity
C_L	:	Lift coefficient
C_{w_2}, C_{w_3}	:	Whirl component of velocity
d	:	Mean diameter of the turbine
$d_1, d_2 \ldots d_5$	:	Function of end dimensions of beam
$d_1, d_2 \ldots d_9$	:	Coefficient of polynomial
e	:	Offset of rotating beam

E	:	Young's modulus
$f(\vec{X})$	:	Function of vector $\vec{X}$ and objective function
$\bar{f}$	:	Mean value of function $f(\vec{X})$
g	:	Acceleration due to gravity
$g_j(\vec{X})$	:	j^{th} constraint
G	:	Shear modulus
$\bar{G}$	:	Some function of constraints
h_o	:	Stagnation enthalpy
h_1, h_2, h_3	:	Blade height at stations 1, 2 and 3
h_N, h_R	:	Height of nozzle and rotor blades
$H_{i,j}$	:	A variable coefficient
$[H_i]$	:	A positive definite symmetric matrix
i	:	Angle of incidence and an index
I_{xx}, I_{yy}, I_{xy}	:	Moment of inertia about xx, yy and xy axes
$I_{\bar{x}\bar{x}}, I_{\bar{y}\bar{y}}, I_{\bar{x}\bar{y}}$	:	Moment of inertia about $\bar{x}\bar{x}$, $\bar{y}\bar{y}$ and $\bar{x}\bar{y}$ axes
j	:	An index
J	:	A parameter
k	:	An index
$\bar{k}$	:	Clearance
K_1, K_2	:	Weightage to mixed objective function
$[K]$	:	Element stiffness matrix
$[\underline{K}]$	:	Stiffness matrix of structure
l	:	Length of an element
L	:	Length of cantilever beam
L_i	:	Functional variable of element length l

m	:	Mass rate of flow of gases
$\bar{m}$	:	A function of stagger angle
M_a, M_w	:	Bending moment
$M_{C_2}, M_{C_3}, M_{V_3}$	:	Mach number corresponding to C_2, C_3 and V_3
$[M]$	:	Element mass matrix
$[\underset{\sim}{M}]$	:	Mass matrix of structure
n_D	:	Number of degree of freedom of one node
n_E	:	Number of element
n_N, n_R	:	Number of nozzle and rotor blades
N	:	Revolution per second
p_{o1}, p_{o2}, p_{o3}	:	Stagnation pressure at stations 1, 2 and 3
p_1, p_2, p_3	:	Static pressure at stations 1, 2 and 3
$p_{o2\ rel}$, $p_{o3\ rel}$	:	Stagnation pressure for relative velocities
p_c	:	Critical pressure
p_j	:	Specified probability of j^{th} constraint
$p_v(z), p_w(z)$, $P(z)$	:	Specified parameter of z
$\bar{P}$	:	A parameter
$P[g_j]$	:	Probability of function g_j
P_i	:	Load in i^{th} degree of freedom
$P_{i,j,k}$, $Q_{i,j,k}$, $R_{i,j,k}$	:	A variable parameter
r_k	:	Response factor for sequential minimization
r_{root}, r_{tip}	:	Radius of root and tip

R	:	Degree of reaction at mean radius
$\bar{R}$	:	Gas constant
R_e	:	Reynolds number
$(R_e)_N, (R_e)_R$	:	Reynolds number for nozzle and rotor
R_{root}	:	Degree of reaction at the root of rotor blade
s_N, s_R	:	Spacing of nozzle and rotor blades
S	:	Entropy
S_i	:	An integral variable
$\vec{S}_i$	:	i^{th} direction vector
t	:	Depth or thickness
$\bar{t}$	:	Time parameter
t_e	:	Trailing edge thickness
t_{eq}	:	Equivalent thickness or depth or rectangular section
t_N, t_R	:	Maximum thickness of nozzle and rotor blades
T	:	Temperature
$\bar{T}$	:	Kinetic energy of the element
T_{o1}, T_{o2}, T_{o3}	:	Stagnation temperature at station 1, 2 and 3
T_1, T_2, T_3	:	Temperature at station 1, 2 and 3
T_2', T_3', T_3''	:	Temperatures as shown in T-S diagram
$u_1, u_2 \ldots u_i$	:	Nodal degree of freedom of element
$\bar{u}_1, \bar{u}_2 \ldots \bar{u}_i$	:	Nodal degree of freedom of element
U	:	Tangential velocity
$\bar{U}$	:	Strain energy
$\vec{U}$	:	Nodal displacement vector of structure

U_i	:	An integral variable
v	:	Displacement in xz plane
V_2, V_3	:	Relative velocity at station 2 and 3
V_i	:	An integral variable
$\vec{V}_i$	:	Vector combination of penalty function
w	:	Displacement in yz plane
x, y, z	:	Coordinate axes
x_1, x_2, x_m	:	Value of x at 1, 2 and point m
$\bar{x}, \bar{y}$	:	Coordinate of centroid
x', y'	:	Axes inclined from x, y
x_c, y_c	:	Camber line coordinates
$\vec{X}$	:	n-dimensional vector
$\vec{X}, \vec{Y}$	:	Vectors of random variables
$\vec{X}_i$	:	i^{th} vector of design variables
$\vec{X}_o$	:	Starting design vector
$y(x)$	:	A dependent variable of x
Y, Y_N, Y_R	:	Loss coefficients defined from pressure drop
Y_k, Y_p, Y_s	:	Clearance, profile and secondary loss coefficients
z_e	:	Distance of first node of the element from root
α	:	Depth taper ratio = depth at root/depth at tip
α_1, α_2	:	Stator blade angle at inlet and outlet or gas angles of cascade at inlet and outlet
α_1', α_2'	:	Blade angle of cascade at inlet and outlet
α_3	:	Swirl angle
α_c	:	Included angle of divergence of walls of annulus

α_m	:	Mean angle
α_s	:	Stagger angle
β	:	Breadth taper ratio = breadth at root/breadth at tip
β_2, β_3	:	Rotor blade angle at inlet and outlet
β_m	:	Mean blade angle
γ	:	Ratio of specific heat
δ	:	Angle of deviation
Δ_t	:	Tip clearance of the rotor blade
ΔT_{os}	:	Stagnation temperature drop
ϵ	:	Angle of gas deflection
ε	:	Small quantity
η_s	:	Stage efficiency
η_{TS}	:	Total to static efficiency
$\theta, \theta_1, \theta_2$	:	Twist of equivalent rectangular section
$\bar{\theta}$	:	Angle between S_i and gradient of penalty function at minimizing length τ^*
θ'	:	Blade camber angle
$\lambda, \lambda_N, \lambda_R$	:	Blade loss coefficient defined from temperature drop
$\lambda_{cN}, \lambda_{cR}$	:	Parameters for nozzle and rotor
λ_j	:	Kuhn-Tucker multipliers
$\bar{\mu}, \bar{\mu}_1, \bar{\mu}_2$	:	Viscosity of gases
ρ_1, ρ_2, ρ_3	:	Gas density at station 1, 2 and 3 respectively
ρ_m	:	Mass density of blade a beam material
σ_{ct}	:	Centrifugal tensile strength

σ_g	:	Stress due to pressure force and gas bending
σ_{max}	:	Maximum stress at the root
σ_{zz}	:	Stress in radial direction
τ^*	:	The minimizing step length in the direction S_i
ϕ	:	Flow coefficient
$\overline{\phi}$	:	Angle between centroidal axes and principal axes
$\phi(X,Y_k)$	:	Penalty function
ψ	:	Stage temperature drop coefficient
$\omega(1),\omega(2)...$	:	Natural frequency of vibration, cycle/sec

Subscript

1,2,3	:	Station number
b	:	Bending
N	:	Nozzle
r	:	Radius r
root	:	Value at root of blade
R	:	Rotor
tip	:	Value at tip of blade

Superscript

(u)	:	Upper limit of variable
(l)	:	Lower limit of variable.
Frequency ratio	:	Ratio of modal frequency to frequency of fundamental mode of uniform beam with the same root cross section and without shear deformation effects.

SYNOPSIS

RAM SAJIWAN GUPTA
Ph.D.
Department of Mechanical Engineering
Indian Institute of Technology Kanpur
August, 1977

AUTOMATED OPTIMUM DESIGN OF AXIAL FLOW GAS TURBINE STAGE

A computational capability for the automated optimum design of axial flow gas turbine stage to satisfy aerodynamic and mechanical constraints is developed in the present work. More specifically an axial flow gas turbine stage is designed for maximum efficiency and/or minimum weight to satisfy strength, natural frequency and deflection requirements along with the behavior constraints due to aerodynamic considerations.

A survey of the available literature shows that mostly gas turbines are designed by conventional methods either from aerodynamic or mechanical considerations and the use of computers in this area is confined to the study of flow behavior or performance analysis. The study of vibration and strength has been carried out for idealized individual blades without considering their interaction with actual turbine design. The potentialities of optimization techniques have not yet been fully exploited by the turbomachine designers. In the present work an attempt has been made to develop a unified procedure for the design of axial flow gas turbines

and to replace the conventional turbine design processes by more sophisticated design methods developed recently.

In the present work the mean diameter of turbine, rotor blade chord to mean diameter ratio, nozzle blade chord to mean diameter ratio, nozzle blade spacing to mean diameter ratio, rotor blade spacing to mean diameter ratio, gas angle relative to the rotor blade at inlet, gas angle relative to the rotor blade at outlet and axial velocity of flow across the stage are taken as the design variables.

A linear combination of losses (one minus efficiency) and weight (mass) of the gas turbine stage is taken as the objective for minimization. The major losses like profile loss, tip clearance loss and secondary loss have been accounted for in calculating the efficiency. The three dimensional effects have been included by assuming a free vortex flow. The effect of Reynolds number on the stage efficiency has also been considered. The various air properties used in the computations are obtained by fitting polynomial equations in the data using least squares method. The weight (mass) of the stage is taken as the sum of the weights (masses) of the disc, rotor blades and nozzle blades. An iterative method has been developed for the computation of the efficiency of the stage and the method has been found to converge within three to four iterations. Bounds are placed on the flow coefficient, stage temperature drop coefficient, degree of reaction at the mean radius and at the root, and Mach number by considering the aerodynamic behavior of the gas flow in the turbine stage.

The vibration analysis of beams having rectangular cross sections has been made using finite element technique. A new beam element has been developed by considering the bending deflection, bending slope, shear deflection and shear slope in two mutually perpendicular planes as nodal degrees of freedom. With these degrees of freedom the coupling effect due to pretwist can be accounted for accurately. The effects of taper, twist, rotation, shear deformation and rotary inertia are considered in deriving the stiffness and mass matrices of the element. The various special cases from this general element are also derived. The first four natural frequencies and mode shapes have been computed for several cases and the effects of breadth and depth taper ratios, twist angle, shear deformation, offset and rotation on the natural frequencies of vibration of cantilever beams are studied. The present numerical results are compared with those available in the literature wherever possible and have been found to be in good agreement even when the beam is idealized with only four finite elements.

The tapered and twisted blade of airfoil cross section has been converted into an equivalent tapered and twisted cantilever beam of rectangular section for the purpose of vibration and stress analysis. The forces due to pressure and gas bending are assumed to act at the nodal points of the finite elements. The tip deflection and the stresses due to

the nodal forces are computed before calculating the natural frequencies of the idealized blade. The centrifugal stress, which can be calculated from the known dimensions of blade, is also included in computing the total stress induced in the blade. The Cholesky decomposition of symmetric banded matrices has been applied in solving the equilibrium equations and in obtaining a partial solution to the eigen value problem by Rayleigh-Ritz sub-space iteration algorithm. This algorithm solves the eigen value problem directly without a transformation to the standard form.

The constrained optimum design problem is cast as a nonlinear mathematical programming problem. The interior penalty function method, with a variable metric unconstrained minimization technique is used to solve the optimum design problem. The computation of the gradient and slope of the function has been carried out by backward finite difference method.

Five problems have been solved to demonstrate the effectiveness and generality of the optimization procedure developed. Out of these one problem has been solved by considering only side constraints in order to find the effect of the behavior constraints on the optimum point. The results of this problem show that a lesser value of objective can be obtained by neglecting the behavior constraints; however, some of the behavior (response) quantities may take abnormal values

at the optimum point as no bounds are placed on them. It has also been found that the effects of rotation, shear deformation and rotary inertia do not change the optimum results appreciably. In most of the cases, the stress at the root and the degree of reaction at the root of the rotor blade have reached their limiting values at the optimum point. Two different starting points taken in the case of maximization of efficiency gave approximately the same results. A sensitivity analysis has been conducted to find the effect of each of the design variables on the objective as well as on the response quantities. It has been found that efficiency is more sensitive to the chord and the spacing of the rotor blades while weight (mass) is most sensitive to the mean diameter of the gas turbine rotor.

The contributions of the present work can be summarized as follows: (i) Development of a beam finite element for the vibration analysis of rotating, doubly tapered and pre-twisted Timoshenko beams, (ii) Application of the finite element developed for the deflection, stress and vibration analysis of rotor blades having airfoil section, (iii) Computerization of air properties for application in gas flow design problems, (iv) Development of a computer programme for the automated optimum design of gas turbine rotor stage with aerodynamic and mechanical constraints, (v) Study of sensitivity of losses, weight and other response quantities of the turbine stage with respect to the design variables.

CHAPTER 1

INTRODUCTION

The application of classical aerodynamics in the design of turbomachinery, made the gas turbine to become a reality during the second world war. By replacing the conventional power units, gas turbines are now a days being being used successfully in space, aviation, marine, nuclear, rail-road, vehicular, cryogenic and petro-chemical applications. The rapid application of gas turbine plants in all phases of power generation is credited not only to the many advantages inherent in these plants, but also to the current technological progress. In gas turbine designs, the attainment of high temperature and high rotative speed alongwith the associated high efficiency has been possible due to the metallurgical advances made and the background of fluid mechanics, thermodynamics and gas dynamics accumulated.

The analytical procedures used in designing turbomachines have now undergone a major revision. The empirical relations used in the design process are being replaced by more sophisticated methods of analysis. These methods provide detailed information regarding static and dynamic loads as well as machine response in the form of stresses and deflections.

In recent years, turbines of considerable size and capacity are being produced with many stages. Along with the

demand for larger gas turbines, factors like efficiency and component weight have become major design considerations. The reduction in weight, while maintaining safe stress levels, has required a more detailed knowledge of load and stress distribution. The increased component flexibility resulting from weight reduction will lead to larger deflections that must be controlled during steady state and transient operating conditions.

In the present work an attempt has been made to maximize the efficiency and/or minimize the weight of an axial flow gas turbine stage by considering deflection, stress and vibration aspects along with aerodynamic requirements.

1.1 Review of Literature

Since the present work deals with the automated optimum design of gas turbine rotor stage with mechanical design considerations, the available literature is reviewed under the headings of aerodynamic design of gas turbines, mechanical design of gas turbine blades and optimum design of turbomachines.

1.1.1 Aerodynamic Design of Gas Turbines

The major developments in the design of gas turbines began during the second world war. In his first authoritative book on the subject of steam and gas turbines, Stodola[1] has given the details of earliest practical gas turbine developed by Holzwarth in 1908. In 1948, Reeman[2] published the details

of a simple jet propulsion turbine for aircraft application. Emmert[3] gave a procedure for designing gas turbines for power plants using two-dimensional theory by considering mechanical aspects. Georgian[4] published the design data of an experimental gas turbine used at Bengal Engineering College, Shibpur, India.

Carter[5] discussed various approaches for incorporating three dimensional design modifications. Johnston and Knight[6] reported the comparative results of two and three dimensional designs having free vortex blading for a single stage gas turbine of radius ratio 1.37. Wu and Wolfenstein[7] applied streamline curvature method to satisfy the radial equilibrium conditions in axial flow compressor and turbine designs. Hawthorne and Ringrose[8] developed the actuator disc theory of compressible flow in free vortex turbomachinery to take into account the three dimensional effects in turbomachine design. In his book, Horlock[9] has reported the plots of Carmichael for determining the axial velocity distribution in the constant angle method of three dimensional design. Smith and Johnston[10] designed, fabricated and conducted the performance tests of an experimental single stage turbine and also studied the applicability of Wu's method of design. Shaw[11] presented a method of designing blades in which the design of blade roots for heavy duty operation was discussed. Davis and Millar[12] compared the matrix and stream line curvature methods for axial flow turbomachines. A number of works have been reported at the

symposium entitled "Technical Advances in Gas Turbine Design" conducted by the Institution of Mechanical Engineers[13]. The NASA special publications[14,15] give comprehensive references in the area of gas turbine analysis, design and application.

The application of high speed digital computers is also being made in solving design analysis and flow problems of gas turbines. Carter, Platt and Lenherr[16] developed a computer program, analysed the geometry and design point performance of axial flow turbines by making use of stream-filament procedure and developed a correlation for total pressure loss coefficient. Glassman[17] also reported the development of a computer programme for predicting the design analysis of axial flow turbines. Wasserbauer and Glassman[18] developed a programme for predicting the off-design performance of radial inflow turbines.

1.1.2 Mechanical Design of Gas Turbine Blades

The blade design is not complete without the consideration of stress, deflection and vibrational aspects. Hodge[19] considered the stress analysis of gas turbine blades. Pollmann[20] included temperature effects in analysing hollow gas turbine blades. Manson[21] studied stresses in the blades and discs of gas turbines. Most of these investigators used conventional methods of strength of materials in their analyses. Further information regarding stresses in blades has been compiled by Cox[22] and Sawyer[23] in their handbooks on gas

turbines. Very little information is available on the magnitude of deflection in gas turbine blading.

Considerable amount of work has been published on the vibration analysis of single turbomachinery blade. The important references in this direction are shown in Figure 1.1 under the categories of tapered beam, rotating beam, pre-twisted beam, asymmetric beam, and uniform beam (by finite element method).

The effect of taper on vibration has been considered by Thomson[24] using matrix methods. Martin[25] analysed the tapered beam vibration problem by using perturbation method. Carnegie and Thomos[26] obtained the natural frequencies of long tapered blades using finite difference technique. Rao and Carnegie[27] determined the frequencies of lateral vibration of tapered cantilever beams by the use of Ritz-Galerkin process. Mabie and Rogers[28] obtained the frequencies of vibration of doubly tapered cantilever beams with end mass using Bessel functions and presented the results in dimensionless form for various taper ratios.

The effect of rotation on the vibration of beam has been considered by many investigators. Plunkett[29] studied free and forced vibration of rotating blades using matrix methods. Lo and Renbarger[30] found the bending vibrations of a rotating beam by applying Rayleigh-Ritz method. Boyce, DiPrima and Handelman[31] reported about the vibration of rotating beams of constant cross section using Rayleigh-Ritz and Southwell

procedure. Yntema[32] presented a simplified procedure and charts for rapid estimation of bending frequencies of rotating beams using Rayleigh-Ritz method. Carnegie, Stirling and Fleming[33] studied the vibration characteristics of turbine blading using finite difference technique.

The effect of pre-twist has been studied by many research workers. Mendelson and Gendler[34] used station functions in analysis and performed experiments to determine the effect of twist on the vibration of cantilevers. Rosard[35] found the natural frequencies of twisted cantilevers by Myklestad method. DiPrima and Handelman[36], Carnegie[37] and Dawson[38] applied the Rayleigh-Ritz method for the vibration analysis of twisted beams. Rao[39] analysed the flexural vibrations of pretwisted beams of rectangular cross section by Galerkin procedure.

The vibration of beams having asymmetrical section has also been considered by many authors. Garland[40] obtained the normal modes and frequencies of beams having noncollinear elastic and mass axes using Rayleigh-Ritz method. Targoff[41] presented the matrices associated with the bending and coupled bending-torsion vibration of beams using Holzer-Myklestad procedure. Mendelson and Gendler[42] determined the coupled bending-torsion vibrations of cantilever beams by means of station functions. Carnegie and Dawson[43] obtained the vibration characteristics of straight blades of asymmetrical airfoil cross section by applying transformation method.

The combined effects of taper, pre-twist, rotation and asymmetry has also been reported in the literature. Targoff[44] considered twist and rotation to study the bending vibrations of beams using matrix methods. Rao and Carnegie[45] presented a numerical procedure for the determination of frequencies and mode shapes of lateral vibration of blades allowing for the effects of pre-twist and rotation. Houbolt and Brooks[46] solved the differential equations of motion for combined flapwise bending, chordwise bending and torsion of twisted nonuniform rotor blades by using Rayleigh-Ritz method. Carnegie, Dawson and Thomas[47] applied finite difference technique to study the vibration characteristics of cantilever blading including the effects of asymmetry and pre-twist. Carnegie and Thomas[48] obtained the coupled bending-bending frequencies of pre-twisted tapered blading using finite difference technique. Banerjee and Rao[49] applied Galerkin method to analyse the coupled bending-torsion vibrations of rotating blades and compared their results with experimental findings. Isakson and Eisley[50] and Montoya[51] found the natural frequencies in coupled bending and torsion of twisted rotating and nonrotating blades. Krupka and Baumanis[52] included the effects of rotary inertia and shear deflection in analysing the bending-bending mode of vibration of a rotating tapered and twisted turbomachine blade using Myklestad method.

The finite element technique has also been applied by many irvestigators, mostly for the vibration analysis of uniform beams. All these investigations differ one from the other in the nodal degrees of freedom taken for deriving the elemental stiffness and mass matrices. McCalley[53] derived the consistent mass and stiffness matrices by selecting total deflection and total slope as nodal coordinates. Archer[54] analysed beams having different boundary conditions. Kapur[55] took bending deflection, shear deflection, bending slope and shear slope as nodal degrees of freedom and derived the elemental matrices of beams having linearly varying inertia. Carnegie, Thomas and Documaki[56] analysed uniform beams by taking few internal nodes in the element. Nickel and Sector[57] used total deflection, total slope and bending slopes of two ends and bending slope of the mid point of the element as degrees of freedom to derive the element stiffness and mass matrices of order seven. Thomas and Abbas[58] analysed uniform Timoshenko beams by taking total deflection, total slope and derivatives of bending slope as nodal degrees of freedom.

The study of banded group of blades has been reported by some investigators. Campbell[59] made an experimental investigation of low pressure blades grouped by lashing wires and stated an empirical relation between the natural frequencies of rotating and non-rotating blades. Prohl[60] analysed the problem of high pressure turbine blades by Holzer's technique and

obtained the first two natural frequencies. In a subsequent paper Prohl[61] presented a case study for determining vibrational amplitude and stresses at resonance. Bhide[62] studied the free vibrations of packetted high pressure blades by assuming the blades to be straight, untwisted and uniform cantilevers and applied finite element method to get the solution. Bajaj[63] studied the free vibration characteristics of packetted turbine blades of high pressure section using finite element method by considering the blades to be untwisted tapered cantilevers.

1.1.3 Optimum Design of Turbomachines

Optimization techniques are versatile and can be applied to a large class of engineering problems. So far they have been mostly applied to structural engineering problems, and to a lesser extent, to other types of design problems. Fox and Kapoor[64] reported a capability for the minimum weight optimum design of planar truss-frame structures with inequality constraints on the maximum dynamic displacement, stress and natural frequencies using the method of feasible directions. Rao[65] presented the optimum design of aircraft wings with strength, stability, frequency and flutter constraints using finite element idealization and interior penalty function approach. A review of the application of optimization techniques in mechanical design has been published by Seireg[66]. Raphael

and James[67] published a programme through which a wing section was optimized for weight. Reddy and Rao[68] applied optimization techniques in the automated optimum design of machine tool structures with constraints on rigidity and chatter stability. Hati and Rao[69,70] presented deterministic and probabilistic procedures for the determination of optimum machining conditions for jobs involving single and multiple operations. Rao[71] reported a capability for the minimum weight design of bridge girders for electric overhead travelling cranes.

Very few papers are available regarding the application of optimization techniques in the design of turbomachines. George[72] reported about the optimization of a rocket engine turbine using differential calculus approach. Balje[73] applied optimization techniques in the design of axial flow turbines to obtain maximum stage efficiency. He solved the problem by considering six design variables; nozzle angle at the outlet of stator blade, blade angle at the outlet of rotor blade, blade height to rotor diameter ratio, blade chord to rotor diameter ratio of nozzle blades, blade chord tor rotor diameter ratio of rotor blade, and the degree of partial admission. Upper and lower bounds on the design variables were the constraints and Wood's technique, which is essentially a pattern search method, was employed in obtaining the solution of the problem. Swift[74] published a flow chart for optimizing pump-turbine designs using computers and reported the transient behavior of

a pump-turbine. Kar and Reddy[75] found the optimum shape of the impeller of a pump by using differential calculus approach. Gupta[76] optimized the radial impeller of a pump by using graphical procedure. Saravanamuttoo and MacIsaac[77] published about the use of hybrid computer simulation of single-spool turbojet engine for optimizing the thrust response of gas turbines. Yadav and Gupta[78] optimized the channel circulation loss of a centrifugal compressor. Blaho[79] discussed the optimum design of axial flow fans from the view point of losses using experimental curves. Paranjpe and Murthy[80] discussed about the optimization and standardization of steam turbine blade profiles. In this work the authors discussed only a comparative procedure without giving any specific data of the problem.

1.2 Objective and Scope of the Present Work

It can be seen from the available literature that the potentialities of optimization techniques have not been exploited much by gas turbine designers. It is observed that the designers considered either aerodynamic aspects only or mechanical aspects only in designing gas turbines. This might be due to the complex aerodynamic fluid flow behavior present in turbines that gives rise to troublesome behavior constraints which, in the presence of constraints on the mechanical behavior, makes the problem more complicated. In the present work the automated

optimum design of axial flow gas turbine stage is considered by including both aerodynamic and mechanical considerations.

The weight of the stage and the losses of the stage have been considered in formulating a compound objective function. This permits the designer to optimize gas turbines either for weight or for losses depending on the specific purpose of the machine. By giving different weights to the individual objective functions, a parametric study can be conducted to find the relative effects of the two objectives on the optimum design.

The analysis used in this work accounts for the Reynolds number effects and makes use of free vortex theory to include three dimensional effects in turbines. The various behaviour constraints which arise due to fluid flow for the efficient operation of the stage are included. From mechanical design point of view, constraints are placed on the deflection, stress and fundamental natural frequency of vibration of the blade.

A finite element procedure is developed for finding the stresses, deflection and natural frequencies of vibration of turbine blades. This procedure takes into account the considerations like taper, twist, asymmetry, rotation, rotary inertia and shear deformation of the blade along with the gas loading. Although the idealization of gas turbine blades can also be made by using more complex elements like flat or

curved triangular plate elements, the beam element has been used in the present work as it gives reasonably good results with lesser number of degrees of freedom and requires lesser computer time.

In the optimization of complex problems using finite element method, a designer is generally confronted with two problems, namely, the computer storage and the computer time. To economize computer time, the eigen value problem has been solved by using one of the most efficient solution techniques developed by Bathe and Wilson[81] for large structural systems. In Bathe and Wilson technique, the Rayleigh-Ritz sub-space iteration algorithm, which solves the eigen value problem directly without transformation to the standard form, is used. Before solving the eigen value problem, the deflection and stresses due to gas forces have been calculated to make use of the available stiffness matrix. In this work, the Cholesky decomposition of symmetric matrices, storing only the upper triangular matrix, is used for solving the equilibrium equations.

In order to avoid storage of the necessary air properties in tabular form, the air properties have been computerised with polynomial approximations using least squares technique.

The constrained optimum design problem has been cast as a nonlinear mathematical programming problem. The interior penalty function method, with a variable metric unconstrained

minimization technique, is used to solve the optimum design problem. The minimizing step lengths in the unconstrained minimization are determined by cubic interpolation method. The computation of the gradient and the slope of the functions has been carried out by using backward difference method.

1.3 Organization of the Thesis

The thesis is organized into eight chapters and five appendices. After the introductory chapter, the design philosophy, objective function, design constraints and design variables of the problem are stated in Chapter 2. The problem of optimum design of axial flow gas turbine stage is also formulated in this chapter.

The evaluation of the objective function, which includes derivation of expressions for the weight of stage and the losses in stage is considered in Chapter 3. The iterative procedure involved in finding the efficiency (one minus losses) from the known data and the computation of the geometrical properties of airfoil section are also discussed in this chapter.

The development of finite element procedure for analysing turbine blades with consideration of taper, twist, rotation, rotary inertia and shear deformation is given in Chapter 4. The method of evaluating the constraints of the optimization problem is discussed in Chapter 5. A procedure for

converting airfoil cross section into an equivalent rectangular section is also presented in this chapter.

Chapter 6 deals with the optimization algorithm used in the present work. The reasons for using the penalty function formulation, with a variable metric unconstrained minimization method, along with the computational details are given in this chapter.

Several illustrative examples are presented in Chapter 7 to show the effectiveness of the present approach for the design of axial flow turbines. The results of sensitivity analysis are also presented in this chapter. The conclusions drawn from the present work and the scope for further extension of the work are stated in Chapter 8.

The polynomial equations used in the calculation of profile losses are given in Appendix A. The polynomial equations for evaluating the various air properties are stated in Appendix B. Appendix C gives the formulation of various matrices required in evaluating element stiffness and mass matrices of Chapter 4. In Appendix D, the elements of stiffness and mass matrices of a tapered beam element are presented. Appendix E contains a description and other details of the computer programme developed for the optimum design of gas turbine rotor stage.

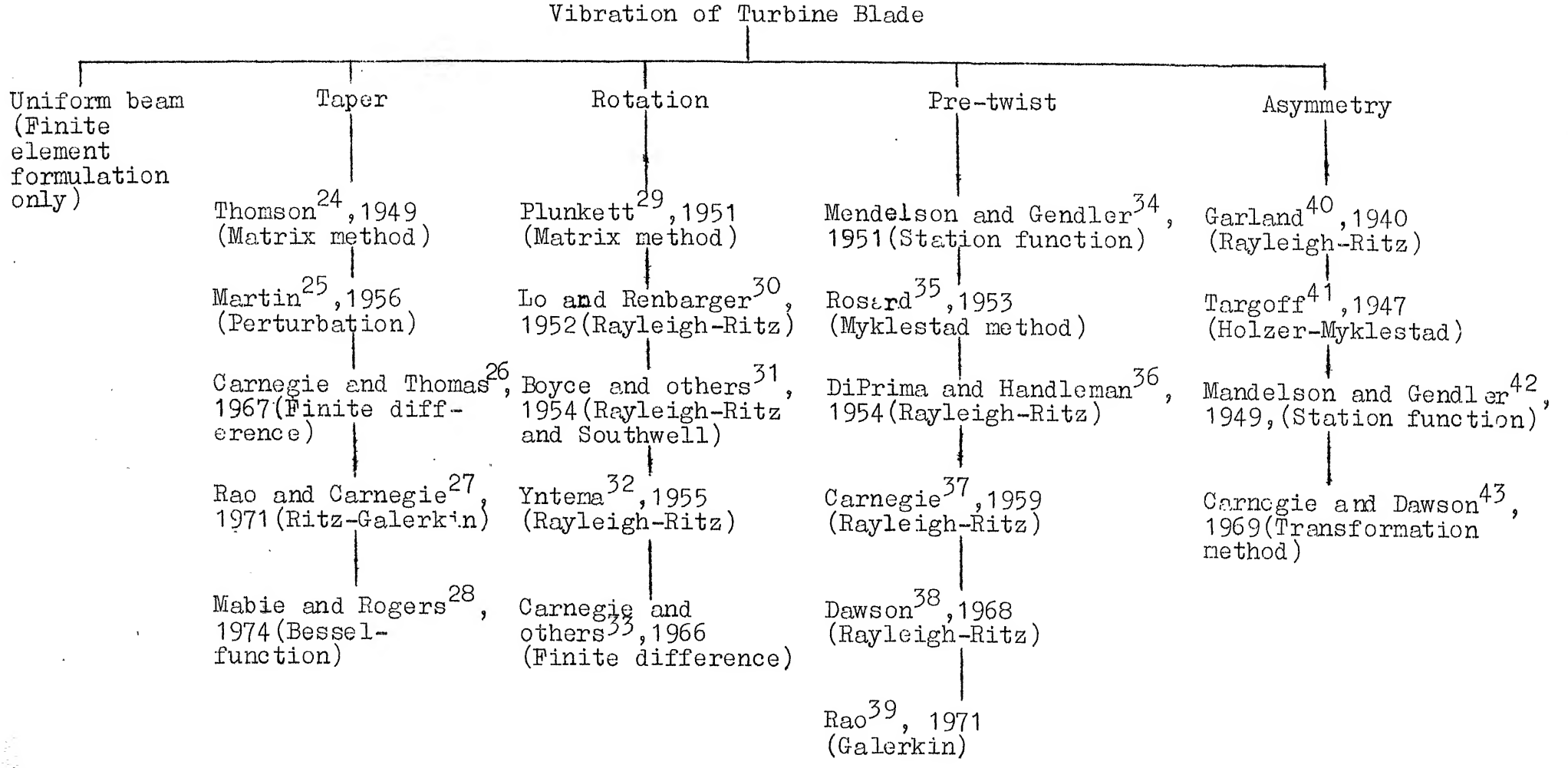
Vibration of Turbine Blade
Uniform beam (Finite element formulation only)
Taper
Thomson[24], 1949 (Matrix method)
Martin[25], 1956 (Perturbation)
Carnegie and Thomas[26], 1967 (Finite difference)
Rao and Carnegie[27], 1971 (Ritz-Galerkin)
Mabie and Rogers[28], 1974 (Bessel-function)
Rotation
Plunkett[29], 1951 (Matrix method)
Lo and Renbarger[30], 1952 (Rayleigh-Ritz)
Boyce and others[31], 1954 (Rayleigh-Ritz and Southwell)
Yntema[32], 1955 (Rayleigh-Ritz)
Carnegie and others[33], 1966 (Finite difference)
Pre-twist
Mendelson and Gendler[34], 1951 (Station function)
Rosard[35], 1953 (Myklestad method)
DiPrima and Handleman[36], 1954 (Rayleigh-Ritz)
Carnegie[37], 1959 (Rayleigh-Ritz)
Dawson[38], 1968 (Rayleigh-Ritz)
Rao[39], 1971 (Galerkin)
Asymmetry
Garland[40], 1940 (Rayleigh-Ritz)
Targoff[41], 1947 (Holzer-Myklestad)
Mandelson and Gendler[42], 1949, (Station function)
Carnegie and Dawson[43], 1969 (Transformation method)

Figure 1.1 (continued)

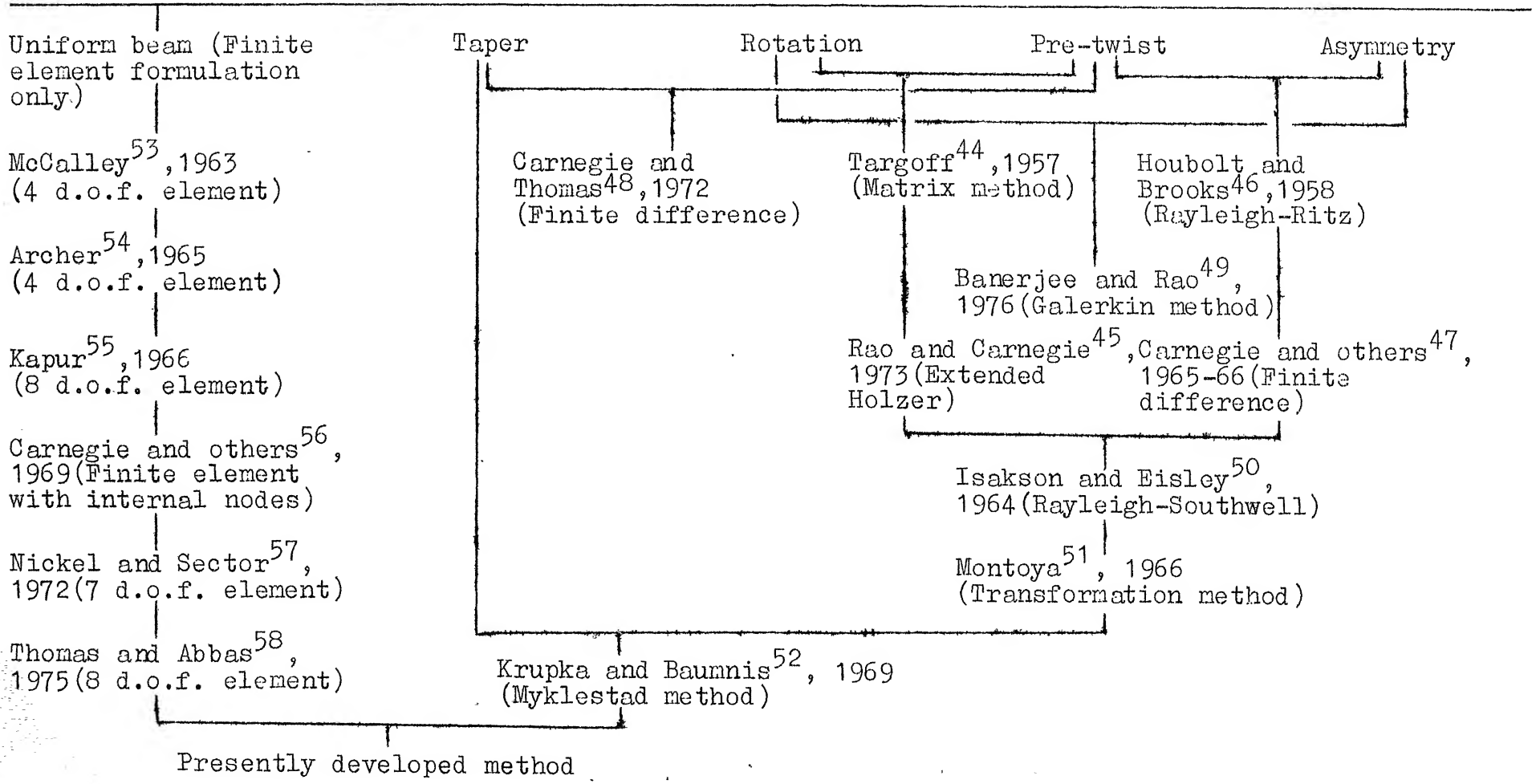

Figure 1.1 Reference Chart on Turbine Blade Vibration (Single Blade Analysis)

CHAPTER 2

FORMULATION OF THE OPTIMIZATION PROBLEM

When a means for predicting the behavior of any design within a particular design concept is available, limitations on the performance and other external constraints on the design are stated and an acceptance criterion is established, it is possible to cast the design modification problem in the form of a mathematical programming problem.

2.1 Design Philosophy

Any general design problem can be formulated and solved according to either deterministic or probabilistic design philosophy. If all the quantities affecting the design problem are deterministic, the design problem can be solved according to the deterministic design philosophy. On the other hand, if some of the design parameters are random in nature, the design problem has to be solved according to the probabilistic design philosophy.

In the deterministic design philosophy, a general mathematical programming problem can be stated as follows:

Minimize a multivariable function $f(\vec{X})$ where $\vec{X}$ is a n-dimensional vector consisting of X_j, $j = 1, 2, \ldots, n$, subjected to the given constraints $g_i(\vec{X})\{\leq, =, \geq\} 0$, $i = 1, 2, \ldots, m$. The function $f(\vec{X})$ is called the objective function and the vector $\vec{X}$ is termed as design vector.

In the probabilistic design philosophy, a general mathematical programming problem can be stated as follows:

Minimize the multivariable function $\bar{f}(\vec{X}, \vec{Y})$ subjected to the probabilistic constraints $P[g_j(\vec{X}, \vec{Y})\{\leq, =, \geq\} 0] \geq p_j$, $j = 1, 2, \ldots, m$, where $\vec{X}$ is the vector of design variables, and $\vec{Y}$ is the vector of other parameters affecting the design problem. Here the components of $\vec{X}$ and $\vec{Y}$ are assumed to be random variables, $\bar{f}$ represents the mean value of the objective function and $P[g_j(\vec{X}, \vec{Y})\{\leq, =, \geq\} 0] \geq p_j$ denotes that the j^{th} constraint has to be satisfied with a probability of greater than or equal to some specified quantity, p_j, $j = 1, 2, \ldots, m$, where $0 \leq p_j \leq 1$.

In the present work, only the deterministic design philosophy is used for the optimization of axial flow gas turbine stage.

2.2 Objective Function

A design problem usually has several solutions which may satisfy the specified functional requirements adequately. The objective function in a general optimization problem represents a basis for choice between alternate acceptable designs. In most of the practical design problems the minimization of weight, cost, volume or losses, or maximization of profit, rigidity or efficiency is taken as the objective. In the case of gas turbines used in aerospace applications the

minimization of weight is one of the most important criteria while in the case of gas turbines used in stationary power plants, the maximization of efficiency represents a more useful criterion. In some cases a mixed objective function representing a linear combination of weight and efficiency will be a more useful objective. In this work the mixed objective function is used so that the optimum design of aerospace turbines or industrial turbines can be obtained from the same computer program going · proper weightages to weight and efficiency in the objective function.

2.3 Design Constraints

In a realistic gas turbine design generally the following requirements are to be met from aerodynamic, vibrational and strength considerations:

(i) The rotational velocity of the rotor should be within some upper and lower bounds.

(ii) The aspect ratio (height/chord) of rotor and nozzle blades should be within some specified upper and lower bounds.

(iii) The pitch-chord ratio of the rotor and nozzle blades should be within the specified upper and lower bounds.

(iv) The relative gas velocity angles at inlet and outlet of rotor blades β_2 and β_3 should be within some specified upper and lower bounds.

(v) The axial velocity of flow should be within some upper and lower bounds.

(vi) The actual pressure ratio across the nozzle blades should be below the critical pressure ratio.

(vii) The Mach number at the exit from the stage should be less than a specified value.

(viii) The included angle of divergence of the turbine annulus walls should not exceed the specific upper limit.

(ix) The flow coefficient (ϕ) and the stage temperature drop coefficient (ψ) should lie within some upper and lower bounds.

(x) The degree of reaction at mean radius should be within some upper and lower bounds while the degree of reaction at the root of rotor blades should be a non-negative quantity.

(xi) The fundamental natural frequency of the blades should be away from the forcing frequency of the blade in order to avoid resonance.

(xii) The stresses developed at the root of the rotor blade should be less than the permissible value.

(xiii) The tip deflection of the rotor blade should be less than some specific value.

2.4 Design Variables

Once the objective function and the design constraints are specified the mathematical programming problem can be stated as soon as the design variables are identified. For the design of a gas turbine stage, the following parameters are taken as design variables:

X_1 = Mean diameter of the rotor, d

X_2 = Ratio of the chord of rotor blade to mean diameter, $\frac{c_R}{d}$

X_3 = Ratio of the chord of nozzle blade to mean diameter, $\frac{c_N}{d}$

X_4 = Ratio of spacing to diameter at mean radius of the nozzle blades, $\frac{s_N}{d}$

X_5 = Ratio of spacing to diameter at mean radius of the rotor blades, $\frac{s_R}{d}$

X_6 = Relative angle of the velocity triangle at the inlet of the rotor blade at mean radius, β_2

X_7 = Relative angle of the velocity triangle at the exit of the rotor blade at mean radius, β_3

X_8 = Axial velocity of flow across the stage, C_a.

Thus the vector of design variables $\vec{X}$ becomes

$$\vec{X} \equiv \begin{Bmatrix} X_1 \\ X_2 \\ X_3 \\ X_4 \\ X_5 \\ X_6 \\ X_7 \\ X_8 \end{Bmatrix} \equiv \begin{Bmatrix} d \\ c_R/d \\ c_N/d \\ s_N/d \\ s_R/d \\ \beta_2 \\ \beta_3 \\ C_a \end{Bmatrix} \qquad (2.1)$$

It can be noted that the nozzle angle α_2 can be taken as a design variable in place of the axial velocity C_a as they are related by the equation

$$C_a = \frac{U}{\tan \alpha_2 - \tan \beta_2} \tag{2.2}$$

where U is the tangential velocity of the rotor at mean radius.

2.5 Optimization Problem

The optimization problem can now be stated as follows:

Minimize

$$f(\vec{X}) = K_1(1 - \eta_s) + K_2 \rho_m \left\{ \frac{\pi \beta c_R (d-h_R)^2}{2(1+\beta)} + n_R h_R A_R + n_N h_N A_N \right\} \tag{2.3}$$

subject to

$$g_1 = \frac{U^{(l)}}{U} - 1.0 \leq 0 \tag{2.4}$$

$$g_2 = \frac{U}{U^{(u)}} - 1.0 \leq 0 \tag{2.5}$$

$$g_3 = \left(\frac{c_R}{d}\right)^{(l)} - \left(\frac{c_R}{d}\right) \leq 0 \tag{2.6}$$

$$g_4 = \left(\frac{c_R}{d}\right) - \left(\frac{c_R}{d}\right)^{(u)} \leq 0 \tag{2.7}$$

$$g_5 = \left(\frac{c_N}{d}\right)^{(l)} - \left(\frac{c_N}{d}\right) \leq 0 \tag{2.8}$$

$$g_6 = \left(\frac{c_N}{d}\right) - \left(\frac{c_N}{d}\right)^{(u)} \leq 0 \tag{2.9}$$

$$g_7 = \left(\frac{s_N}{c_N}\right)^{(l)} - \left(\frac{s_N}{c_N}\right) \leq 0 \tag{2.10}$$

$$g_8 = \left(\frac{s_N}{c_N}\right) - \left(\frac{s_N}{c_N}\right)^{(u)} \leq 0 \tag{2.11}$$

$$g_9 = \left(\frac{s_R}{c_R}\right)^{(l)} - \left(\frac{s_R}{c_R}\right) \leq 0 \tag{2.12}$$

$$g_{10} = \left(\frac{s_R}{c_R}\right) - \left(\frac{s_R}{c_R}\right)^{(u)} \leq 0 \tag{2.13}$$

$$g_{11} = \beta_2^{(l)} - \beta_2 \leq 0 \tag{2.14}$$

$$g_{12} = \beta_2 - \beta_2^{(u)} \leq 0 \tag{2.15}$$

$$g_{13} = \beta_3^{(l)} - \beta_3 \leq 0 \tag{2.16}$$

$$g_{14} = \beta_3 - \beta_3^{(u)} \leq 0 \tag{2.17}$$

$$g_{15} = \frac{c_a^{(l)}}{c_a} - 1.0 \leq 0 \tag{2.18}$$

$$g_{16} = \frac{c_a}{c_a^{(u)}} - 1.0 \leq 0 \tag{2.19}$$

$$g_{17} = \frac{p_{o1}}{p_2} - \frac{p_{o1}}{p_c} \leq 0 \tag{2.20}$$

$$g_{18} = M_{c_3} - M_{c_3}^{(u)} \leq 0 \tag{2.21}$$

$$g_{19} = \alpha_c - \alpha_c^{(u)} \leq 0 \tag{2.22}$$

$$g_{20} = \phi^{(l)} - \phi \leq 0 \tag{2.23}$$

$$g_{21} = \phi - \phi^{(u)} \leq 0 \tag{2.24}$$

$$g_{22} = \psi^{(l)} - \psi \leq 0 \tag{2.25}$$

$$g_{23} = \psi - \psi^{(u)} \leq 0 \tag{2.26}$$

$$g_{24} = R^{(l)} - R \leq 0 \tag{2.27}$$

$$g_{25} = R - R^{(u)} \leq 0 \tag{2.28}$$

$$g_{26} = \alpha_2^{(l)} - \alpha_2 \leq 0 \tag{2.29}$$

$$g_{27} = R_{root}^{(l)} - R_{root} \leq 0 \tag{2.30}$$

$$g_{28} = \frac{N}{\omega(1)} - 1.0 \leq 0 \tag{2.31}$$

$$g_{29} = \sigma_{max} - \sigma^{(u)} \leq 0 \tag{2.32}$$

$$g_{30} = \frac{\Delta_t}{\Delta_t^{(u)}} - 1.0 \leq 0 \tag{2.33}$$

where

$f(\vec{X})$ = mixed objective function

K_1 = weightage given to the minimization of losses in the objective function

η_s = stage efficiency

K_2 = weightage given to the minimization of weight of stage in the objective function

ρ_m = mass density of disc and blade material

β = chord taper ratio

c_R = chord of rotor blade at mean radius

h_R = mean height of rotor blades

n_R = number of rotor blades

A_R = cross-sectional area of rotor blade at the mean radius

n_N = number of nozzle blades

h_N = mean height of nozzle blades

A_N = cross-sectional area of nozzle blade at the mean radius

c_N = chord of nozzle blades at mean radius

s_N = spacing of nozzle blades at mean radius

s_R = spacing of rotor blades at mean radius

p_{o1} = stagnation pressure at the inlet of the stage

p_2 = static pressure at the inlet of the rotor blades

p_c = critical pressure

M_{C_3} = Mach number at the exit of the rotor blade calculated from the absolute velocity C_3

α_c = included angle of divergence of flared turbine annulus

R = degree of reaction at mean radius

α_2 = nozzle blade angle at the outlet

R_{root} = degree of reaction at the root of the rotor blade

N = rotational speed of the rotor (revolutions per second)

$\omega(1)$ = first natural frequency of vibration of rotor blade (cycles per second)

σ_{max} = maximum stress at the root

Δ_t = tip deflection of the rotor blade

l = superscript denoting the lower bound

u = superscript denoting the upper bound

The quantities p_2, p_c, M_{C_3}, α_c, $\emptyset$, , R, α_2, R_{root}, Δ_t and stresses are dependent on the design variables X_i and hence the constraint equations (2.20) to (2.33) are called the behavior constraints. The relation between the behavior quantities and the design variables cannot be expressed directly in closed form. However, for any given design vector $\vec{X}$, the behavior quantities can be evaluated numerically upto any desired accuracy. The analysis procedure to be adopted for determining the behavior quantities is considered in Chapters 3, 4 and 5.

Equations (2.4) to (2.19) represent the geometrical or side constraints, which impose limits on the size of the design variables.

It can be seen that the objective function of equation (2.3) is a non-linear function of the design variables, and the side constraints of equations (2.4) to (2.19) are linear while the behavior constraints are non-linear. Hence the mathematical programming problem formulated above is a non-linear programming problem.

CHAPTER 3

EVALUATION OF OBJECTIVE FUNCTION OF AXIAL FLOW GAS TURBINE STAGE

The essential purpose of a turbine is to obtain work output from a gas which drops in pressure and hence in temperature while passing through the machine. There are two basic types of gas turbines, namely, radial flow and axial flow turbines. The radial turbine is similar in appearance to a centrifugal compressor, but with a flow in the inward direction and nozzle vanes replacing the diffuser vanes. The radial turbine has been used in some small gas turbines where compactness is more important than performance. In an axial flow turbine, the gas flow has components of velocity parallel to the axial and tangential directions of the machine but has little radial velocity. The range of applications of axial flow turbines is very wide. There is no alternative to the axial flow turbine for the designer who seeks to have high flow per unit frontal area and high efficiency coupled with a reasonably high enthalpy drop per stage. In axial flow turbine designs, we want the machine to have a higher efficiency with a lesser weight. That is why the losses of the turbine stage and its weight have been taken as objectives in the present work. The procedure for evaluating these objective functions is discussed in some detail in this chapter.

3.1 Two Dimensional Fluid Flow Idealization in a Gas Turbine Stage

Figure 3.1(a) shows a gas turbine stage consisting of two rows of blades, one stationary and the other rotating. In the 'stator' or 'nozzle' row, the tangential velocity of the fluid is increased in the direction of rotation and the fluid is accelerated at the expense of a pressure drop. The tangential velocity in the direction of rotation is reduced across the 'rotor' row and tangential forces are exerted by the fluid on the rotor blades which produce a torque on the output shaft. Thus the absolute kinetic energy of the fluid is reduced across the rotor. There may be some acceleration of the fluid relative to the moving blades together with some drop in pressure and temperature. A multistage turbine is made up of several stages, each stage consisting of first a nozzle row and then a rotor row.

For machines having high hub to tip ratio, there cannot be large radial components of velocity between the annular walls and the flow conditions are not very much different at different radii. For such machines the two dimensional analysis is sufficiently accurate. In two dimensional analysis, the flow velocity triangles are drawn for the conditions of mean radius, but these triangles are assumed to be valid for other radial sections as well.

3.2 Velocity Triangles

Figure 3.1(b) shows the velocity triangle for an axial flow turbine stage alongwith the nomenclature employed. The gas enters the row of nozzle blades with a static pressure p_1, temperature T_1 and velocity C_1, expands to p_2, T_2 and leaves with an increased velocity C_2 at an angle α_2. The rotor blade inlet angle will be chosen to suit the direction β_2 of the gas velocity V_2 relative to the blade at inlet. β_2 and V_2 are found by vectorial subtraction of the blade speed U from the absolute velocity C_2. After being deflected, and usually further expanded, in the rotor blade passages, the gas leaves at p_3, T_3 with relative velocity V_3 at an angle β_3. The vectorial addition of U and V_3 yields the magnitude and direction of the gas velocity at exit from the stage, C_3 and α_3. The angle α_3 is known as the swirl angle.

In a single stage turbine, C_1 will be axial, i.e. $\alpha_1 = 0$ and $C_1 = C_a$ where C_a is the axial velocity of flow. If on the other hand, the stage is typical of many in a multi stage turbine, C_1 and α_1 will probably be equal to C_3 and α_3 so that the same blade shapes can be used in successive stages. The quantity $(C_{w_2} + C_{w_3})$ represents the change in whirl (or tangential) component of momentum per unit mass flow which produces the useful torque.

3.3 Temperature-Entropy (T - S) Diagram for a Stage

Figure 3.2 represents the temperature-entropy diagram for a stage. The full and chain dotted lines connect the stagnation and static states respectively. The stagnation temperature T_{o2} is equal to T_{o1} because no work is done in the nozzles; and the short horizontal portion of the full line represents the stagnation pressure drop, $(p_{o1} - p_{o2})$, due to friction in nozzles. The losses are ofcourse exaggerated in this figure. When obtaining the temperature equivalent of the velocity of the gas leaving the nozzle row, we may say that ideally the gas would be expanded from T_{o1} to T'_2 but due to friction the temperature at the nozzle exit will be T_2 which is somewhat higher than T'_2. The expansion of the gas in the moving blade passage reduces its pressure to p_3. Isentropic expansion in the whole stage would result in a final temperature T'_3, and in the rotor blade passages alone T''_3. The expansion with friction leads to a final temperature T_3. As no work is done by the gas relative to the blades, the stagnation temperature relative to the blade at point 3, $T_{o3\ rel}$, will be equal to $T_{o2\ rel}$. The stagnation pressures relative to the blade at inlet and outlet are represented by $p_{o2\ rel}$ and $p_{o3\ rel}$ respectively.

3.4 Losses and Efficiency

Horlock[82] has discussed about losses and efficiency of full admission turbines and Yahya[83] has discussed about losses in axial flow turbines with partial admission. Here the information regarding losses and efficiency of axial flow turbines with full admission is summarized.

3.4.1 Blade Losses due to Flow of Fluid in an Axial Flow Turbine Stage

An overall blade loss coefficient Y (or λ) must account for the following sources of friction loss:

(a) Profile loss - associated with the boundary layer growth over the blade profile (including separation loss under adverse conditions of extreme angles of incidence or high inlet Mach number).

(b) Annulus loss - associated with the boundary layer growth on the inner and outer walls of the annulus shown in Figure 3.3(a).

(c) Secondary flow loss - arising from the secondary flows which are always present when a wall boundary layer is turned through an angle by an adjacent curved surface. This loss is shown in Figure 3.3(b).

(d) Tip clearance loss - near the rotor blade tip the gas does not follow the intended path, fails to contribute its quota of work output and interacts with the outer wall boundary

layer. The radial tip clearance and side clearance for shrouded blades are shown in Figures 3.3(c) and 3.3(d) respectively.

The profile loss coefficient Y_p is measured directly in the cascade tests. The annulus and secondary flow losses cannot be easily separated, and they are accounted for by a secondary loss coefficient Y_s. The tip clearance loss coefficient, which normally arises only for rotor blades, will be denoted by Y_k. Thus the total loss coefficient Y comprises of the accurately measured two dimensional loss Y_p, plus the three dimensional loss $(Y_s + Y_k)$ which must be deduced from the turbine stage test results.

3.4.2 Definition of the Loss Coefficients

Benson[84] reviewed the methods for assessing the loss coefficients in radial gas turbines while the various loss coefficients used in axial flow compressors and gas turbine designs have been defined, compared and discussed in detail by Brown[85]. Referring to Figure 3.2, the most common loss coefficient for the nozzle blades may be defined either by

$$\lambda_N = \frac{T_2 - T_2'}{(C_2^2/2c_p)} \qquad \text{or} \qquad Y_N = \frac{p_{o1} - p_{o2}}{p_{o1} - p_2} \tag{3.1}$$

Both λ and Y express the proportion of the leaving energy which is degraded by friction. Although Y_N can be measured relatively

easily in cascade tests, λ_N can be used more easily in designs. It can be shown that λ_N and Y_N are not very different numerically. Similarly the loss coefficient for the rotor blades is defined as

$$\lambda_R = \frac{T_3 - T_3''}{(V_3^2/2c_p)} \quad \text{or} \quad Y_R = \frac{p_{o2\ rel} - p_{o3\ rel}}{p_{o3\ rel} - p_3} \qquad (3.2)$$

3.4.3 Definition of Efficiency

The isentropic stage efficiency or the total-to-total stage efficiency η_s is defined as

$$\eta_s = \frac{T_{o1} - T_{o3}}{T_{o1} - T'_{o3}} = \frac{1}{1 + [(T_{o3} - T'_{o3})/(T_{o1} - T_{o3})]} \qquad (3.3)$$

From Figure 3.1(c) it can be seen that

$$T_{o3} - T'_{o3} \approx (T_3 - T'_3) = (T_3 - T_3'') + (T_3'' - T'_3) \qquad (3.4)$$

But $(T'_2/T'_3) = (T_2/T_3'')$ because both of them are equal to $(\frac{p_1}{p_2})^{\frac{(\gamma-1)}{\gamma}}$. Rearranging and subtracting one from both sides of equation (3.4), one gets

$$\frac{T_3'' - T'_3}{T'_3} = \frac{T_2 - T'_2}{T'_2} \quad \text{or} \quad (T_3'' - T'_3) \approx (T_2 - T'_2)\frac{T_3}{T_2} \qquad (3.5)$$

Hence

$$\eta_s \simeq \frac{1}{1 + \left[\{(T_3 - T_3'') + \frac{T_3}{T_2}(T_2 - T_2')\}/(T_{o1} - T_{o3})\right]} \tag{3.6}$$

$$\simeq \frac{1}{1 + \left[\{\lambda_R (\frac{V_3^2}{2c_p}) + (\frac{T_3}{T_2}) \lambda_N (\frac{C_2^2}{2c_p})\}/(T_{o1} - T_{o3})\right]} \tag{3.7}$$

Alternatively, by substituting $V_3 = C_a \sec \beta_3$, $C_2 = C_a \sec \alpha_2$, and

$$c_p'(T_{o1} - T_{o3}) = U C_a(\tan \beta_3 + \tan \beta_2)$$

$$= U C_a\left[\tan \beta_3 + \tan \alpha_2 - (\frac{U}{C_a})\right], \tag{3.8}$$

equation (3.7) can be written in the form

$$\eta_s = \frac{1}{1 + \frac{1}{2}\frac{C_a}{U}\left[\frac{\lambda_R \sec^2 \beta_3 + (\frac{T_3}{T_2}) \beta_N \sec^2 \alpha_2}{\tan \beta_3 + \tan \alpha_2 - (\frac{U}{C_a})}\right]} \tag{3.9}$$

Because $Y \simeq \lambda$, the loss coefficients Y_R and Y_N may replace λ_R and λ_N in equations (3.7) and (3.9) if desired.

A second definition, the total-to-static efficiency, η_{TS}, for a stage is given by

$$\eta_{TS} = \frac{T_{o1} - T_{o3}}{T_{o1} - T_3'} \tag{3.10}$$

The isentropic stage efficiency should generally be used in multi stage turbines where the exhaust velocity from a stage is not lost.

3.5 Evaluation of the Efficiency of a Gas Turbine Stage

In Chapter 2 we identified eight design variables at mean radius as: diameter of the rotor, d; chord to diameter ratio of the rotor blades, $\frac{c_R}{d}$; chord to diameter ratio of the nozzle blades, $\frac{c_N}{d}$; spacing to diameter ratio of nozzle blades, $\frac{s_N}{d}$; spacing to diameter ratio of rotor blades, $\frac{s_R}{d}$; gas angle for rotor blade at inlet, β_2; gas angle for rotor blade at outlet, β_3 and the axial velocity of flow across the stage, C_a. In optimization procedure, the efficiency of the turbine stage is to be evaluated at various trial values of these design variables.

In the design of axial flow gas turbine stage it is assumed that the stagnation pressure at inlet to stage (p_{o1}), stagnation temperature at inlet to stage (T_{o1}), mass flow rate across the stage (m) and the speed of the rotor (N in revolutions per second) are the preassigned parameters.

Further we assume that the properties of air like specific heat at constant pressure, c_p, gas constant, $\bar{R}$, viscosity of gas, $\bar{\mu}$, and ratio of specific heat γ are known or can be calculated from suitable formulas.

In the following subsections the equations necessary for evaluating the isentropic stage efficiency or total-to-total stage efficiency η_s are developed sequentially. It is essential to assume a trial value in the beginning to calculate a more accurate value of the efficiency η_s. Thus the process is iterative and has to be continued until the values of η_s in two consecutive iterations are sufficiently close to each other.

3.5.1 Calculation of the Parameters of Velocity Triangle and Blade Heights

The tangential velocity of the rotor, U, can be calculated as

$$U = \pi d N \tag{3.11}$$

With the known values of U, C_a, β_2 and β_3, the velocity triangles (Figure 3.1(b)) at inlet and outlet of the rotor can be drawn and their parameters can be calculated using the following equations once the value of C_a is assumed constant across the stage.

$$\phi = \frac{C_a}{U} \tag{3.12}$$

$$R = \frac{\phi}{2} (\tan \beta_3 - \tan \beta_2) \tag{3.13}$$

$$\tan \alpha_2 = \tan \beta_2 + \frac{1}{\phi} \tag{3.14}$$

$$\tan \alpha_3 = \tan \beta_3 - \frac{1}{\phi} \tag{3.15}$$

$$C_2 = \frac{C_a}{\cos \alpha_2} \tag{3.16}$$

$$C_3 = \frac{C_a}{\cos \alpha_3} \tag{3.17}$$

$$V_2 = \frac{C_a}{\cos \beta_2} \tag{3.18}$$

$$V_3 = \frac{C_a}{\cos \beta_3} \tag{3.19}$$

$$C_{w_2} = C_2 \sin \alpha_2 \tag{3.20}$$

$$C_{w_3} = C_3 \sin \alpha_3 \tag{3.21}$$

where $\emptyset$ and R represent the flow coefficient and the degree of reaction respectively.

The stagnation temperature drop ΔT_{os} in the stage and the blade loading coefficient or the temperature drop coefficient can be calculated as

$$\Delta T_{os} = \frac{U\, C_a(\tan \beta_2 + \tan \beta_3)}{c_p} \tag{3.22}$$

and

$$\psi = \frac{2c_p \Delta T_{os}}{U^2} \tag{3.23}$$

The temperature equivalent of the outlet velocity is $\frac{C_2^2}{2c_p}$ and hence

$$T_2 = T_{o2} - \frac{C_2^2}{2c_p} = T_{o1} - \frac{C_2^2}{2c_p} \tag{3.24}$$

Assuming a guess value for the loss coefficient of the nozzle blades, λ_N, equation (3.1) gives

$$T_2' = T_2 - \lambda_N \frac{C_2^2}{2c_p} \tag{3.25}$$

The pressure p_2 can be found from the isentropic relation as

$$p_2 = p_{o1} / \left(\frac{T_{o1}}{T_2'}\right)^{\frac{\gamma}{(\gamma-1)}} \tag{3.26}$$

By ignoring the effect of friction, the critical pressure ratio can be calculated as

$$\frac{p_{o1}}{p_c} = \left(\frac{\gamma + 1}{2}\right)^{\frac{\gamma}{(\gamma-1)}} \tag{3.27}$$

where p_c is the critical pressure. The actual pressure ratio $\frac{p_{o1}}{p_2}$ is kept well below the critical pressure ratio for avoiding choking of the nozzle. The density ρ_2, annulus area A_2 and the throat area of the nozzle A_{2N} are calculated from the relations:

$$\rho_2 = \frac{p_2}{\overline{R}\, T_2} , \tag{3.28}$$

$$A_2 = \frac{m}{\rho_2 C_a} , \tag{3.29}$$

and

$$A_{2N} = \frac{m}{\rho_2 C_2} = A_2 \cos \alpha_2 \tag{3.30}$$

We now assume that the C_1 is axial i.e. $C_1 = C_a$ and hence $\alpha_1 = 0$. The temperature equivalent of the inlet kinetic energy is $\frac{C_1^2}{2c_p}$ and hence the annulus area required in plane 1 can be calculated as follows:

$$T_1 = T_{o1} - \frac{C_1^2}{2c_p} , \tag{3.31}$$

$$p_1 = p_{o1} \left(\frac{T_1}{T_{o1}}\right)^{\frac{\gamma}{(\gamma-1)}} , \tag{3.32}$$

$$\rho_1 = \frac{p_1}{\bar{R}\, T_1} , \tag{3.33}$$

and

$$A_1 = \frac{m}{1 \cdot C_a} \tag{3.34}$$

Similarly at the outlet of the stage, we have

$$T_{o3} = T_{o1} - \Delta T_{os} , \tag{3.35}$$

$$T_3 = T_{o3} - \frac{C_3^2}{2c_p} , \tag{3.36}$$

$$p_{o3} = p_{o1}\left(1 - \frac{\Delta T_{os}}{\eta_s\, T_{o1}}\right)^{\frac{\gamma}{(\gamma-1)}} , \tag{3.37}$$

$$p_3 = p_{o3}\left(\frac{T_3}{T_{o3}}\right)^{\frac{\gamma}{(\gamma-1)}} , \tag{3.38}$$

$$\rho_3 = \frac{p_3}{\overline{R}\, T_3}, \tag{3.39}$$

and

$$A_3 = \frac{m}{\rho_3 C_a} \tag{3.40}$$

The rotor blade height h_R and the nozzle blade height h_N can be calculated from the blade heights h_1, h_2 and h_3 at planes 1, 2 and 3 using the relations

$$h_1 = \frac{A_1 N}{U} \tag{3.41}$$

$$h_2 = \frac{A_2 N}{U} \tag{3.42}$$

$$h_3 = \frac{A_3 N}{U} \tag{3.43}$$

$$h_R = \frac{h_2 + h_3}{2} \tag{3.44}$$

$$h_N = \frac{h_1 + h_2}{2} \tag{3.45}$$

The turbine annulus is flared as shown in Figure 3.4. It is desired that the included angle of divergence of the wall α_c should not exceed a certain limiting value. If the blade breadth is approximately taken as the chord of the blade, α_c is related to the other parameters as

$$\tan \alpha_c = \frac{(h_3 - h_1)}{2} \cdot \frac{1}{d\ \{(\frac{c_N}{d}) + 1.25(\frac{c_R}{d})\}} \tag{3.46}$$

It is necessary to check the Mach number at the exit of the stage, M_{C_3}, because if this is too high, the friction losses may become unduly large. The Mach number at the exit is computed as

$$M_{C_3} = \frac{C_3}{(\gamma \bar{R} T_3)^{1/2}} \tag{3.47}$$

The loss coefficient λ_R can be calculated as

$$\lambda_R = \frac{T_3 - T_3''}{V_3^2/2c_p} \tag{3.48}$$

where

$$T_3'' = T_2/(\frac{p_2}{p_3})^{\frac{(\gamma-1)}{\gamma}} \tag{3.49}$$

3.5.2 Calculation of Gas Angles Along the Radius by Considering Three-Dimensional Effects

In actual practice, the shape of the velocity triangle varies from root to tip of the blade since the blade speed U increases along with the radius. Another reason is that the whirl component in the flow at outlet from the nozzles causes the static pressure and temperature to vary across the annulus. With a uniform pressure at inlet or with a small variation in pressure (due to smaller whirl component), it is clear that the pressure drop across the nozzle will vary giving rise to a corresponding variation in efflux velocity C_2. Twisted

blading designed to take account of the changing gas angles is called vortex blading.

It can be shown that if the elements of the fluid are to be in radial equilibrium ($\frac{1}{\rho}\frac{dp}{dr} = \frac{C_w^2}{r}$), an increase in static pressure from root to tip is necessary whenever there is a whirl component of velocity. The gas turbine designer cannot talk of impulse or 50 percent reaction stages as the rotor stage pressure or temperature drop increases from root to tip and therefore the reaction will also increase from the root to the tip.

The design method used in the present analysis, which takes into account these three dimensional effects, is called the radial equilibrium free vortex design. The assumptions of this analysis are:

(i) The stagnation enthalpy h_o is constant over the annulus (i.e. $\frac{dh_o}{dr} = 0$).

(ii) The axial velocity is constant over the annulus.

(iii) The whirl velocity is inversely proportional to the radius.

By using the subscript r to represent a quantity at any general radius r, the following relations can be derived for calculating the angles α_{2r}, α_{3r}, β_{2r} and β_{3r} at any general radius:

$$\tan \alpha_{2r} = \left(\frac{d}{d_r}\right)_2 \tan \alpha_2 \qquad (3.50)$$

$$\tan \alpha_{3r} = \left(\frac{d}{d_r}\right)_3 \tan \alpha_3 \tag{3.51}$$

$$\tan \beta_{2r} = \left(\frac{d}{d_r}\right)_2 \tan \alpha_2 - \left(\frac{d_r}{d}\right)_2 \frac{U}{C_a} \tag{3.52}$$

$$\tan \beta_{3r} = \left(\frac{d}{d_r}\right)_3 \tan \alpha_3 + \left(\frac{d_r}{d}\right)_3 \frac{U}{C_a} \tag{3.53}$$

These general relations can be specialized to obtain the blade angles at the root and at the tip of the stage as:

$$\tan \alpha_{2 \text{ root}} = \left(\frac{d}{d - h_2}\right) \tan \alpha_2 \tag{3.54}$$

$$\tan \alpha_{3 \text{ root}} = \left(\frac{d}{d - h_3}\right) \tan \alpha_3 \tag{3.55}$$

$$\tan \beta_{2 \text{ root}} = \left(\frac{d}{d - h_2}\right) \tan \alpha_2 - \left(\frac{d - h_2}{d}\right) \frac{U}{C_a} \tag{3.56}$$

$$\tan \beta_{3 \text{ root}} = \left(\frac{d}{d - h_3}\right) \tan \alpha_3 + \left(\frac{d - h_3}{d}\right) \frac{U}{C_a} \tag{3.57}$$

$$\tan \alpha_{2 \text{ tip}} = \left(\frac{d}{d + h_2}\right) \tan \alpha_2 \tag{3.58}$$

$$\tan \alpha_{3 \text{ tip}} = \left(\frac{d}{d + h_3}\right) \tan \alpha_3 \tag{3.59}$$

$$\tan \beta_{2 \text{ tip}} = \left(\frac{d}{d + h_2}\right) \tan \alpha_2 - \left(\frac{d + h_2}{d}\right) \frac{U}{C_a} \tag{3.60}$$

$$\tan \beta_{3 \text{ tip}} = \left(\frac{d}{d + h_3}\right) \tan \alpha_3 + \left(\frac{d + h_3}{d}\right) \frac{U}{C_a} \tag{3.61}$$

It is desirable always to have a positive value of the degree of reaction at the root of the blade, R_{root}, which can be calculated from the following relation:

$$R_{root} = \frac{C_a d}{2U(d - h_R)} \{\tan \beta_{3root} - \tan \beta_{2root}\} \qquad (3.62)$$

3.5.3 Blade Angles and Blade Profile

It is important to note that the velocity triangles yield the gas angles but not the blade angles. We have shown how to establish the gas angles at all radii and the blade height. We have also taken some trial value of spacing and chord of the blade. The next step is to choose the stator and the rotor blade shapes which will accept the gas incidence upon the leading edge and deflect it through the required angle with minimum loss. For calculating blade angles we should know the value of deviation.

Carter and Hughes[86] have calculated the deviation (δ) in potential flow through a variety of compressor and turbine cascades. The cascade geometry is shown in Figure 3.5. It has been suggested that the un-stalled low speed deviation for the turbine cascades may be written as

$$\delta = \bar{m}\, \theta' \sqrt{\frac{s}{c}} \qquad (3.63)$$

where $\bar{m}$ is a function of the stagger α_s as indicated in Figure 3.6(a) and θ' is the blade camber angle. The angle

θ' is related to the blade angles (α_1' and α_2') of the cascade and the gas angles of the cascade (α_1 and α_2) at inlet and outlet as

$$\theta' = \alpha_1' + \alpha_2' = (\alpha_1 + i) + (\alpha_2 + \delta) = \epsilon + i + \delta \qquad (3.64)$$

where i is the angle of incidence and ϵ is the gas deflection which is equal to $(\alpha_1 + \alpha_2)$. At design conditions, the angle of incidence is assumed to be zero and hence the equation of deviation becomes

$$\delta = \bar{m}(\alpha_1 + \alpha_2 + \delta)\sqrt{\frac{s}{c}} \qquad (3.65)$$

The solution of equation (3.65) gives the deviation as

$$\delta = \frac{\bar{m}(\alpha_1 + \alpha_2)\sqrt{\frac{s}{c}}}{(1 - \bar{m}\sqrt{\frac{s}{c}})} \qquad (3.66)$$

In the present analysis, a constant value of $\bar{m} = 0.1$ has been assumed which is reasonably good for the blade having parabolic arc camber line. Thus we can calculate the blade angles at the outlet of the nozzle stage α_2' and the outlet of the rotor blade β_3' from the relations given below. The inlet stator and rotor blade angles will then correspond to α_1 and β_2 respectively as incidence is assumed to be zero.

$$\alpha_2' = \alpha_2 + \delta_N = \alpha_2 + \frac{\bar{m}(\alpha_1 + \alpha_2)\sqrt{\frac{s_N}{c_R}}}{(1 - \bar{m}\sqrt{\frac{s_N}{c_R}})} \qquad (3.67)$$

$$\beta_3' = \beta_3 + \delta_R = \beta_3 + \frac{\bar{m}(\beta_2 + \beta_3)\sqrt{\frac{s_R}{c_R}}}{(1 - \bar{m}\sqrt{\frac{s_R}{c_R}})} \qquad (3.68)$$

The blade angles at the root and the tip for free vortex blading can be calculated by replacing α_2 and α_3 of equations (3.54) to (3.61) by α_2' and β_3' of equations (3.67) and (3.68).

The next step is to fix the blade profiles. Two series of profiles have been specially designed for turbines by Dunavant and Erwin[87]. The details of the two series are given in Table 3.1 and in Figure 3.7. The primary series A_3K_7 (Figure 3.7(a)) is for reaction blades in which there is acceleration through the cascades. The shape of the camber line gives a rapid turning in the forward part of the blade, where the Mach numbers are low. The secondary series $B_1E_1I_1$ (Figure 3.7(b)) is for conditions approaching zero reaction. The loading is distributed more evenly along the chord, since there is less change in the average Mach number through the channel. The camber line coordinates and the blade thickness y_t have been given as a percentage of the chord in Table 3.1 for which $\frac{dy_c}{dx_{c(0.5)}} = 0.8574$, leading edge radius = 4.407% of chord; $\frac{dy_c}{dx_{c(95)}} = -0.1602$, trailing edge radius = 1.000% of chord for primary blade and for secondary blade

$\frac{dy_c}{dx_c(0.5)}$ = 0.5657, leading edge radius = 3.300% of chord; and

$\frac{dy_c}{dx_c(95)}$ = -0.2017, trailing edge radius = 1.000% of chord.

The above-mentioned profiles (A_3K_7 and $B_1E_1I_1$) are suitable for a particular set of inlet and outlet angles. If the gas angles are changed, we will have to select another set of profiles whose mean line coordinate should match with the new gas angles. In this way we will have to store a huge amount of data in an automated design procedure which may not be practically feasible. This problem can be solved if we find the mean line of the profile by satisfying certain desired conditions and then superimpose the thickness distribution of either the primary or the secondary profiles from Table 3.1 depending on the requirements.

In Figure 3.8, the line 1-2 represents the chord of the blade and the curve 1-m-2 the camber where the maximum camber with respect to the chord occurs at the point m. The angle between the chord line (x-axis) and the axial direction (X-axis) is given by the stagger angle α_s. We assume the location of the point m depending on the type of blading (reaction or impulse) and hence the coordinates of m (namely, x_m and y_m) are known. It is required that the gas should enter at point 1 (when $y = y_1$) at an angle α_1 and it should leave at point 2 (when $y = y_2$) at an angle α_2. Hence the following conditions are to be satisfied by the camber line of Figure 3.8:

$$\begin{aligned}
&\text{At } x = x_1 = x^{(l)} : \quad y = y_1 \quad \text{and} \quad \frac{dy}{dx} = \alpha_1 \\
&\text{At } x = x_2 = x^{(u)} : \quad y = y_2 \quad \text{and} \quad \frac{dy}{dx} = \alpha_2 \qquad (3.69) \\
&\text{At } x = x_m \quad\quad : \quad y = y_m \quad \text{and} \quad \frac{dy}{dx} = 0
\end{aligned}$$

Thus there are six conditions to be met by the camber line and hence a polynomial of degree five can be fitted exactly. Once the equation of the mean line is obtained, we can superimpose the thickness distribution from Table 3.1 to obtain the required profile of the blade. The upper and lower profile curves of the blade section have been interpolated as fourth order polynomials from 23 data points using least squares method of curve fitting. These boundary profiles have been expressed as $y^{(u)}(x)$ and $y^{(l)}(x)$ respectively in Fig. 3.8.

3.5.4 Estimation of Design Point Performance of the Stage

Once the major parameters of the stage are decided, the design point performance of the stage can be calculated. The method used is due to Ainby and Mathieson[88] which estimates the performance on flow conditions at the mean diameter of the annulus. Reference 88 describes how to calculate the performance of a turbine over a range of operating conditions, but we shall be concerned here only to find efficiency at the design point. A start is made using the two correlations for profile loss coefficient Y_p obtained from cascade data (shown

in Figures 3.6(b) and 3.6(c)). These refer to nozzle-type blades ($\beta_2 = 0$) and impulse type blades ($\beta_2 = \beta_3$) of conventional profiles having thickness to chord ratio ($\frac{t}{c}$) of 0.2 and a trailing edge thickness to pitch ratio, ($\frac{t_e}{s}$), of 0.02. The rotor blade notation is used in Figure 3.6 and the flow relative to any blade row is considered. When the nozzle row is being considered, β_2 becomes α_1 and β_3 becomes α_2. The values of Y_p in Figure 3.6 refer to the blades operating at zero incidence, i.e. when the gas inlet angle β_2 is also the blade inlet angle. The incidence is assumed to be zero and the thickness to chord ratio of the rotor and nozzle blades is also assumed as 0.2. All the curves of Figures 3.6(b) and 3.6(c) have been computerised in the form of polynomials. The polynomial equations of the various curves are given in Appendix A. The method of estimation of the design point performance can be stated by the following steps.

Step (i): Estimate the profile losses of rotor and nozzle blades as follows:

$$(Y_p)_R = \left[Y_{p(\beta_2 = 0)} + \left(\frac{\beta_2}{\beta_3}\right)^2 \{ Y_{p(\beta_2 = \beta_3)} - Y_{p(\beta_2 = 0)} \} \right] \left(\frac{t_R/c_R}{0.2}\right)^{\beta_2/\beta_3} \qquad (3.70)$$

$$(Y_p)_N = \left[Y_{p(\alpha_1 = 0)} + \left(\frac{\alpha_1}{2}\right)^2 \left\{ Y_{p(\alpha_1 = \alpha_2)} - Y_{p(\alpha_1 = 0)} \right\} \right] \left(\frac{t_N/c_N}{0.2}\right)^{\alpha_1/\alpha_2} \quad (3.71)$$

Step (ii): The secondary and tip clearance loss data for Y_s and Y_k have been correlated using the concepts of lift and drag coefficients. By defining the mean angles α_m and β_m as

$$\tan \alpha_m = \frac{(\tan \alpha_2 - \tan \alpha_1)}{2} \quad (3.72)$$

and

$$\tan \beta_m = \frac{(\tan \beta_3 - \tan \beta_2)}{2} \quad (3.73)$$

the lift coefficients for nozzle and rotor are calculated from the relations

$$(C_L)_N = 2\left(\frac{s_N}{c_N}\right)(\tan \alpha_1 + \tan \alpha_2) \cos \alpha_m \quad (3.74)$$

and

$$(C_L)_R = 2\left(\frac{s_R}{c_R}\right)(\tan \beta_2 + \tan \beta_3) \cos \beta_m \quad (3.75)$$

Dunham and Came[89] suggest that the method of reference 88 would be applicable to a wider range of turbines if the following secondary and tip clearance loss correlations are used

$$\lambda_{c_N} = 0.0334 \left(\frac{c_N}{h_N}\right)\left(\frac{\cos \alpha_2}{\cos \alpha_1}\right) \tag{3.76}$$

$$\lambda_{c_R} = 0.0334 \left(\frac{c_R}{h_R}\right)\left(\frac{\cos \beta_3}{\cos \beta_2}\right) \tag{3.77}$$

Thus the sum of the secondary and tip clearance loss coefficients of the rotor and the nozzle are given by:

$$(Y_s + Y_k)_R = \{ \lambda_{c_R} + B\left(\frac{c_R}{h_R}\right)\left(\frac{\bar{k}}{c}\right)^{0.78} \} \{ \frac{(C_L)^2_R}{(s_R/c_R)} \} \left(\frac{\cos^2 \beta_3}{\cos^3 \beta_m}\right) \tag{3.78}$$

$$(Y_s + Y_k)_N = \{ \lambda_{c_N} + 0.0 \} \{ \frac{(C_L)^2_N}{(s_N/c_N)} \} \left(\frac{\cos^2 \alpha_2}{\cos^3 \alpha_m}\right) \tag{3.79}$$

where $\bar{k}$ is the clearance and B is a constant depending upon the type of clearance. The value of B is 0.50 for a radial tip clearance and 0.25 for a shrouded blade with side clearance as shown in Figures 3.3(c) and 3.3(d).

Step (iii): The total loss coefficient for nozzle and rotors can be calculated as:

$$Y_N = (Y_p)_N + (Y_s + Y_k)_N \tag{3.80}$$

$$Y_R = (Y_p)_R + (Y_s + Y_k)_R \tag{3.81}$$

Step (iv): From the known Y_N and Y_R, the iterated (improved) loss parameters λ_{N_i} and λ_{R_i} are obtained as:

$$\lambda_{N_i} = \frac{Y_N T_2'}{T_{o1}} \tag{3.82}$$

and

$$\lambda_{R_i} = \frac{Y_R T_3''}{T_{o3\ rel}} \tag{3.83}$$

where $$T_{o3rel} = T_3 + \frac{V_3^2}{2c_p} \tag{3.84}$$

It can be observed that λ_{R_i} is greater than λ_{N_i} by virtue of tip leakage loss in the rotor blades. With the new values of λ_{N_i} and λ_{R_i}, an improved value of the isentropic efficiency is calculated by making use of relation (3.7) as:

$$\eta_{si} = \frac{1}{1 + \left[\left\{ \lambda_{R_i} \left(\frac{V_3^2}{2c_p}\right) + \left(\frac{T_3}{T_2}\right) \lambda_{N_i} \left(\frac{C_2^2}{2c_p}\right)\right\} / (T_{o1} - T_{o3}) \right]} \tag{3.85}$$

It is to be remembered that we started with a trial value of the nozzle loss coefficient λ_N and the isentropic stage efficiency η_s and now we obtained iterated (improved) values of these quantities as λ_{N_i} and η_{s_i}. It is desired that finally we should get $\lambda_{N_i} = \lambda_N$ and $\eta_{s_i} = \eta_s$. Both these requirements may not be met at a time. When convergence is not achieved, we start a new iteration taking λ_{N_i} and η_{s_i} as the guess values and finally we stop the iterative procedure when

n_{s_i} converges within a specified accuracy. In the present work, the iteration procedure is terminated whenever $|n_s - n_{si}| \leq .0005$. Finally the number of nozzle blades n_N and rotor blades n_R are calculated from the known value of spacing to diameter ratio as

$$n_N = \frac{\pi d}{s_N} \tag{3.86}$$

and

$$n_R = \frac{\pi d}{s_R} \tag{3.87}$$

Further the Mach numbers corresponding to the velocities V_3 and C_2 (namely M_{V_3} and M_{C_2}) can be computed as:

$$M_{V_3} = \frac{V_3}{(\gamma \bar{R} \bar{T}_3)^{1/2}} \tag{3.88}$$

$$M_{C_2} = \frac{C_2}{(\gamma \bar{R} \bar{T}_2)^{1/2}} \tag{3.89}$$

The values of M_{V_3} and M_{C_2} are to be kept below the critical value.

3.5.5 Correction for Reynolds Number Effect

The applicability of the correlations of profile losses given in section 3.5.4 is limited by the Reynolds number of the flow (R_e). The Reynolds number effects on turbomachines are discussed in references 90 and 91. The Reynolds number of

the flow should be in the region of $1X10^5$ to $3X10^5$, with R_e defined in terms of the blade chord c, density ρ and the relative velocity at the outlet of the blade row. We can calculate the Reynolds number for the nozzle and rotor blades, $(R_e)_N$ and $(R_e)_R$, by assuming a constant (known) value of viscosity $\bar{\mu}$ ($\bar{\mu} = \bar{\mu}_2 = \bar{\mu}_3$) for air as

$$(R_e)_N = \frac{\rho_2 C_2 c_N}{\bar{\mu}_2} \tag{3.90}$$

and

$$(R_e)_R = \frac{\rho_3 V_3 c_R}{\bar{\mu}_3} \tag{3.91}$$

The Reynolds number for a turbine stage R_e is taken as the arithmatic mean of R_e for the nozzle and rotor as

$$R_e = \frac{(R_e)_N + (R_e)_R}{2} \tag{3.92}$$

If the value of R_e given by equation (3.92) differs much from $2X10^5$, an approximate correlation can be made to the isentropic efficiency η_s by modifying it to $(\eta_s)_{R_e}$ as follows:

$$(\eta_s)_{R_e} = 1 - \left(\frac{2X10^5}{R_e}\right)^{0.2} (1 - \eta_s) \tag{3.93}$$

All the steps followed in section 3.5 have been shown in the form of a flow chart in Figure 3.9.

3.6 Determination of Air Properties

The computation of energy and work of gases in the present chapter are based on the temperature-entropy diagram. This requires a knowledge of the values of specific heat of air at constant pressure, c_p, at various temperatures. These values of c_p are taken from air tables and stored in the computer in the form of polynomials obtained by using least squares method. These polynomial expressions for c_p are given in Appendix B. An alternative approach for the calculation of energy and work is to make use of the enthalpy-entropy and enthalpy-temperature relations. Again these calculations require air tables to obtain the various properties. For this purpose, all the air properties tabulated by Keenan and Kaye[92] have been computerised in the form of polynomials using the technique of least squares and the results are reported in Appendix B.

3.7 Computation of the Geometrical Properties of Airfoil Sections

In order to evaluate the weight of a stage, the areas of cross section of nozzle and rotor blades are needed. Moreover, some other geometrical properties of the airfoil like moments of inertia are required for computing the stresses in blades. Hence the computation of the geometrical properties of airfoil sections is considered in this section.

The blade angles and blade profiles were fixed in section 3.5.3. The equations of upper profile $y^{(u)}(x)$ and lower profile $y^{(l)}(x)$ were obtained as fourth order polynomials (Figure 3.8) by making use of least squares fit. Let these curves be expressed in a general form as

$$y = c_5x^4 + c_4x^3 + c_3x^2 + c_2x + c_1$$

Since the evaluation of the geometrical properties of the airfoil requires y^2 and y^3, these can be expressed as.

$$y^2 = d_9x^8 + d_8x^7 + d_7x^6 + d_6x^5 + d_5x^4 + d_4x^3 + d_3x^2 + d_2x + d_1 \qquad (3.94)$$

where $d_9 = c_5^2$, $d_8 = 2c_5c_4$, $d_7 = 2(c_3c_5 + c_4^2)$,

$d_6 = 2(c_4c_3 + c_2c_5)$, $d_5 = (2c_5c_1 + 2c_2c_4 + c_3^2)$,

$d_4 = 2(c_4c_1 + c_2c_3)$, $d_3 = (2c_1c_3 + c_2^2)$

$d_2 = 2c_1c_2$, $d_1 = c_1^2$ (3.95)

and,

$$y^3 = (d_9c_5)x^{12} + (d_8c_5 + d_9c_4)x^{11} + (d_7c_5 + d_8c_4 + d_9c_3)x^{10}$$
$$+ (d_6c_5 + d_7c_4 + d_8c_3 + d_9c_2)x^9 + (d_5c_5 + d_6c_4 + d_7c_3$$
$$+ d_8c_2 + d_9c_1)x^8 + (d_4c_5 + d_5c_4 + d_6c_3 + d_7c_2 + d_8c_1)x^7$$
$$+ (d_3c_5 + d_4c_4 + d_5c_3 + d_6c_2 + d_7c_1)x^6 + (d_2c_5 + d_3c_4$$

$$+ d_4c_3 + d_5c_2 + d_6c_1)x^5 + (d_1c_5 + d_2c_4 + d_3c_3 + d_4c_2$$

$$+ d_5c_1)x^4 + (d_1c_4 + d_2c_3 + d_3c_2 + d_4c_1)x^3 + (d_1c_3 +$$

$$d_2c_4 + d_3c_1)x^2 + (d_1c_2 + d_2c_1)x + d_1c_1 \qquad (3.96)$$

Thus from the known values of c_1, c_2, c_3, c_4 and c_5, the coefficients of the polynomials of y^2 and y^3 for upper and lower curves can be calculated. The geometrical properties of the airfoil section can be evaluated as follows:

Area of cross-section of the airfoil = $A = \int_{x^{(l)}}^{x^{(u)}} \int_{y^{(l)}(x)}^{y_2^{(u)}(x)} dy\, dx$

(3.97)

i.e., $$A = \int_{x^{(l)}}^{x^{(u)}} \{y^{(u)}(x) - y^{(l)}(x)\}\, dx$$

$$= \{(c_5^{(u)} - c_5^{(l)})\frac{x^5}{5} + (c_4^{(u)} - c_4^{(l)})\frac{x^4}{4} + (c_3^{(u)} - c_3^{(l)})$$

$$\frac{x^3}{3} + (c_2^{(u)} - c_2^{(l)})\frac{x^2}{2} + (c_1^{(u)} - c_1^{(l)})x\}_{x^{(l)}}^{x^{(u)}}$$

(3.98)

where the subscripts (u) and (l) represent the values corresponding to upper and lower curves respectively. Further,

x coordinate of the centroid = $\bar{x} = \frac{1}{A}\{ \int_{x^{(l)}}^{x^{(u)}} \int_{y^{(l)}(x)}^{y^{(u)}(x)} x\, dx\, dy \}$

$$= \frac{1}{A}\{ \int_{x^{(l)}}^{x^{(u)}} x\,(y^{(u)}(x) - y^{(l)}(x)\, dx)\} \qquad (3.99)$$

y coordinate of the centroid $= \bar{y} = \frac{1}{A}\left[\int_{x^{(l)}}^{x^{(u)}} \int_{y^{(l)}(x)}^{y^{(u)}(x)} y \, dx \, dy \right]$

$$= \frac{1}{2A}\left[\int_{x^{(l)}}^{x^{(u)}} \{ y^{(u)^2}(x) - y^{(l)^2}(x) \} \, dx \right] \qquad (3.100)$$

Moment of inertia about x axis $= I_{xx} = \int_{x^{(l)}}^{x^{(u)}} \int_{y^{(l)}(x)}^{y^{(u)}(x)} y^2 \, dx \, dy$

$$= \frac{1}{3}\left[\int_{x^{(l)}}^{x^{(u)}} \{ y^{(u)^3}(x) - y^{(l)^3}(x) \} \, dx \right] \qquad (3.101)$$

Moment of inertia about y axis $= I_{yy} = \int_{x^{(l)}}^{x^{(u)}} \int_{y^{(l)}(x)}^{y^{(u)}(x)} x^2 \, dx \, dy$

$$= \frac{1}{2}\left[\int_{x^{(l)}}^{x^{(u)}} x^2 \{ y^{(u)}(x) - y^{(l)}(x) \} \, dx \right] \qquad (3.102)$$

Product of inertia $= I_{xy} = \int_{x^{(l)}}^{x^{(u)}} \int_{y^{(l)}(x)}^{y^{(u)}(x)} x \, y \, dx \, dy$

$$= \frac{1}{2}\left[\int_{x^{(l)}}^{x^{(u)}} x\{ y^{(u)^2}(x) - y^{(l)^2}(x) \} \, dx \right] \qquad (3.103)$$

If $x^{(l)} = 0$, $x^{(u)}$ will be equal to the chord of the blade, c.

3.8 Evaluation of the Objective Function

Once the blade angles and the chords of rotor and nozzle blades are decided, the cross sectional areas of rotor blade (A_R) and nozzle blade (A_N) can be calculated by making use of the analysis of section 3.7. The efficiency of the stage η_s and the other blade parameters have been calculated in section 3.5. Suitable breadth ratio is also assumed. Now we can calculate the objective function $f(\vec{X})$ using equation (2.3). Since it is a mixed type of objective function, where the first part represents losses of the stage and second part represents the weight of rotor disc, rotor blades and nozzle blades, suitable values of K_1 and K_2 are to be assumed depending on the application of gas turbine.

Since the procedure indicated in section 3.5 for computing the isentropic efficiency is iterative, it is necessary to see the nature of convergence of the procedure. For this the isentropic efficiency of a gas turbine stage is computed using different trial values of efficiency and convergence criteria. The results are shown in Table 3.2. It can be seen that the efficiency converged essentially to the same value for all trial efficiencies; however, lesser number of iterations are required when the trial efficiency is assumed to be 0.9. The results obtained with two different values of ε (the difference between the current trial value of efficiency and the calculated value of efficiency in any iteration) show that more number of iterations are required with smaller (more stringent) values of ε.

TABLE 3.1

Mean Line, Thickness Distribution and Coordinates for Primary and Secondary Turbine-blade Series

Sl. No.	x_c	Primary turbine blade (reaction blading) A_3K_7 mean line coordinate for $C_{L_o}=1.0$ and thickness distribution in % of chord		Secondary turbine blade (impulse) $B_1E_1I_1$ mean line and thickness distribution	
		y_c Mean line coordinate % of chord	y_t Thickness distribution % of chord	y_c % of chord	y_t % of chord
1	0.0	0	0	0	0
2	0.5	0.397		0.336	
3	1.25	0.836	3.469	0.718	2.583
4	2.5	1.428	4.972	1.253	3.282
5	5.0	2.359	6.918	2.128	4.041
6	10.0	3.689	9.007	3.480	5.007
7	15.0	4.597	9.827	4.506	5.592
8	20.0	5.217	10.000	5.291	6.995
9	25.0	5.623	9.899	5.862	8.063
10	30.0	5.852	9.613	6.261	9.025
11	35.0	5.936	9.106	6.514	9.727
12	40.0	5.897	8.594	6.642	10.000
13	45.0	5.753	7.913	6.652	9.725
14	50.0	5.516	7.152	6.551	9.009
15	55.0	5.200	6.339	6.342	8.016
16	60.0	4.814	5.500	6.016	6.908
17	65.0	4.367	4.661	5.551	5.848
18	70.0	3.870	3.848	4.983	5.000
19	75.0	3.328	3.087	4.332	4.312
20	80.0	2.746	2.406	3.680	3.624
21	85.0	2.133	1.830	2.824	2.936
22	90.0	1.485	1.387	1.953	2.248
23	95.0	0.801	1.101	0.948	1.560
24	100	0.0	0.0	0.0	0.0

TABLE 3.2

Convergence Study of Isentropic Efficiency

Sl. No.	Trial value of efficiency	For ε = .0005		For ε = .00005	
		Converged value of efficiency	No. of iterations required	Converged value of efficiency	No. of iterations required
1	.60	.92015686	3	.92015349	4
2	.65	.92015617	3	.92015351	4
3	.70	.92015556	3	.92015352	4
4	.75	.92015501	3	.92015353	4
5	.80	.92015453	3	.92015353	4
6	.85	.92015410	3	.92015410	3
7	.90	.92014484	2	.92015373	3
8	.95	.92015338	3	.92015338	3
9	1.00	.92015306	3	.92015306	3
10	1.05	.92015279	3	.92015279	3

Data: $d = .432$ m, $\frac{c_R}{d} = .046$, $\frac{c_N}{d} = .04$, $\frac{s_N}{d} = .035$, $\frac{s_R}{d} = .044$, $\beta_2 = .358$, $\beta_3 = .960$, $C_a = 272$ m/sec, $p_{o1} = .4 \times 10^6$ N/m^2, $T_{o1} = 1100$ K, $m = 20$ Kg, $N = 250$ rps, radial clearance is assumed.

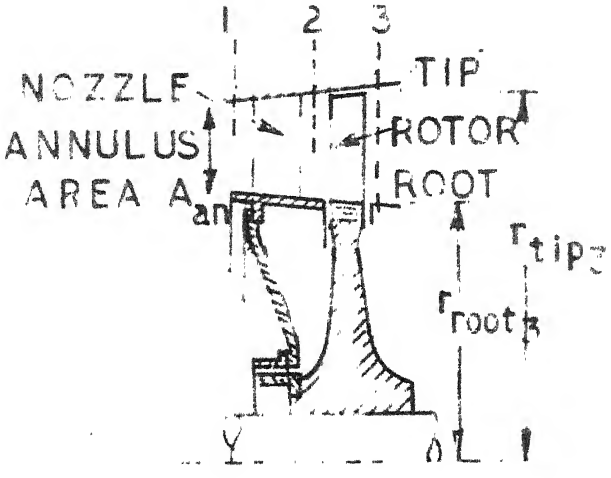

(a) TURBINE STAGE.

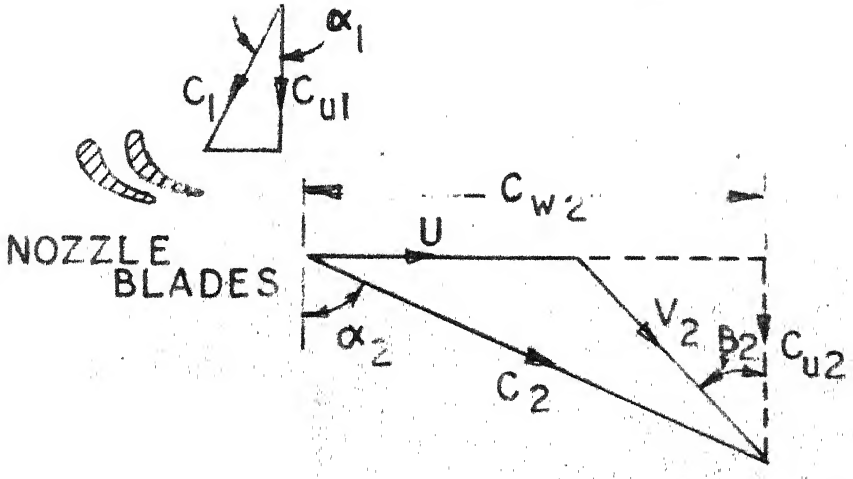

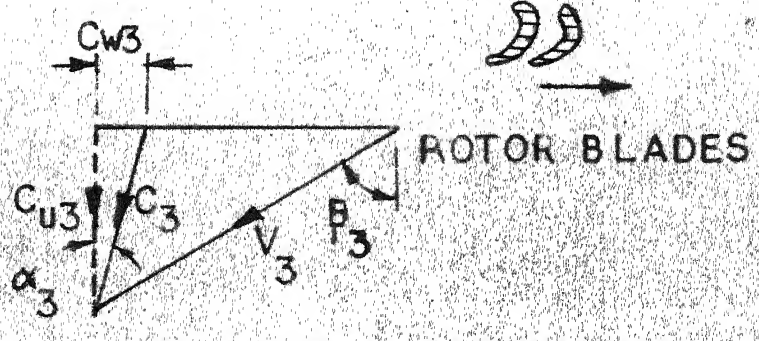

(b) VELOCITY TRIANGLE

FIG. 3-1 AXIAL FLOW TURBINE STAGE

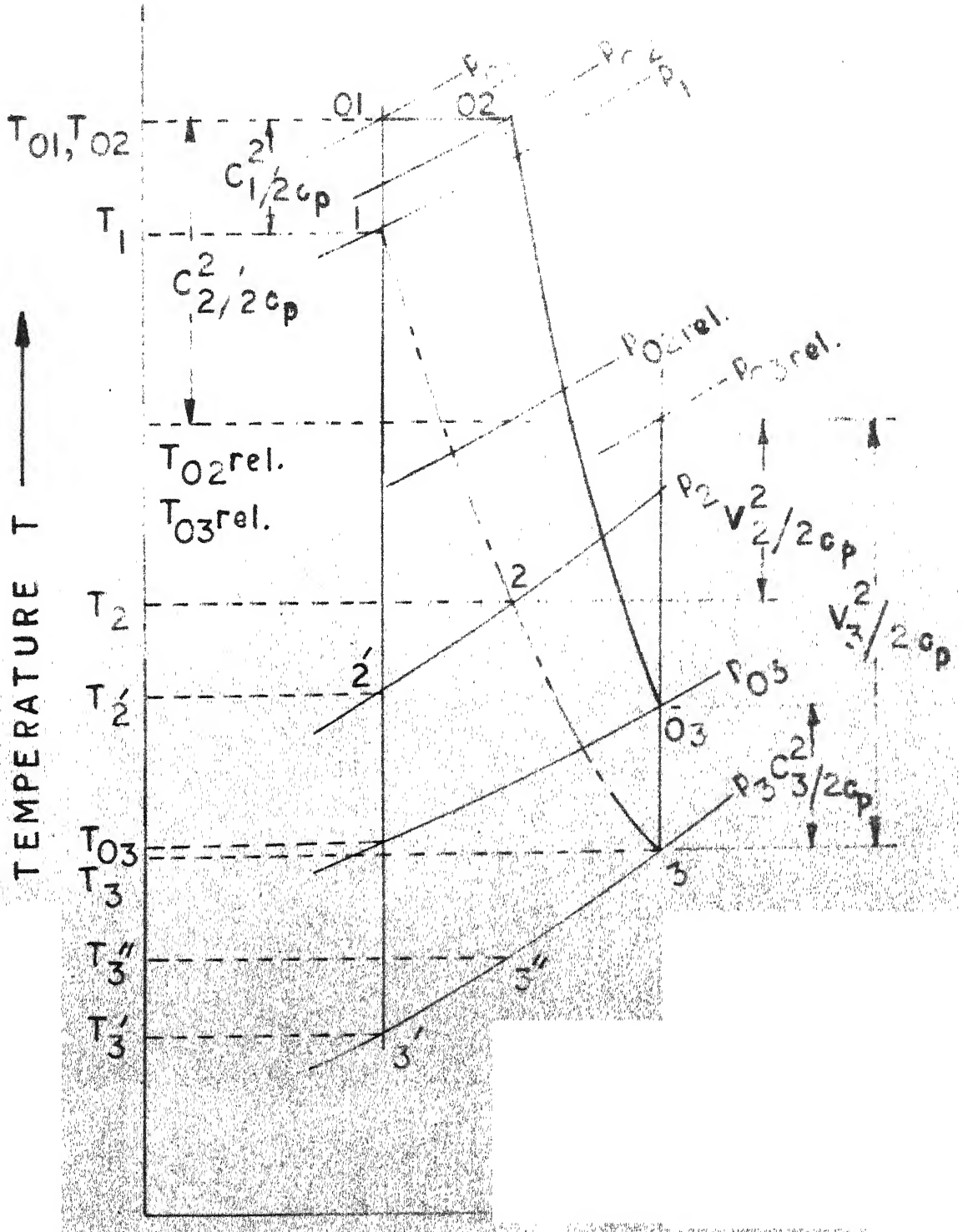

FIG. 3·2 TEMPERATURE–ENTROPY DIAGRAM FOR A REACTION STAGE.

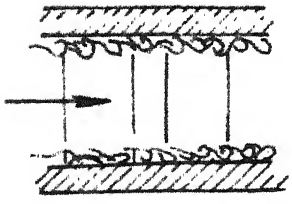

(a) ANNULU DRAG

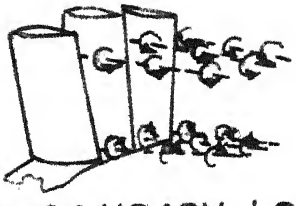

(b) SECONDARY LOSSES.

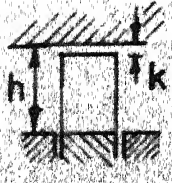

(c) RADIAL TIP CLEARANCE.

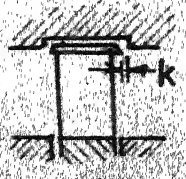

(d) SHROUDED BLADE WITH SIDE CLEARANCE.

FIG. 3.3 LOSSES AND CLEARANCES.

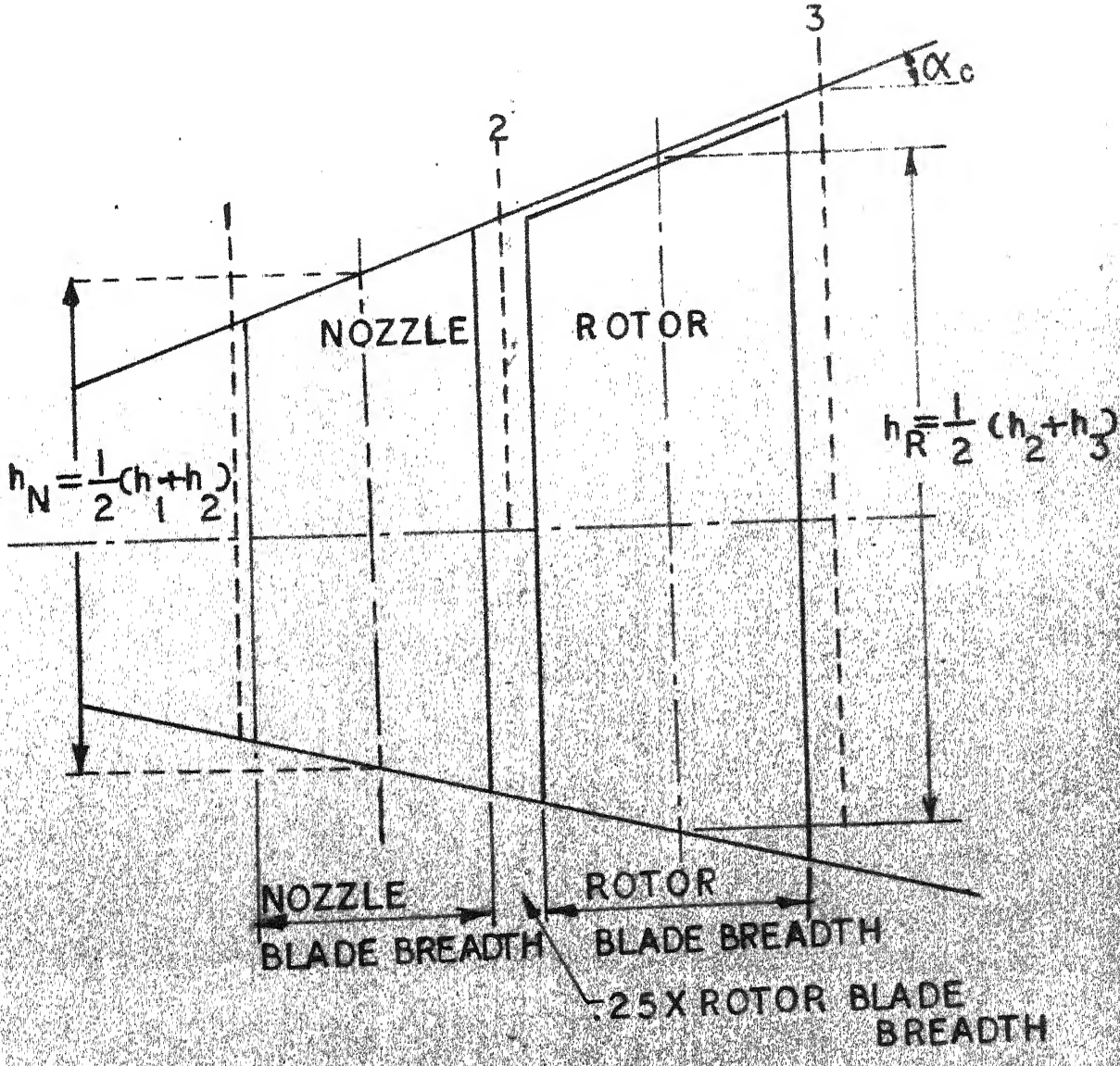

FIG. 3.4 FLARED TURBINE ANNULUS.

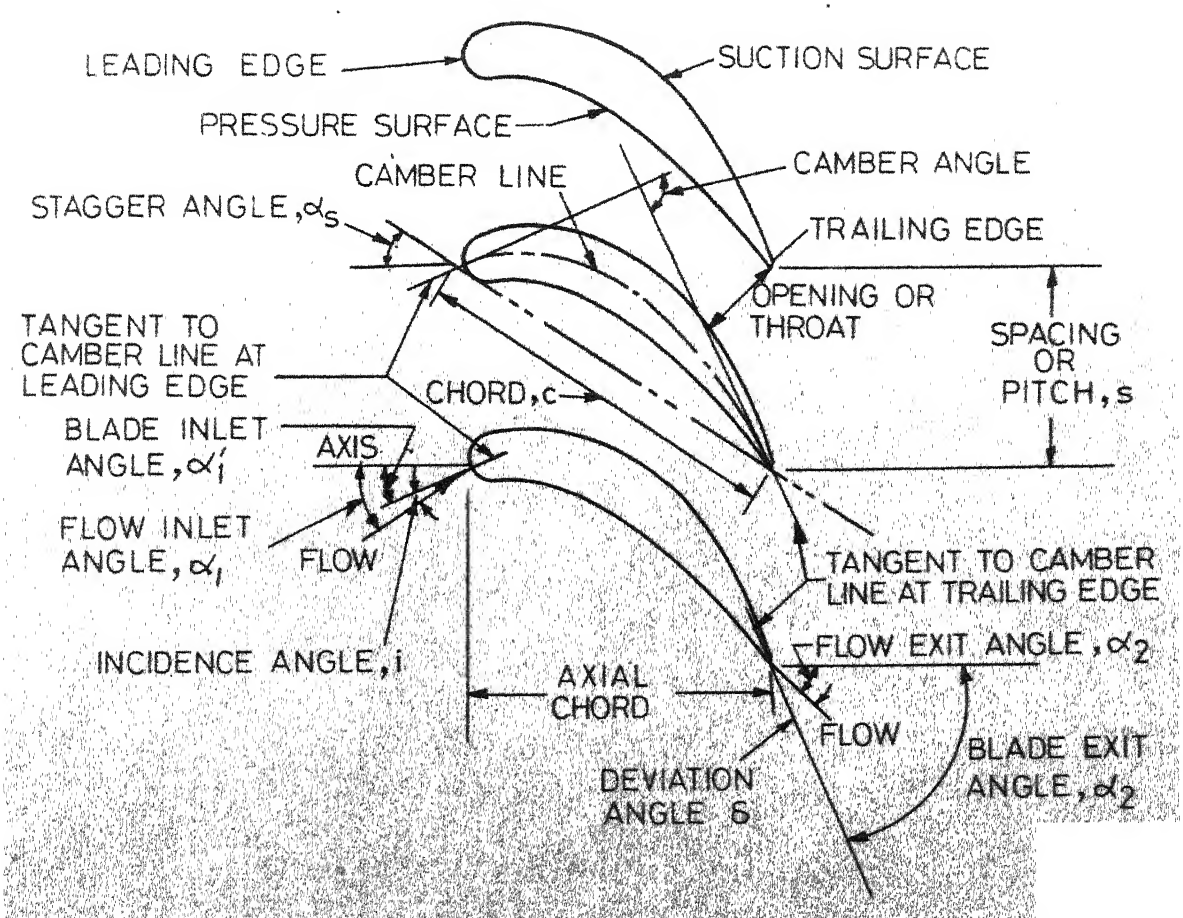

FIG. 3.5 CASCADE GEOMETRY AND TERMINOLOGY

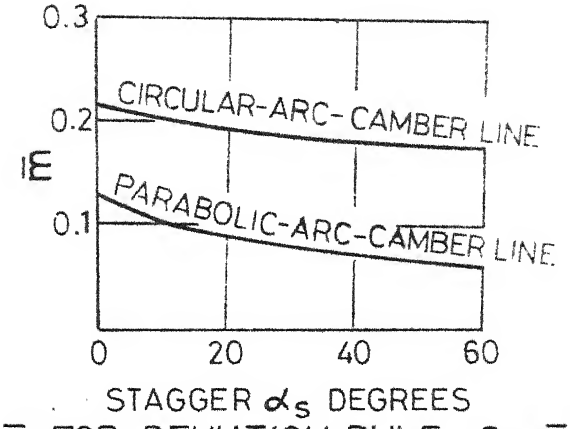

(a) CONSTANT $\bar{m}$ FOR DEVIATION RULE $\delta = \bar{m}\theta\sqrt{s/c}$

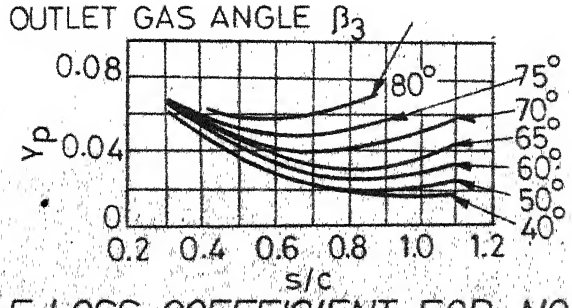

(b) PROFILE LOSS COEFFICIENT FOR NOZZLE BLADES
$\beta_2 = 0$ ($t/c = 0.2$)

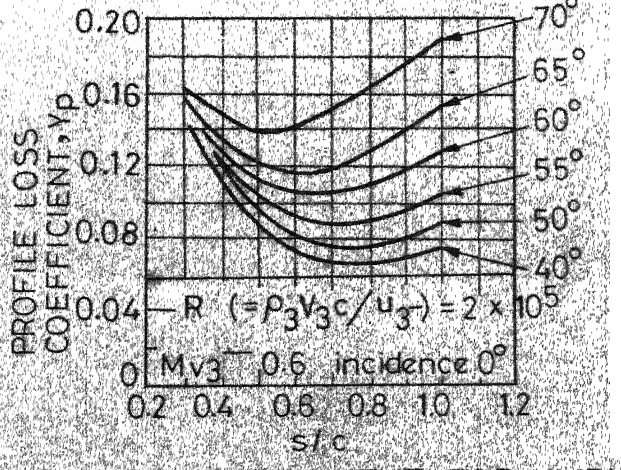

(c) PROFILE LOSS COEFFICIENT FOR IMPULSE BLADES
$\beta_2 = \beta_3$ ($t/c = 0.20$)

FIG. 3.6 CONSTANT $\bar{m}$ AND PROFILE LOSS COEFFICIENT

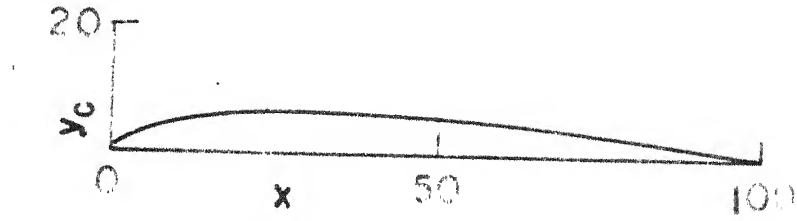

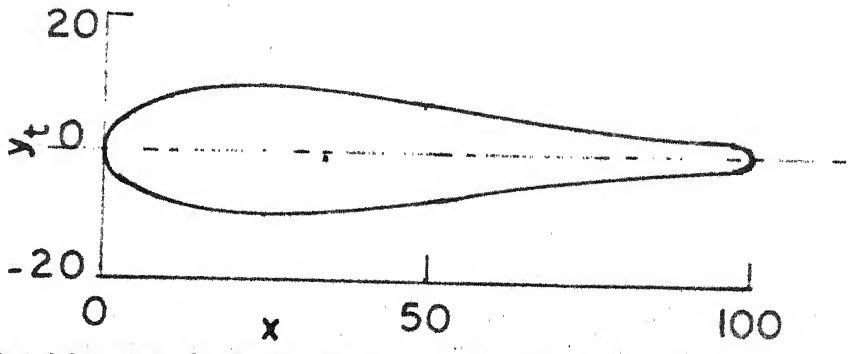

(a) CAMBER LINE AND PROFILE SHAPE FOR REACTION BLADING.

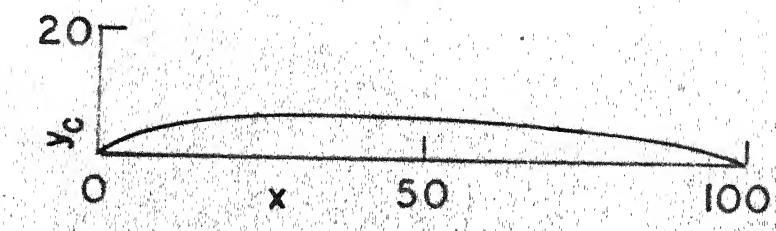

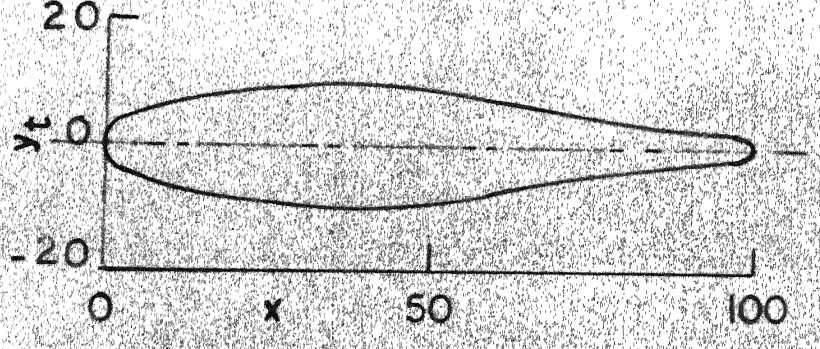

(b) CAMBER LINE AND PROFILE SHAPE FOR IMPULSE BLADING.

FIG.3·7 CAMBER LINE AND PROFILE SHAPES.

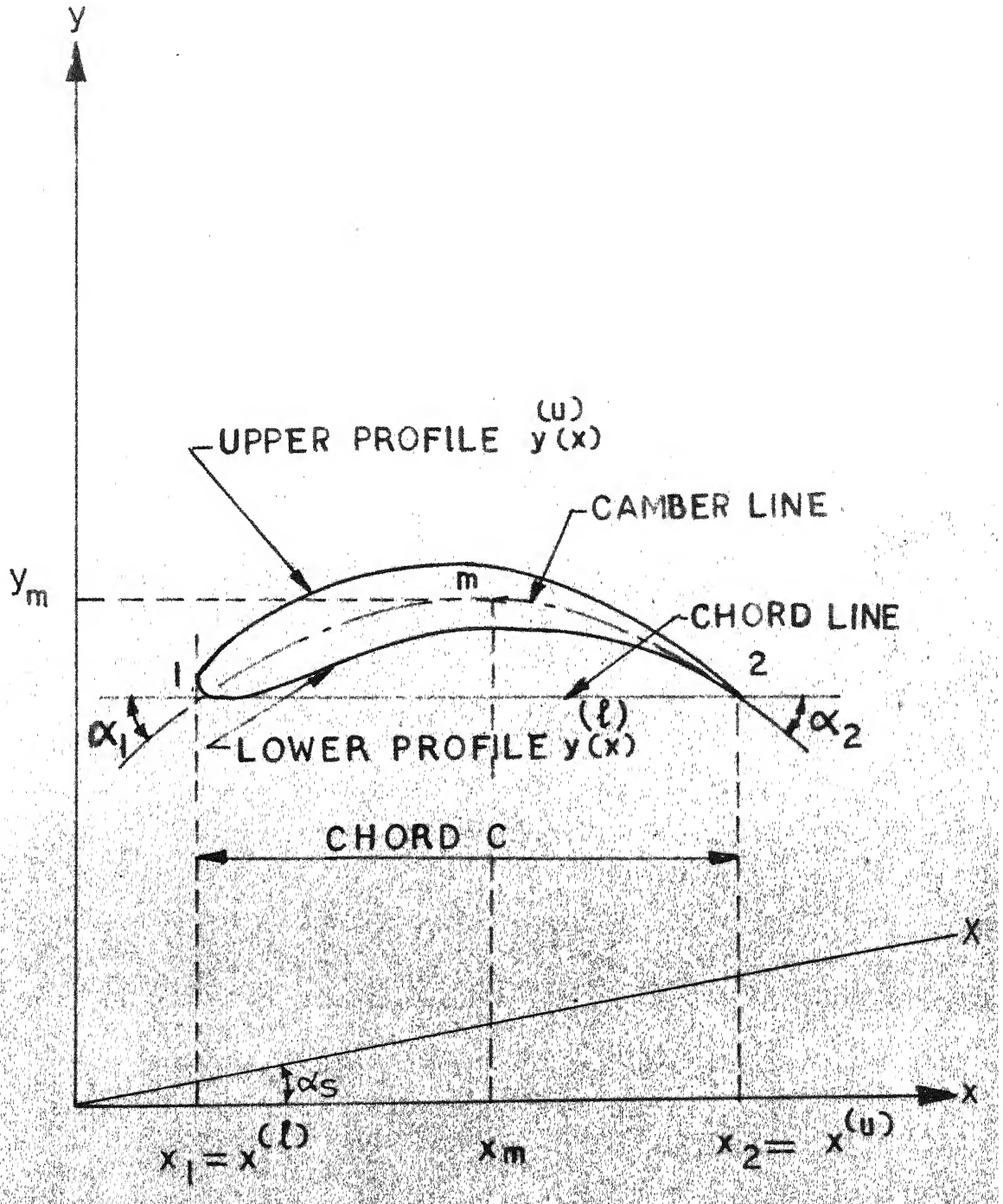

FIG. 3.8 CAMBER LINE AND PROFILE SHAPE OF BLADE SECTION.

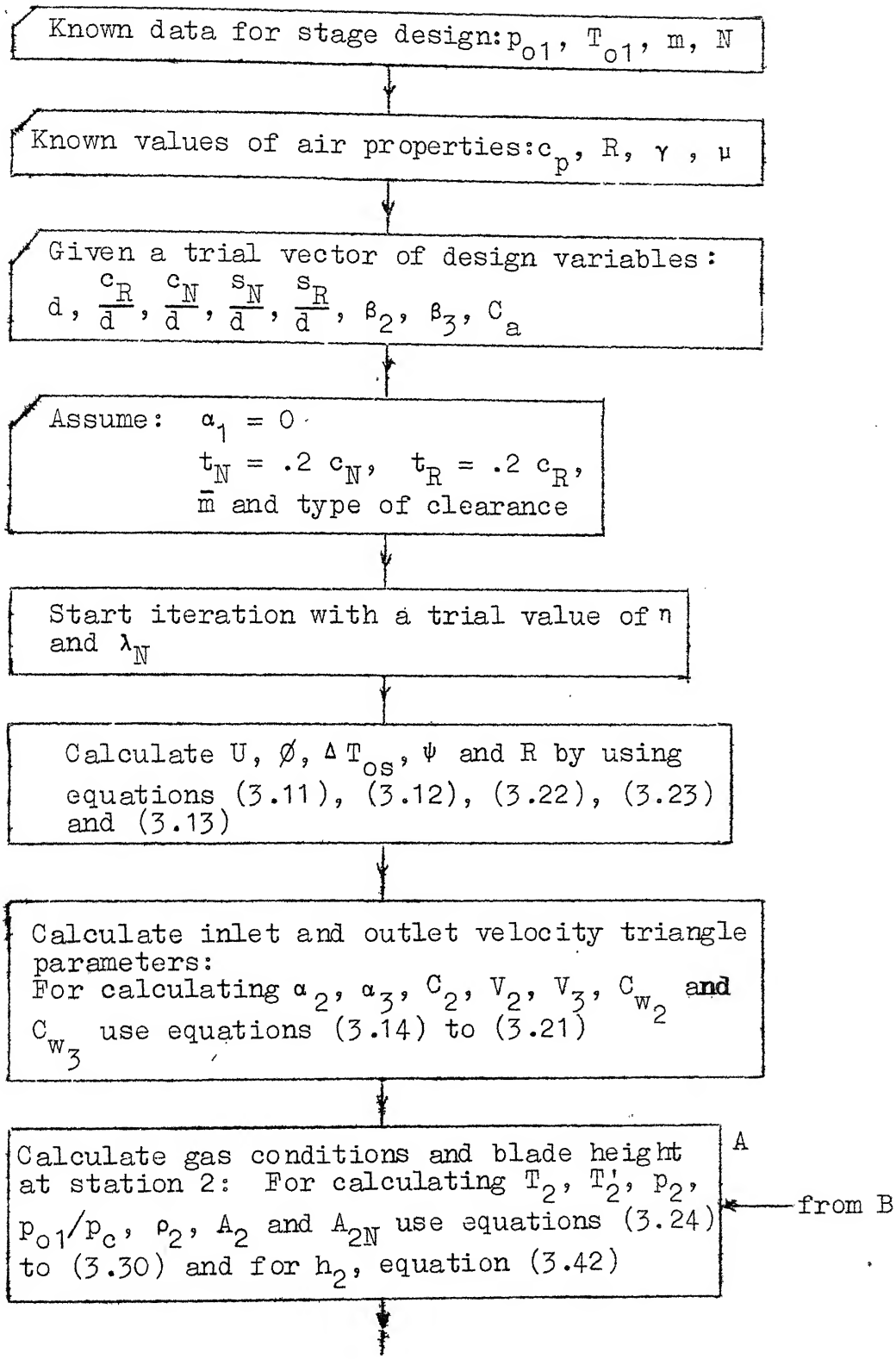
Known data for stage design: p_{o1}, T_{o1}, m, N
Known values of air properties: c_p, R, γ, μ
Given a trial vector of design variables: d, $\frac{c_R}{d}$, $\frac{c_N}{d}$, $\frac{s_N}{d}$, $\frac{s_R}{d}$, β_2, β_3, C_a
Assume: $\alpha_1 = 0$
$t_N = .2\ c_N$, $t_R = .2\ c_R$,
$\bar{m}$ and type of clearance
Start iteration with a trial value of η and λ_N
Calculate U, ϕ, ΔT_{os}, ψ and R by using equations (3.11), (3.12), (3.22), (3.23) and (3.13)
Calculate inlet and outlet velocity triangle parameters:
For calculating α_2, α_3, C_2, V_2, V_3, C_{w_2} and C_{w_3} use equations (3.14) to (3.21)
Calculate gas conditions and blade height at station 2: For calculating T_2, T_2', p_2, p_{o1}/p_c, ρ_2, A_2 and A_{2N} use equations (3.24) to (3.30) and for h_2, equation (3.42)
A
from B

Continued...

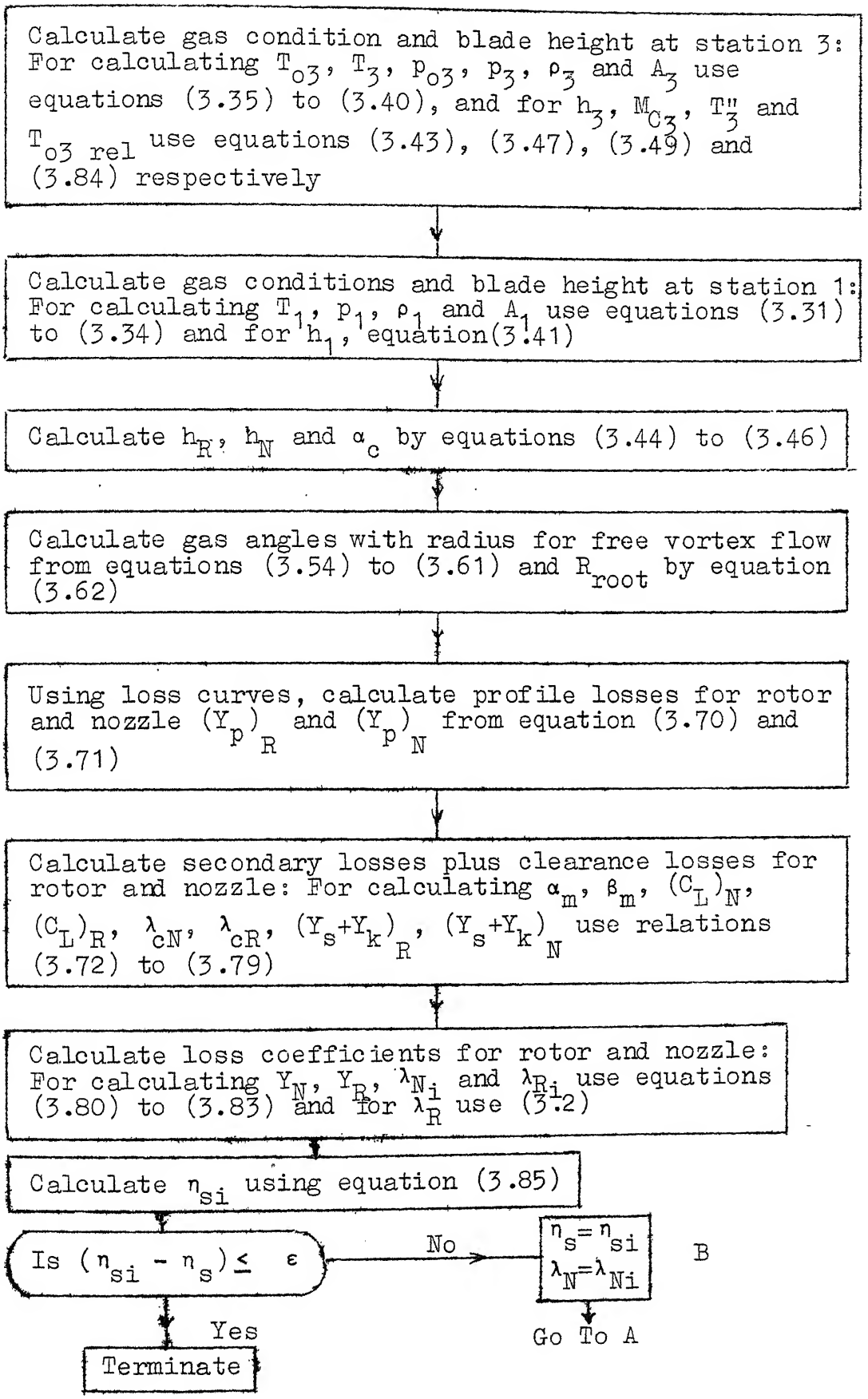

Figure 3.9. Flow Chart for Calculation of Efficiency

CHAPTER 4

FINITE ELEMENT VIBRATION ANALYSIS OF ROTATING TIMOSHENKO BEAMS

In finite element method, the domain of the continuum is discretized into a number of disjointed subdomains called elements defined by a set of points which are called nodes. The elements may not be connected at the nodes, but also along the interelement boundaries. Then the unknown field variables are approximated by a set of assumed functions, which are expressed in terms of the field variables at the nodes by suitable interpolation formulas. The characteristics of the continuum are predicted from the characteristics of the elements.

The need for finite element method arose from the fact that (1) exact solutions for complex differential equations encountered in continuum approach have not been possible except for very few idealized cases and (2) with the advent of digital computers the approximate methods of solution like Ritz method, Galerkin technique and finite difference method, have come into vogue. Most well studied mathematically, among the approximate methods is the finite difference method which is mathematical discretization of differential equations. However, the method suffers from the inherent drawback that it cannot handle complicated boundary conditions, irregular change in geometry and material properties. Amongst the approximate techniques, the finite element method can be considered as one of the most

powerful and versatile physical discretization scheme presently available for the numerical solution of complex continuum problems using digital computers. Nonlinearity, orthotropy, considerations of cutouts, irregular boundaries and complicated boundary conditions can all be incorporated in the analysis without much difficulty.

In this chapter a new finite element is developed to find the natural frequencies and mode shapes of beams in bending-bending mode of vibration by taking into account taper, pre-twist and rotation simultaneously. The coupling that exists between the flexural and torsional vibration is not considered. The taper and the angle of twist are assumed to vary linearly along the length of the beam. The element stiffness and mass matrices are derived and the effects of offset, rotation, pre-twist, depth and breadth taper ratios and rotary inertia and shear deformation on the natural frequencies are studied. Various special cases of beam vibration are obtained from the general equations derived.

4.1 Displacement Model

Figure 4.1(a) shows a doubly tapered, twisted beam element of length l with the nodes as 1 and 2. The breadth, depth and the twist of the element are assumed to be linearly varying along its length. The breadth and depth at the two nodal points are shown as b_1, t_1 and b_2, t_2 respectively. The

pretwist at the two nodes is denoted by θ_1 and θ_2. Figure 4.1(b) shows the nodal degrees of freedom of the element where bending deflection, bending slope, shear deflection and shear slope in the two planes are taken as the nodal degrees of freedom. Figure 4.1(c) shows the angle of twist θ at any section z. The beam is assumed to rotate about the x-x axis at a speed of Ω radians per second.

The total deflections of the element in the y and x directions at a distance z from node 1, namely, w(z) and v(z) are taken as

$$\begin{aligned} w(z) &= w_b(z) + w_s(z) \\ v(z) &= v_b(z) + v_s(z) \end{aligned} \tag{4.1}$$

where $w_b(z)$ and $v_b(z)$ are the deflections due to bending in the yz and xz planes, respectively, and $w_s(z)$ and $v_s(z)$ are the deflections due to shear in the corresponding planes.

The displacement models for $w_b(z)$, $w_s(z)$, $v_b(z)$ and $v_s(z)$ are assumed to be polynomials of third degree. They are similar in nature except for the nodal constants. These expressions are given by:

$$w_b(z) = \frac{u_1}{l^3}(2z^3 - 3lz^2 + l^3) + \frac{u_2}{l^3}(3lz^2 - 2z^3)$$

$$- \frac{u_3}{l^2}(z^3 - 2lz^2 + l^2z) - \frac{u_4}{l^2}(z^3 - lz^2)$$

$$w_s(z) = \frac{u_5}{l^3}(2z^3 - 3lz^2 - l^3) + \frac{u_6}{l^3}(3lz^2 - 2z^3)$$

$$- \frac{u_7}{l^2}(z^3 - 2lz^2 + l^2z) - \frac{u_8}{l^2}(z^3 - lz^2)$$

$$v_b(z) = \frac{u_9}{l^3}(2z^3 - 3lz^2 - l^3) + \frac{u_{10}}{l^3}(3lz^2 - 2z^3)$$

$$- \frac{u_{11}}{l^2}(z^3 - 2lz^2 + l^2z) - \frac{u_{12}}{l^2}(z^3 - lz^2) \qquad (4.2)$$

$$v_s(z) = \frac{u_{13}}{l^3}(2z^3 - 3lz^2 - l^3) + \frac{u_{14}}{l^3}(3lz^2 - 2z^3)$$

$$- \frac{u_{15}}{l^2}(z^3 - 2lz^2 + l^2z) - \frac{u_{16}}{l^2}(z^3 - lz^2)$$

where u_1, u_2, u_3 and u_4 represent the bending degrees of freedom and u_5, u_6, u_7 and u_8 are the shear degrees of freedom in yz plane, u_9, u_{10}, u_{11} and u_{12} represent the bending degrees of freedom and u_{13}, u_{14}, u_{15} and u_{16} the shear degrees of freedom in xz plane.

4.2 Element Stiffness Matrix

The total strain energy $\bar{U}$ of a beam of length l, due to bending and shear deformation including rotary inertia and rotation effects is given by:

$$\bar{U} = \int_0^l \left[\left\{ \frac{EI_{xx}}{2} \left(\frac{\partial^2 w_s}{\partial z^2}\right)^2 + EI_{xy} \frac{\partial^2 w_b}{\partial z^2} \cdot \frac{\partial^2 v_b}{\partial z^2} + EI_{yy} \left(\frac{\partial^2 v_b}{\partial z^2}\right)^2 \right\} \right.$$

$$+ \frac{\mu A_G}{2} \left(\frac{\partial w_s}{\partial z}\right)^2 + \left(\frac{\partial v_s}{\partial z}\right)^2 \}] \, dz + \frac{1}{2} \int_o^l P(z) \left(\frac{\partial w_b}{\partial z} + \frac{\partial w_s}{\partial z}\right)^2 dz$$

$$+ \frac{1}{2} \int_o^l P(z) \left(\frac{\partial v_b}{\partial z} + \frac{\partial v_s}{\partial z}\right)^2 dz - \int_o^l p_w(z) \, (w_b + w_s) \, dz$$

$$- \int_o^l p_v(z) \, (v_b + v_s) \, dz \qquad (4.3)$$

where E = Young's modulus, I_{xx} = moment of inertia about xx axis, I_{yy} = moment of inertia about yy axis, I_{xy} = moment of inertia about xy axis, μ = shear coefficient, G = shear modulus and

$$P(z) = \int_{R+z_e+z}^{L+e} m \, \Omega^2 \, \xi \, d\xi \approx \frac{\rho_m A \, \Omega^2}{2} [(L + e)^2 - (R + z_e + z)^2] \qquad (4.4)$$

where the mass per unit length (m) is assumed to be a constant for simplicity.

$$p_w(z) = \rho_m A \, \Omega^2 \, (w_b + w_s) \qquad (4.5)$$

$$p_v(z) = \rho_m A \, \Omega^2 \, (v_b + v_s) \qquad (4.6)$$

where e is the offset ρ_m is the mass density and z_e is the distance of the first node of the element from the root of the beam as shown in Figure 4.1(d).

As the cross section of the element changes with z and as the element is twisted, the cross sectional area A, and the moments of inertia I_{xx}, I_{yy} and I_{xy} will be functions of z:

$$A(z) = b(z)\,t(z) = \{b_1 + (b_2 - b_1)\frac{z}{l}\}\{t_1 + (t_2 - t_1)\frac{z}{l}\}$$

$$= \frac{1}{l^2}(c_1 z^2 + c_2 l z + c_3 l^2) \qquad (4.7)$$

where

$$\left.\begin{aligned} c_1 &= (b_2 - b_1)(t_2 - t_1) \\ c_2 &= b_1(t_2 - t_1) + t_1(b_2 - b_1) \\ c_3 &= b_1 t_1 \end{aligned}\right\}, \qquad (4.8)$$

$$\left.\begin{aligned} I_{xx}(z) &= I_{x'x'}\cos^2\theta + I_{y'y'}\sin^2\theta \\ I_{yy}(z) &= I_{y'y'}\cos^2\theta + I_{x'x'}\sin^2\theta \\ I_{xy}(z) &= (I_{x'x'} - I_{y'y'})\frac{\sin 2\theta}{2} \end{aligned}\right\} \qquad (4.9)$$

where x'x' and y'y' are the axes inclined at an angle θ, the angle of twist, at any point in the element, to the original axes xx and yy as shown in Figure 4.1(c). The value of $I_{x'y'} = 0$ and the values of $I_{x'x'}$ and $I_{y'y'}$ can be computed as:

$$I_{x'x'}(z) = \frac{b(z)\,t^3(z)}{12} = \frac{1}{12l^4}\{a_1 z^4 + a_2 l z^3 + a_3 l^2 z^2 + a_4 l^3 z + a_5 l^4\} \qquad (4.10)$$

where

$$a_1 = (b_2 - b_1)(t_2 - t_1)^3$$

$$a_2 = b_1(t_2 - t_1)^3 + 3(b_2 - b_1)(t_2 - t_1)^2 t_1$$

$$a_3 = 3\ b_1 t_1 (t_2 - t_1)^2 + (b_2 - b_1)(t_2 - t_1)t_1^2$$

$$a_4 = 3b_1 t_1^2 (t_2 - t_1) + (b_2 - b_1)t_1^3$$

$$a_5 = b_1 t_1^3 \qquad (4.11)$$

$$I_{y'y'}(z) = \frac{t(z).b^3(z)}{12} = \frac{1}{12l^4}\{d_1 z^4 + d_2 l z^3 + d_3 l^2 z^2 + d_4 l^3 z + d_5 l^4\} \qquad (4.12)$$

where

$$d_1 = (t_2 - t_1)(b_2 - b_1)^3$$

$$d_2 = t_1 (b_2 - b_1)^3 + 3(t_2 - t_1)(b_2 - b_1)^2 b_1$$

$$d_3 = 3\{t_1 b_1 (b_2 - b_1)^2 + (t_2 - t_1)(b_2 - b_1)b_1^2\} \qquad (4.13)$$

$$d_4 = 3t_1 b_1^2 (b_2 - b_1) + (t_2 - t_1)b_1^3$$

$$d_5 = t_1 b_1^3$$

By substituting the expressions of w_b, w_s, v_b, v_s, A, I_{xx}, I_{xy} and I_{yy} from equations (4.2), (4.7) and (4.9) in equation (4.3), the strain energy U can be expressed as:

$$\bar{U} = \frac{1}{2}\ \vec{u}^{\,T}[K]\ \vec{u} \qquad (4.14)$$

where $\vec{u}$ is the vector of nodal displacements $u_1, u_2, \ldots, u_{16}$, and $[K]$ is the elemental stiffness matrix of order 16.

Denoting the integrals

$$\int_0^1 EI_{xx}\left(\frac{\partial^2 w_b}{\partial z^2}\right)^2 dz = [u_1\ u_2\ u_3\ u_4]^T [AK][u_1\ u_2\ u_3\ u_4], \quad (4.15)$$

$$\int_0^1 EI_{yy}\left(\frac{\partial^2 v_b}{\partial z^2}\right)^2 dz = [u_9\ u_{10}\ u_{11}\ u_{12}]^T [BK][u_9\ u_{10}\ u_{11}\ u_{12}], \quad (4.16)$$

$$\int_0^1 \mu AG\left(\frac{\partial w_s}{\partial z}\right)^2 dz = [u_5\ u_6\ u_7\ u_8]^T [CK][u_5\ u_6\ u_7\ u_8], \quad (4.17)$$

$$\int_0^1 EI_{xy}\left(\frac{\partial^2 w_b}{\partial z^2}\right)^2 \left(\frac{\partial^2 v_b}{\partial z^2}\right) dz = [u_1\ u_2\ u_3\ u_4]^T [DK][u_9\ u_{10}\ u_{11}\ u_{12}] \quad (4.18)$$

$$\int_0^1 P(z)\left(\frac{\partial w_b}{\partial z}\right)^2 dz = [u_1\ u_2\ u_3\ u_4]^T [EK][u_1\ u_2\ u_3\ u_4] \quad (4.19)$$

and

$$\int_0^1 2\rho_m A\,\Omega^2 (w_b^2) dz = [u_1\ u_2\ u_3\ u_4]^T [FK][u_1\ u_2\ u_3\ u_4] \quad (4.20)$$

The element stiffness matrix can be expressed as

$$[K] = \begin{bmatrix} [AK]+[EK]-[FK] & [EK]-[FK] & [DK] & [0] \\ [EK]-[FK] & [CK]+[EK]-[FK] & [0] & [0] \\ [DK] & [0] & [BK]+[EK]-[FK] & [EK]-[FK] \\ [0] & [0] & [EK]-[FK] & [CK]+[EK]-[FK] \end{bmatrix} \quad (4.21)$$

where [AK], [BK], [CK], [DK], [EK] and [FK] are symmetric matrices of order 4 and their elements are formulated in Appendix C. [0] is a null matrix of order 4.

4.3 Element Mass Matrix

The kinetic energy of the element $\bar{T}$ including the effects of shear deformation and rotary inertia is given by

$$\bar{T} = \int_0^l \frac{\rho_m}{2} \left[A\left(\frac{\partial w_b}{\partial \bar{t}} + \frac{\partial w_s}{\partial \bar{t}}\right)^2 + A\left(\frac{\partial v_b}{\partial \bar{t}} + \frac{\partial v_s}{\partial \bar{t}}\right)^2 + I_{yy}\left(\frac{\partial^2 v_b}{\partial z\, \partial \bar{t}}\right) \right.$$

$$\left. + 2I_{xy}\left(\frac{\partial^2 w_b}{\partial z\, \partial \bar{t}}\right)\left(\frac{\partial^2 v_b}{\partial z\, \partial \bar{t}}\right) + I_{xx}\left(\frac{\partial^2 w_b}{\partial z\, \partial \bar{t}}\right)^2 \right] dz \qquad (4.22)$$

By defining

$$\int_0^l \rho_m A \left(\frac{\partial w_b}{\partial \bar{t}}\right)^2 dz = [\dot{u}_1\ \dot{u}_2\ \dot{u}_3\ \dot{u}_4]^T [AM][\dot{u}_1\ \dot{u}_2\ \dot{u}_3\ \dot{u}_4], \qquad (4.23)$$

$$\int_0^l \rho_m I_{xx}\left(\frac{\partial^2 w_b}{\partial z\, \partial \bar{t}}\right)^2 dz = [\dot{u}_1\ \dot{u}_2\ \dot{u}_3\ \dot{u}_4]^T [BM][\dot{u}_1\ \dot{u}_2\ \dot{u}_3\ \dot{u}_4], \qquad (4.24)$$

$$\int_0^l \rho_m I_{yy}\left(\frac{\partial^2 v_b}{\partial z\, \partial \bar{t}}\right)^2 dz = [\dot{u}_9\ \dot{u}_{10}\ \dot{u}_{11}\ \dot{u}_{12}]^T [CM][\dot{u}_9\ \dot{u}_{10}\ \dot{u}_{11}\ \dot{u}_{12}] \qquad (4.25)$$

and

$$\int_0^l \rho_m I_{xy}\left(\frac{\partial^2 w_b}{\partial z\, \partial \bar{t}}\right)\left(\frac{\partial^2 v_b}{\partial z\, \partial \bar{t}}\right) = [\dot{u}_1\ \dot{u}_2\ \dot{u}_3\ \dot{u}_4]^T [DM][\dot{u}_9\ \dot{u}_{10}\ \dot{u}_{11}\ \dot{u}_{12}] \qquad (4.26)$$

where $\dot{u}_i$ denotes the time derivative of the nodal displacement u_i, $i = 1, 2, \ldots, 16$, the kinetic energy of the element can be expressed as

$$\bar{T} = \frac{1}{2} \dot{\vec{u}}^T [M] \dot{\vec{u}} \tag{4.27}$$

where M is the mass matrix given by

$$[K]_{16 \times 16} = \begin{bmatrix} [AM]+[BM] & [AM] & [DM] & [0] \\ [AM] & [AM] & [AM] & [0] \\ [DM] & [AM] & [AM]+[CM] & [AM] \\ [0] & [0] & [AM] & [AM] \end{bmatrix} \tag{4.28}$$

and [AM], [BM], [CM] and [DM] are symmetric matrices of order 4 whose elements are defined in Appendix C.

Boundary Conditions:

The following boundary conditions are to be applied depending on the type of end conditions:

Free end : $\frac{\partial w_s}{\partial z} = 0$ and $\frac{\partial v_s}{\partial z} = 0$ (4.29)

Clamped end: $w_s = 0$, $w_b = 0$, $v_s = 0$, $v_b = 0$, $\frac{\partial w_b}{\partial z} = 0$

and $\frac{\partial v_b}{\partial z} = 0$ (4.30)

Hinged end: $w_s = 0$, $w_b = 0$, $v_s = 0$ and $v_b = 0$ (4.31)

4.4 Special Cases

The various special cases of the beam vibration problem can be solved by applying one or more of the following four conditions:

(a) For non-rotating beams:

$$\Omega = 0 \quad \text{which results in} \quad [EK] = [FK] = [0] \tag{4.32}$$

(b) For uniform beams:

By setting $b_2 = b_1$ and $t_2 = t_1$, one obtains

$$\begin{aligned} c_1 &= c_2 = 0 \quad \text{and} \quad c_3 = b_1 t_1 \\ a_1 &= a_2 = a_3 = a_4 = 0 \quad \text{and} \quad a_5 = b_1 t_1^3 \\ d_1 &= d_2 = d_3 = d_4 = 0 \quad \text{and} \quad d_5 = t_1 b_1^3 \end{aligned} \tag{4.33}$$

(c) For neglecting the effect of shear deformation:

$w_s = v_s = 0$ so that equations (1) and (2) become

$$w(z) = w_b(z) \quad \text{and} \quad v_z = v_b(z) \tag{4.34}$$

Due to this, the order of [K] and [M] matrices reduces from 16 to 8.

(d) For beams without pre-twist:

In this case there will be no coupling between the moment of inertia terms and one obtains:

$$\begin{aligned} I_{xx} &= I_{x'x'} \\ I_{yy} &= I_{y'y'} \\ I_{xy} &= 0 \end{aligned} \tag{4.35}$$

For vibration in yz plane, $v_b = v_z = 0$

For vibration in xz plane, $w_b = w_s = 0$

Few of the special cases of practical interest are discussed below.

4.4.1 Classical Tapered, Twisted and Rotating Beam

This case is obtained by neglecting shear deformation in the general case. When the conditions of equation (4.34) are applied, the [K] and [M] matrices reduce to:

$$[K] = \begin{bmatrix} [AK] + [EK] - [FK][DK] & \\ [DK] & [BK] + [EK] - [FK] \end{bmatrix} \quad (4.36)$$

and

$$[M] = \begin{bmatrix} [AM] + [BM] & [DM] \\ [DM] & [AM] + [CM] \end{bmatrix} \quad (4.37)$$

4.4.2 Non-rotating, Tapered and Twisted Beam with Shear Deformation and Rotary Inertia

This case can be obtained by applying the condition of equation (4.32) to the most general case. Here the mass matrix [M] remains same as one given in equation (4.28) while the stiffness matrix [K] reduces to the following

$$[K] = \begin{bmatrix} [AK] & [0] & [DK] & [0] \\ [0] & [CK] & [0] & [0] \\ [DK] & [0] & [BK] & [0] \\ [0] & [0] & [0] & [CK] \end{bmatrix} \quad (4.38)$$

4.4.3 Classical Tapered and Twisted Non-rotating Beam

By applying the non-rotating condition of equation (4.32) along with equation (4.34), the stiffness and mass matrices reduce to order 8 and are given by

$$[K] = \begin{bmatrix} [AK] & [DK] \\ [DK] & [BK] \end{bmatrix} \tag{4.39}$$

and

$$[M] = \begin{bmatrix} [AM] + [BM] & [DM] \\ [DM] & [AM] + [CM] \end{bmatrix} \tag{4.40}$$

4.4.4 Non-rotating, Untwisted and Tapered Beam with Shear Deformation and Rotary Inertia

In this case the non-rotating condition of equation (4.32), the uniform beam condition of equation (4.33) and the no-twist condition of equation (4.35) are applied simultaneously. The beam may vibrate either in yz plane or in xz plane.

In the special case of a non-rotating, untwisted beam vibrating in the yz plane the element stiffness and mass matrices will be of order 8 and can be expressed as follows:

$$[K] = \begin{bmatrix} [A] & [0] \\ [0] & [B] \end{bmatrix} \tag{4.41}$$

and

$$[M] = \begin{bmatrix} [C] + [D] & [C] \\ [C] & [C] \end{bmatrix} \tag{4.42}$$

where [A], [B], [C] and [D] are symmetric matrices of order 4 whose elements are given in Appendix D.

4.4.5 Classical Non-rotating, Untwisted and Tapered Beam

If shear deformation is neglected from the case discussed in section 4.4.4, the following simplified form of stiffness and mass matrices of classical, non-rotating, untwisted and tapered beam will be obtained:

$$[K] = [A] \tag{4.43}$$

$$[M] = [C] + [D] \tag{4.44}$$

where [A], [C] and [D] are symmetric matrices of order 4 whose elements are given in Appendix D.

4.4.6 Non-rotating, Untwisted and Uniform Beam with Shear Deformation and Rotary Inertia

If the conditions (a), (b) and (d) are applied one gets the following expressions for [K] and [M] for non-rotating uniform beams without pre-twist but with a consideration of rotary inertia and shear deformation effects (for vibrations in y-z plane):

$$K = \frac{EI_{xx}}{l^3}\begin{bmatrix} 12 & -12 & -6l & -6l & 0 & 0 & 0 & 0 \\ & 12 & 6l & 6l & 0 & 0 & 0 & 0 \\ & & 4l^2 & 2l^2 & 0 & 0 & 0 & 0 \\ & & & 4l^2 & 0 & 0 & 0 & 0 \\ & & & & 36J & -36J & -3lJ & -3lJ \\ & & & & & 36J & 3lJ & 3lJ \\ & & & & & & 4l^2J & -l^2J \\ & \text{Symmetric} & & & & & & 4l^2J \end{bmatrix} \qquad (4.45)$$

$$M = \frac{\rho_m Al}{420}\begin{bmatrix} 156+36\bar{P} & 54-36\bar{P} & 22l-3l\bar{P} & 13l-3l\bar{P} & 156 & 54 & 22l & 13l \\ & 156+36\bar{P} & -13l+3l\bar{P} & 22l+3l\bar{P} & 54 & 156 & -13l & 22l \\ & & 4l^2+4l^2\bar{P} & -3l^2-l^2\bar{P} & 22l & -13l & 4l^2 & -3l^2 \\ & & & 4l^2-4l^2\bar{P} & 13l & 22l & -3l^2 & 4l^2 \\ & & & & 156 & 54 & 22l & 13l \\ & & & & & 156 & -13l & 22l \\ & & & & & & 4l^2 & -3l^2 \\ & \text{Symmetric} & & & & & & 4l^2 \end{bmatrix} \qquad (4.46)$$

where $J = \dfrac{\mu G b_1 t_1 l^2}{30EI_{xx}}$,

and $\bar{P} = \dfrac{14I_{xx}}{b_1 t_1 l^2}$

4.4.7 Classical, Non-rotating, Untwisted and Uniform Beam

Equations (4.45) and (4.46) further reduce to the following well-known equations if the effects of shear deformation and rotary inertia are neglected.

$$[K] = \frac{EI_{xx}}{l^3}\begin{bmatrix} 12 & -12 & -6l & -6l \\ & 12 & 6l & 6l \\ & & 4l^2 & 2l^2 \\ \text{Symmetric} & & & 4l^2 \end{bmatrix} \tag{4.47}$$

$$[M] = \frac{\rho_m b_1 t_1}{420}\begin{bmatrix} 156 & 54 & -22l & 13l \\ & 156 & -13l & 22l \\ & & 4l^2 & -3l^2 \\ \text{Symmetric} & & & 4l^2 \end{bmatrix} \tag{4.48}$$

4.5 Numerical Results:

The element stiffness and mass matrices developed are used for the dynamic analysis of cantilever beams. By using the standard procedures of structural analysis, the eigen value problem can be stated as:

$$([\underset{\sim}{K}] - \omega^2 [\underset{\sim}{M}])\,\vec{\underset{\sim}{U}} = \vec{0} \tag{4.49}$$

where $[\underset{\sim}{K}]$ and $[\underset{\sim}{M}]$ denote the stiffness and mass matrices of the structure respectively, $\vec{\underset{\sim}{U}}$ indicates nodal displacement vector of the structure, and ω is the natural frequency of vibration.

4.5.1 Convergence Study

A study of the convergence properties of the element is made by taking special case of a uniform beam discussed by Thomas and Abbas[58]. The results are shown in Table 4.1 and

the convergence can be seen to be quite good. It can be observed that the eigen values converge to the exact values even with four elements. The convergence of the natural frequencies of a rotating pretwisted doubly tapered cantilever beam has also been studied by considering the effects of rotary inertia and shear deformation and the results are shown in Table 4.2. In this case also it is found that reasonably accurate results can be obtained even by using four finite elements.

4.5.2 Rotating Beam Results

The effects of shear deformation and depth taper ratio on the natural frequencies of a rotating twisted beam are shown in Figure 4.2 for a beam of length 0.254 m, offset zero, depth at root 0.00865 m, breadth at root 0.0173 m, twist 45°, rotation 100 r.p.m. and breadth taper ratio 3. The material properties of the beam are taken same as those given in Table 4.2. The effect of shear deformation is found to reduce the frequencies at higher modes while at lower nodes the results are nearly unaffected. There is an increase in the frequencies of vibration with an increase in the depth taper ratio in the first, second and fourth modes while a decrease has been observed in the case of third mode (vibration in a perpendicular plane). Figure 4.3 shows the variation of natural frequencies with breadth taper ratio. In this case the

data is same as in the case of Figure 4.2.

In Figures 4.4 and 4.5 the variation of frequency ratio with rotation and pre-twist is studied. It can be seen that frequency ratio changes slightly with the rotation but appreciably with the twist. At higher modes (in Figure 4.5) the effect of twist can be seen to be more pronounced. It is also observed that the frequency ratio increases with an increase in the twist in the case of first and third modes while it decreases with an increase of the twist in the case of second and fourth modes of vibration.

In Figure 4.6 the effect of offset is studied for a twisted blade having 60° twist with other data same as that of Figure 4.4. The frequency values are shown in Table 4.3. It is observed that an increase in offset changes the frequency ratio more at higher values of rotation. The frequency ratio has been found to increase with an increase in the offset.

4.5.3 Non-rotating and Twisted Beam Results

Figure 4.7 shows a comparison of the results given by the finite element method with those reported by Rosard for a uniform beam of 0.0254 m x 0.00635 m cross section and 0.2794 m length for 0° to 30° twist. It can be seen that results are quite comparable.

Figures 4.8 and 4.9 represent the frequency ratio of an uniform beam and a twisted beam for first four modes

when the angle of twist is varied from 0° to 90°. The length of the beam is taken as 0.254 m and the cross section as 0.076 x 0.038 times the length of beam. The results are shown for Timoshenko beams where shear deformation effects are considered and for beams where shear deformation effects are neglected. The frequency values are also shown in Tables 4.4 and 4.5. It can be seen that the shear deformation effect is comparatively more at higher modes of vibration and also frequency ratio changes at a higher rate with an increase in the twist angle at higher modes. The present results are found to agree well with those given by Mabie and Rogers[28] (Table 4.4).

Figures 4.10 and 4.11 give the variation of modal frequencies with breadth taper ratio for beams having 0°, 30°, 60° and 90° twist with constant depth taper ratio while Figures 4.12 and 4.13 show similar variations for beam with constant breadth taper ratio and varying depth taper ratios. The beam dimensions are same as used for Figures 4.8 and 4.9. Again the effects of breadth and depth tapers are seen to be pronounced at higher modes of vibration. Here also the effect of shear deformation is seen to reduce the modal frequencies at higher rate at higher modes of vibration in all the cases.

The effect of cross sectional dimensions for the same area of cross section on the natural frequencies is also studied and the results are shown in Table 4.6. The present results are found to agree well with those available in the literature.

4.5.4 Non-rotating and Untwisted Beam Results

Tables 4.7 and 4.8 show a comparison of the natural frequencies of a non-rotating untwisted tapered beam for various combinations of depth and breadth taper ratios. Six finite elements are used to model the beam. It is observed that for constant depth taper ratio the frequency ratio of all the four modes increases with breadth taper ratio while for constant breadth taper ratio the frequency ratio decreases for the first mode and increases for the second, third and fourth modes with an increase in the depth taper ratios. The shear deformation effects reduce the frequency of modal vibration. The present results can be seen to compare well with those reported by Mabie and Rogers.

4.6 Conclusion

The finite element procedure developed for the eigen value analysis of rotating, doubly tapered and twisted Timoshenko beams has been found to give reasonably accurate results even with four finite elements. The effects of breadth and depth taper ratios, twist angle, shear deformation, offset and rotation on the natural frequencies of vibration of cantilever beams are found. The element developed is expected to be useful for the dynamic analysis of blades of roto-dynamic machines.

TABLE 4.1

Natural Frequencies (Hz) of an Untwisted Uniform Beam

Number of elements	First mode	Second mode	Third mode	Fourth mode
1	849.3	5005.0	12278.4	23240.1
2	846.1	4012.2	9531.6	15877.0
3	845.9	3996.3	8895.3	14410.0
4	845.8	3991.8	8861.4	13909.6
5	845.8	3990.4	8846.6	13865.5
6	845.8	3989.8	8840.7	13843.1
7	845.8	3989.7	8838.1	13832.4
8	845.8	3989.5	8836.8	13827.1
Exact	845.8	3988.9	8834.2	13818.1

Data: Length of beam = .254 m, breadth = .0762 m, depth = .08 $\sqrt{12}$ x length of beam, E = 2.07 x 10^{11} N/m^2, G = 3/8 E, mass density = 800 kg/m^3, shear coefficient = 2/3.

TABLE 4.2

Convergence Study of Natural Frequencies (Hz) of a Tapered, Twisted and Rotating Beam

Number of elements	First mode	Second mode	Third mode	Fourth mode
1	304.30	1191.66	2327.07	4552.23
2	296.22	1161.70	1779.50	4106.83
3	295.03	1155.97	1746.55	3747.04
4	294.85	1154.94	1741.39	3697.05
5	294.78	1154.67	1739.99	3689.82
6	294.78	1154.58	1739.40	3683.98
7	294.78	1154.54	1739.25	3683.91
8	294.78	1154.50	1739.10	3683.85

Data: Length of beam = 0.1524 m, breadth at root = .0254 m, depth at root = .0046 m, depth taper ratio = 2.29, breadth taper ratio = 2.56, twist angle = 45°, shear coefficient = .833, $E = 2.07 \times 10^{11}$ N/m^2, $G = E/2.6$, offset = 0, mass density = 800 kg/m^3, rotational speed = 250 revolutions/second.

TABLE 4.3

Effect of Offset on Natural Frequencies (Hz) of a Rotating Twisted Beam

Mode shape	Twist	Offset = 0				Offset = 0.0254 m			
		RPS = 0	100	200	300	0	100	200	300
I	0°	286.4	271.9	222.6	91.0	286.4	276.7	244.8	177.5
	30°	299.5	285.3	237.5	119.7	299.5	289.8	258.3	193.5
	60°	323.2	309.7	264.8	164.3	323.2	313.8	283.5	223.4
	90°	347.1	334.3	292.4	203.9	347.1	338.1	309.2	253.6
II	0°	901.3	897.0	883.0	861.0	901.0	898.0	889.0	874.0
	30°	890.0	886.0	872.0	850.0	890.0	887.0	878.0	863.0
	60°	861.4	857.0	844.0	821.0	861.4	859.0	850.0	835.0
	90°	810.6	806.0	793.0	770.0	810.6	808.0	800.0	786.0
III	0°	1789.0	1802.0	1838.0	1898.0	1790.0	1806.0	1854.0	1931.0
	30°	2081.0	2092.0	2124.0	2176.0	2081.0	2096.0	2138.0	2206.0
	60°	2569.0	2578.0	2604.0	2647.0	2569.0	2581.0	2615.0	2672.0
	90°	2993.0	3000.0	3022.0	3059.0	2993.0	3002.0	3032.0	3080.0
IV	0°	5478.0	5482.0	5493.0	5512.0	5478.0	5483.0	5498.0	5523.0
	30°	5219.0	5224.0	5241.0	5267.0	5219.0	5226.0	5247.0	5282.0
	60°	4799.0	4805.0	4820.0	4846.0	4799.0	4806.0	4826.0	4860.0
	90°	4039.0	4045.0	4064.0	4094.0	4039.0	4047.0	4071.0	4111.0

Continued...

Table 4.3 (Continued)

Mode shape	Twist	Offset = 0.0508 m				Offset = 0.0762 m			
		RPS = 0	100	200	300	0	100	200	300
I	0°	286.4	281.4	265.2	233.9	286.4	286.0	284.0	279.0
	30°	299.5	294.0	277.5	246.0	299.5	298.6	295.5	289.1
	60°	323.2	317.8	300.9	269.8	323.2	321.8	317.4	309.3
	90°	347.1	341.8	325.2	295.1	347.1	345.5	340.4	331.4
II	0°	901.3.	900.0	895.0	887.0	901.0	901.0	901.0	900.0
	30°	890 0	889.0	884.0	877.0	890.0	890.0	890.0	890.0
	60°	861.4	860.0	856.0	850.0	861.0	862.0	863.0	864.0
	90°	810.6	810.0	807.0	801.4	810.6	811.0	813.0	817.0
III	0°	1789.0	1810.0	1869.0	1964.0	1789.0	1814.0	1884.0	1997.0
	30°	2081.0	2099.0	2152.0	2236.0	2081.0	2103.0	2165.0	2266.0
	60°	2569.0	2583.0	2627.0	2698.0	2569.0	2586.0	2638.0	2723.0
	90°	2993.0	3005.0	3042.0	3102.0	2993.0	3007.0	3052.0	3123.0
IV	0°	5478.0	5484.0	5503.0	5533.0	5478.0	5485.0	5507.0	5544.0
	30°	5219.0	5228.0	5254.0	5296.0	5219.0	5229.0	5260.0	5310.0
	60°	5799.0	4808.0	4833.0	4874.0	4799.0	4809.0	4839.0	4888.0
	90°	4039.0	4049.0	4078.0	4127.0	4039.0	4051.0	4086.0	4143.0

Data: Length of beam = 0.1524 m, breadth at root = .0254 m, depth at root = 0.00103 m, depth taper ratio = 1, breadth taper ratio = 1, shear coefficient = .833, $E = 2.07 \times 10^{11}$ N/m^2, $G = E/2.6$, mass density = 800 kg/m^3, Number of elements = 6.

TABLE 4.4

Effect of Depth and Breadth Taper Ratios on Natural Frequencies (Hz) of a Tapered Twisted Beam with Shear Deformation and Rotary Inertia Effects

Mode shape	Twist	$\alpha = 3$					$\beta = 3$				$\alpha = 1$
		$\beta = 1$	$\beta = 2$	$\beta = 3$	$\beta = 4$	$\beta = 5$	$\alpha = 1$	$\alpha = 2$	$\alpha = 4$	$\alpha = 5$	$\beta = 1$
I	0°	141.9	170.2	187.6	199.7	208.6	169.2	180.2	193.0	197.2	123.8
	30°	150.2	176.8	193.3	204.9	213.5	170.5	183.9	200.3	205.8	126.0
	60°	162.6	189.0	205.0	216.2	224.5	174.2	192.4	214.3	221.3	130.8
	90°	173.8	200.9	217.2	228.4	236.7	179.1	202.1	227.9	235.9	136.4
II	0°	336.9	359.2	373.9	384.8	393.2	283.0	339.4	398.0	415.8	246.8
	30°	333.1	354.6	369.1	379.9	388.3	281.4	335.7	392.3	409.6	245.0
	60°	323.0	341.4	355.0	365.5	374.0	276.9	325.0	376.1	392.0	239.8
	90°	302.6	317.6	331.2	342.4	351.6	269.8	307.9	347.6	360.1	230.7
III	0°	594.3	634.3	659.4	678.2	693.3	854.9	713.1	631.3	614.4	770.9
	30°	725.1	707.0	711.1	718.9	726.6	864.9	747.0	697.0	691.1	818.8
	60°	894.7	828.4	810.3	805.3	805.1	890.7	821.5	811.5	816.3	914.8
	90°	986.9	902.7	883.1	876.9	874.9	923.6	891.9	879.8	878.9	999.7
IV	0°	1462.6	1506.0	1534.1	1555.9	1574.0	2226.4	1727.5	1428.8	1362.1	2139.0
	30°	1602.5	1358.8	1265.4	1217.2	1188.3	1169.3	1226.0	1294.8	1317.3	1473.8
	60°	1470.9	1242.7	1164.4	1128.2	1109.2	1150.5	1149.3	1181.1	1196.9	1382.0
	90°	1240.7	1089.3	1043.3	1025.2	1018.3	1122.2	1055.9	1044.1	1049.2	1251.6
I	Ref. 28	142.0	170.3	187.8	199.9	208.9	169.4	180.4	193.2	197.3	124.0
III	(No	596.3	636.4	661.7	680.6	695.7	861.7	716.4	633.1	615.8	776.9
IV	twist)	1472.1	1515.6	1543.6	1565.9	1584.1	2264.9	1743.1	1435.6	1366.7	2175.3

Data: Length of beam = 0.254 m, breadth at root = .076xLength, depth at root = 0.038xLength shear coefficient = .833, $E = 2.07 \times 10^{11}$ N/m^2, $G = E/2.6$, mass density = 800 kg/m^3, Number of elements = 6.

TABLE 4.5

Effect of Depth and Breadth Taper Ratios on Natural Frequencies (Hz) of a Tapered Twisted Beam without Shear Deformation Effect

Mode shape	Pre-twist	Depth taper ratio $\alpha = 3$					Breadth taper ratio $\beta = 3$				$\alpha = 1$
		$\beta = 1$	$\beta = 2$	$\beta = 3$	$\beta = 4$	$\beta = 5$	$\alpha = 1$	$\alpha = 2$	$\alpha = 4$	$\alpha = 5$	$\beta = 1$
I	0°	141.9	170.3	187.7	199.9	208.8	169.3	180.4	193.2	197.4	123.9
	30°	150.3	176.9	193.5	205.1	213.7	170.7	184.1	200.5	206.0	126.1
	60°	162.8	189.2	205.3	216.4	224.8	174.4	192.6	214.5	221.5	130.9
	90°	173.9	201.2	217.4	228.7	237.0	179.4	202.3	228.2	263.3	136.5
II	0°	338.4	360.6	375.3	386.1	394.5	283.8	340.5	399.5	417.4	247.6
	30°	334.5	355.9	370.4	381.2	389.6	282.3	336.8	393.8	411.1	245.9
	60°	324.2	342.6	356.1	366.7	375.2	277.7	326.0	377.3	393.3	240.5
	90°	303.6	318.5	332.0	343.3	352.5	270.5	308.7	348.5	361.1	231.3
III	0°	596.2	636.3	661.6	680.5	695.6	860.2	715.9	633.2	616.1	775.5
	30°	728.5	709.8	713.8	721.5	729.2	870.3	750.3	699.3	693.4	824.4
	60°	901.0	832.9	814.2	809.0	808.7	896.6	825.8	815.4	820.2	922.6
	90°	995.8	908.9	888.5	881.9	879.7	930.0	897.5	885.1	884.2	1010.0
IV	0°	1710.5	1427.9	1320.6	1264.3	1230.3	1190.2	1270.1	1358.2	1388.4	1542.1
	30°	1637.9	1378.4	1280.6	1230.2	1199.9	1183.8	1240.7	1310.4	1333.2	1507.0
	60°	1497.0	1257.4	1176.0	1138.4	1118.6	1164.4	1161.3	1192.6	1208.6	1409.0
	90°	1255.4	1098.7	1051.3	1032.7	1025.7	1135.3	1065.1	1051.6	1056.5	1271.2
I	Ref.28	141.9	170.3	187.8	199.9	208.9	169.4	180.4	193.2	197.3	123.9
III	(No	596.3	636.4	661.7	680.6	695.7	861.7	716.4	633.1	615.8	776.9
IV	twist)	1472.1	1515.6	1543.6	1565.9	1584.1	2264.5	1743.1	1435.6	1366.7	2175.3

Data: Length of beam = .254 m, Breadth at root = .076 length, Depth at root = .038 length, Shear coefficient = .833, Mass density = 800 Kg/m^3, $E = 2.07 \times 10^{11}$ N/m^2, $G = 3/8\ E$

TABLE 4.6

Effect of Fixed End Cross Sectional Dimensions on Natural Frequencies (Hz) of Tapered Twisted Beam with Shear Deformation Effects having Constant Area of Cross Section at Fixed End

Ratio of breadth to thickness at fixed end, (b_1/t_1)	Pre-twist	Mode shapes			
		I	II	III	IV
3.0/1.0	0°	445.2	1331.6	1632.8	3780.4
	30°	481.4	1306.0	2008.0	4279.4
	60°	536.2	1249.5	2517.7	3995.1
	90°	585.5	1137.0	2844.2	3390.6
2.5/1.2	0°	532.7	1131.5	1938.1	4436.4
	30°	554.4	1118.1	2159.3	3867.3
	60°	593.8	1079.4	2509.9	3609.1
	90°	631.8	1006.9	2713.5	3229.1
2.0/1.5	0°	662.2	920.4	2376.1	5337.8
	30°	670.8	914.8	2463.9	3301.9
	60°	689.5	897.7	2626.4	3167.1
	90°	709.8	869.6	2702.7	3034.8
3.0/1.0	Ref.28	448.3	-	1674.7	3988.3
2.5/1.2	(No	537.9	-	2009.6	4786.0
2.0/1.5	twist)	672.4	-	2512.0	5982.5

Data: Length of beam = .254 m, Constant root area = .000762 m^2, Depth taper ratio = 3, Breadth taper ratio = 2, Shear coefficient = .833, Mass density = 800 Kg/m^3, $E = 2.07 \times 10^{11}$ N/m^2, $G = 3/8\ E$.

TABLE 4.7

Comparison of Frequency Ratios$^{\oplus}$ for Various Depth and Breadth Taper Ratios of Non-rotating, Untwisted and Tapered Beam

Method*		Depth taper ratio $\alpha = 3$					Breadth taper ratio $\beta = 3$				$\alpha = 1$
		$\beta = 1$	$\beta = 2$	$\beta = 3$	$\beta = 4$	$\beta = 5$	$\alpha = 1$	$\alpha = 2$	$\alpha = 4$	$\alpha = 5$	$\beta = 1$
First mode	(a)	1.1452	1.3741	1.5144	1.6124	1.6849	1.3668	1.4556	1.5582	1.5920	1
	(b)	1.1454	1.3743	1.5148	1.6124	1.6850	1.3668	1.4556	1.5584	1.5923	1
	(c)	1.1369	1.3626	1.5010	1.5971	1.6680	1.3505	1.4413	1.5444	1.5786	0.9905
Second mode	(a)	4.8104	5.1337	5.3381	5.4905	5.6125	6.9511	5.7789	5.1073	4.9679	6.2670
	(b)	4.8124	5.1361	5.3404	5.4928	5.6149	6.9528	5.7805	4.1103	4.9715	6.2685
	(c)	4.6650	4.9759	5.1708	5.3156	5.4313	6.5228	5.5543	4.9670	4.8432	5.8850
Third mode	(a)	11.8752	12.2260	12.4526	12.6318	12.7788	18.2701	14.0614	11.5805	11.0251	17.5484
	(b)	11.8957	12.2477	12.4771	12.6549	12.8024	18.2998	14.0867	11.6056	11.0554	17.5797
	(c)	11.1177	11.4410	11.6491	11.8091	11.9413	15.9423	12.9227	10.9327	10.4713	15.3303
Fourth mode	(a)	22.3834	22.7437	22.9902	23.1798	23.3410	35.1250	26.3652	21.1320	19.9375	34.3857
	(b)	22.5186	22.8936	23.1429	23.3399	23.5060	35.3637	26.5329	21.3052	20.1406	34.6158
	(c)	20.0672	20.3905	20.6016	20.7663	20.9054	28.1545	22.9438	19.2481	18.3606	27.5757

Data: Length of beam = .254 m, Breadth at root = .0762 m, Depth at root = .0254 m, Shear coefficient = .833, Mass density = 800 Kg/m^3, $E = 2.07 \times 10^{11}$ N/m^2, $G = 3/8\ E$

* Method (a) : Mabie and Rogers[28]
Method (b) : Finite element without shear deformation effect
Method (c) : Finite element with shear deformation effect

$^{\oplus}$ Frequency ratio: Ratio of modal frequency to frequency of fundamental mode of uniform beam with the same root cross section and without shear deformation effects.

TABLE 4.8

Comparison of Natural Frequencies (Hz) for Various Depth and Breadth Taper Ratios of Non-rotating, Untwisted and Tapered Beam

Method*		Depth taper ratio $\alpha = 3$					Breadth taper ratio $\beta = 3$				$\alpha = 1$
		$\beta = 1$	$\beta = 2$	$\beta = 3$	$\beta = 4$	$\beta = 5$	$\alpha = 1$	$\alpha = 2$	$\alpha = 4$	$\alpha = 5$	$\beta = 1$
First mode	(a)	374.25	449.04	494.98	526.90	550.60	446.66	475.66	509.21	520.24	326.79
	(b)	374.31	449.10	495.03	526.90	550.65	446.65	475.69	509.28	520.36	326.79
	(c)	371.53	445.30	490.50	521.90	545.10	441.34	471.00	504.70	515.86	323.67
Second mode	(a)	1571.99	1677.63	1744.43	1794.25	1834.10	2271.54	1888.48	1669.00	1623.46	2048.00
	(b)	1572.63	1678.42	1745.18	1795.00	1834.90	2272.09	1889.00	1670.00	1624.65	2048.47
	(c)	1524.47	1626.08	1689.77	1737.10	1774.90	2131.60	1815.10	1623.17	1582.70	1923.17
Third mode	(a)	3880.70	3995.34	4069.40	4127.94	4175.97	5970.70	4595.14	3784.40	3602.88	5734.63
	(b)	3887.40	4002.44	4077.40	4135.50	4183.71	5980.20	4600.34	3792.60	3612.81	5744.86
	(c)	3633.15	3738.79	3806.80	3859.10	3902.30	5209.80	4223.00	3572.70	3421.90	5009.80
Fourth mode	(a)	7314.68	7432.40	7512.96	7574.92	7627.59	1147.85	8615.90	6905.73	6515.36	11236.90
	(b)	7358.86	7481.40	7562.86	7627.23	7681.54	1155.65	8670.68	6962.32	6581.76	11312.10
	(c)	6557.77	6663.40	6732.40	6786.40	6831.67	9200.60	7497.80	6290.10	6000.06	9011.47

Data: Length of beam = .254 m, Breadth at root = .0762 m, Depth at root = .0254 m, Shear coefficient = .833, Mass density = 800 Kg/m^3, $E = 2.07 \times 10^{11}$ N/m^2, $G = 3/8\ E$

* Method (a) : Mabie and Rogers[28]
Method (b) : Finite element without shear deformation effect
Method (c) : Finite element with shear deformation effect.

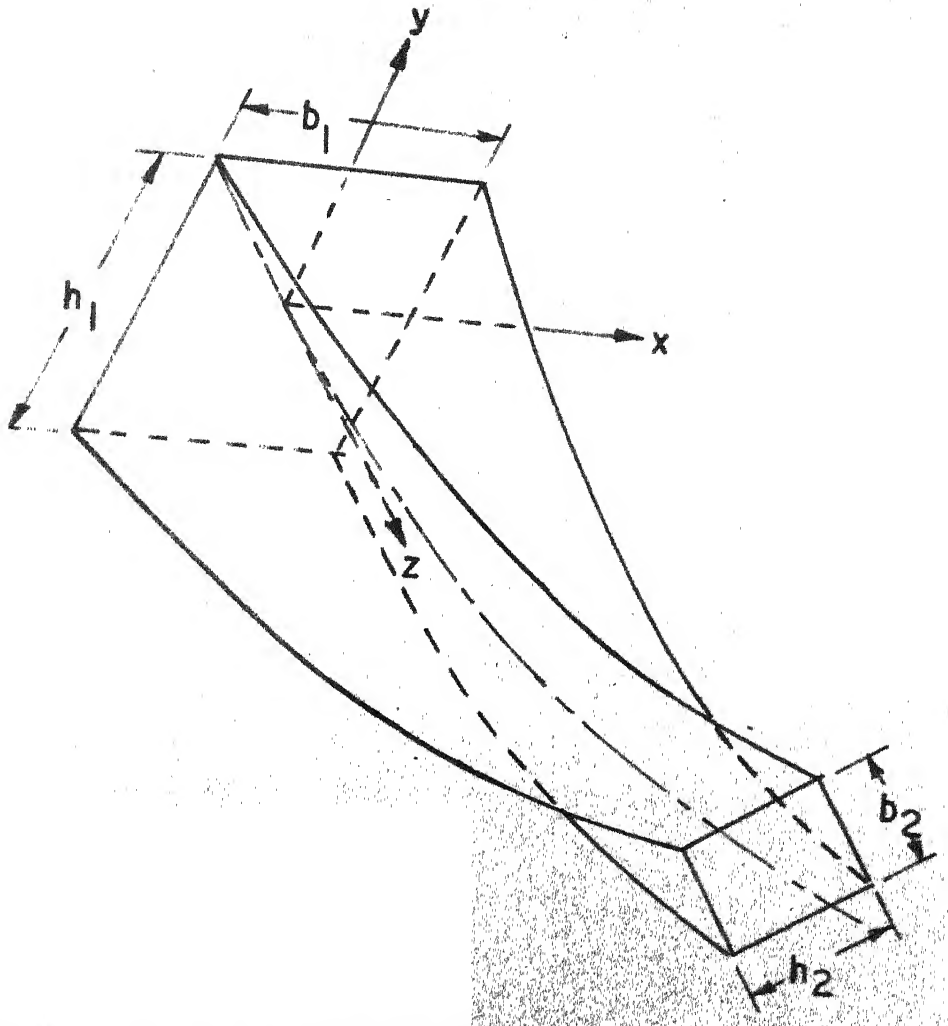

(a) AN ELEMENT OF TAPERED AND TWISTED BEAM.

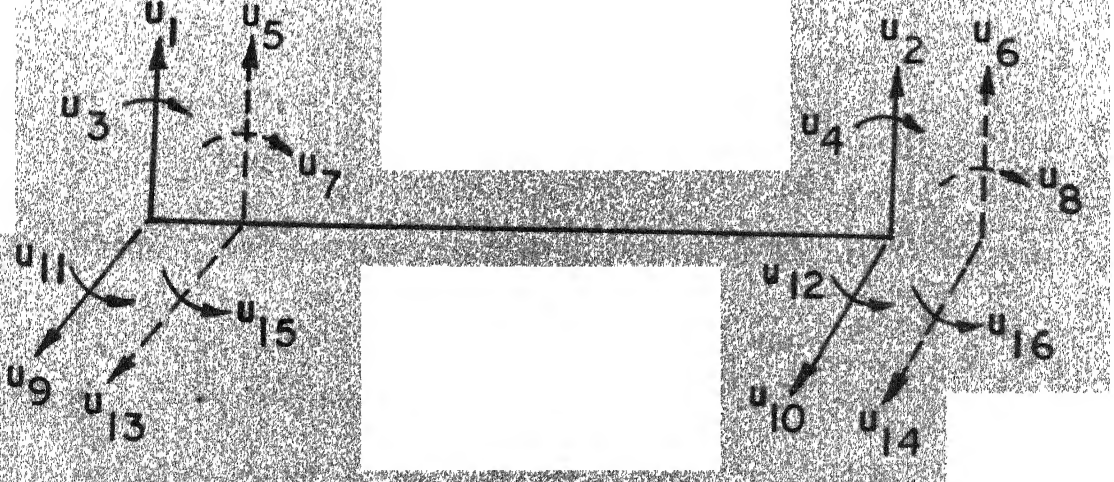

(b) DEGREES OF FREEDOM OF AN ELEMENT.

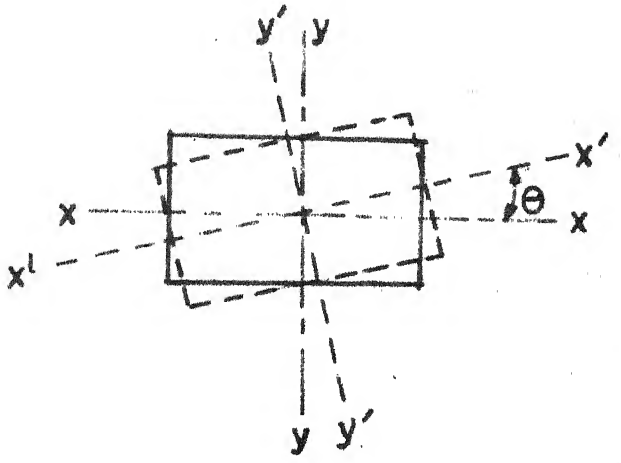

(c) ANGLE OF TWIST θ

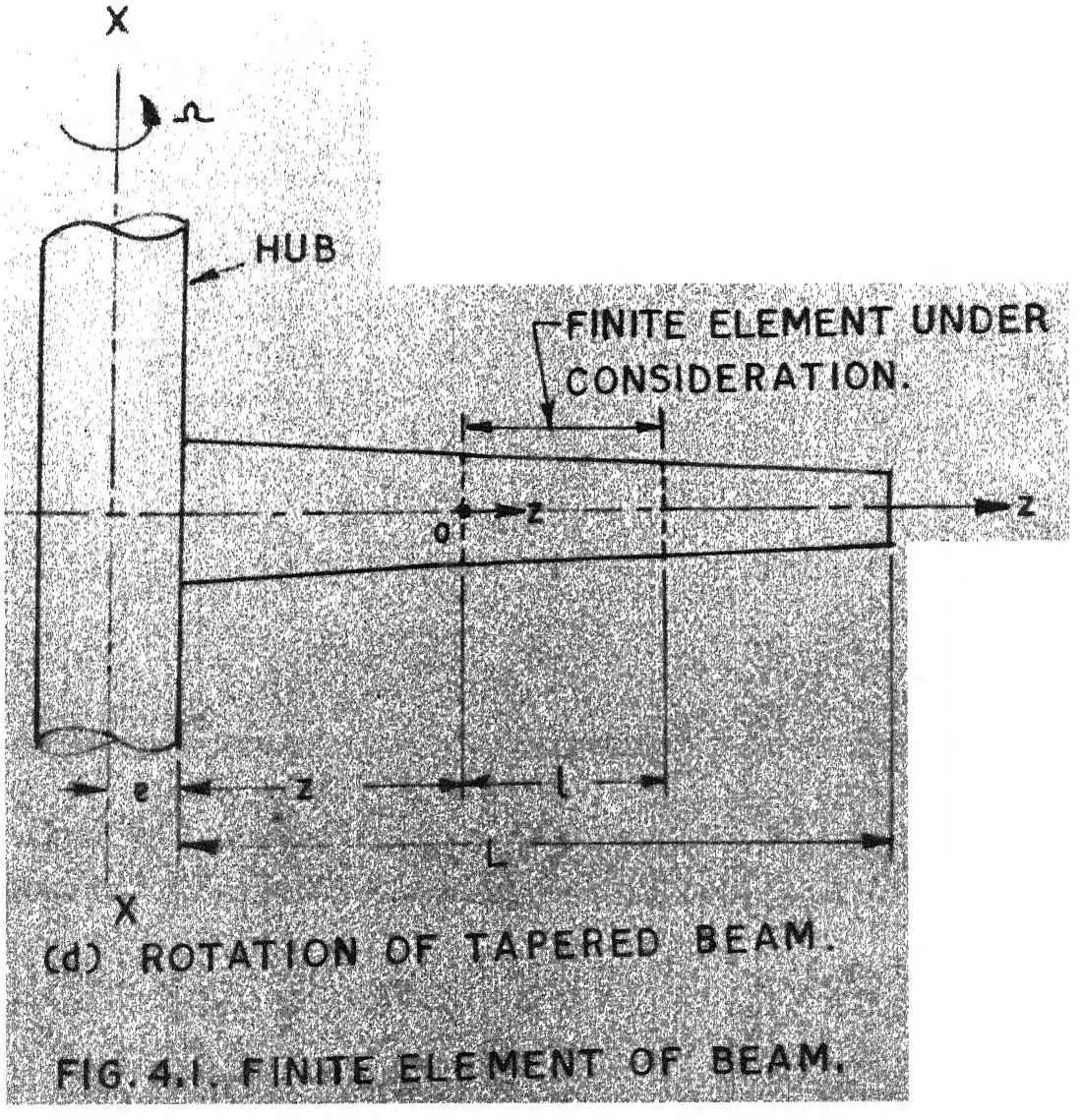

(d) ROTATION OF TAPERED BEAM.

FIG. 4.1. FINITE ELEMENT OF BEAM.

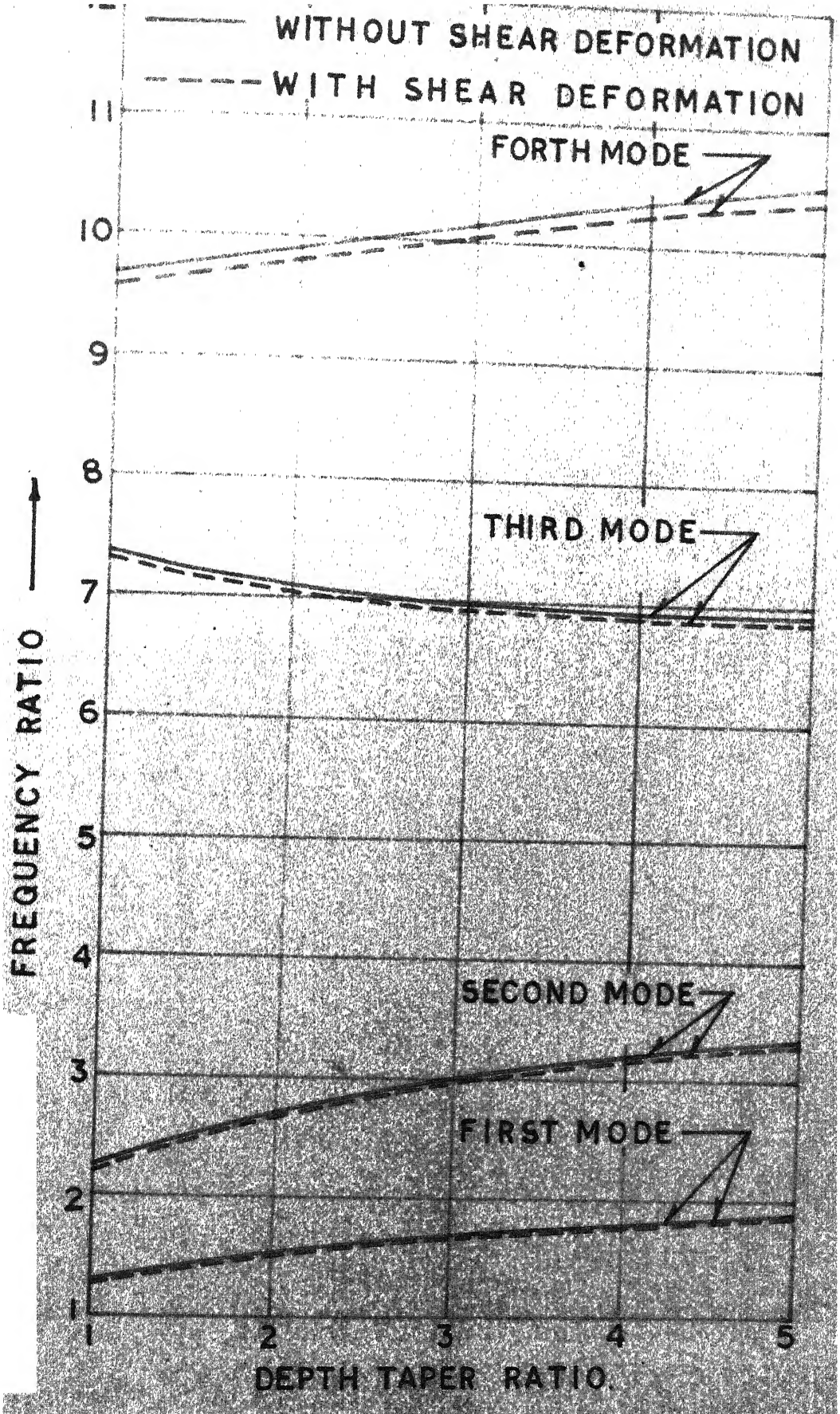

FIG.42 EFFECT OF DEPTH TAPER RATIO AND SHEAR DEFORMATION ON FREQUENCY RATIO OF ROTATING BEAM.

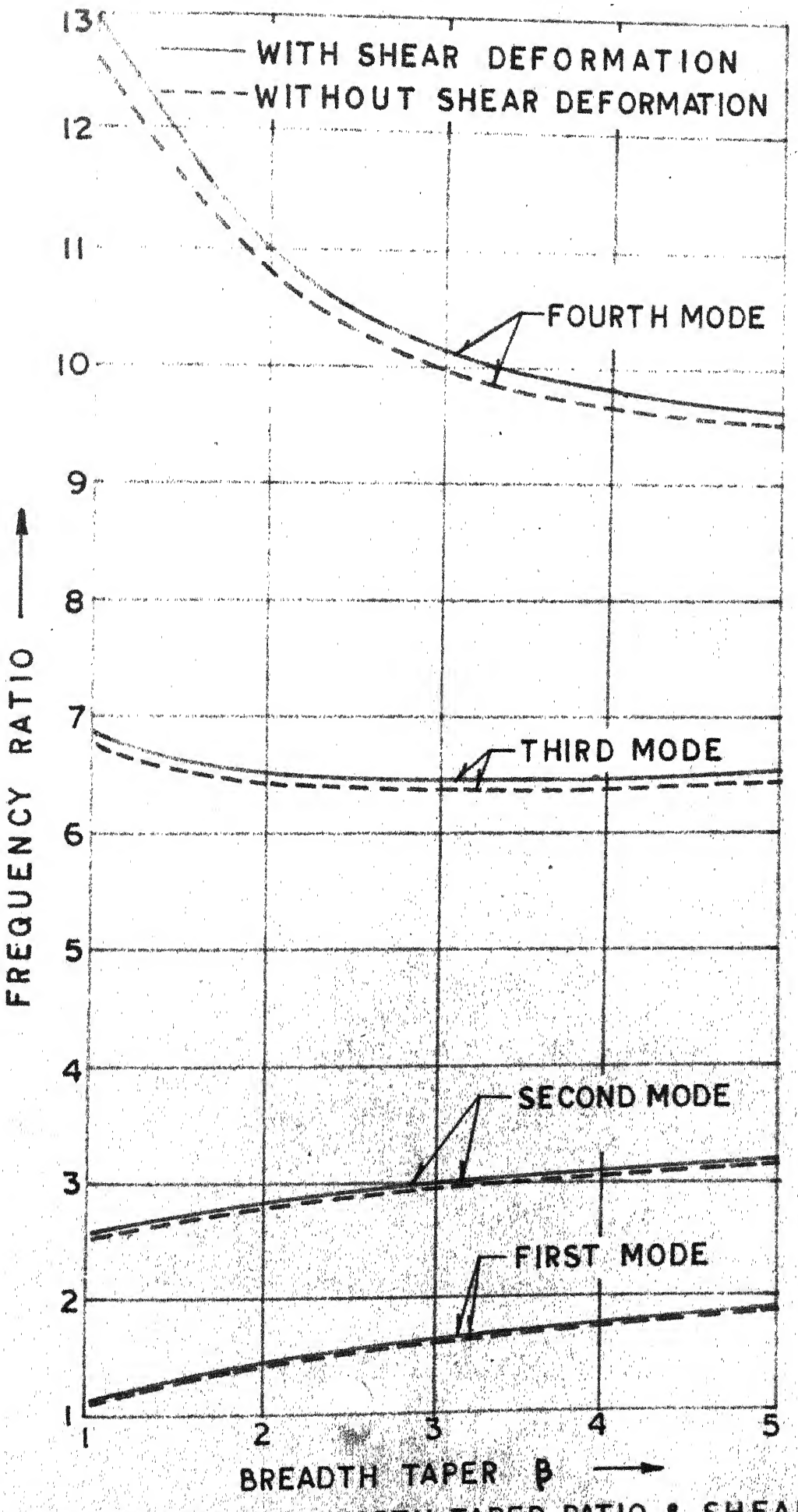

FIG.4.3 EFFECT OF BREADTH TAPER RATIO & SHEAR DEFORMATION ON FREQUENCY RATIO OF ROTATING BEAM.

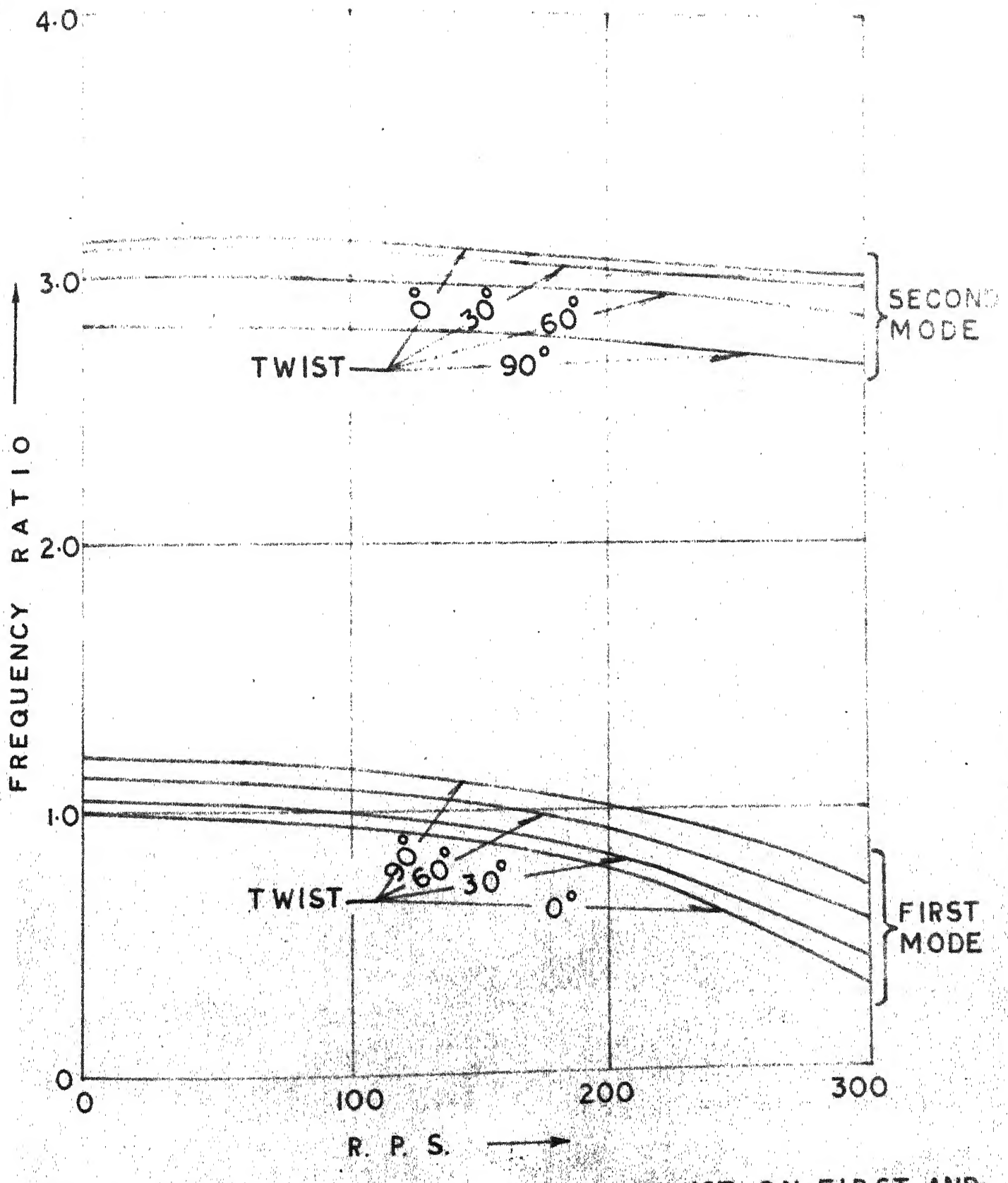

FIG. 4.4 EFFECT OF ROTATION AND TWIST ON FIRST AND SECOND NATURAL FREQUENCY.

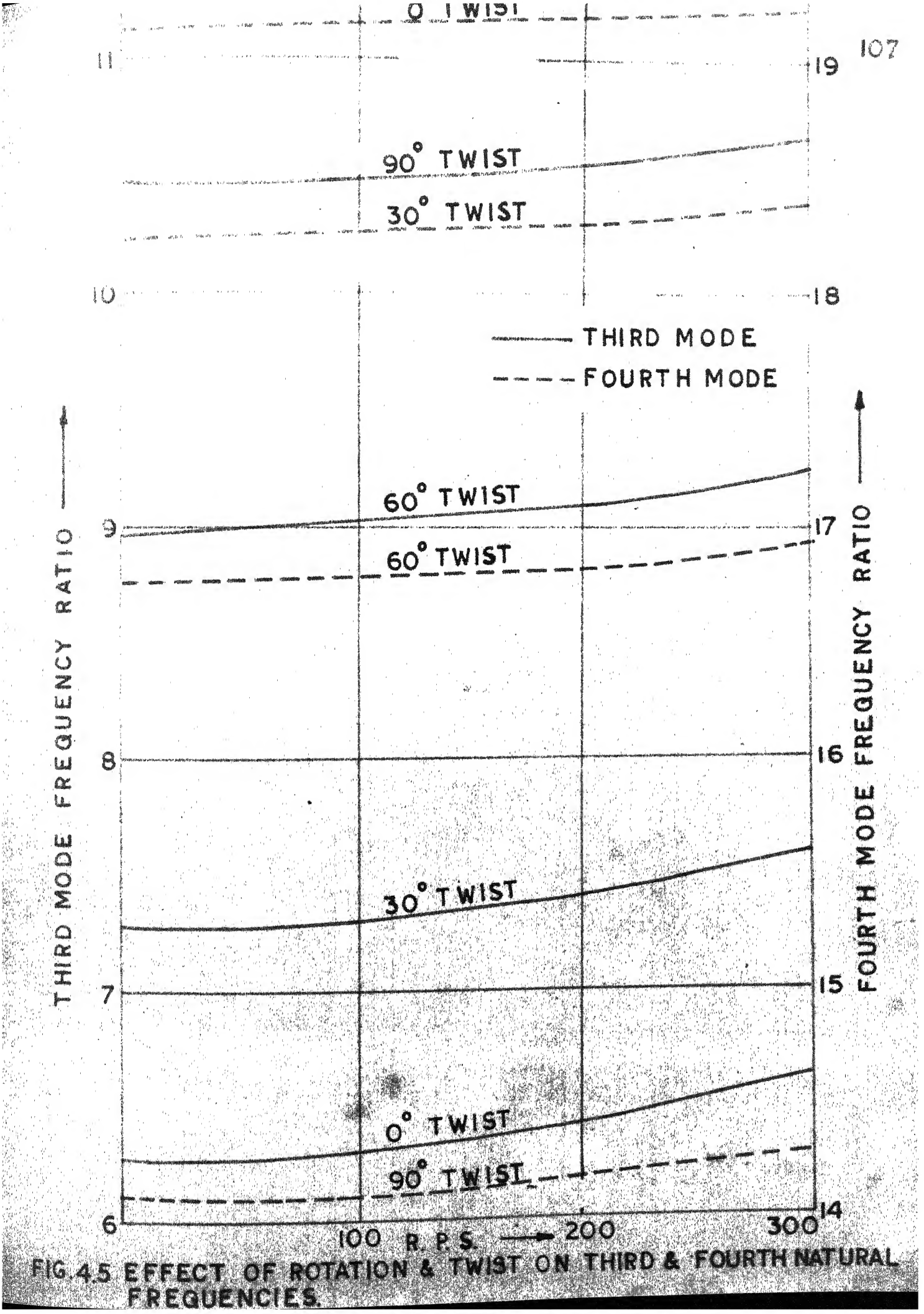

FIG. 4.5 EFFECT OF ROTATION & TWIST ON THIRD & FOURTH NATURAL FREQUENCIES.

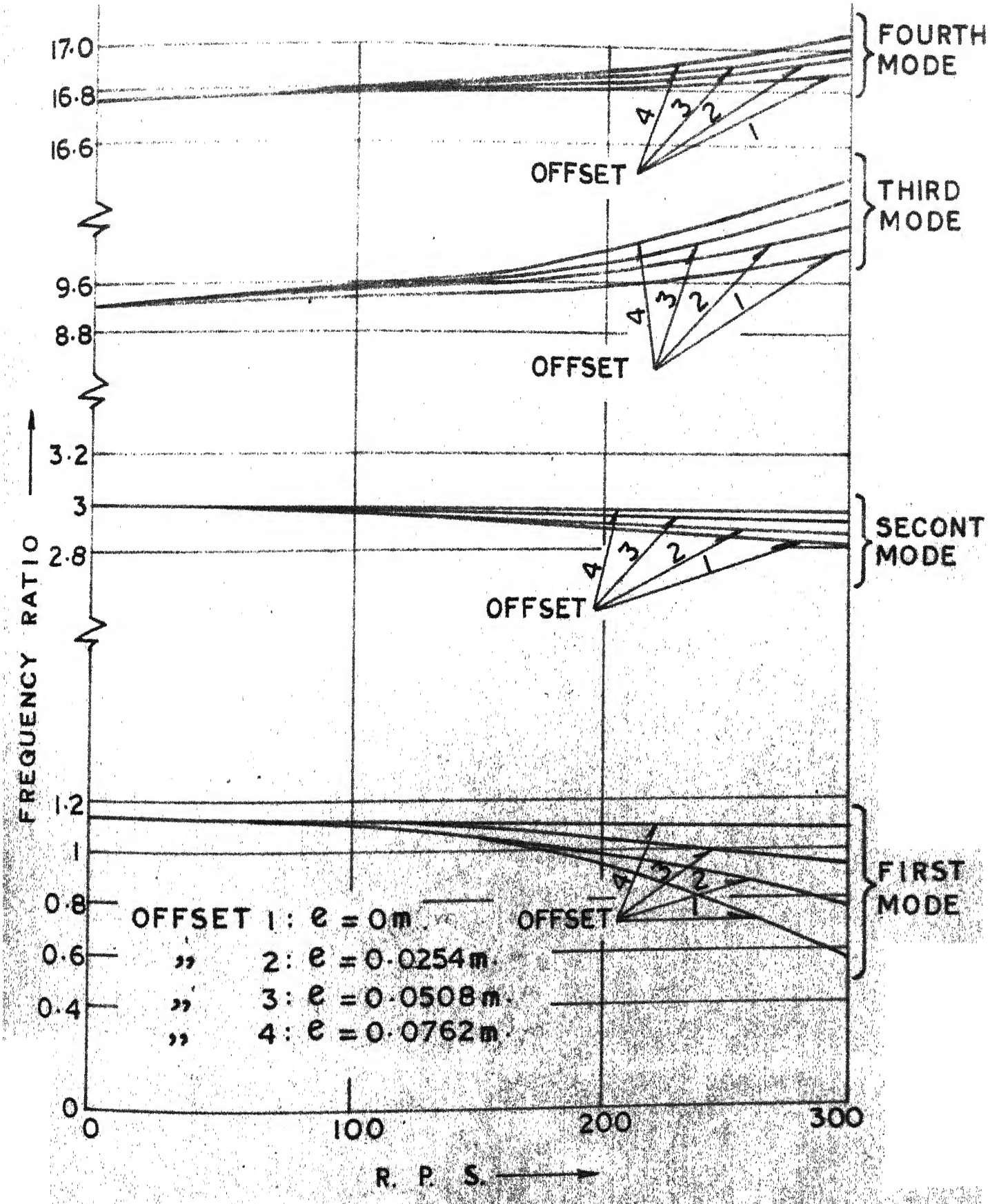

FIG.4.6 EFFECT OF OFFSET AND ROTATION ON FREQUENCY RATIO.

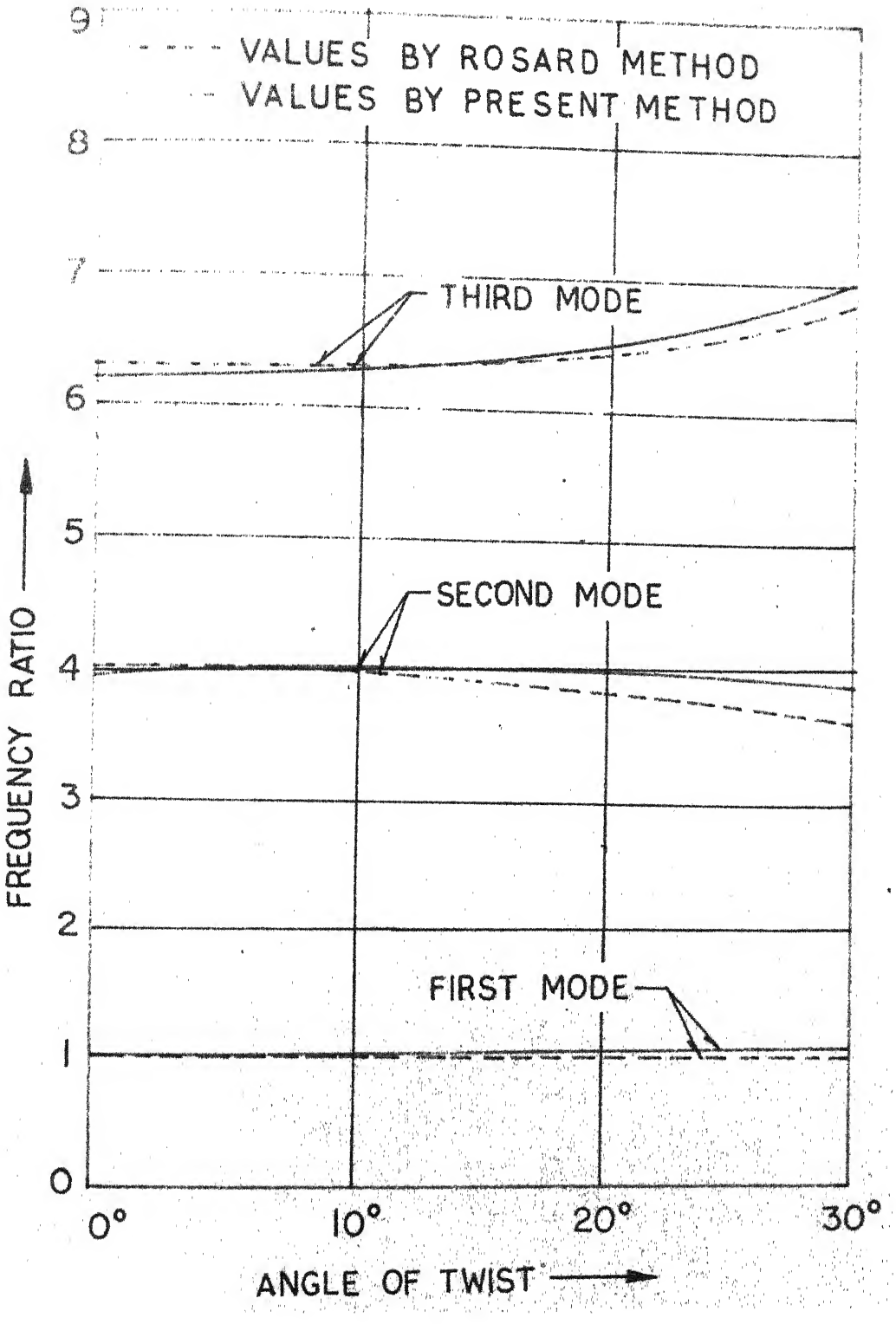

FIG 4.7 COMPARISON OF RESULTS FOR AN UNIFORM TWISTED BEAM.

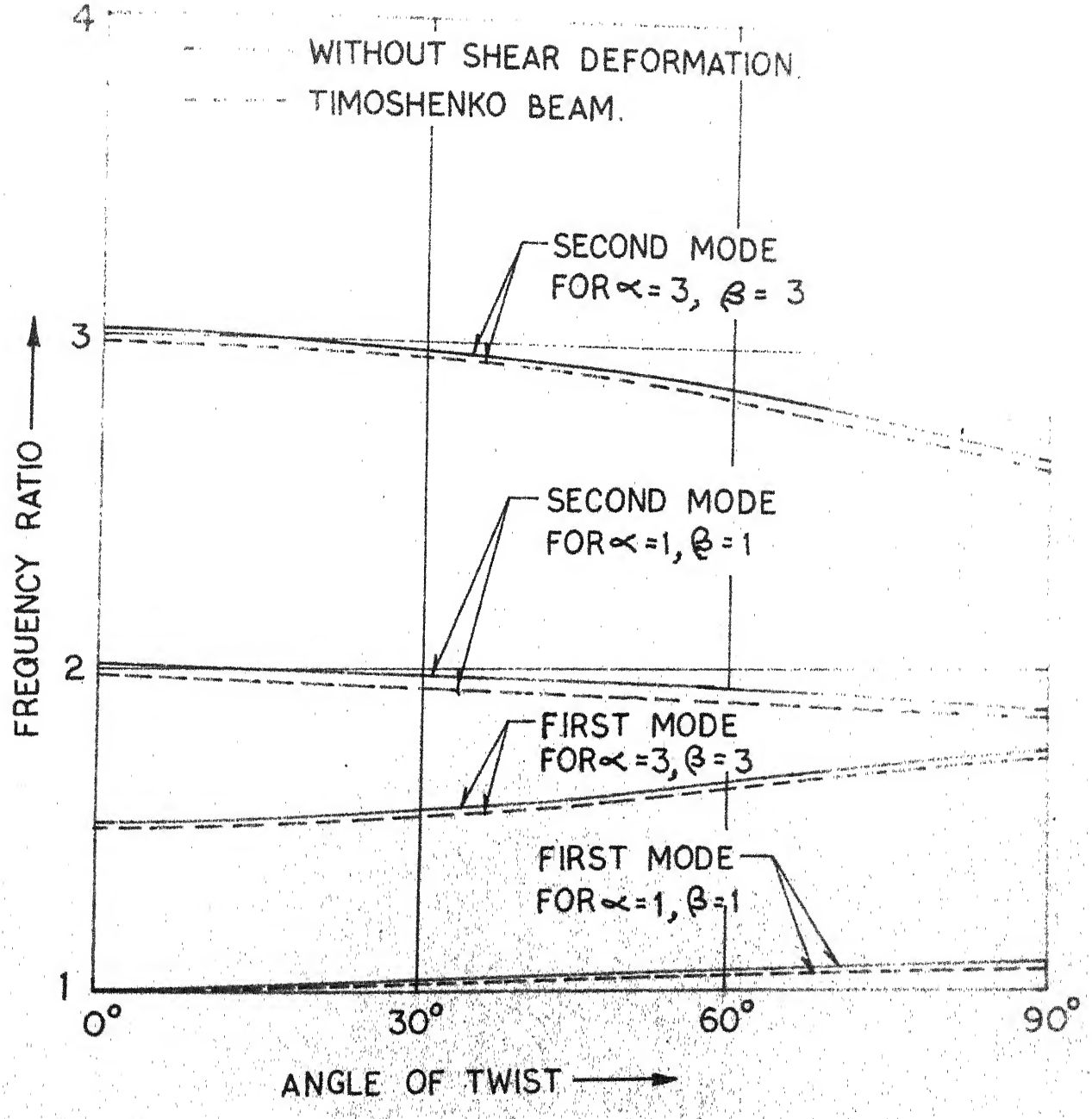

FIG. 4.8. EFFECTS OF SHEAR DEFORMATION AND ANGLE OF TWIST ON THE FIRST & SECOND NATURAL FREQUENCIES.

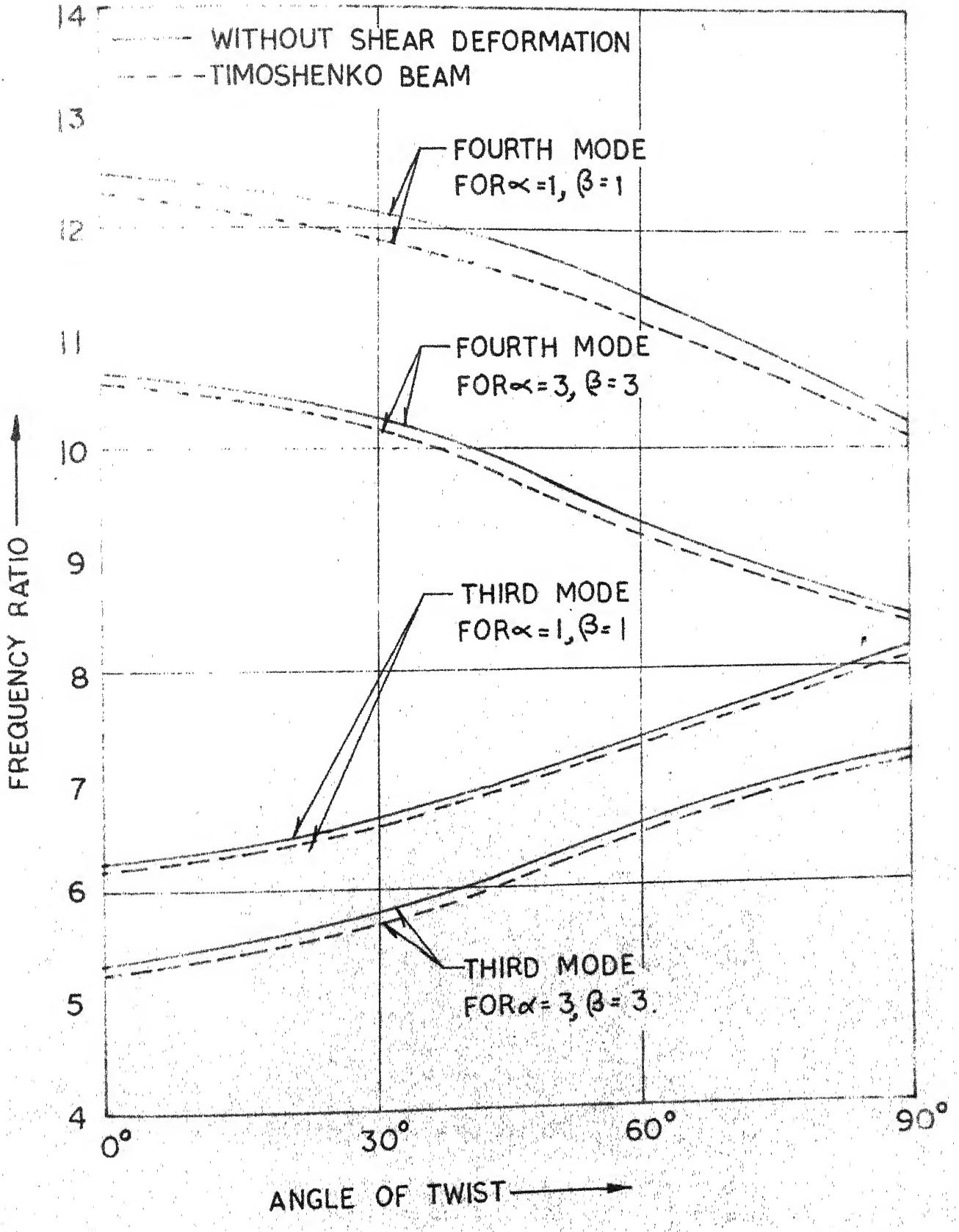

FIG 4.9 EFFECTS OF SHEAR DEFORMATION & ANGLE OF TWIST ON THE THIRD & FOURTH NATURAL FREQUENCIES.

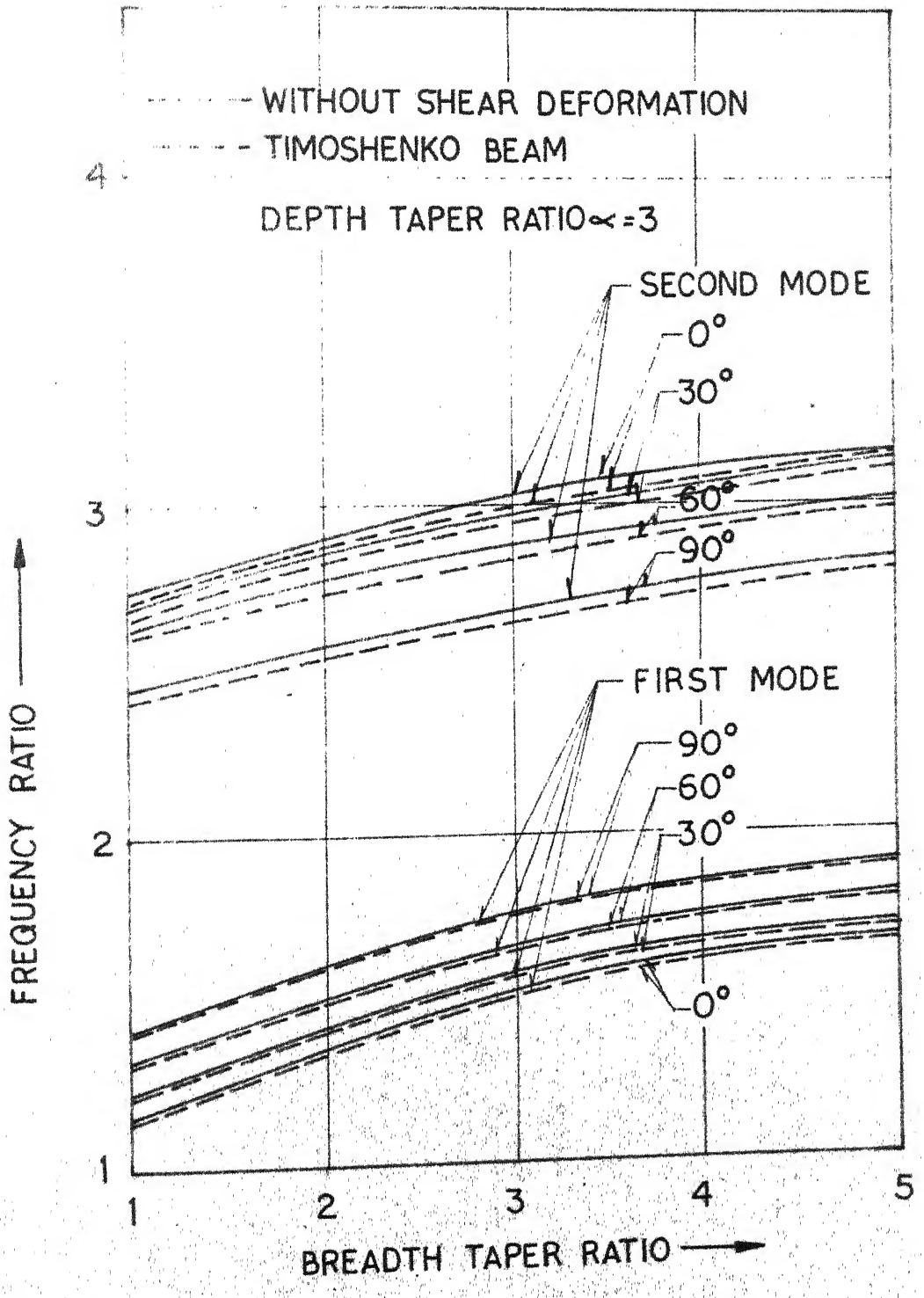

FIG.4.10 EFFECTS OF SHEAR DEFORMATION & BREADTH TAPER RATIO ON THE FIRST & SECOND NATURAL FREQUENCIES OF A TWISTED BEAM.

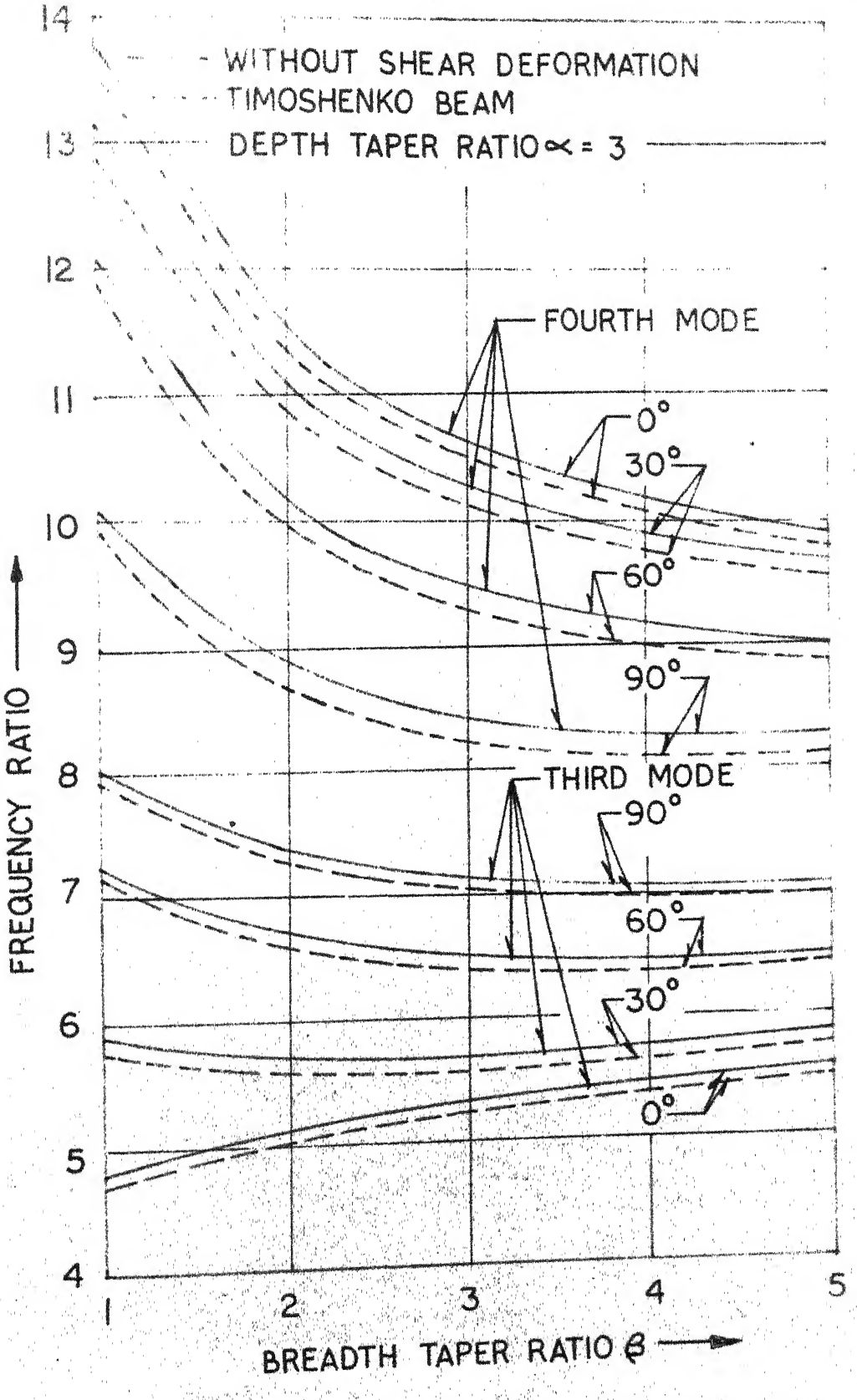

FIG 4.11 EFFECTS OF SHEAR DEFORMATION & BREADTH TAPER RATIO ON THE THIRD & FOURTH NATURAL FREQUENCIES OF A TWISTED BEAM.

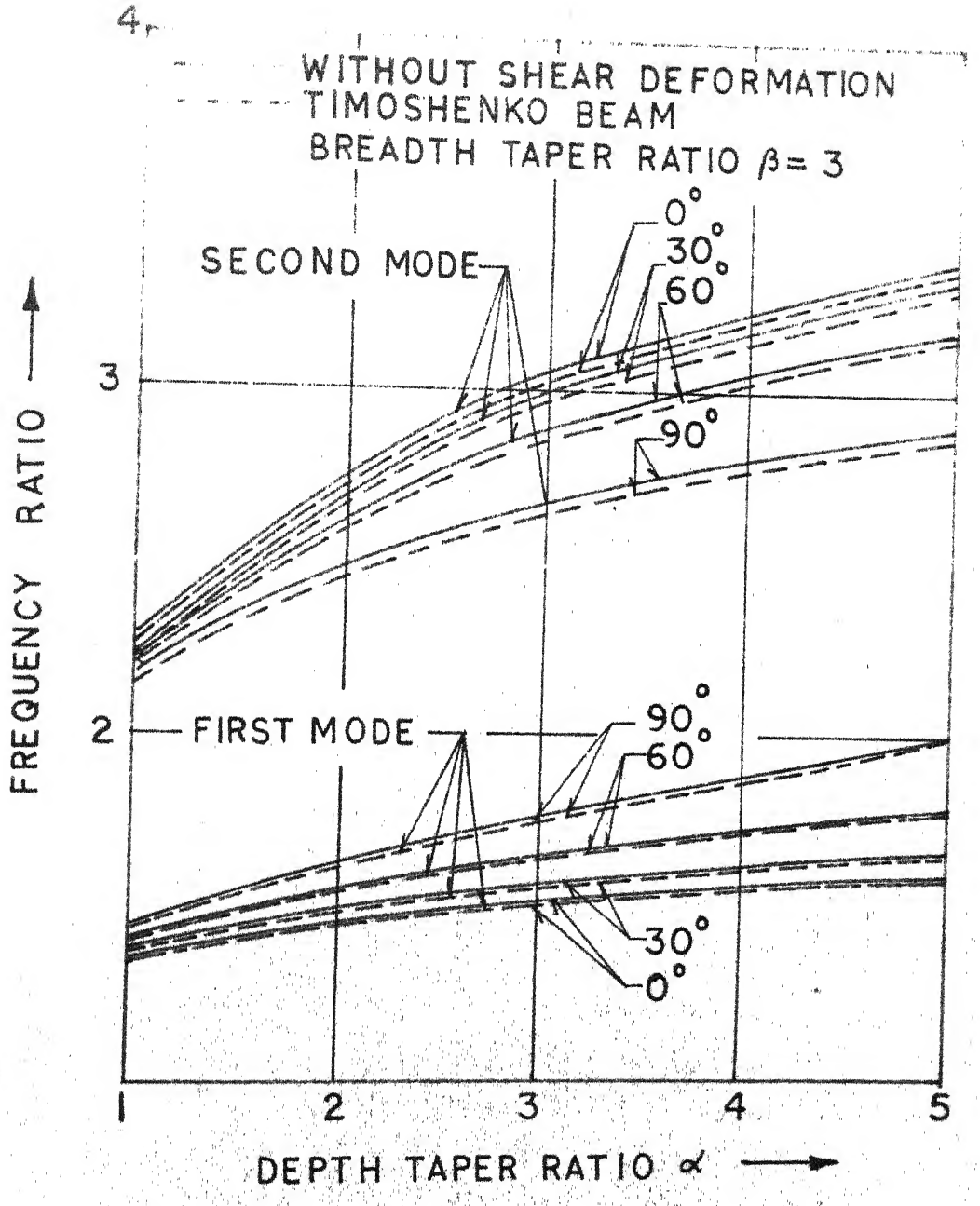

FIG 4.12 EFFECTS OF SHEAR DEFORMATION AND DEPTH TAPER RATIO ON THE FIRST & SECOND NATURAL FREQUENCIES OF A TWISTED BEAM

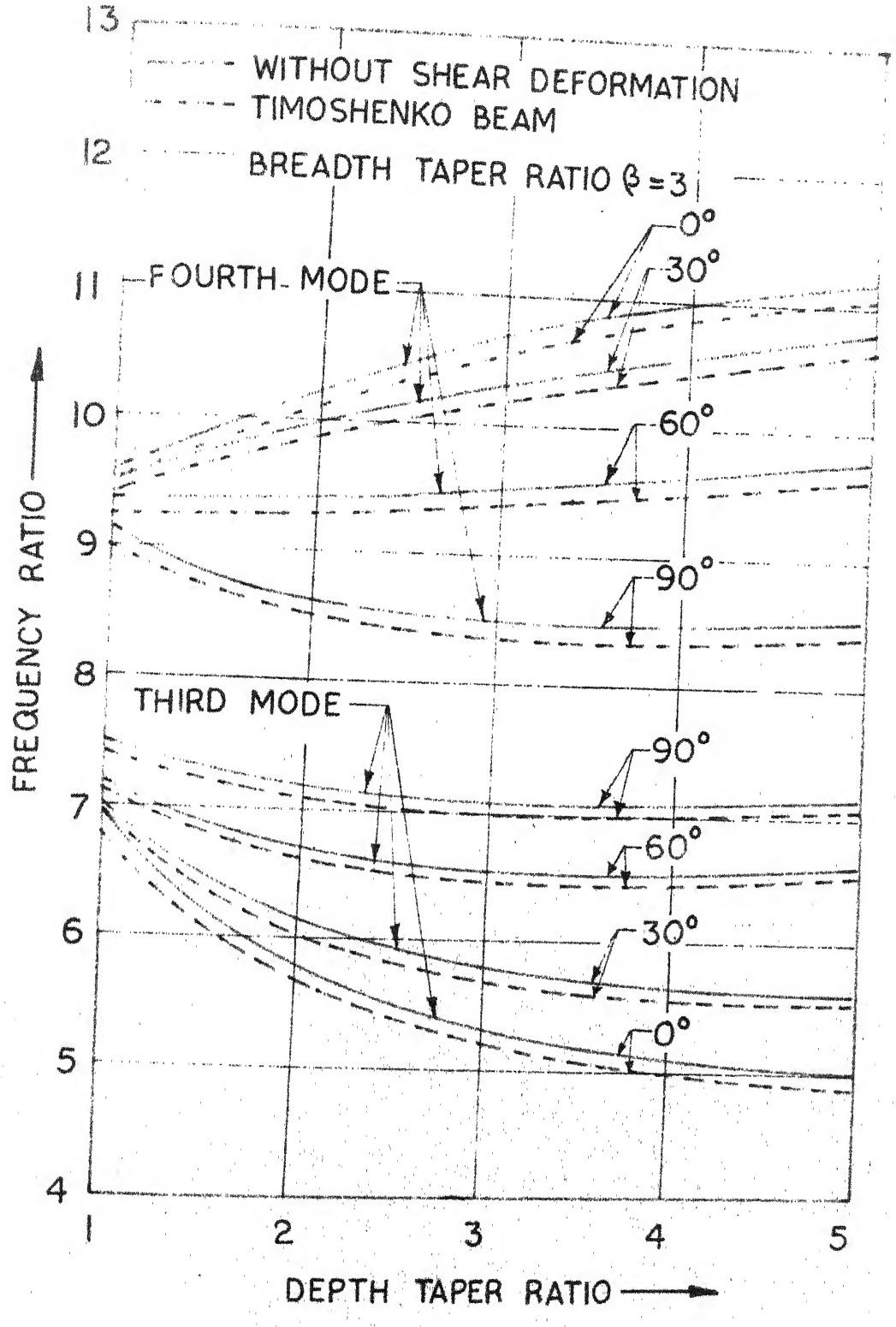

FIG 4.13 EFFECTS OF SHEAR DEFORMATION & DEPTH TAPER RATIO ON THE THIRD & FOURTH NATURAL FREQUENCIES OF A TWISTED BEAM.

CHAPTER 5

EVALUATION OF CONSTRAINTS

The optimization problem has been formulated in Chapter 2 and the method of calculating the objective function was discussed in Chapter 3. In Chapter 4, the vibration analysis of tapered pretwisted rectangular beams has been considered using the finite element method. The method of evaluating the constraints of the optimization problem is discussed in this chapter so that the numerical techniques of optimization discussed in Chapter 6 can be applied for solving the problem.

5.1 Blade Idealization

Generally the turbomachine blades are idealized as cantilever beams of rectangular cross section. Refinements in idealization can be made by including the effects of taper, pretwist, rotation, shear deformation and rotary inertia as described in Chapter 4. In order to apply the analysis procedure of Chapter 4, the airfoil section has to be replaced by an equivalent rectangular section with pretwist. A method of replacing a rotor blade of airfoil section by a doubly tapered and pretwisted cantilever beam of rectangular cross section is described in the following subsections.

5.1.1 Equivalent Rectangular Section of an Airfoil Section

From the known values of area A and moments of inertia I_{xx}, I_{xy} and I_{yy} (computed in section 3.7), the moments of inertia $I_{\bar{x}\bar{x}}$, $I_{\bar{x}\bar{y}}$ and $I_{\bar{y}\bar{y}}$ with respect to $\bar{x}$ and $\bar{y}$ axes passing through the centroid of the airfoil section can be computed using the parallel axes relations as:

$$I_{\bar{x}\bar{x}} = I_{xx} - A\,\bar{y}^2 \tag{5.1}$$

$$I_{\bar{y}\bar{y}} = I_{yy} - A\,\bar{x}^2 \tag{5.2}$$

$$I_{\bar{x}\bar{y}} = I_{xy} - A\,\bar{x}\bar{y} \tag{5.3}$$

We then define a rectangular section having twist θ, breadth b_{eq} and height t_{eq} to be equivalent to the given airfoil section by equating their areas, and moments of inertia about $\bar{x}$ and $\bar{y}$ axes (Figure 5.1). Thus

Area of the rectangle = $A = b_{eq}\, t_{eq}$ (5.4)

Moment of inertia of the rectangle about $\bar{x}$ axis =

$$I_{\bar{x}\bar{x}} = \frac{1}{12} b_{eq}\, t_{eq}^3 \cos^2\theta + \frac{1}{12} t_{eq}\, b_{eq}^3 \sin^2\theta \tag{5.5}$$

Moment of inertia of rectangle about $\bar{y}$ axis =

$$I_{\bar{y}\bar{y}} = \frac{1}{12} t_{eq}\, b_{eq}^3 \cos^2\theta + \frac{1}{12} b_{eq}\, t_{eq}^3 \sin^2\theta \tag{5.6}$$

The three unknown parameters θ, b_{eq} and t_{eq} can be found by solving the three equations (5.4) to (5.6) simultaneously. Here it is assumed that $I_{\bar{x}\bar{y}}$ is negligible compared to $I_{\bar{x}\bar{x}}$ and $I_{\bar{y}\bar{y}}$. From equations (5.4) and (5.5), one gets

$$\frac{12 I_{\bar{x}\bar{x}}}{A} = t_{eq}^2 \cos^2\theta + b_{eq}^2 \sin^2\theta = t_{eq}^2 \cos^2\theta + b_{eq}^2 - b_{eq}^2 \cos^2\theta \tag{5.7}$$

i.e.,

$$\cos^2\theta = \frac{12 I_{\bar{x}\bar{x}} - b_{eq}^2 A}{A(t_{eq}^2 - b_{eq}^2)} \tag{5.8}$$

Similarly from equations (5.4) and (5.6),

$$\sin^2\theta = \frac{12 I_{\bar{y}\bar{y}} - A b_{eq}^2}{A(t_{eq}^2 - b_{eq}^2)} \tag{5.9}$$

Equations (5.8) and (5.9) give

$$\frac{12 I_{\bar{x}\bar{x}} - A b_{eq}^2}{A(t_{eq}^2 - b_{eq}^2)} + \frac{12 I_{\bar{y}\bar{y}} - A b_{eq}^2}{A(t_{eq}^2 - b_{eq}^2)} = 1 \tag{5.10}$$

By substituting the value of b_{eq} from equation (5.4), equation (5.10) gives

$$t_{eq}^4 - \frac{12}{A}(I_{\bar{x}\bar{x}} + I_{\bar{y}\bar{y}}) t_{eq}^2 + A^2 = 0 \tag{5.11}$$

where roots are given by

$$t_{eq} = \left[\frac{6}{A}(I_{\bar{x}\bar{x}} + I_{\bar{y}\bar{y}}) \pm \left\{ \frac{9}{A^2}(I_{\bar{x}\bar{x}} + I_{\bar{y}\bar{y}})^2 - A^2 \right\}^{0.5} \right]^{0.5} \qquad (5.12)$$

and

$$b_{eq} = \frac{A}{t_{eq}} \qquad (5.13)$$

Finally the twist can be obtained from equations (5.8) and (5.9) as

$$\tan\theta = \frac{\sin\theta}{\cos\theta} = \left\{ (12I_{\bar{y}\bar{y}} - b_{eq}^2 A)/(12I_{\bar{x}\bar{x}} - b_{eq}^2 A) \right\}^{0.5} \qquad (5.14)$$

Notice that equations (5.12) and (5.13) give two equivalent rectangular sections whose orientations are perpendicular to each other. Out of these, we select the one having a larger value of b_{eq} compared to t_{eq} as the desired equivalent section.

In Figure 5.1, z-axis will be in the radially outward direction, x-axis will be along the chord direction and xyz axes form a right handed coordinate system. The origin of $\bar{x}\bar{y}\bar{z}$ system will be at the centroid of the cross section of the blade at the root. Since the airfoil section changes from point to point along the length of the blade (z-axis), the value of θ which defines the directions of degrees of freedom with respect to $\bar{x}$-axis will also change from point to point.

5.1.2 Equivalent Doubly Tapered and Twisted Rectangular Cantilever Beam of a Rotor Blade

Generally turbine blades having airfoil shapes are tapered from root to tip as shown in Figure 5.2. The taper is such that the value of (area of tip/area of root) lies between 1/4 and 1/3. In this work the taper in chord or breadth (β) has been fixed as 2 and the taper in thickness (α) has been assumed as 1.5. The chord lengths at root and tip are calculated in terms of the known chord length at mean radius (c_R) as:

$$(c_R)_{root} = \frac{2\beta\, c_R}{(1+\beta)} \tag{5.15}$$

$$(c_R)_{tip} = (c_R)_{root}/\beta \tag{5.16}$$

The blade angles β_{2root}, β_{3root} at root and β_{2tip}, β_{3tip} at tip are already calculated from the free vortex analysis.

Once the values of $(c_R)_{root}$, β_{2root} and β_{3root} are known, we can get the equivalent rectangular section of dimensions $(b_{eq})_{root}$, $(t_{eq})_{root}$ and twist θ_{root} at root by using the procedure of section 5.1.1. Similarly using the values $(c_R)_{tip}$, β_{2tip} and β_{3tip} we can obtain an equivalent rectangular section of dimensions $(b_{eq})_{tip}$, $(t_{eq})_{tip}$ and twist θ_{tip} at tip. Hence the pretwist of equivalent blade will be

$$\theta = \theta_{tip} - \theta_{root} \tag{5.17}$$

Thus the actual rotor blade is idealized as a doubly tapered cantilever beam of length h_R and pretwist θ whose end dimensions are $(b_{eq})_{root}$ and $(t_{eq})_{root}$ at the root and $(b_{eq})_{tip}$ and $(t_{eq})_{tip}$ at the tip. If the airfoil blade itself has an original pretwist of θ_o, the total pretwist of the blade would be $(\theta + \theta_o)$.

5.2 Rotor Blade Stresses

After obtaining the idealized (equivalent) blade section we have to verify whether the stage design is consistent with the permissible stresses in the rotor blades. For this we assume that simple approximate methods are adequate for preliminary design calculations. The final design has to be checked by laying out the blade cross section at several radii between root and tip, and performing an accurate stress analysis on the lines indicated by Sternlicht[23]. Among the various types of stresses induced in rotor blades, only centrifugal stress, gas bending stress and stress due to pressure force are important and hence are considered in this work.

5.2.1 Centrifugal Tensile Stress

When the rotational speed of the rotor (N revolutions/second) is specified, the allowable centrifugal tensile stress, σ_{ct}, places a limit on the annulus area A_{an} but it does not affect the chord length of the blade. The maximum value of

the centrifugal stress occurs at the root of the blade and is given by

$$(\sigma_{ct})_{max} = \frac{\rho_m \Omega^2 r_{tip}}{A_{root}} \int_{r_{root}} A_r r \, dr \qquad (5.18)$$

where ρ_m is the mass density of the blade material, Ω is the angular velocity of the blade (rad/sec), A_r is the cross sectional area of the blade at any radius r and A_{root} is the cross sectional area of the blade at root. In practice the integration of equation (5.18) is performed either graphically or numerically. However, if the blade is of uniform cross section, equation (5.18) reduces to

$$(\sigma_{ct})_{max} = \frac{\rho_m \Omega^2}{2} (r_{tip}^2 - r_{root}^2) = \frac{\rho_m \Omega^2 A_{an}}{2\pi}$$

$$= 2\pi N^2 \rho_m A_{an} \qquad (5.19)$$

where r_{tip} and r_{root} indicate the radii of tip and root of the blade respectively. A_{an} is the annulus area of the turbine at mean height of rotor blade. A rotor blade is usually tapered in chord and thickness. For preliminary design calculations it is sufficiently accurate (and on the safe side) to assume that the assumed taper reduces the stress to 2/3 of the value for an untapered blade[93]. Thus the approximate value of the maximum centrifugal stress induced in the rotor blade can be taken as

$$(\sigma_{ct})_{max} = \frac{4}{3} \pi N^2 \rho_m A_{an} \qquad (5.20)$$

Note that in a multistage turbine, the maximum centrifugal stress will occur at the root of the blade of the last stage where the fluid density is least and the annulus area, therefore, is largest.

The centrifugal stresses can also be calculated using the finite element technique. For this, two additional degrees of freedom (in axial direction) are required in each element, which will increase the size of the elemental stiffness and mass matrices. The total number of degrees of freedoms for the blade will also increase which means some more computational time. Hence the simpler procedure stated above has been employed in calculating the centrifugal stresses.

5.2.2 Stresses Due to Gas Bending and Pressure Force

The force arising from the change in the angular momentum of the gas in tangential direction, which produces the useful torque, also produces a gas bending moment about the axial direction, namely, M_w, as shown in Figure 5.3. There may be a change of momentum in axial direction (when $C_{a_3} \neq C_{a_2}$) and with reaction blading there will be a pressure force

$$= (p_2 - p_3) \frac{\pi d\, h_R}{n_R} \qquad (5.21)$$

per blade of the rotor where d is the diameter of rotor, h_R is the height of rotor, n_R is the number of rotor blades and p_2

and p_3 are the pressures. This pressure force will give rise to a gas bending moment M_a about the tangential direction. By resolving these bending moments into components parallel to the principal axes $(\bar{X} - \bar{Y})$ of the blade cross section, the maximum stresses can be calculated. The moments along $\bar{X}$ and $\bar{Y}$ are given by

$$\text{Along } \bar{X} : \quad M_{\bar{X}} = M_w \cos(\theta - \alpha_s) + M_a \sin(\theta - \alpha_s)$$

$$\text{Along } \bar{Y} : \quad M_{\bar{Y}} = M_a \cos(\theta - \alpha_s) - M_w \sin(\theta - \alpha_s)$$

so that

$$\text{stress induced} = \frac{\bar{Y}}{I_{\bar{X}\bar{X}}} M_{\bar{X}} + \frac{\bar{X}}{I_{\bar{Y}\bar{Y}}} M_{\bar{Y}} \qquad (5.22)$$

Equation (5.22) assumes that $M_{\bar{X}}$ and $M_{\bar{Y}}$ are constant along the length of the blade. The stress induced in the blade can be computed more accurately if the variation of $M_{\bar{X}}$ and $M_{\bar{Y}}$ along the length of the blade is considered. This can be done without much difficulty using the finite element formulation.

For this, a twisted and tapered blade has to be divided into strips of height δh and the bending moments calculated from the average force acting on each strip. For simplicity, these strips can be taken to be same as the finite elements used for the blade analysis. In the present work, the stresses due to gas bending and pressure forces have been calculated by using the finite element technique discussed in

Chapter 4 as it will not require any additional degrees of freedom per element. For calculating the stresses, forces are applied at the nodal points in the directions of the nodal degrees of freedom and then the deflections due to loading are obtained by applying standard techniques of matrix structural analysis. Once the deflections are available, the stresses at any section can be calculated by using the relations from the theory of structures. The procedure adopted in finding the vector of nodal loads is given below.

(i) Forces due to gas bending:

The quantity $(C_{w_2} + C_{w_3})$ represents the change in the whirl (or tangential) component of momentum per unit mass flow. This quantity, which produces the useful torque, can be calculated by using the procedure described in section 3.5. Thus force due to momentum change = $(C_{w_2} + C_{w_3})$ per unit mass flow.

The mass flow per finite element $= \frac{m}{n_R \cdot n_E}$

where m is the total mass flow and n_E is the number of finite elements (of equal length) in the blade.

Therefore, force due to gas bending per element =

$$(C_{w_2} + C_{w_3}) \frac{m}{n_R \, n_E} \qquad (5.23)$$

(in Y-direction)

The length of each finite element is given by $\frac{h_R}{n_E}$. Figure 5.4 shows the degrees of freedom associated with a blade element and the nodal distances from the axis of rotation along with the end dimensions of the equivalent beam. The distance of the i^{th} node from the axis of rotation (z_i) is given by

$$z_{i+1} = \{\frac{1}{2}(d - h_R) + i\,\frac{h_R}{n_E}\} \;;\; i = o,1,2,\ldots,n_E \qquad (5.24)$$

The whirl component of velocity varies with the radius and in such cases the free vortex relation is assumed to be valid so that

$$(C_{w_2} + C_{w_3})\,\frac{d}{2} = \text{constant} \qquad (5.25)$$

By assuming that the end nodes share half the load as compared to the middle nodes, we can specify the gas bending loads P_i corresponding to the i^{th} degree of freedom by the following expressions:

$$P_1 \simeq (C_{w_2} + C_{w_3})\,\frac{m}{n_R\, n_E}\,(\frac{d}{2})(\frac{n_E}{2z_1\, n_E + h_R}) \qquad (5.26)$$

$$P_{(n_E n_D+1)} \simeq (C_{w_2} + C_{w_3})\,\frac{m}{n_R\, n_E}\,(\frac{d}{2})(\frac{n_E}{2z_{n_E}\, n_E + h_R}) \qquad (5.27)$$

$$P_{(in_D+1)} = (C_{w_2}+C_{w_3})\frac{m}{n_R\, n_E}\cdot\frac{d}{2z_{(i+1)}} \;;\; i = 1,2,\ldots,(n_E-1) \qquad (5.28)$$

where n_D is the number of degrees of freedom at a node, which is equal to 4 in the present case. Since all these forces P_1, P_5, P_9,...,$P_{(n_E n_D+1)}$ act in Y direction, they have to be resolved into components parallel to $\bar{X}$ and $\bar{Y}$ axes before solving the static equilibrium problem.

(ii) Forces due to gas pressure:

The total pressure force acting at the annulus will be $(p_2 - p_3)\ \pi d\ h_R$. Thus the pressure force per element will be approximately

$$\frac{(p_2 - p_3)\ \pi d\ h_R}{n_R\ n_E} \tag{5.29}$$

Here again, we assume that the end nodes share half the load as compared to the middle nodes. We can specify the loading due to pressure at the end and middle nodes by the following relations:

$$P_3 = \frac{\pi}{2}\left(\frac{z_1 + z_2}{2}\right)\frac{h_R(p_2 - p_3)}{n_E\ n_R} \tag{5.30}$$

$$P_{(n_E n_D+3)} = \frac{\pi}{2}\left(\frac{z_{(n_E)} + z_{(n_E+1)}}{2}\right) \cdot \frac{h_R(p_2 - p_3)}{n_E\ n_R} \tag{5.31}$$

$$P_{(i.n_D+3)} = \pi\ z_i\ \frac{h_R(p_2 - p_3)}{n_E\ n_R}\ ;\quad i = 1,2,\ldots,(n_E-1) \tag{5.32}$$

Since all these loads P_3, P_7,...,$P_{(n_E n_D+3)}$ act along X direction, they have to be resolved into components parallel to $\bar{X}$ and $\bar{Y}$ axes before solving the static equilibrium problem.

Once the load vector is computed, we can get the nodal deflections corresponding to the various degrees of freedom of the beam (in $\bar{X}$ and $\bar{Y}$ directions) by solving the equilibrium equations $[K]\ \vec{U} = \vec{P}$ where [K] is the assembled stiffness matrix, $\vec{U}$ is the vector of nodal displacements and $\vec{P}$ is vector of nodal loads. The maximum deflection will occur at the free end of the cantilever and its magnitude can be found as

$$\Delta_t = (u^2_{(n_E n_D+1)} + u^2_{(n_E n_D+3)})^{0.5} \tag{5.33}$$

where u_i are the displacement degrees of freedom of the structure.

In Chapter 4, the displacement due to bending (w_b) was expressed in terms of the vector of nodal displacements (u_i) of the element. For the first element of the blade in which the stress would be maximum, the bending deflection w_b in the $\bar{Y}\bar{Z}$ plane is given by (by neglecting the effect of shear deformation):

$$w_b(z) = \frac{u_1}{l^3}(2z^3 - 3lz^2 + l^3) + \frac{u_5}{l^3}(3lz^2 - 2z^3) -$$

$$\frac{u_2}{l^2}(z^3 - 2lz^2 + l^2z) - \frac{u_6}{l^2}(z^3 - lz^2) \tag{5.34}$$

where l is the length of the element, which is equal to h_R/n_E and z is the coordinate measured along the $\bar{Z}$-axis

(Figure 5.4). The stress σ_{zz} and the strain e_{zz} are related with w_b as

$$\sigma_{zz} = E\, e_{zz} = -yE\frac{\partial^2 w_b}{\partial z^2} = -Ey\left\{\frac{u_1}{l^3}(12z - 6l) + \frac{u_5}{l^3}(6l - 12z) - \frac{u_2}{l^2}(6z - 4l) - \frac{u_6}{l^2}(6z - 2l)\right\} \tag{5.35}$$

where y is the distance of the fibre measured along $\bar{Y}$-axis from the neutral axis.

The maximum value of stress $(\sigma_{zz})_{max}$ will occur at $y = (t_{eq})_{root}/2$ and $z=0$. Thus $(\sigma_{zz})_{max}$ is given by

$$(\sigma_{zz})_{max} = -E\frac{(t_{eq})_{root}}{2}\left\{-\frac{6u_1}{l^2} + \frac{6u_5}{l^2} + \frac{4u_2}{l} + \frac{2u_6}{l}\right\} \tag{5.36}$$

Since node 1 is fixed, $u_1 = u_2 = 0$ and hence the equation (5.36) simplifies to

$$(\sigma_{zz})_{max} = -E\frac{(t_{eq})_{root}}{2}\left(\frac{6u_5}{l^2} + \frac{2u_6}{l}\right) = -\frac{E(t_{eq})_{root}}{l}\left(\frac{3u_5}{l} + u_6\right) \tag{5.37}$$

By proceeding in a similar manner, the maximum stress induced due to the displacement of the beam in $\bar{X}\bar{Z}$ plane can be obtained as

$$(\sigma_{zz})_{max} = -\frac{E\,(b_{eq})_{root}}{l}\left(\frac{3u_7}{l} + u_8\right) \tag{5.38}$$

Thus the total maximum stress induced due to gas bending and pressure force (σ_g) can be found as

$$\sigma_g = \left|\frac{E(t_{eq})_{root}}{l}\left(\frac{3u_5}{l} + u_6\right)\right| + \left|\frac{E(b_{eq})_{root}}{l}\left(\frac{3u_7}{l} + u_8\right)\right| \quad (5.39)$$

Finally the total maximum stress induced at the root (σ_{max}) will be

$$\sigma_{max} = \sigma_g + (\sigma_{ct})_{max} \quad (5.40)$$

where σ_g is given by equation (5.39) and $(\sigma_{ct})_{max}$ by equation (5.20).

5.3 Deflection, Stress, Vibration and Other Constraints

By idealizing the blade as a rectangular, tapered, twisted and rotating cantilever beam, its deflection, stress and the fundamental natural frequency can be found using the finite element analysis as described in sections 5.1, 5.2, 4.4 and 4.5. Then the mechanical constraints can be evaluated in the manner indicated in section 2.5. The other behavior constraints of section 2.5 can also be evaluated by using the values computed in Chapter 3.

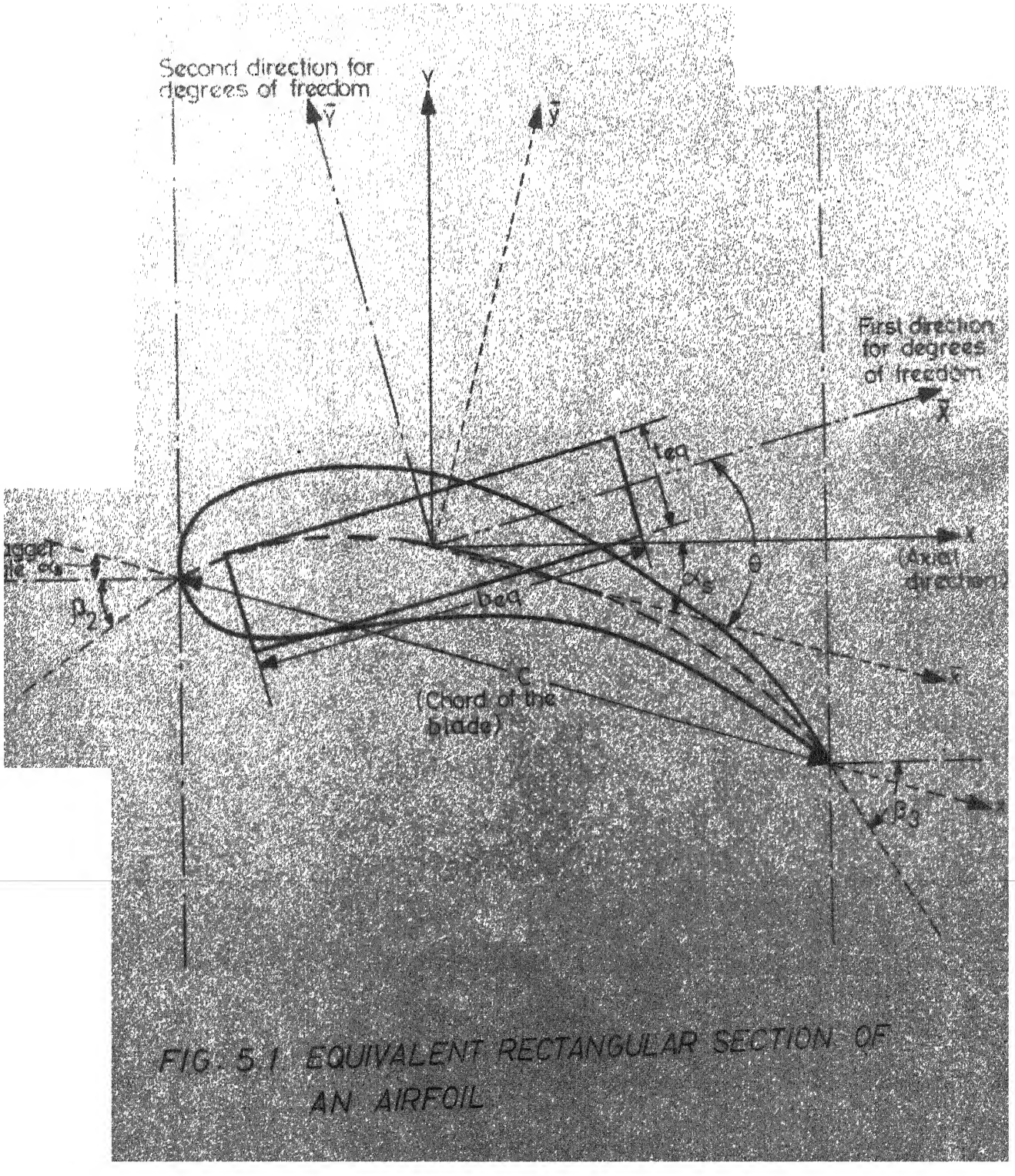

FIG. 5.1 EQUIVALENT RECTANGULAR SECTION OF AN AIRFOIL

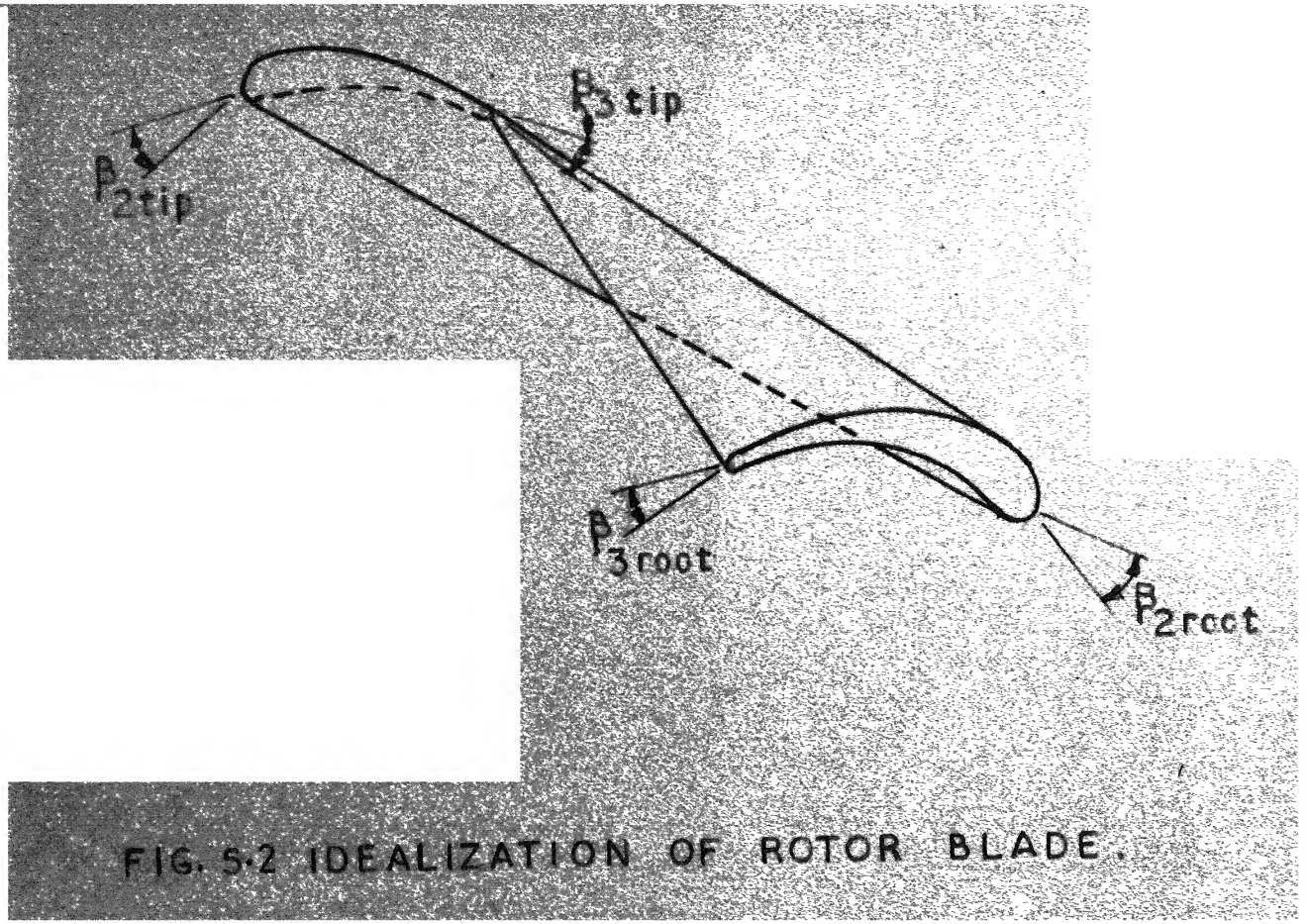

FIG. 5·2 IDEALIZATION OF ROTOR BLADE.

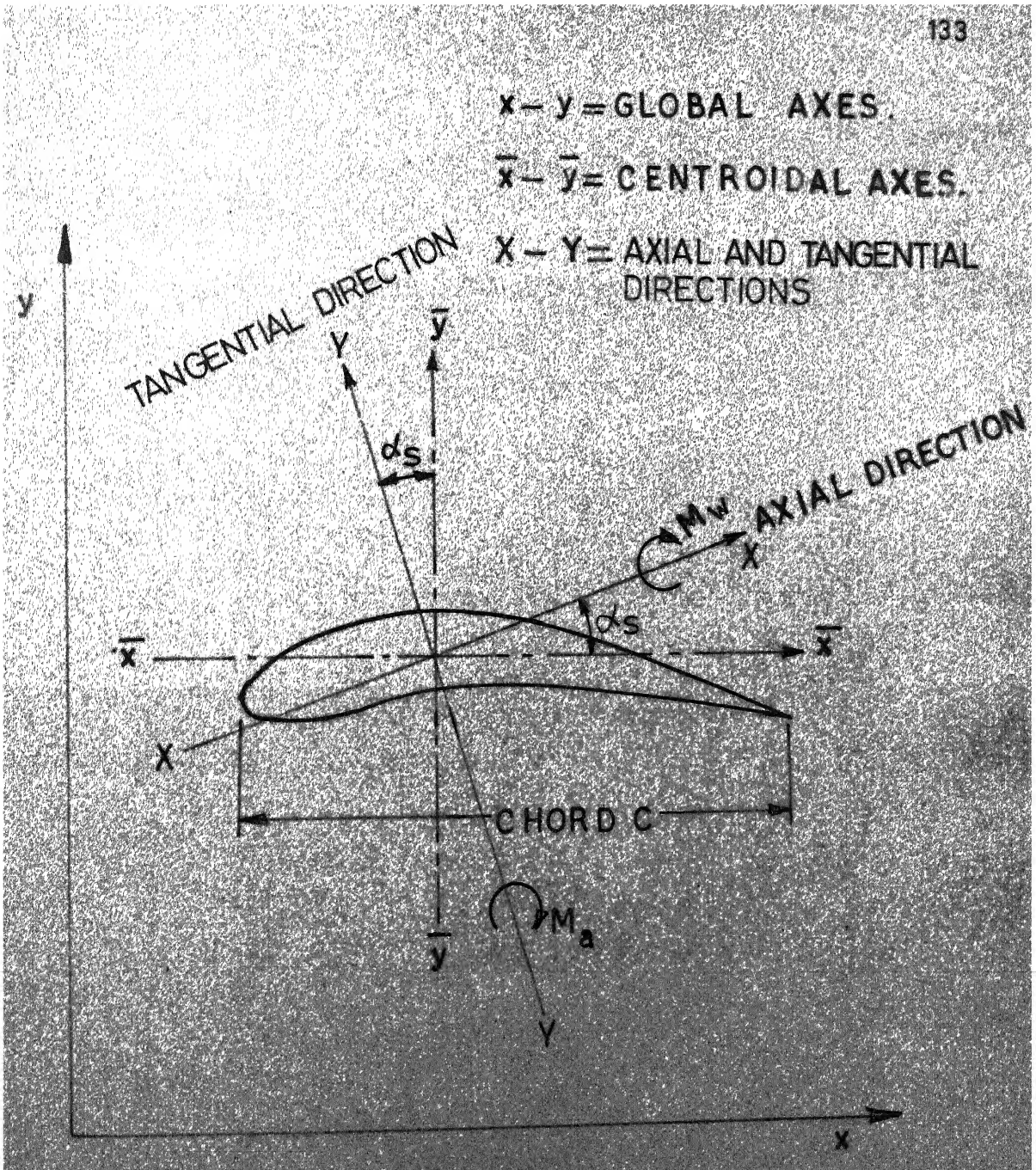

FIG. 5.3 MOMENTS DUE TO GAS BENDING AND PRESSURE FORCES.

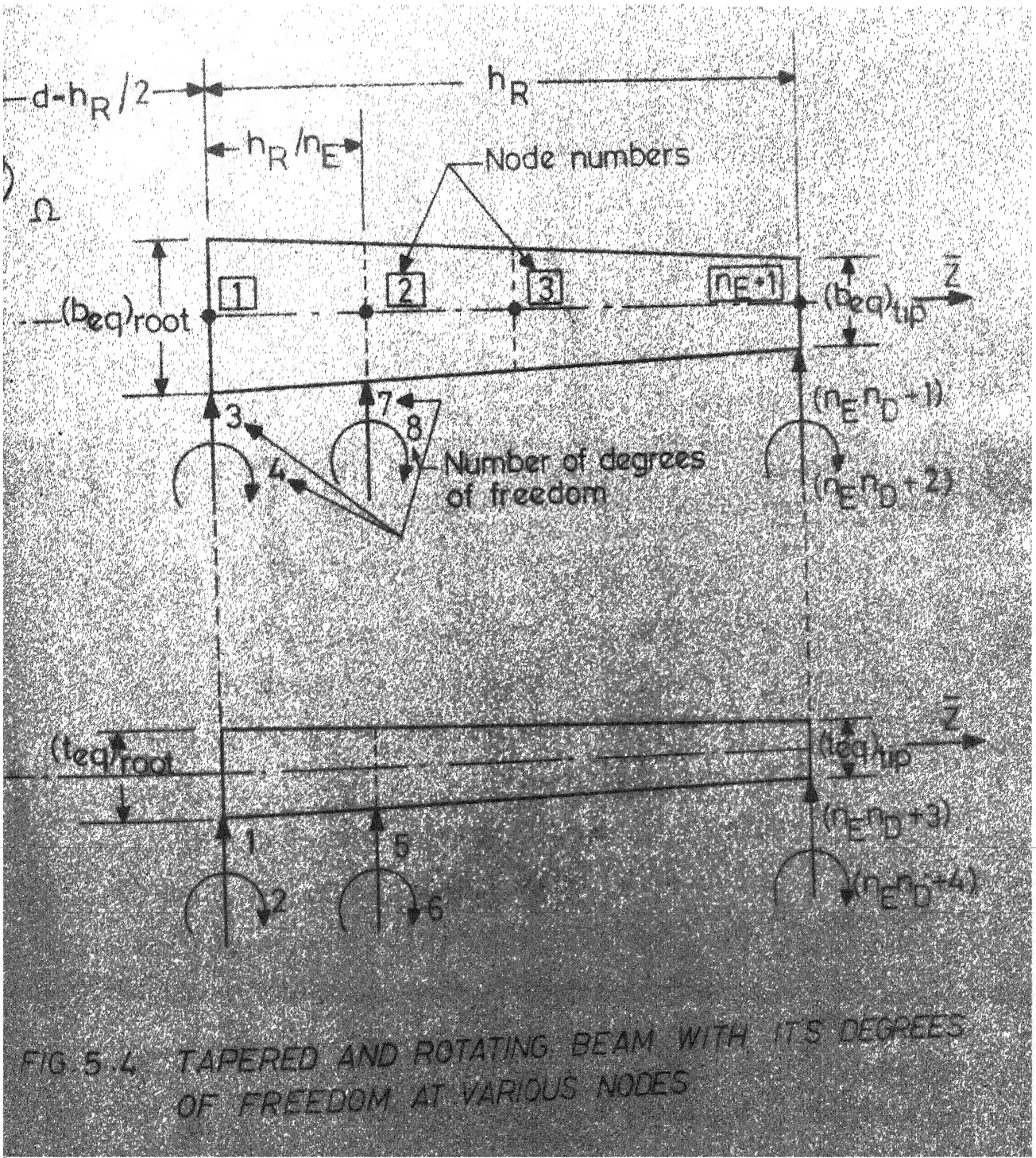

FIG. 5.4 TAPERED AND ROTATING BEAM WITH ITS DEGREES OF FREEDOM AT VARIOUS NODES

CHAPTER 6

OPTIMIZATION METHOD

In Chapter 2, the problem of optimum design of gas turbine stage has been formulated as a nonlinear mathematical programming problem. The methods of computing objective function and constraints have been developed in Chapters 3, 4 and 5. The choice of the method of optimization and its description is the topic of this chapter.

6.1 Choice of the Method

The three general classes of widely used nonlinear programming methods are as follows:

(a) Gradient projection method of Rosen[94] which was subsequently modified by Goldfarb[95]: Though this method works well with linear constraints, its efficiency is considerably reduced in the case of nonlinear constraints.

(b) Feasible direction method of Zontendijk[96]: This method is based on the generation of usable feasible directions at constraint boundaries. Although this method works in a direct manner in solving the problem, the analyses during optimization have to be done accurately as they influence the rate of convergence and accuracy.

(c) Penalty function methods: These methods are quite reliable and their sequential nature allows a gradual approach to criticality of constraints. The methods allow coarse approximations to be used during early stages of the optimization procedure and finer or more accurate approximations during the final stages. The computational time, however, is expected to be slightly more in these methods as the minimization problem has to be solved a number of times. If computational time is to be reduced, the penalty function methods allow the use of approximate analysis without effecting the accuracy and stability of the procedure. In the present work the penalty function method of Fiacco and McCormick[97] is used as it has been found to be quite reliable.

6.2 Penalty Function Methods

Penalty function methods transform the basic problem into alternative formulations such that numerical solutions are sought by solving a sequence of unconstrained minimization problems.

Let the basic optimization problem be of the form:

Find $\vec{X}$ such that

$$f(\vec{X}) \rightarrow \text{minimum} \tag{6.1}$$

and

$$g_j(\vec{X}) \leq 0 \ , \quad j = 1, 2, \ldots, m$$

This problem is converted into an unconstrained minimization problem by constructing a function of the form

$$\phi(\vec{X}, r_k) = f(\vec{X}) + r_k \sum_{j=1}^{m} \overline{G}\ g_j(\vec{X}) \tag{6.2}$$

where $\overline{G}$ is some function of the constraints.

If the minimization of the ϕ-function is repeated for a sequence of values of the response factor r_k, the solution may be brought to converge to that of the original constrained problem given by equation (6.1).

6.3 Fiacco-McCormick Interior Penalty Function Method

In this method, the objective function is augmented with a penalty term consisting of the constraints as

$$\phi(\vec{X}, r_k) = f(X) - r_k \sum_{j=1}^{m} \frac{1}{g_j(\vec{X})} \tag{6.3}$$

where $\phi(\vec{X}, r_k)$ is called the penalty function. The minimization of ϕ-function is performed for a decreasing sequence of r_k so that

$$r_{k+1} < r_k \tag{6.4}$$

Equation (6.3) requires a feasible starting point and, in the present work, it is found by a process of trial and error. Since each of the designs generated during the optimization

process lies inside the acceptable design space, the method is classified as interior penalty function formulation.

6.4 Davidon-Fletcher-Powell Variable Metric Unconstrained Minimization Method

In the penalty function formulations, since a sequence of unconstrained minimizations has to be performed, the selection of an efficient method of unconstrained minimization becomes very important. All the methods of unconstrained minimization find a sequence of improved approximations to the optimum according to the iteration:

$$\vec{X}_{i+1} = \vec{X}_i + \tau^* \vec{S}_i \qquad (6.5)$$

where

$\vec{X}_{i+1}$ = the design vector corresponding to the minimum of $\emptyset$-function along the current search direction $\vec{S}_i$

$\vec{X}_i$ = the starting design vector

τ^* = the minimizing step length in the direction $\vec{S}_i$.

There are several methods available for finding the search direction $\vec{S}_i$ in equation (6.5).

In the present work, the Davidon-Fletcher-Powell Variable Metric method[98] is used. This method can be considered as a quasi-Newton algorithm, and is a very powerful general procedure for finding a local unconstrained minimum of a

function of many variables[99]. In this method, the i^{th} search vector $\vec{S}_i$ in equation (6.5) is computed as follows:

$$\vec{S}_i = -[H_i]\,\nabla\phi(\vec{X}) \tag{6.6}$$

where $\phi(\vec{X}_i)$ denotes the gradient of the ϕ-function at $\vec{X}_i$ and $[H_i]$ is a positive definite symmetric matrix. The matrix $[H_i]$ is updated according to the following procedure:

$$[H_{i+1}] = [H_i] + [A_i] + [B_i] \tag{6.7}$$

where

$$[A_i] = \frac{\tau^* \vec{S}_i \vec{S}_i^T}{\vec{S}_i^T \vec{V}_i} \tag{6.8}$$

$$[B_i] = \frac{[H_i]\,\vec{V}_i \vec{V}_i^T [H_i]^T}{\vec{V}_i^T [H_i]\,\vec{V}_i} \tag{6.9}$$

and

$$\vec{V}_i = \nabla\phi(\vec{X}_{i+1}) - \nabla\phi(\vec{X}_i) \tag{6.10}$$

The updating of $[H_i]$ preserves the symmetric positive definiteness of $[H_{i+1}]$ which ensures the stability of the procedure. The positive definiteness of $[H_{i+1}]$ is influenced only by the accuracy with which τ^* is determined. To start with $[H_o]$ is taken as the identity matrix in the present work.

6.5 One Dimensional Minimization Method

In the present work, the one dimensional minimization is accomplished by cubic interpolation method. In this method, the algorithm used to compute τ^* is reapplied until the cosine of the angle between the vectors $\vec{S}_i$ and $\nabla\phi_{i+1}$ at the minimizing step length τ^* is sufficiently small (ε), i.e.

$$\cos\bar{\theta} = \frac{\vec{S}_i^T \cdot \nabla\phi_{i+1}}{|\vec{S}_i| \cdot |\nabla\phi_{i+1}|} < \varepsilon \quad , \tag{6.11}$$

This ensures that $\vec{X}_{i+1}$ is the minimum along the direction $\vec{S}_i$. In the present work, the value of ε is taken as 0.05. However to reduce the computer time, the number of cubic interpolations is limited to three.

6.6 Additional Considerations and Convergence Criteria

(i) Starting point $\vec{X}_o$

For the minimization of $\phi(\vec{X}, r_1)$, the starting feasible point $\vec{X}_o$ is found by a process of trial and error. Each subsequent stage used the solution of the previous stage as a starting point. In some cases, the overall procedure may be accelerated by employing an extrapolation technique[99] to determine starting points for subsequent unconstrained minimization cycles (after two or more minimization stages have been completed). Starting points obtained by extrapolation must be

checked to ensure that they satisfy the constraints, because at each stage, it is necessary to start the unconstrained minimization of $\phi(\vec{X}, r_k)$ from an acceptable design point.

(ii) Initial value of r_k

If r_1 is large, the function is easy to minimize, but the minimum may lie far from the desired solution of the original constrained minimization problem. On the other hand, if r_1 is small the function will be hard to minimize. In the present work, the value of r_1 is chosen such that

$$1.25f(\vec{X}) \leq \phi(\vec{X}_o, r_1) \leq 2.00f(\vec{X}_o) \tag{6.12}$$

(iii) Subsequent values of r_k

The total number of r_k's to be employed is given as an input to the problem and the values of r_{k+1} are found by using the ratio

$$\frac{r_{k+1}}{r_k} = 0.1 \tag{6.13}$$

(iv) Initial positive definite matrix $[H_o]$

The identity matrix $[I]$ is used for the initial $[H_o]$.

(v) Updating the $[H_i]$ matrix

Whenever the cosine of the angle between $\vec{S}$ and $\nabla\phi$ is less than -0.1, the matrix $[H_{i+1}]$ is taken as $[H_i]$. Otherwise equation (6.7) is used to find $[H_{i+1}]$.

(vi) Restarting the [H] matrix

In the case of highly distorted or eccentric functions, it might occur after few iterations that $\vec{S}_i^T \cdot \nabla\emptyset_i$ is positive, indicating that $\vec{S}_i$ is not a direction of descent. When this happens, the remedy is to set $[H_i]$ back to H_o and proceed as if starting over again.

(vii) Termination of minimization of each r_k

For each r_k, the minimization of the $\emptyset$-function is terminated whenever the predicted percentage difference between the current and the optimal $\emptyset$-values is less than a small number. Thus the convergence criterion can be expressed as

$$\frac{\nabla\emptyset_i^T [H_i] \nabla\emptyset_i}{2\emptyset_i} = \frac{\vec{S}_i^T \nabla\emptyset_i}{2\emptyset_i} < \varepsilon \qquad (6.14)$$

where ε is a small quantity. The value of ε used in the present work varied from about 0.10 for r_1 to 0.0005 for higher r_k.

(viii) Gradient of $\emptyset$-function

The gradient of the $\emptyset$-function can be expressed as

$$\nabla\emptyset = \nabla f + r \sum_{j=1}^{m} \frac{1}{g_j^2} \cdot \nabla g_i \qquad (6.15)$$

However the gradient of the $\emptyset$-function has been calculated by using the backward difference formula in the present work. An

efficient method of evaluating the gradients of static deflection, natural frequencies and eigen vectors has been suggested by Reddy[100].

(ix) Number of cubic interpolations

A maximum of five cubic interpolations are allowed in each one dimensional search problem. Out of these, only the final interpolation involves the evaluation of the gradient $\nabla\phi$. All preliminary interpolations use a perturbation scheme to determine the dot product $\vec{S}^T \cdot \nabla\phi$ as

$$\vec{S}^T \cdot \phi = \frac{\phi(\tau^+) - \phi(\tau^-)}{(\tau^+ - \tau^-)} \tag{6.16}$$

where τ^+ and τ^- define the step length.

(x) Kuhn-Tucker conditions

Before stopping the minimization process of any problem, the Kuhn-Tucker conditions are tested as the necessary conditions for the optimum. Mathematically these conditions can be expressed by:

$$\frac{\partial f}{\partial X_i} + \sum_{j \in J} \lambda_j \frac{g_j}{X_i} = 0 , \quad i = 1, 2, \ldots, n \tag{6.17}$$

$$\lambda_j \geq 0 , \quad j \in J \tag{6.18}$$

where λ_j are called the Kuhn-Tucker multipliers and J is the set of indices of active constraints. It is important to note

that the Kuhn-Tucker conditions are necessary and sufficient for a global minimum only in the case of convex programming problems. However, equations (6.17) and (6.18) can be used as the necessary conditions to test the minimum of any practical design problem.

(xi) Relative minima

In order to see whether any relative minima exists in the design space, two completely different starting points may be used for the sequence of minimizations for any example. If the two sequences lead to the same optimum design (except for a small difference that might occur due to numerical instability), it can be assumed that local optimum is same as the global optimum.

(xii) Reducing the total computational time

It has been observed that some of the automated optimum design problems take longer time to satisfy the prescribed convergence criteria even after reaching very near to the optimum design point. This happens whenever the function being minimized is highly distorted or eccentric. In such cases, it may not be worthwhile to try to reach the exact minimum to obtain about 0.5 or 1% decrease in the objective at the expense of 40 to 50% more computing time. This type of situation can be identified by manually inspecting the progress of the optimization path at various stages.

CHAPTER 7

NUMERICAL EXAMPLES AND SENSITIVITY ANALYSIS

A computer program has been developed to implement the optimization procedure described in Chapter 6. The program contains twenty one subroutines along with the main program. The details of the subroutines and their calling sequence are discussed in Appendix E. The program developed is quite general and can be used for the optimization of any axial flow turbine. Other problems in the area of design of turbomachines can also be solved by making slight modifications to the present program. The flow diagram for Cholesky decomposition of symmetric banded matrices used to obtain a partial solution to the eigen value problem has been also shown in Appendix E. To demonstrate the effectiveness and flexibility of the program developed, the design of an axial flow gas turbine stage is considered. The problem is solved with different objective functions under different constraint sets. The data pertinent to the design of the stage along with the material properties of blades and gas properties are given in Table 7.1.

7.1 Maximization of Isentropic Stage Efficiency

The maximization of isentropic stage efficiency or minimization of losses is considered as the first example. The effects of rotation, taper and twist of the blade are considered

in the finite element idealization. Since the effects of shear deformation and rotary inertia on the first natural frequency are expected to be very small, they have been neglected during computations to save computer time (by reducing the nodal degrees of freedom by fifty percent). The components of the design vector are taken as:

X_1 = Mean diameter of rotor

X_2 = Ratio of the chord of rotor blade to mean diameter

X_3 = Ratio of the chord of nozzle blade to mean diameter

X_4 = Ratio of spacing to diameter at mean radius of the nozzle blades

X_5 = Ratio of spacing to diameter at mean radius of rotor blades

X_6 = Relative angle of the velocity triangle at inlet of the rotor blade at mean radius

X_7 = Relative angle of the velocity triangle at the exit of the rotor blade at mean radius

X_8 = Axial velocity of flow across the stage.

The constraints of the problem can be stated as follows:

$$g_1 = \frac{50}{U} - 1.0 \leq 0 \tag{7.1}$$

$$g_2 = \frac{U}{400} - 1.0 \leq 0 \tag{7.2}$$

$$g_3 = \frac{h_R}{8d} - X_2 \leq 0 \tag{7.3}$$

$$g_4 = X_2 - \frac{h_R}{2d} \leq 0 \tag{7.4}$$

$$g_5 = \frac{h_N}{10d} - X_3 \leq 0 \tag{7.5}$$

$$g_6 = X_3 - \frac{h_N}{2d} \leq 0 \tag{7.6}$$

$$g_7 = 0.5 - \frac{X_4}{X_3} \leq 0 \tag{7.7}$$

$$g_8 = \frac{X_4}{X_3} - 1.0 \leq 0 \tag{7.8}$$

$$g_9 = 0.5 - \frac{X_5}{X_2} \leq 0 \tag{7.9}$$

$$g_{10} = \frac{X_5}{X_2} - 1.0 \leq 0 \tag{7.10}$$

$$g_{11} = 0.01 - X_6 \leq 0 \tag{7.11}$$

$$g_{12} = X_6 - 1.0 \leq 0 \tag{7.12}$$

$$g_{13} = \frac{40}{57} - X_7 \leq 0 \tag{7.13}$$

$$g_{14} = X_7 - 1.4 \leq 0 \tag{7.14}$$

$$g_{15} = \frac{50.0}{X_8} - 1.0 \leq 0 \tag{7.15}$$

$$g_{16} = \frac{X_8}{400} - 1.0 \leq 0 \tag{7.16}$$

$$g_{17} = \frac{p_{o1}}{p_2} - \frac{p_{o1}}{p_c} \leq 0 \tag{7.17}$$

$$g_{18} = M_{c_3} - 1.0 \leq 0 \tag{7.18}$$

$$g_{19} = \frac{12\alpha}{\pi} \frac{c}{} - 1.5 \leq 0 \tag{7.19}$$

$$g_{20} = 0.25 - \emptyset \leq 0 \tag{7.20}$$

$$g_{21} = \emptyset - 2.0 \leq 0 \tag{7.21}$$

$$g_{22} = 0.5 - \psi \leq 0 \tag{7.22}$$

$$g_{23} = \psi - 6.0 \leq 0 \tag{7.23}$$

$$g_{24} = 0.3 - R \leq 0 \tag{7.24}$$

$$g_{25} = R - 0.7 \leq 0 \tag{7.25}$$

$$g_{26} = \frac{40}{57} - \alpha_2 \leq 0 \tag{7.26}$$

$$g_{27} = 0.01 - R_{root} \leq 0 \tag{7.27}$$

$$g_{28} = \frac{N}{\omega(1)} - 1.0 \leq 0 \tag{7.28}$$

$$g_{29} = \frac{\sigma}{0.30x10^9} - 1.0 \leq 0 \tag{7.29}$$

$$g_{30} = \frac{\Delta_t}{0.05\ h_R} - 1.0 \leq 0 \tag{7.30}$$

The starting values of the design variables are taken as $X_1 = 0.432$, $X_2 = 0.046$, $X_3 = 0.040$, $X_4 = 0.035$, $X_5 = 0.044$, $X_6 = 20.5°$, $X_7 = 54.57°$ and $X_8 = 272.0$.

The upper and lower bounds as well as the optimum values of the design variables are shown in Table 7.2. The bounds on the behavior constraints and the values of the response quantities at the starting and optimum designs are shown in Table 7.3. The progress of the optimization path, showing the cumulative number of one dimensional minimizations versus objective function (losses or one minus efficiency) is shown in Figure 7.1. In this figure, the variation of penalty function and mass of the stage has also been represented. The results of optimization show that there is a 30.5% reduction in the objective function. The optimum point corresponds to an increase in the efficiency of the stage by 2.48% and a reduction in weight of the stage by 55.3% compared to the starting design vector. None of the side constraints is active at the optimum point. The constraints on stress and degree of reaction at root have become active (out of the behavior constraints) at the optimum point. It can be observed that X_3, X_4 and X_5 have not changed much from starting point while the other variables show appreciable change from the initial starting point. The optimum point has been found with 3 values of r_k in 15 one dimensional minimization steps which required about 61 minutes of computer time on an IBM 7044 computer.

Although the point obtained at the end of 15 one dimensional steps (with 3 values of r_k) can be taken as the optimum (evident from Figure 7.1), the minimization is carried

for three more values of r_k which required an additional computational time of 70 minutes. The results obtained with 6 values of r_k are compared with those obtained with 3 values of r_k in Tables 7.2 and 7.3. It can be seen that while the first 3 values of r_k reduced the objective function (one minus efficiency) from 0.0813 to 0.0565, the additional 3 values of r_k could reduce it to 0.0557 only. Thus no significant reduction in the objective could be achieved by proceeding beyond 3 values of r_k. Since this behavior is characteristic of the interior penalty function method, all the subsequent examples are solved by using 3 values of r_k only.

In order to test whether the optimum point found corresponds to a local minimum or the absolute minimum in the design space, the same example has been solved with a second starting design vector whose components are $X_1 = 0.276$, $X_2 = 0.056$, $X_3 = 0.068$, $X_4 = 0.059$, $X_5 = 0.028$, $X_6 = 18.6°$, $X_7 = 52.5°$ and $X_8 = 252.7$. The progress of the optimization path is shown in Figure 7.2. This plot is similar to Figure 7.1 and the optimum point obtained ($f = 0.0543$) also compares well with that of the previous case ($f = 0.0557$). The starting and the optimum designs of the two cases are compared in Tables 7.2 and 7.3. The optimum design variables are also in good agreement with each other. Apart from a small difference that might have occurred due to numerical instability, the two optimum points appear to be same. Although, merely on the

basis of two trial starting designs, it is hard to say that the minimum obtained is the absolute minimum over the design space; finding the similar optimum design by starting from two different initial designs is at least a pointer in that direction.

7.2 Minimization of Weight

In the second example, the optimization of weight (mass) of the axial flow gas turbine stage is considered. The effects of rotation, taper and twist of the blade are considered in the deflection and vibration analysis of blades. The constraints, design variables and their bounds are same as in the case of the first example (first starting point).

The optimization results are shown in Tables 7.2 and 7.3. The progress of the optimization path, showing the cumulative number of one dimensional minimizations versus the objective function is shown in Figure 7.3. The optimization results show that there is a 80.5% reduction in the objective function (mass). Out of all the side and behavior constraints, only the degree of reaction at root and the stress at the root of the rotor blade have become active at the optimum point. Comparatively X_6, X_7 and X_8 have not changed much from their initial starting values. From Figure 7.3 it can be observed that the losses decreased by small amount first and then increased at a faster rate. This indicates that the reduction in weight can be obtained only at the cost of efficiency. For

this example, the computer time required is 60 minutes on an IBM 7044 computer for 15 one dimensional minimization steps.

7.3 Optimization of Weighted Combination of Efficiency and Mass

The minimization of a weighted sum of efficiency and weight (mass) of the gas turbine stage is considered in the third example. The constraints, design variables and their bounds are same as in the case of example 2. The blade has been idealized as a rotating, tapered and twisted cantilever beam by neglecting the effects of shear deformation and rotary inertia. The magnitude of losses and mass (weight) of the stage are normalized such that their contributions will be equal at the starting design point. The optimization results are given in Tables 7.4 and 7.5. The progress of the optimization path is shown in Figure 7.4, where the variations of penalty function, losses and mass of the stage with the number of one dimensional minimizations are shown. It is observed that there is a 45% reduction in the objective function while the efficiency increased by 1.65% and the weight reduced by 69.5%. The variables X_4, X_6 and X_7 have not changed much from the starting point. The constraints on the degree of reaction at the root and the stress have become active at the optimum point. It can be seen that the reduction in losses or mass of the stage is less in this case compared to the case where the individual objective function is considered

for optimization. Thus the present results indicate a compromise between efficiency and mass of the stage. Here 15 one dimensional minimization steps required about 62 minutes of computer time on an IBM 7044 computer.

7.4 Optimization of Weighted Combination of Mass and Efficiency (Without Considering Rotation)

In the fourth example, the minimization of weighted sum of efficiency and mass (weight) of the stage is considered. The rotor blade has been idealized by using four tapered and twisted beam elements. The effect of rotation has not been included while computing eigen values of the idealized blade. The shear deformation and rotary inertia effects have also been neglected.

The optimization results of this problem are shown in Tables 7.4 and 7.5. The progress of the optimization path, showing the values of penalty function, objective function, losses and weight versus the number of one dimensional minimization steps is shown in Figure 7.5. In this case, the objective function has decreased by 43%, efficiency has increased by 1.68% and the mass of the stage has decreased by 65.5%. Most of the variables behaved as in the case of third example. The degree of reaction at the root and the stress at the root have become active at the optimum point. The program required about 61 minutes of computer time for 15 one dimensional minimization steps.

7.5 Optimization of Weighted Combination of Efficiency and Mass by Considering Only the Side Constraints

In the fifth problem, a linear combination of the mass and the losses of the stage has been minimized with equal contribution of losses and mass at the starting design point. Only the side constraints (g_1 to g_{16}) are considered with no constraints on the behavior (response) quantities in the problem formulation and solution. The blade has been idealized with four finite elements and the effects of rotation, shear deformation and rotary inertia have been neglected.

The optimization results are shown in Tables 7.4 and 7.5. The progress of optimization path, showing the cumulative number of one dimensional minimizations versus the values of objective function, losses and mass is shown in Figure 7.6. It is found that the objective function was reduced by 47.6% while there is an increase of 2.1% in efficiency and a reduction of 69.3% in mass of the stage. It is observed that although the objective function (losses as well as mass of the stage) has been reduced by a larger amount, the behavior quantities like stress, degree of reaction at root and tip deflection have become larger than the permissible values. This clearly demonstrates the necessity of putting bounds on these response quantities. The program required only about 20 minutes of computer time on IBM 7044 computer for 15 one dimensional minimization steps in this case.

7.6 Sensitivity Analysis

In practice a designer would be interested in knowing how the response quantities vary with a change in the design variables. This type of sensitivity analysis will help the designer in manipulating the design variables to suit some specific requirements. Further, in some cases, the results obtained from the optimization procedure may have to be rounded-off to the nearest practical values of the design variables. Hence a sensitivity analysis of response quantities, namely, objective function, losses, mass, stress, degree of reaction at root and mean radius, first natural frequency, flow coefficient, stage temperature drop coefficient and angle of nozzle blade at outlet, with respect to the various design variables is conducted. In this analysis, the reference design is taken same as the optimum point of example three (section 7.3). The design variables are varied on the negative and positive sides of the reference (optimum) values and the magnitudes of the behavior quantities are plotted against the percentage changes of the design variables in Figures 7.7 to 7.15.

From Figure 7.7 it is observed that the objective function (weighted combination of losses and mass) is quite sensitive to variations in X_1, X_2, X_4 and X_5. The sensitivity of the two components of objective function is shown in Figures 7.8 and 7.9. Figure 7.8 shows that losses are more sensitive to the variables X_2, X_3, X_4 and X_5 compared to the

other four variables. Similarly Figure 7.9 indicates that mass of the stage is more sensitive to the diameter of the turbine compared to the variables X_2, X_7 and X_8. The mass is almost independent of the variables X_3, X_4, X_5 and X_6.

The sensitivity of mechanical response quantities, namely, stress, deflection and fundamental natural frequency with respect to the various design parameters is shown in Figures 7.10 to 7.12. It can be observed that all these quantities are most sensitive to the variables X_1 and X_7 and less sensitive to the other variables.

Figures 7.13 to 7.15 represent the variation of the aerodynamic response quantities, namely, degree of reaction at root, flow coefficient, stage temperature drop coefficient, stator blade angle at outlet and degree of reaction at mean radius with a percentage change in design variables. It can be seen (Figure 7.13) that the degree of reaction at root is more sensitive to the variables X_7 and X_8 compared to the other variables. The stage temperature drop coefficient is found (Figure 7.14) to be quite sensitive to X_1, X_6, X_7 and X_8, and independent of the variables X_2, X_3, X_4 and X_5. The flow coefficient is found to increase (decrease) with increasing values of $X_8(X_1)$ while it is independent of the remaining six variables. Figure 7.15 represents the sensitivity analysis of degree of reaction at mean radius and gas outlet angle of stator blades. It is seen that the degree of reaction is most

sensitive to the variable X_7, less sensitive to X_1, X_6 and X_8, and insensitive to the variables X_2, X_3, X_4 and X_5. Similarly the stator blade outlet angle (α_2) is found to be more sensitive to X_1, X_6 and X_8 and insensitive to the remaining variables (X_2, X_3, X_4, X_5 and X_7).

Similar results have been obtained when the optimum point of example 1 (first starting point) is perturbed. These results are shown in tabular form in Table 7.6.

TABLE 7.1

Data for Optimization Problems

Number of design variables, n = 8

Number of constraints = 30

Number of finite elements in a blade = 4

Number of eigen values computed = 2

Number of degrees of freedom of an element = 8 (since shear deformation effect is neglected)

Maximum number of cubic interpolations used in one dimensional minimization = 3

Maximum number of unconstrained minimuzation steps for any value of penalty parameter = 5

Gas constant, $\bar{R}$ = 287 N-m/Kg-K

Viscosity, $\bar{\mu}$ = 4.0×10^{-5} Kg/m-sec

Ratio of specific heats of the gas, γ = 1.333

Density of the blade material, ρ_m = 800 Kg/m^3

Young's modulus of the material, E = 2.0×10^{11} N/m^2

Shear modulus, G = E/2.6

Stagnation pressure of entering gas in the stage,
p_{o1} = 4.0×10^5 N/m^2

Stagnation temperature of entering gas in the stage,
T_{o1} = 1100 K

Mass flow of the gases across the stage = 20 Kg/sec

Rotational speed of the turbine, N = 250 rps

Radial clearance of the blades, $\bar{k}$ = .000154 m

Breadth taper ratio, β = 2.0

Depth taper ratio, α = 1.5

Shear coefficient, μ = .833

TABLE 7.2

Initial and Optimum Design Variables for Examples 1 and 2

Design variable	Bounds		Maximization of efficiency (Example 1)					Minimization of weight (Example 2)	
			First starting point			Second starting point			
	Lower	Upper	Initial point	Optimum point with 3 r_k	Optimum point with 6 r_k	Initial point	Optimum point	Initial point	Optimum point
X_1	0.064	0.512	0.432	0.3378	0.3370	0.276	0.3254	0.432	0.2764
X_2	0.020	0.080	0.046	0.0611	0.0609	0.056	0.0656	0.046	0.0559
X_3	0.016	0.080	0.040	0.0473	0.0462	0.068	0.0438	0.040	0.0683
X_4	0.008	0.080	0.035	0.0335	0.0322	0.059	0.0309	0.035	0.0595
X_5	0.010	0.080	0.044	0.0428	0.0425	0.028	0.0474	0.044	0.0284
X_6	0.600°	57.0°	20.5°	15.4°	15.2°	18.6°	11.9°	20.5°	18.7°
X_7	40.000°	80.0°	54.57°	59.5°	58.9°	52.5°	58.8°	54.57°	52.8°
X_8	50.000	400.000	272.0	191.4	188.2	252.7	187.0	272.0	252.7
Objective function	-	-	0.0813	0.0565	0.0557	0.122	0.0543	29.939	4.223

TABLE 7.3

Response Quantities at Initial and Optimun Points for Example 1 and 2

Response quantities	Bounds		Maximization of efficiency (Example 1)					Minimization of weight (Example 2)	
			First starting point			Second starting point			
	Lower	Upper	Initial point	Optimum point with 3 r_k	Optimum point with 6 r_k	Initial point	Optimum point	Initial point	Optimum point
Pressure ratio, p_{01}/p_2	-	1.853	1.602	1.262	1.266	1.303	1.128	1.602	1.303
Mach number, M_{C_3}	-	1.000	0.465	0.322	0.315	0.453	0.317	0.465	0.453
Annulus angle, α_c	-	22.5°	15.0°	18.9°	16.92°	18.87°	16.5°	15.0°	20.4°
Flow coefficient	0.25	2.0	0.802	0.721	0.71	1.16	0.732	0.802	1.164
Temperature drop coefficient	0.50	6.0	2.89	2.805	2.76	3.854	2.77	2.89	3.854
Reaction at mean radius	0.30	0.70	0.422	0.502	0.4962	0.569	0.538	0.422	0.569
Angle α_2	40.0°	-	58.2°	58.2°	58.92°	50.1°	57.3°	58.2°	49.9°
Root reaction	0.01	-	0.202	0.04	0.0130	0.088	0.052	0.202	0.088
$\omega(1)$ in rps	250.00	-	975.0	542.0	530.0	455.0	515.0	975.0	455.0
Root stress, N/m^2	-	$.3\times10^9$	$.281\times10^9$	$.297\times10^9$	$.299\times10^9$	$.295\times10^9$	$.299\times10^9$	$.281\times10^9$	$.296\times10^9$
Tip deflection, m	-	3.5×10^{-3}	$.304\times10^{-3}$	$.439\times10^{-3}$	$.443\times10^{-3}$	$.843\times10^{-3}$	$.457\times10^{-3}$	$.304\times10^{-3}$	$.843\times10^{-3}$
OBJ1	-	-	0.0813	0.565	0.0557	0.122	0.0543	0.813	0.122
OBJ2	-	-	21.94	9.80	9.585	4.22	8.818	21.94	4.223

TABLE 7.4

Initial and Optimum Design Variables for Minimization of Weighted Combination of Losses and Mass

Design variables	Bounds		Initial point	Optimum points		
	Lower	Upper		Example 3 (with rotation)	Example 4 (without rotation)	Example 5 (with side constraints only)
X_1	0.064	0.512	0.432	0.3055	0.3117	0.285
X_2	0.020	0.080	0.046	0.0579	0.0615	0.0464
X_3	0.016	0.080	0.040	0.0475	0.0441	0.0457
X_4	0.008	0.080	0.035	0.0338	0.0304	0.0321
X_5	0.010	0.080	0.044	0.390	0.408	0.0327
X_6	0.600°	57.0°	20.5°	19.8°	19.8°	19.5°
X_7	40.0°	80.0°	54.57°	54.8°	54.8°	54.8°
X_8	50.0	400.0	272.0	232.9	231.0	218.2
Objective function	-	-	0.162	0.0895	0.0928	0.0853

TABLE 7.5

Initial and Optimum Response Quantities for Minimization of Weighted Combination of Losses and Mass

Response quantities	Bounds		Initial point	Optimum points		
	Lower	Upper		Example 3 (with rotation)	Example 4 (without rotation)	Example 5 (with side constraints only
Pressure ratio, p_{01}/p_2	-	1.853	1.602	1.309	1.313	1.076
Mach number, M_{C_3}	-	1.0	0.465	0.407	0.400	0.395
Annulus angle, $_c$	-	22.5°	15.0°	20.3°	18.5°	21.0°
Flow coefficient	0.25	2.0	0.802	0.971	0.944	0.954
Temperature drop coefficient	0.50	6.0	2.89	3.458	3.364	3.399
Reaction of mean radius, R	0.30	0.70	0.422	0.515	0.499	0.5194
Angle, $_2$	40.0°	-	58.2°	54.1°	54.6°	54.4°
Root reaction, R_{root}	0.01	-	0.202	0.0517	0.040	-0.099
First natural frequency in rps	250.0	-	975.0	527.0	408.0	392.0
Root stress in N/m^2	-	0.3×10^9	0.281×10^9	0.298×10^9	0.298×10^9	2.298×10^9
Tip deflection in m	-	3.5×10^{-3}	0.304×10^{-3}	0.683×10^{-3}	1.06×10^{-3}	16.20×10^{-3}
OBJ1	-	-	0.813	0.0648	0.0645	0.0603
OBJ2 in Kg	-	-	21.94	6.65	7.54	6.75

TABLE 7.6

Sensitivity Analysis of Example 1

X_i	Point as a % of X_i	OBJ1	OBJ2	Stress $\times 10^9$ N/m^2	Root reaction	Tip deflection $\times 10^{-3}$, m	First natural frequency, Hz	Flow coefficient	Stage temperature drop coefficient	Angle α_2 radians	Degree of reaction at mean radius
	70	.05638	1.279	.5310	.04084	3.470	229	1.031	4.008	.8945	.7177
	80	.05544	3.158	.3837	.04327	1.436	335	.9018	3.507	.9453	.6280
	90	.05560	5.972	.326	.05706	.753	437	.8016	3.117	.9899	.5582
X_1	110	.05806	14.78	.2828	.06088	.2736	654	.6559	2.550	1.064	.4567
	120	.06009	20.96	.2756	.07318	.1782	771	.6012	2.388	1.095	.4187
	130	.06236	28.47	.273	.07984	.1205	892	.555	2.158	1.122	.3864
	140	.06562	37.39	.275	.0826	.0844	1015	.515	2.004	1.147	.3588
	70	.05895	6.869	.4023	.03984	1.222	465	.721	2.805	1.029	.5024
	80	.06028	7.847	.3533	.03975	.845	489	.721	2.805	1.029	.5024
	90	.05798	8.831	.3203	.0398	.6029	515	.721	2.805	1.029	.5024
X_2	120	.06934	11.570	.2703	.03923	.250	597	.721	2.805	1.029	.5024
	130	.08432	12.690	.2624	.03849	.1947	626	.721	2.805	1.029	.5024
	140	.1034	13.61	.2567	.03750	.1539	652	.721	2.805	1.029	.5024
	70	.05955	9.809	.2977	.0395	.440	542	.721	2.805	1.029	.5024
	80	.06110	9.801	.2979	.03891	.441	542	.721	2.805	1.029	.5024
	90	.05869	9.808	.2977	.0394	.440	542	.721	2.805	1.029	.5024
X_3	120	.06733	9.776	.2987	.03643	.443	539	.721	2.805	1.029	.5024
	130	.08150	9.727	.300	.03193	.4418	535	.721	2.805	1.029	.5024
	140	.1002	9.715	.3019	.0349	.4491	534	.721	2.805	1.029	.5024

Continued...

Table 7.6 (continued)

X_i	Point as a % of X_i	OBJ1	OBJ2	Stress $\times 10^9$ N/m^2	Root reaction	Tip deflection $\times 10^{-3}$, m	First natural frequency, Hz	Flow coefficient	Stage temperature drop coefficient	Angle α_2 radians	Degree of reaction at mean radius
	70	.1073	9.648	.303	.02449	.455	528	.7215	2.805	1.029	.5024
	80	.0737	9.759	.299	.03491	.445	538	.7215	2.805	1.029	.5024
	90	.05934	9.804	.2978	.03907	.4405	542	.7215	2.805	1.029	.5024
X_4	120	.06081	9.800	.2980	.03865	.4409	542	.7215	2.805	1.029	.5024
	130	.06125	9.799	.2980	.03852	.4411	542	.7215	2.805	1.029	.5024
	140	.0615	9.802	.2979	.03884	.4411	542	.7215	2.805	1.029	.5024
	70	.1093	9.721	.2789	.03741	.3148	534	.7215	2.805	1.029	.5024
	80	.7519	9.782	.2840	.03903	.355	540	.7215	2.805	1.029	.5024
	90	.05996	9.808	.290	.03971	.3968	542	.7215	2.805	1.029	.5024
X_5	120	.06076	9.806	.3129	.03968	.527	542	.7215	2.805	1.029	.5024
	130	.06163	9.805	.3212	.03964	.574	542	.7215	2.805	1.029	.5024
	140	.06095	9.806	.3288	.03967	.6185	542	.7215	2.805	1.029	.5024
	70	.05433	9.921	.2917	.1090	.4113	553	.7215	2.682	1.006	.5331
	80	.05500	9.886	.2936	.08646	.4205	550	.7215	2.723	1.014	.52299
	90	.05572	9.850	.2956	.0634	.4300	546	.7215	2.764	1.021	.51276
X_6	120	.05826	9.736	.3017	.00913	.460	536	.7215	2.890	1.044	.48117
	130	.05925	9.695	.3038	.0347	.471	532	.7215	2.934	1.052	.4703
	140	.0603	9.653	.3061	.0610	.482	528	.7215	2.978	1.059	.4691
	70	.06300	10.25	.249	-.500	.2365	588	.721	1.667	1.029	-
	80	.05900	10.16	.259	-.366	.2833	578	.721	1.959	1.029	-
X_7	90	.05675	10.03	.2746	-.1952	.3464	565	.721	2.826	1.029	-
	120	.0729	8.313	.429	1.182	.973	425	.721	4.559	1.029	.9408

Continued...

Table 7.6 (continued)

X_i	Point as a % of X_i	OBJ1	OBJ2	Stress $\times 10^9$ N/m^2	Root reaction	Tip deflection $\times 10^{-3}$, m	First natural frequency, Hz	Flow coefficient	Stage temperature drop coefficient	Angle α_2 radians	Degree of reaction at mean radius
	70	.05055	7.329	.3554	-.718	.494	366	.505	1.96	1.152	-
	80	.05096	8.35	.3288	-.382	.468	428	.577	2.244	1.109	-
	90	.0535	9.166	.3103	-.144	.4514	487	.649	2.525	1.067	-
X_8	120	.06293	10.73	.2836	.3256	.4286	643	.8657	3.366	.9608	.6028
	130	.06600	11.05	.2810	.4462	.429	684	.9379	3.647	.9804	.653
	140	.06887	11.28	.2806	.5593	.4348	718	1.010	3.927	.9022	.7033
Values at optimum point		.05651	9.813	.2976	.03986	.4397	543	.7215	2.805	1.029	.502

At optimum point: $X_1 = .33785$, $X_2 = .0610731$, $X_3 = .0473134$, $X_4 = .0334715$, $X_5 = .042786$, $X_6 = .269043$, $X_7 = .1.03085$, $X_8 = 191.435$.

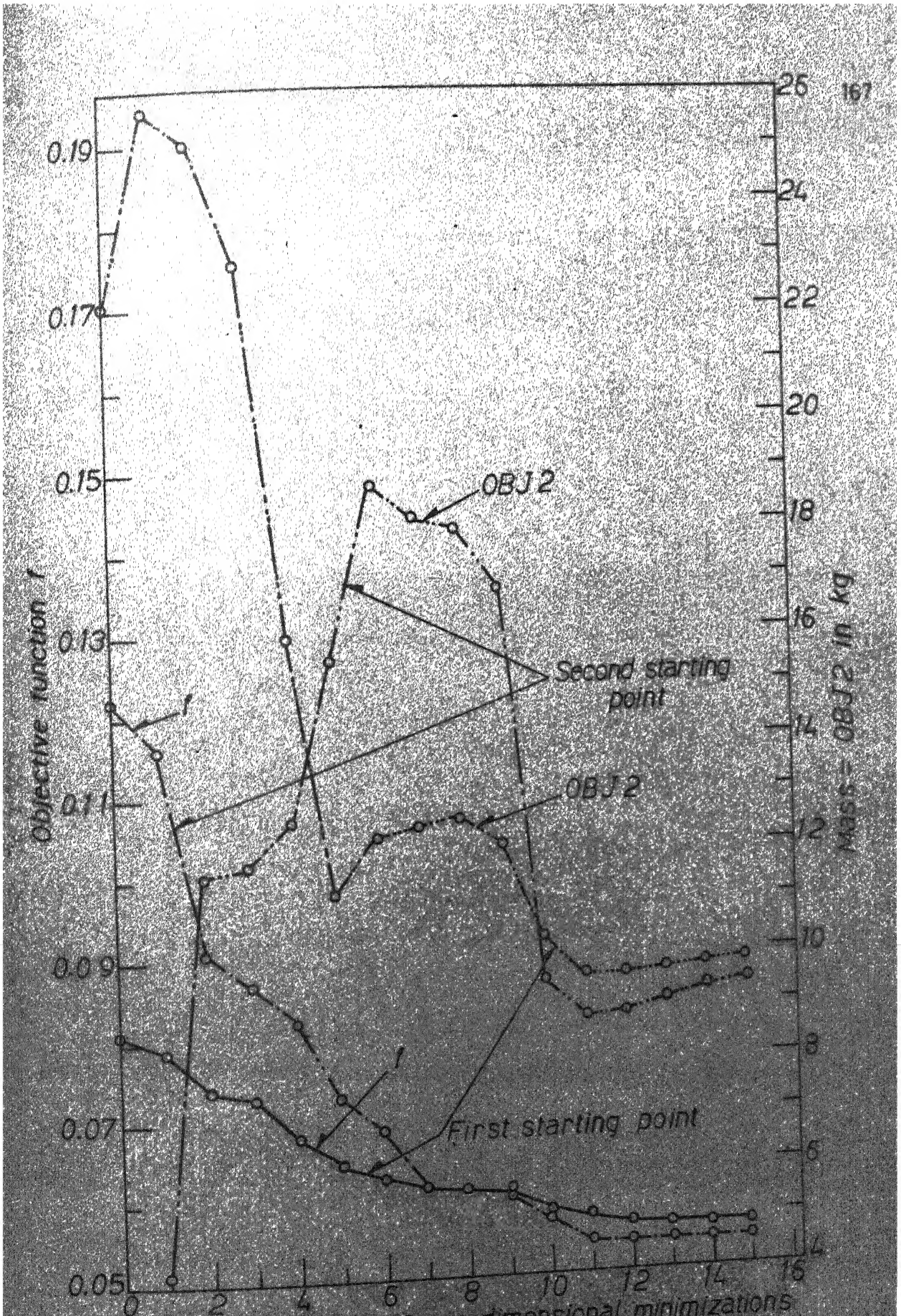

FIG. 7.2 PROGRESS OF OPTIMIZATION PATH FOR EFFICIENCY (SECOND STARTING POINT) AND COMPARISON WITH FIRST STARTING POINT

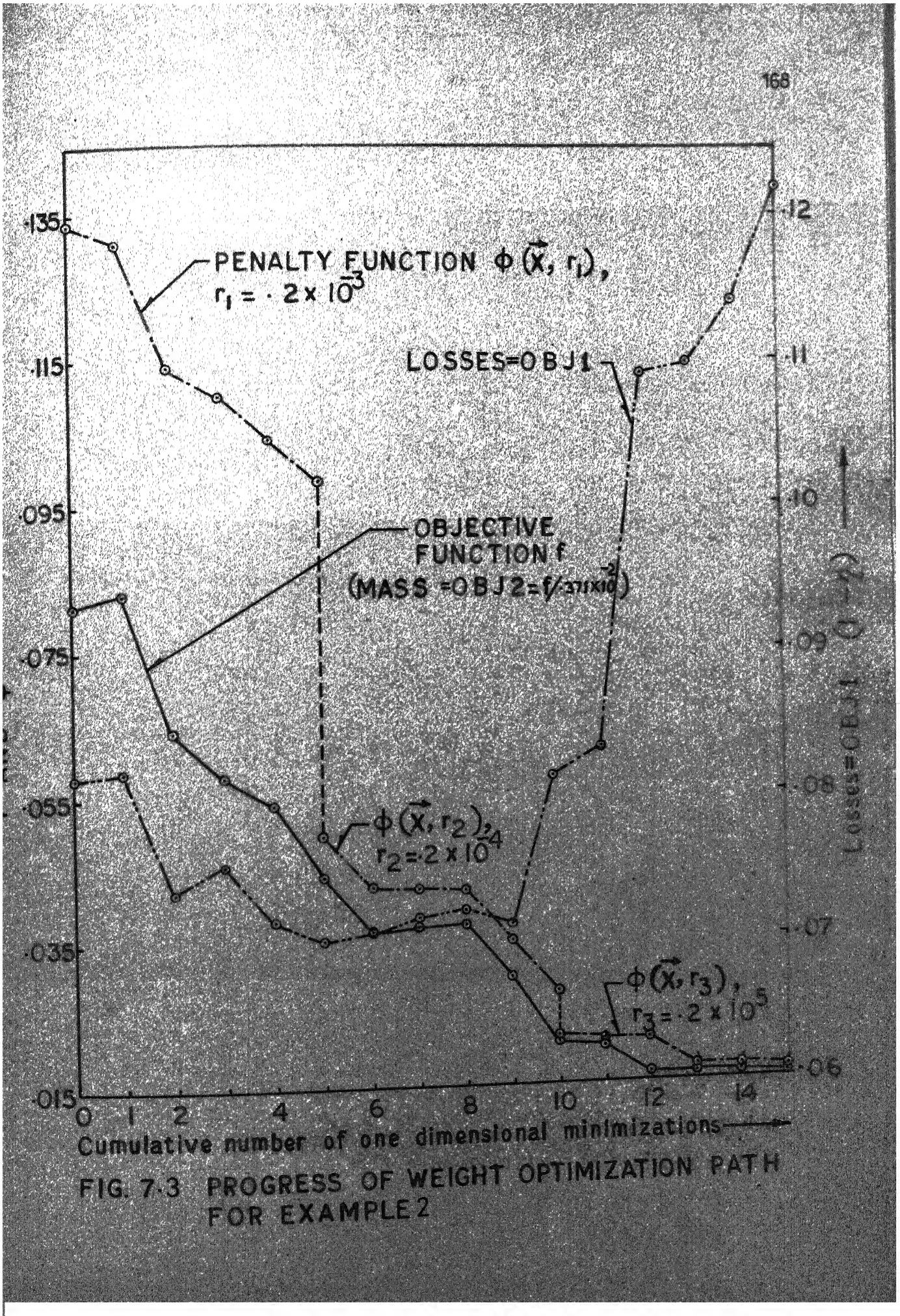

FIG. 7.3 PROGRESS OF WEIGHT OPTIMIZATION PATH FOR EXAMPLE 2

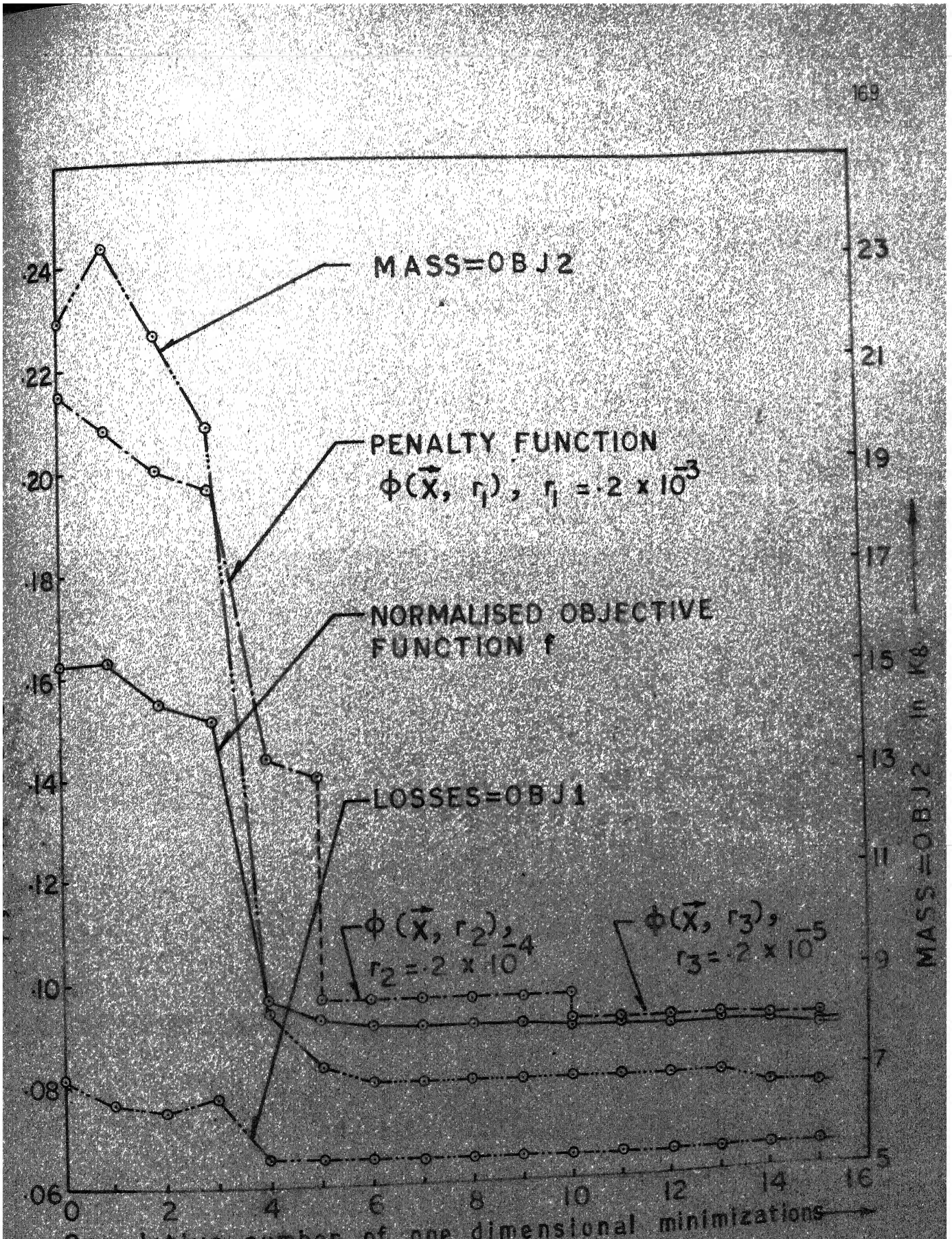

FIG. 7·4 PROGRESS OF OPTIMIZATION PATH (EQUAL WEIGHTAGE TO LOSSES & WEIGHT) FOR EXAMPLE 3

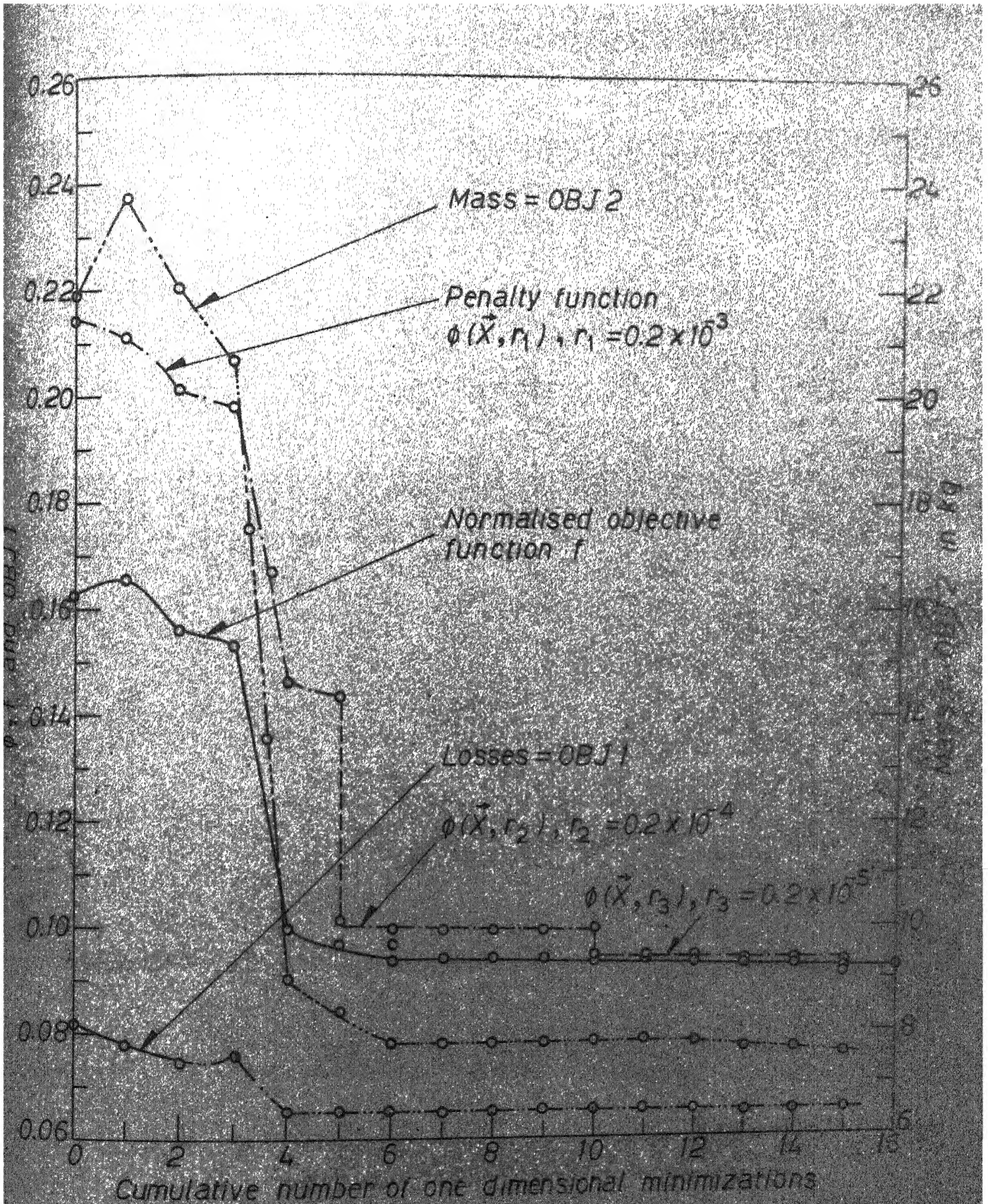

FIG. 7.5 PROGRESS OF OPTIMIZATION PATH (EQUAL WEIGHTAGE TO LOSSES AND MASS) FOR EXAMPLE 4

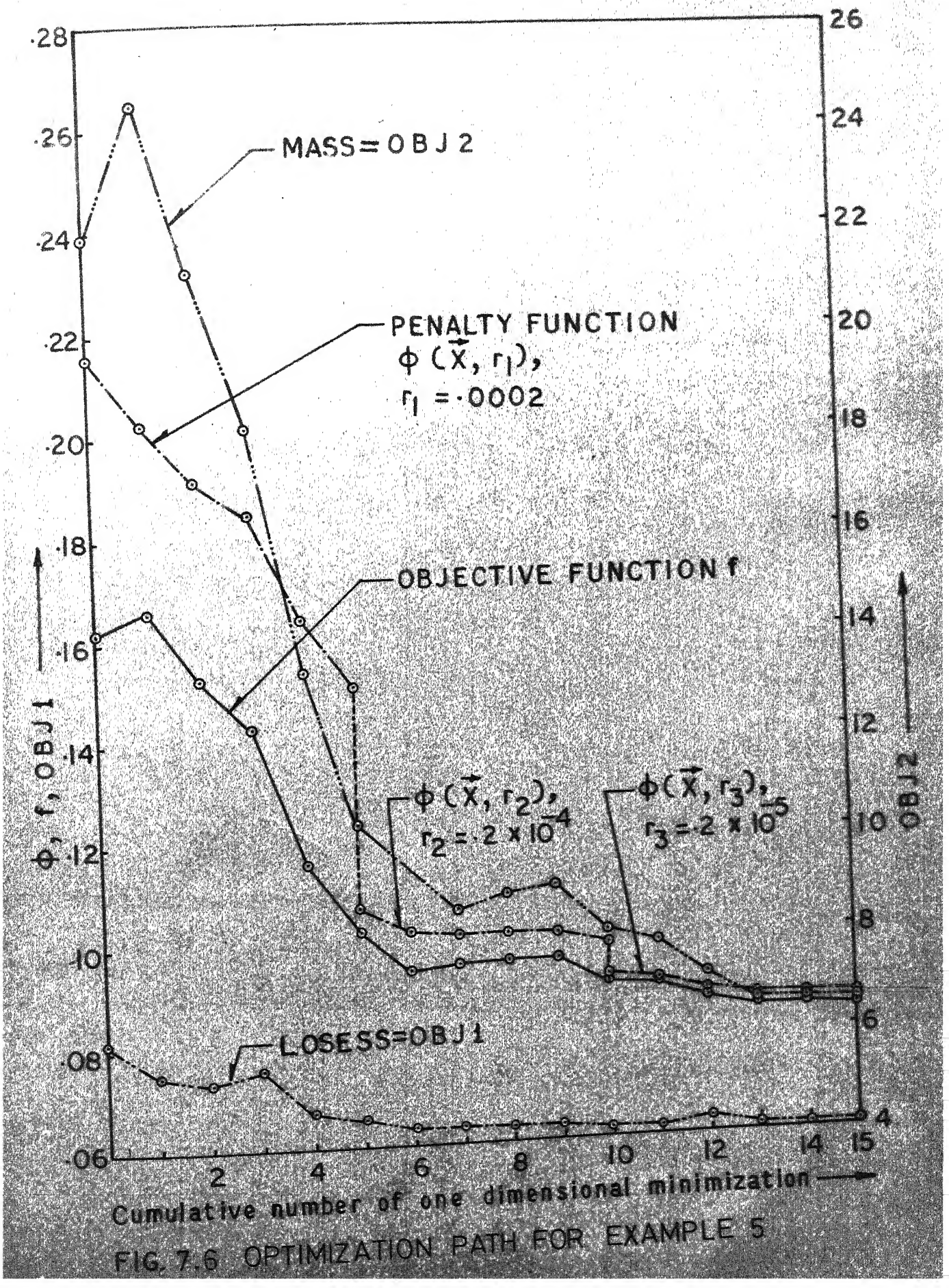

FIG. 7.6 OPTIMIZATION PATH FOR EXAMPLE 5

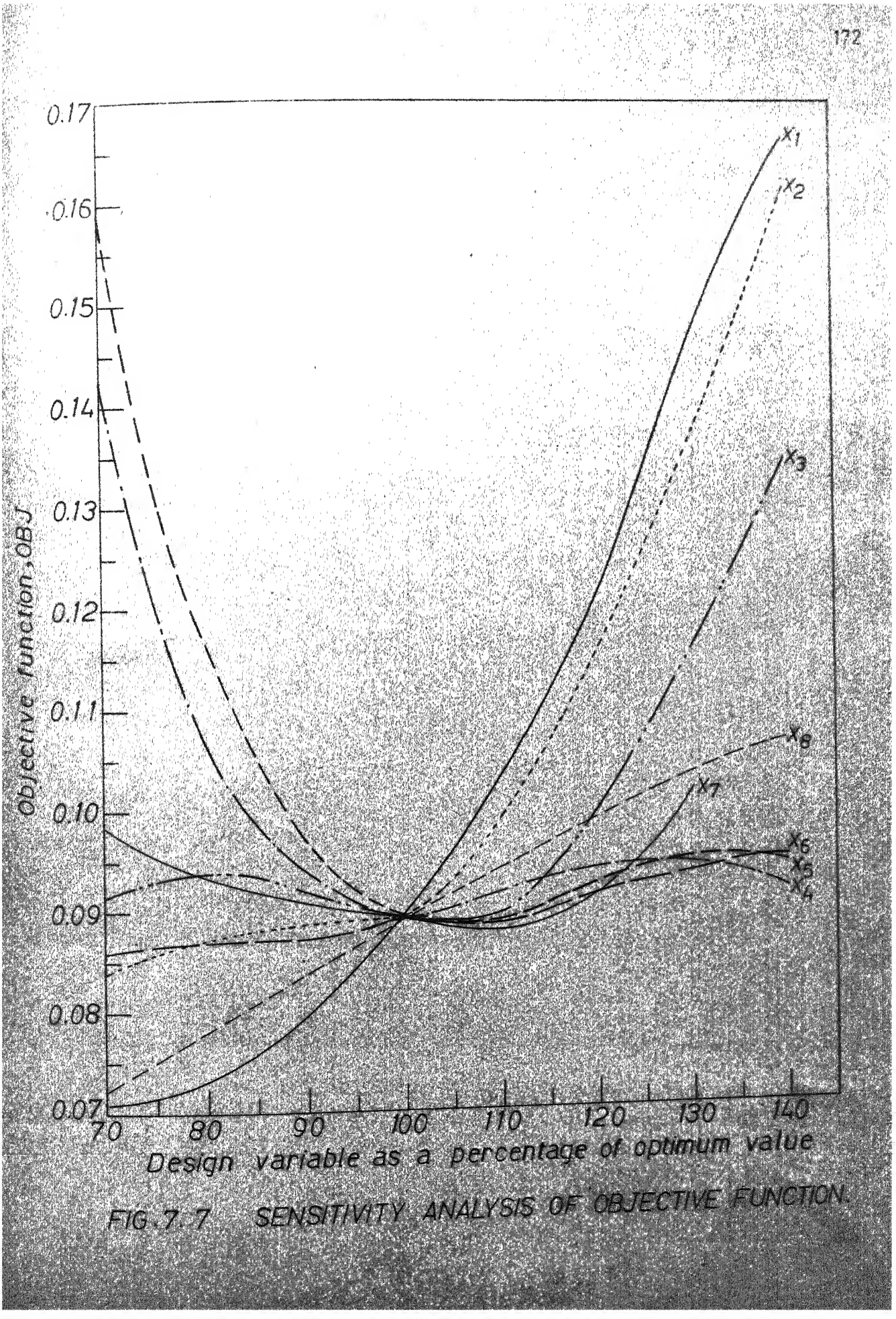

FIG. 7. 7 SENSITIVITY ANALYSIS OF OBJECTIVE FUNCTION.

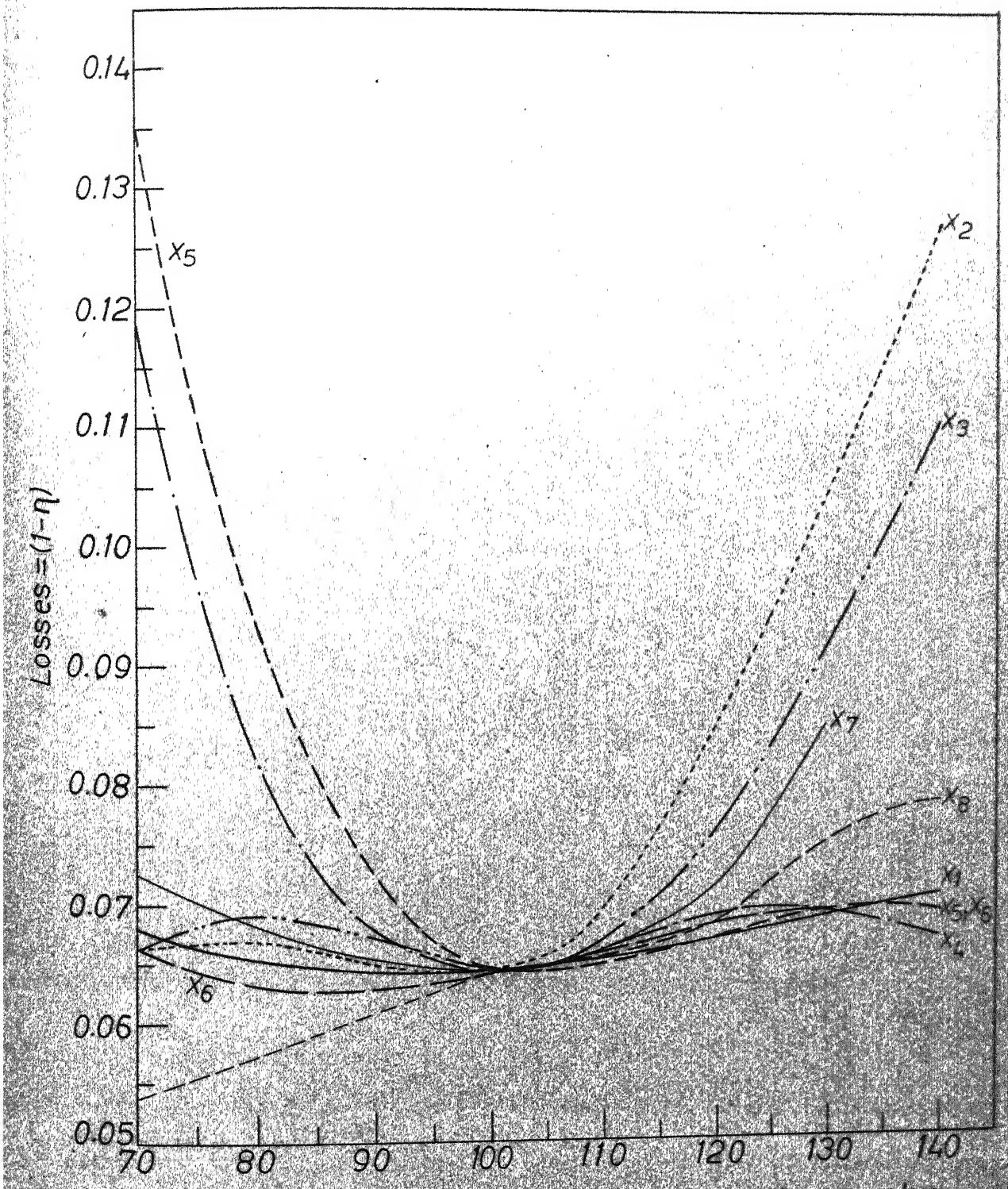

FIG. 7. 8 SENSITIVITY ANALYSIS OF LOSSES.

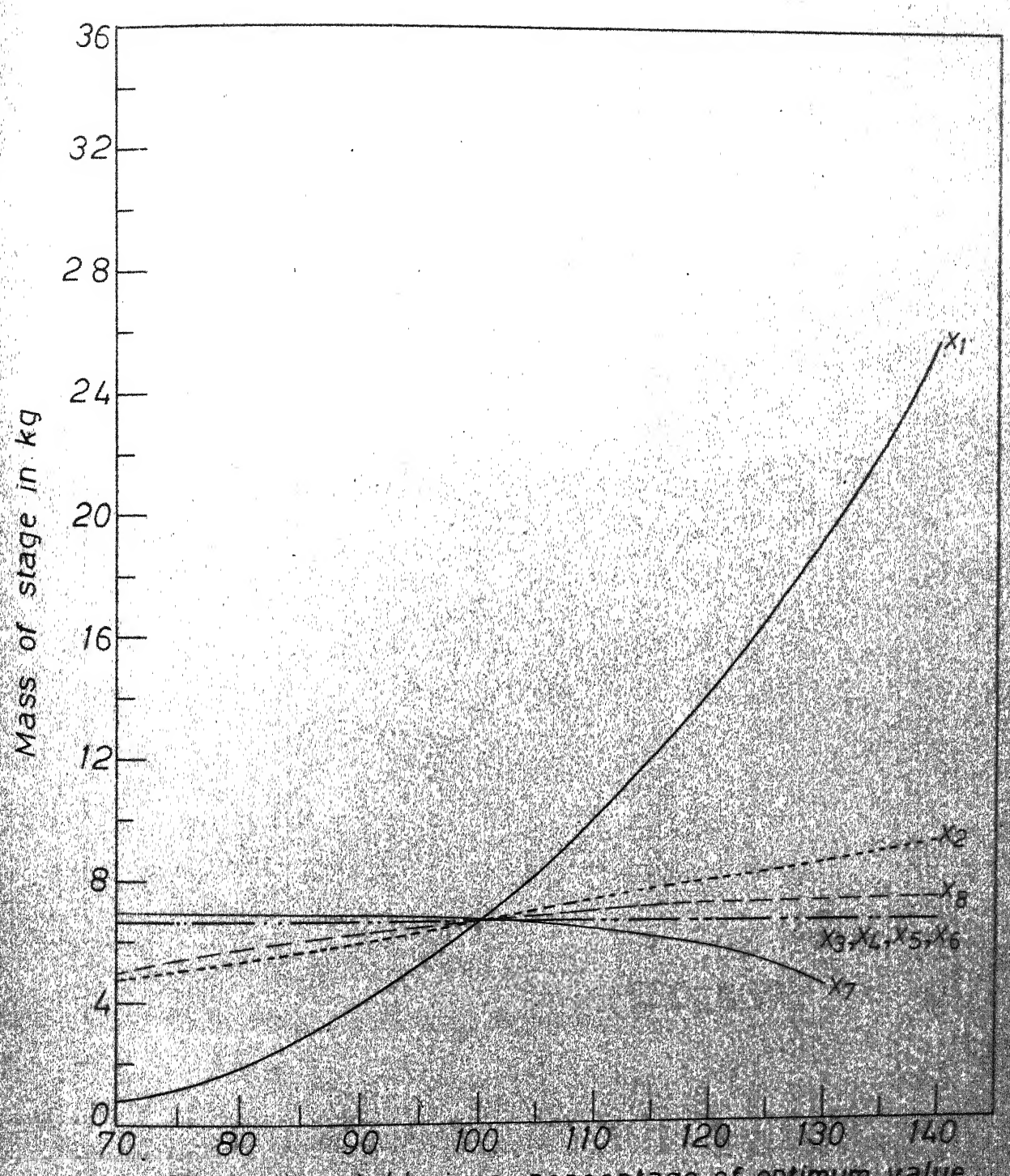

FIG 7.9 SENSITIVITY ANALYSIS OF MASS

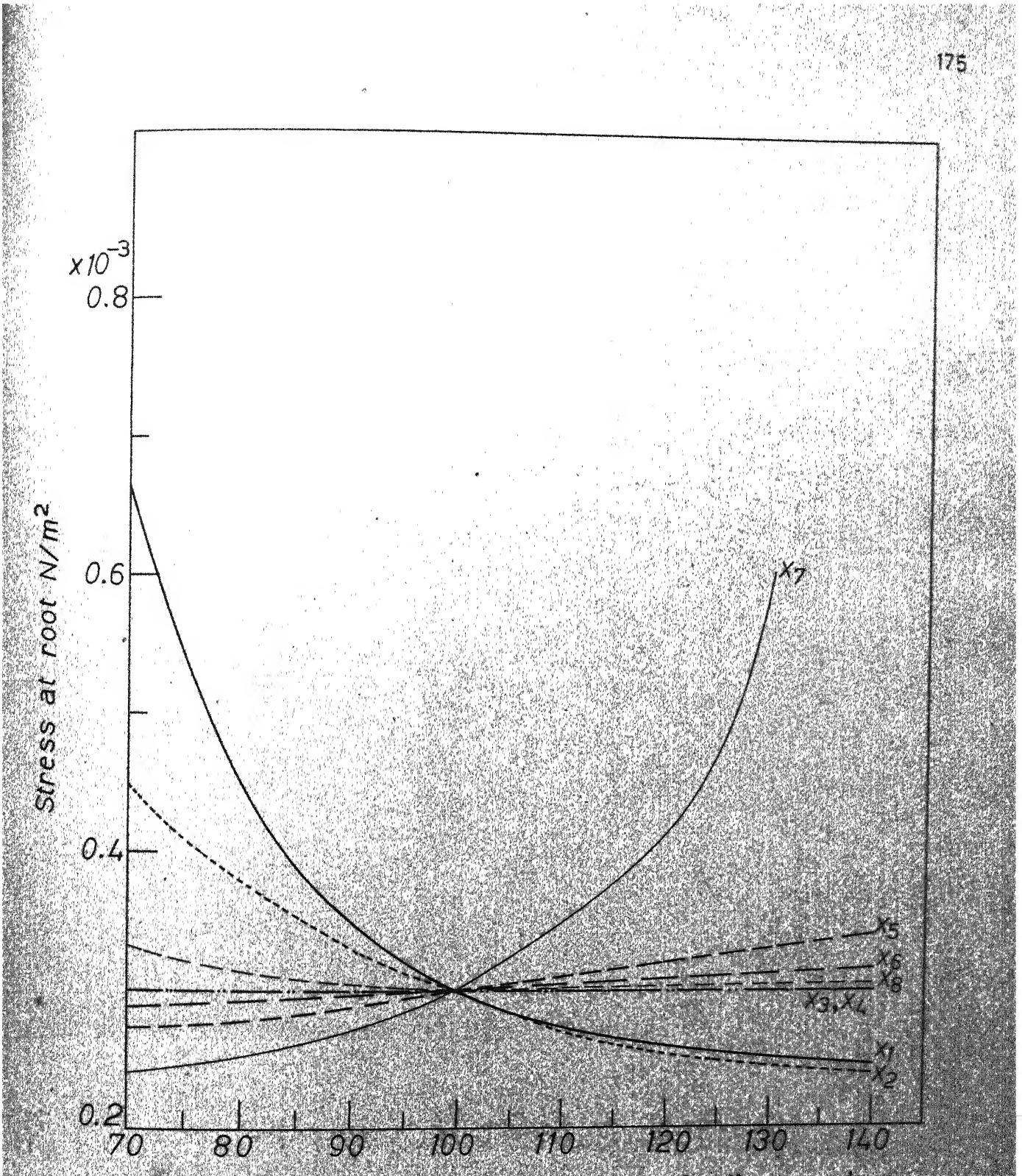

FIG. 7.10 SENSITIVITY ANALYSIS OF STRESS AT ROOT.

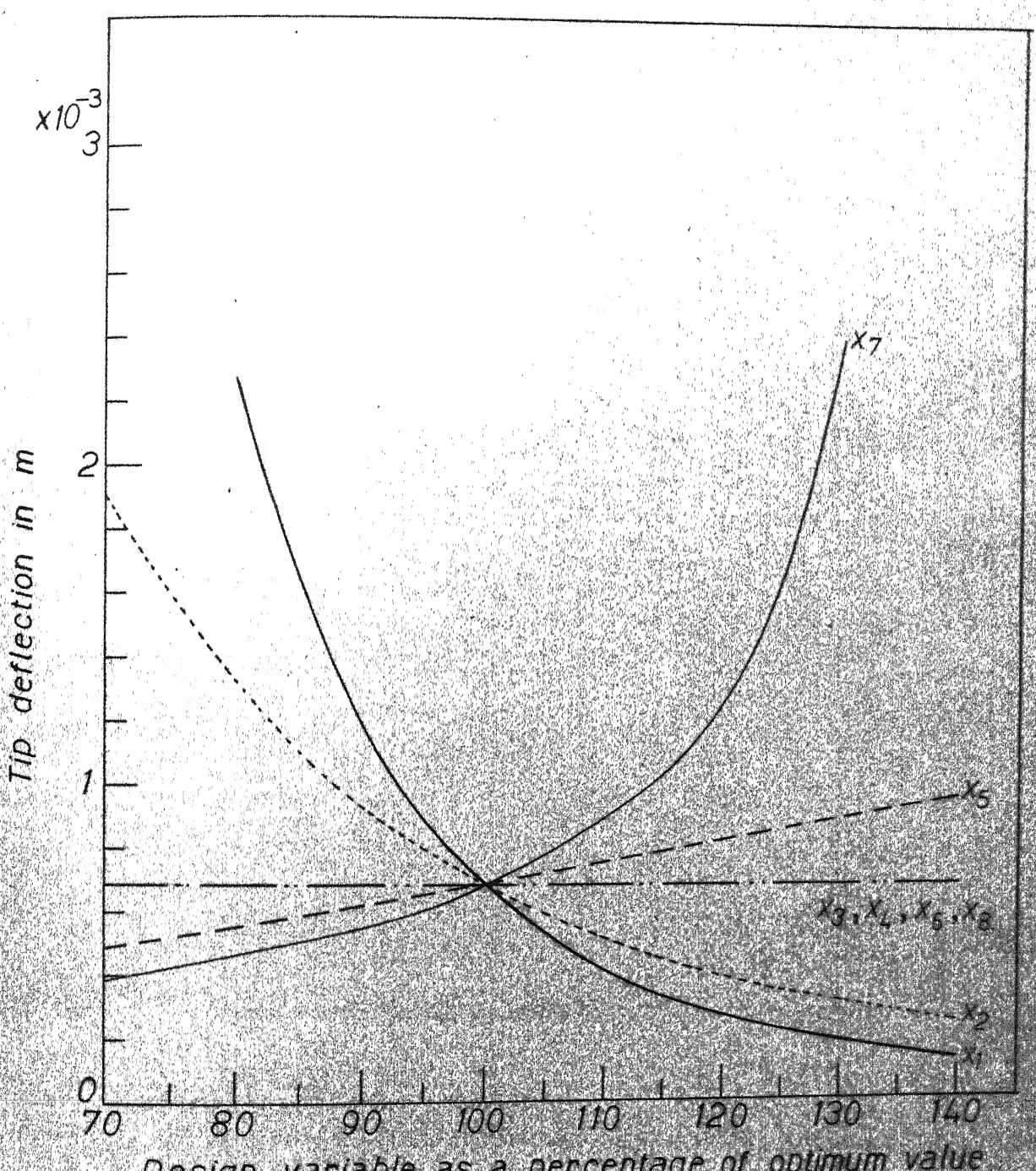

FIG. 7.11 SENSITIVITY ANALYSIS OF TIP DEFLECTION

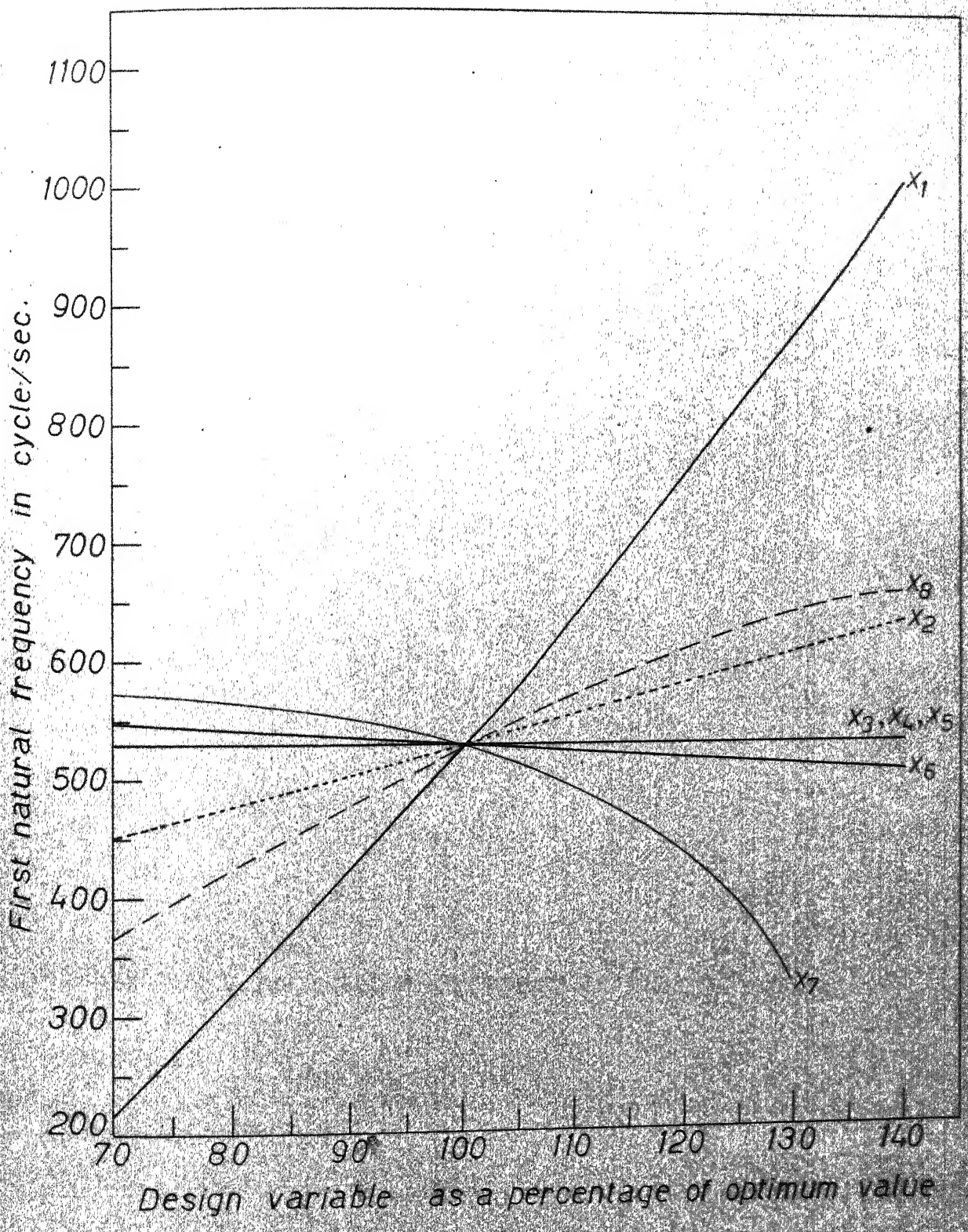

FIG. 7.12 SENSITIVITY ANALYSIS OF FIRST NATURAL FREQUENCY.

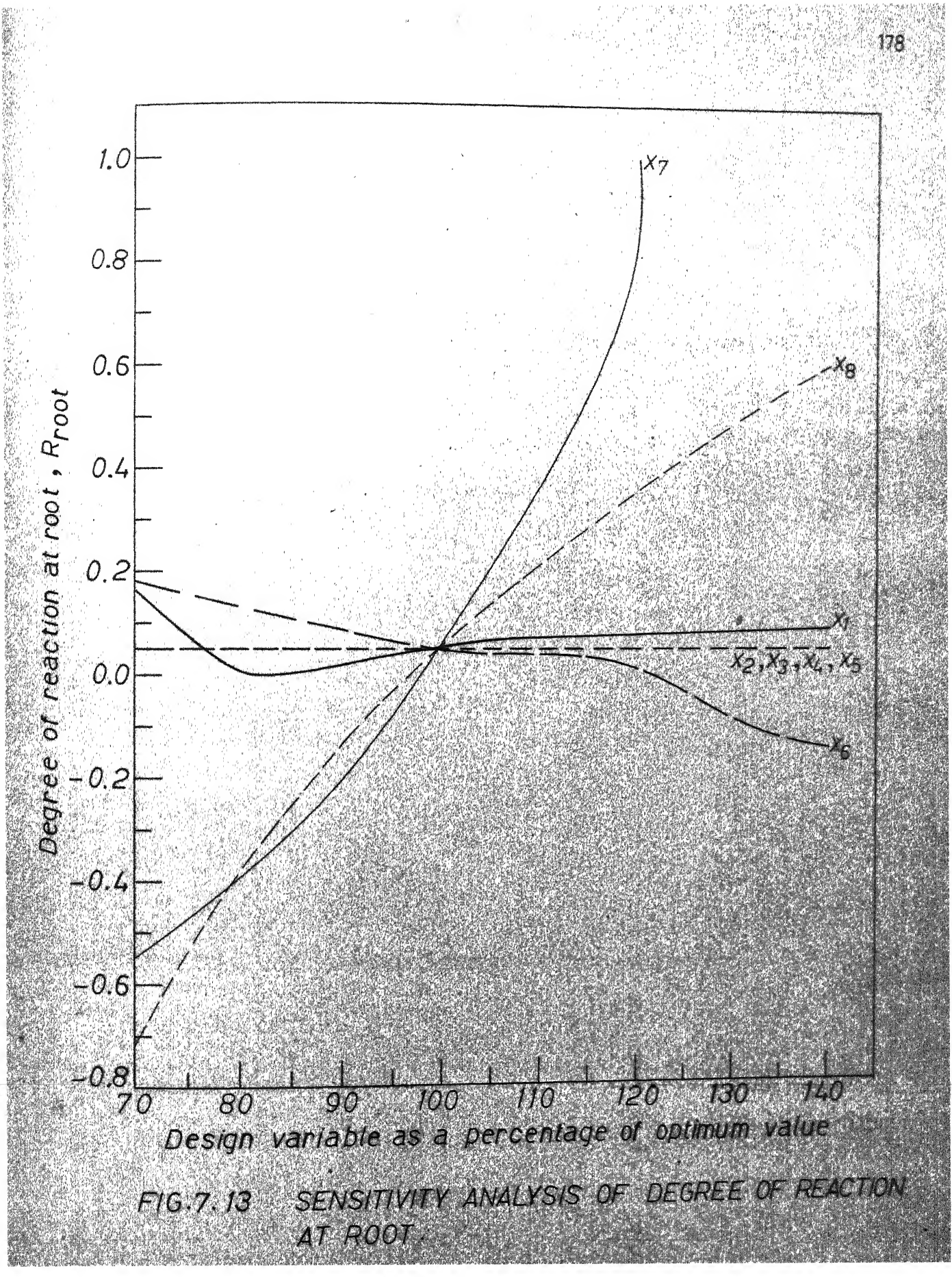

FIG.7.13 SENSITIVITY ANALYSIS OF DEGREE OF REACTION AT ROOT.

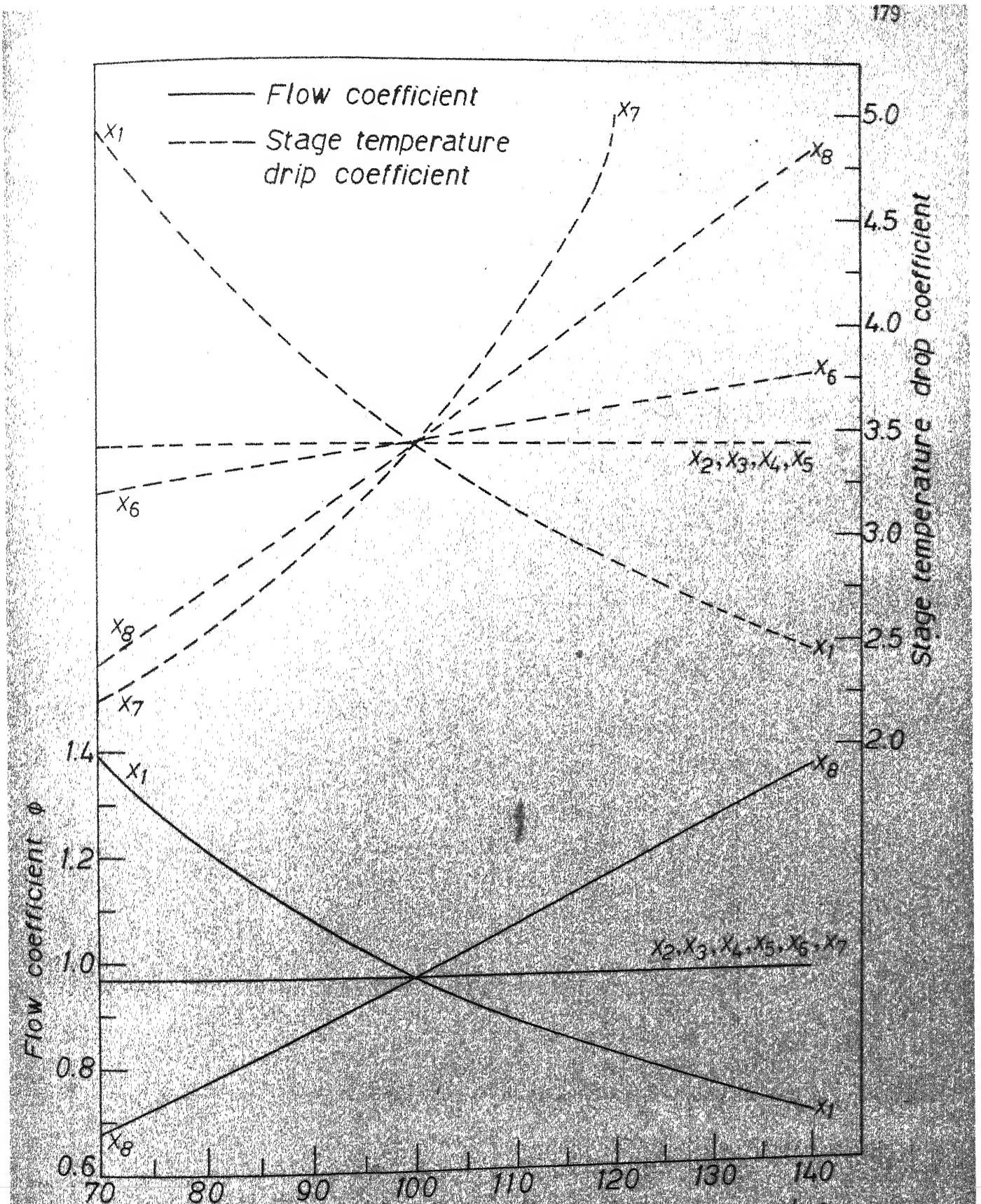

FIG. 7.14 SENSITIVITY ANALYSIS OF FLOW COEFFICIENT AND STAGE TEMPERATURE DROP COEFFICIENT.

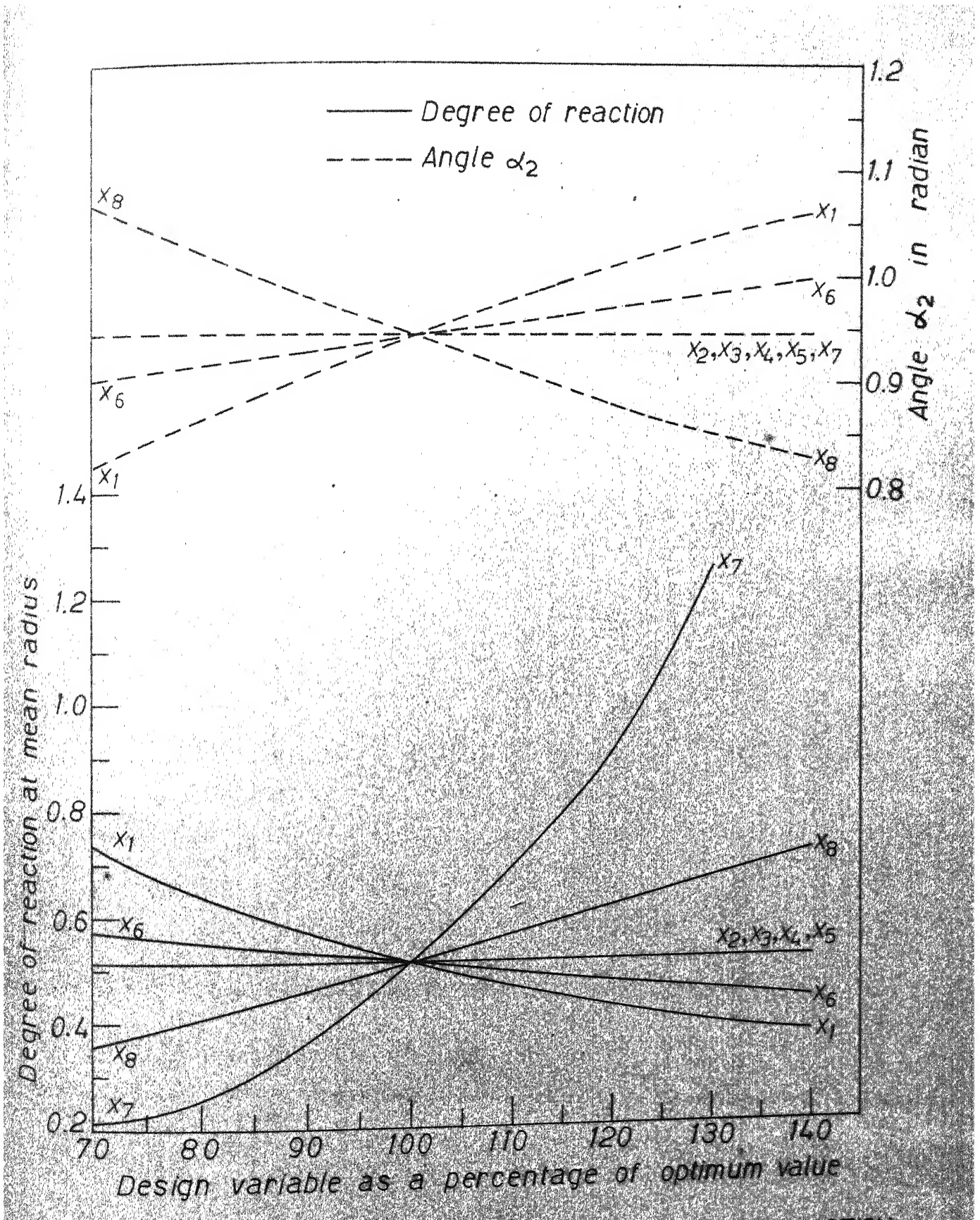

FIG. 7.15 SENSITIVITY ANALYSIS FOR DEGREE OF REACTION AND ANGLE α_2

CHAPTER 8

CONCLUSIONS AND RECOMMENDATIONS

The feasibility of automated optimum design of axial flow gas turbine stage has been demonstrated by the numerical examples of Chapter 7. In this chapter conclusions drawn from the present study are stated and the scope of extension of the present work is suggested.

8.1 Conclusions

(1) Computation of the efficiency of gas turbine stage

The convergence of the iterative method developed for the calculation of efficiency has been found to be very good. The method converged within 3 to 4 iterations irrespective of the initial trial value given. With higher convergence criteria, the number of iterations may increase by one or two.

(2) Computerization of air property relations

The polynomial equations obtained for evaluating the properties of air are quite accurate and the maximum error involved in most of the equations does not exceed 0.0535 percent. These equations would be useful in all analyses involving gas flow.

(3) Vibration and stress analysis of rotor blades

The turbine blade of airfoil section has been converted into an equivalent doubly tapered and twisted rectangular cantilever beam for the purpose of analyzing deflection, stress and natural frequencies of vibration of blade. A new finite element has been developed for the stress and vibration analysis of tapered, twisted and rotating beams by including the effects of shear deformation and rotary inertia. The element developed has been found to give reasonably good results even with four elements.

The results of the tapered beam with varying depth and breadth taper ratios were quite comparable with those reported by Mabie and Rogers[28]. The results of twisted uniform beams were in good agreement with those given by Rosard[35]. The following observations have been made regarding the vibration characteristics of cantilever beams:

(a) The effects of shear deformation and rotary inertia reduce the natural frequencies of vibration of beams.

(b) The natural frequencies increase with an increase in the offset (Figure 4.6).

(c) In certain mode shapes, the natural frequencies increase while in some cases, they decrease with an increase in the rotational speed of the beam.

(d) An increase or decrease of depth or breadth taper ratio changes the frequency ratio of the beam.

(e) The twist also effects in two different ways; it may increase or decrease the frequency ratio of the beam depending on the amount of twist and the mode shape.

(f) The effects of shear deformation, twist, offset and taper ratio have been found to be more predominant on higher modes of vibration.

The Cholesky decomposition of symmetric banded matrices has been used efficiently in solving equilibrium equations and in obtaining a partial solution to eigen value problem by Raleigh-Ritz subspace iteration algorithm.

The stresses due to pressure force, gas bending and centrifugal action have been calculated individually. At the root of the blade, all the three stresses are added to get the maximum stress. The stresses due to pressure and gas bending were calculated by using the finite element analysis. The centrifugal stresses were calculated by using the conventional method. The orders of magnitude of these stresses have been found to be same as the ones reported in reference 93 for a specific case.

(4) Results of optimization

The problem of design of axial flow gas turbine stage has been formulated as a nonlinear programming problem by including the constraints due to mechanical and aerodynamic considerations. The interior penalty function approach with

the root and the stresses in the blade have been found to be active at the optimum point.

By considering the savings realized through the optimization procedure (between 1.65% to 2.48% increase in efficiency of the stage and 65.5% to 80.5% reduction in weight in the examples considered), the computer time of about 60 minutes required for solving one optimization problem is justified. Thus the present procedure gives the designer complete information automatically in the initial design phase.

(5) Results of sensitivity analysis

The results of sensitivity analysis are expected to be useful in rounding off the optimum design variables to the nearest available values. These are also useful in determining the relative importance of the various design variables. This information would be helpful in eliminating some of the less important design variables in future design studies. It has been observed that the losses are most sensitive to the chord and spacing of rotor blades while the mass of the stage is most sensitive to the mean diameter of the rotor. The mechanical response parameters, namely the deflection, stress and fundamental natural frequency of vibration of the blade, have been found to be most sensitive to variations in mean diameter of the rotor and the exit angle of the rotor blade

(β_3). The degree of reaction at root was found to be most sensitive with respect to β_3 and axial velocity of flow.

(6) Computer program

The computer program developed for the automated optimum design of axial flow gas turbine stages involved 21 subroutines. It is quite general and can be used for solving any axial flow gas turbine design problem with different objectives and constraint sets.

8.2 Recommendations for Future Work

1. The loss due to trailing edge thickness, entrance losses, disc friction and windage losses, mechanical losses and partial admission losses (in the case of turbine with partial admission) can also be considered and the overall efficiency of the turbine can be considered for optimization. However, since the present stage of knowledge does not permit quantification of these losses in terms of the design variables of the problem, more research need to be done in this direction.
2. To include the three dimensional effects in the analysis of turbine stage, other methods like stream line curvature method, actuator disc theory etc. can be used instead of the simple free vortex theory used in the present work.

3. The axial displacement degrees of freedom can also be included in the finite element formulation to find the centrifugal stresses induced in the rotor blade more accurately. The other types of stresses like thermal stresses, stress due to root fixing and stresses due to creep and fatigue can also be included in the analysis.
4. The torsional nodal degrees of freedom can also be considered in the finite element analysis to find the coupled bending-bending-torsional frequencies of vibration of turbine blades.
5. No experimental results are available on the natural frequencies of vibration of beams including the effects of rotation, taper and pretwist. Some experiments could be conducted to predict the vibration response of such beams.
6. The vibration analysis of the turbine stage can be made by considering the assembly of rotor disc and blades with root fixing and shrouding.
7. The present optimization method can be extended to find the optimum design of multistage gas turbines.
8. The relative efficiencies of optimization can be studied by solving the problem of optimum design of gas turbine stage by using other optimization methods like gradient projection method, Zoutendijk's feasible direction method and sequential linear programming method.

9. The design problems can be formulated and solved by using a reliability framework.
10. Some experimental test rig for gas turbines can be set-up and the validity of the optimum results can be studied.

REFERENCES

1. Stodola, A., "Steam and Gas Turbines", Vol. I and II, Peter Smith, 1945.

2. Reeman, J., "The Turbine for the Simple Jet Propulsion Engine", Proc. Instn. Mech. Engrs., Vol. 153, 1948, p. 495.

3. Emmert, H.D., "Current Design Practices for Gas Turbine Power Elements", Trans. ASME, Vol. 72, 1950, p. 189.

4. Georgian, J.C., "The Design of Axial Flow Gas Turbines", J. of Instn. of Engrs. (India), Vol. 35, Part II, 1955, p. 1053.

5. Carter, A.D.S., "Three Dimensional Flow Theories for Axial Compressors and Turbines", Proc. Instn. Mech. Engrs., Vol. 159, 1948, p. 41.

6. Johnston, I.H. and Knight, L.R., "Tests on a Single Stage Turbine Comparing the Performance of Twisted with Untwisted Rotor Blades", H.M.S.O., A.R.C., R. and M. No. 2927, 1953.

7. Wu, C.H. and Wolfenstein, L., "Application of Radial Equilibrium Conditions to Axial Flow Compressor and Turbine Design", NACA Rep. 955, 1955.

8. Hawthorne, W.R. and Ringrose, J., "Actuator Disc Theory of Compressible Flow in Free-Vortex Turbomachinery", Proc. Instn. Mech. Engrs., Vol. 178, Part 3, 1963-64, p. 1.

9. Horlock, J.H., "Axial Flow Turbines", Butterworths, London, 1966.

10. Smith, D.J.L. and Johnston, I.H., "Investigations on an Experimental Single Stage Turbine of Conservative Design", A.R.C., R. and M. No. 3541, 1968.

11. Shaw, H., "An Improved Blade Design for Axial Flow Compressor (and Turbine)", The Aeronautical Journal, Vol. 74, 1970, p. 589.

12. Davis, W.R. and Millar, D.A.J., "A Comparison of Matrix and Streamline Curvature Methods of Axial Flow Turbomachine Analysis, From a User's Point of View", J. Engg. for Power, Trans. ASME, Vol. 97, 1975, p. 549.

13. "Technical Advances in Gas Turbine Design", Instn. of Mech. Engrs. Symposium, 1969.

14. Laxminarayana, B., Britsch, W.R. and Gearhart, W.S. (Eds.), "Fluid Mechanics, Acoustics, and Design of Turbomachinery", Parts I and II, NASA, SP-304, 1974.

15. A.J. Glassman (Ed.), "Turbine Design and Application", 3 Volumes, NASA, SP-290, 1975.

16. Carter, A.F., Platt, M. and Lenherr, F.K., "Analysis of Geometry and Design Point Performance of Axial Flow Turbines", Part I, Development of the Analysis Method and Loss Coefficient Correlation, NASA, CR-1181, Sept. 1968; Part II, Computer Programme, NASA, CR-1187, Oct. 1968.

17. Glassman, A.J., "Computer Programme for Predicting Design Analysis of Axial Flow Turbines", NASA, Tech. Notes, TND-6702, 1972.

18. Wasserbauer, C.A. and Glassman, A.J., "Fortran Programme for Predicting Off-design Performance of Radial Inflow Turbines", NASA Tech. Notes: NASA TND-8063, Sept. 1975, p. 55.

19. Hodge, J., "Stressing of Gas Turbine Blading", Engineering, Vol. 182, 1946, p. 4745.

20. Pollmann, E., "Temperatures and Stresses on Hollow Blades for Gas Turbines", NACA TM 1183, Sept. 1947.

21. Manson, S.S., "Stress Investigations in Gas Turbine Discs and Blades", SAE Annual Meeting, Jan. 1948.

22. Cox, H.R. (Ed.), "Gas Turbine Principles and Practice", George Newnes Limited, London, 1955.

23. Sawyer, J.W. (Ed.), "Gas Turbine Engineering Handbook", Gas Turbine Publication, 1966.

24. Thomson, W.T., "Matrix Solution of Vibration of Non-uniform Beams", ASME Paper No. 49A-11, 1949.

25. Martin, A.I., "Some Integrals Relating to Vibration of Cantilever Beams and Approximation for the Effect of Taper on Overtone Frequencies, Aeronautical Quarterly, Vol. 7, 1956, p. 109.

26. Carnegie, W. and Thomas, J., "Natural Frequencies of Long Tapered Cantilevers", Aeronautical Quarterly, Vol. 18, 1967, p. 309.

27. Rao, J.S. and Carnegie, W., "Determination of the Frequencies of Lateral Vibrations of Tapered Cantilever Beams by the Use of Ritz-Galerkin Process", Bulletin of Mechanical Engineering Education, Vol. 10, 1971, p. 239.

28. Mabie, H.H. and Rogers, C.B., "Vibration of Doubly Tapered Cantilever Beam with End Mass and End Support", J. of Acoustical Society of America, Vol. 55, May 1974, p. 986

29. Plunkett, R., "Free and Forced Vibration of Rotating Blades", J. of Aerospace Science, Vol. 18, 1951, p. 278.

30. Lo, H. and Renbarger, J., "Bending Vibrations of a Rotating Beam", Proceedings of First U.S. National Congress on Applied Mechanics, ASME, 1952, p. 75.

31. Boyce, W.E., DiPrima, R.C. and Handelman, G.H., "Vibrations of Rotating Beams of Constant Section", Proceedings of Second U.S. National Congress on Applied Mechanics, ASME, 1954, p. 165.

32. Yntema, R.T., "Simplified Procedures and Charts for the Rapid Estimation of Bending Frequencies of Rotating Beams", NACA-TN 3459, 1955.

33. Carnegie, W., Stirling, C. and Fleming, J., "Vibration Characteristics of Turbine Blading under Rotation — Results of an Initial Investigation and Details of a High-Speed Test Installation", Paper No. 32, Applied Mechanics Convention held at Cambridge, Mass., 1966.

34. Mendelson, A. and Gendler, S., "Analytical and Experimental Investigations of Effect of Twist on Vibration of Cantilevers", NACA TN-2300, 1951.

35. Rosard, D.D., "Natural Frequencies of Twisted Cantilevers", J. of Applied Mechanics, ASME, Vol. 20, 1953, p. 241.

36. DiPrima, R.C. and Handelman, G.H., "Vibration of Twisted Beams", Quarterly of Applied Mathematics, Vol. 12, 1954, p. 241.

37. Carnegie, W., "Vibration of Pretwisted Cantilever Blading", Proceedings of the Institute of Mechanical Engineers, Vol. 173, 1959, p. 343.

38. Dawson, B., "Coupled Bending Vibrations of Pretwisted Cantilever Blading Treated by Rayleigh-Ritz Method", J. of Mech. Engg. Sc., Vol. 10, 1968, p. 381.

39. Rao, J.S., "Flexural Vibration of Pretwisted Beams of Rectangular Cross Section", J. of Aero. Society of India, Vol. 23, 1971, p. 62.

40. Garland, C.F., "The Normal Modes and Vibrations of Beams Having Noncollinear Elastic and Mass Axes", J. of Applied Mechanics, Trans. ASME, 1940, p. A-97.

41. Targoff, W.P., "The Associated Matrixes of Bending and Coupled Bending Torsion Vibration", J. of Aerospace Science, Vol. 14, 1947, p. 177.

42. Mendelson, A. and Gendler, S., "Analytical Determination of Coupled Bending Torsion Vibrations of Cantilever Beams by Means of Station Functions", NACA TN-2185, 1949.

43. Carnegie, W. and Dawson, B., "Vibration Characteristics of Straight Blades of Asymmetrical Aerofoil Cross Section", Aeronautical Quarterly, Vol. 20, p. 178.

44. Targoff, W.P., "The Bending Vibrations of a Twisted Rotating Beam", Proceedings of Third Midwestern Conference on Solid Mechanics, 1957, p. 177.

45. Rao, J.S. and Carnegie, W., "Numerical Procedure for the Determination of the Frequencies and Mode Shapes of Lateral Vibration of Blades Allowing for the Effects of Pretwist and Rotation", International J. of Mech. Engg. Education, Vol. 1, 1973, p. 37.

46. Houbolt, J.C. and Brooks, G., "Differential Equations of Motion for Combined Flapwise Bending Chordwise Bending and Torsion of Twisted Nonuniform Rotor Blades", NACA 1346, 1958.

47. Carnegie, W., Dawson, B. and Thomas, J., "Vibration Characteristics of Cantilever Blading", Proceedings of the Institution of Mechanical Engineers, Vol. 180, 1965-1966, p. 71.

48. Carnegie, W. and Thomas, J., "The Coupled Bending-Bending Vibration of Pretwisted Tapered Blading", J. of Engg. for Industry, Trans. ASME, 1972, p. 255.

49. Banerjee, S. and Rao, J.S., "Coupled Bending-Torsion Vibrations of Rotating Blades", ASME Paper No. 76-GT-43, 1976.

50. Isakson, G. and Eisley, G.J., "Natural Frequencies in Coupled Bending and Torsion of Twisted Rotating and Nonrotating Blades", NASA No. NSG-27-59, 1964.

51. Montoya, J., "Coupled Bending Torsion Vibrations in a Twisted Rotating Blades", Brown Bovery Review, Vol. 53, 1966, p. 216.

52. Krupka, R.M. and Baumanis, A.M., "Bending Mode of a Rotating Tapered Twisted Turbomachine Blade Including Rotary Inertia and Shear Deflection", J. of Engg. for Industry, ASME, Vol. 91, 1969, p. 1017.

53. McCalley, R., "Rotary Inertia Correction for Mass Matrices", General Electric Company, Schenectady, New York, Report No. DIG/SA, 1963, pp. 63-73.

54. Archer, S.S., "Consistent Matrix Formulations for Structural Analysis Using Finite Element Techniques", AIAA J., Vol. 3, 1965, p. 1910.

55. Kapur, K.K., "Vibrations of a Timoshenko Beam Using Finite Element Approach", J. of Acoustical Society of America, Vol. 40, No. 5, 1966, p. 1058.

56. Carnegie, W., Thomas, J. and Documaki, E., "An Improved Method of Matrix Displacement Analysis in Vibration Problems", Aeronautical Quarterly, Vol. 20, 1969, p. 321.

57. Nickel, R. and Sector, G., "Convergence of Consistently Derived Timoshenko Beam Finite Elements", Int. J. Numerical Methods in Engg., Vol. 5, 1972, p. 243.

58. Thomas, J. and Abbas, B.A.H., "Finite Element Model for Dynamic Analysis of Timoshenko Beam", J. of Sound and Vibration, Vol. 41, No. 3, 1975, p. 291.

59. Campbell, W., "Tangential Vibration of Steam Turbine Buckets", Trans. ASME, Vol. 47, 1925, p. 543.

60. Prohl, M.A., "A Method of Calculating Vibration Frequency and Stress of a Banded Group of Turbine Buckets", Trans. ASME, Vol. 80, No. 1, 1958, p. 169.

61. Prohl, M.A. and Weaver, F.L., "High Frequency Vibration of Steam Turbine Buckets", Trans. ASME, Vol. 80, No. 1, 1958, p. 181.

62. Bhide, V.J., "Vibrations of Packetted Turbine Blades", M.Tech. Thesis, Deptt. of Mech. Engg., I.I.T. Kanpur, Aug. 1972.

63. Bajaj, G.R., "Free Vibration of Packetted Turbine Blades – Coupled Bending Bending Torsion Modes", M.Tech. Thesis, Deptt. of Mech. Engg., I.I.T. Kanpur, July 1974.

64. Fox, R.L. and Kapoor, M.P., "Structural Optimization in the Dynamic Response Regime: A Computational Approach", AIAA Journal, Vol. 8, No. 10, 1970.

65. Rao, S.S., "Automated Optimum Design of Aircraft Wings to Satisfy Strength, Stability, Frequency and Flutter Requirements", Ph.D. Thesis, Case Western Reserve University, Cleveland, Jan. 1972.

66. Seireg, A., "A Survey of Optimization of Mechanical Design", J. of Engg. for Industry, Trans. ASME, 1972, p. 495.

67. Raphael, T.H. and James, H.S., "WINDOWWAC (Wing Design Optimization with Aeroelastic Constraints): Program Manual", NASA TM-X-3071, Oct. 1974, p. 184.

68. Reddy, C.P. and Rao, S.S., "Automated Optimum Design of Machine Tool Structures for Static, Rigidity, Natural Frequencies and Regenerative Chatter Stability", J. of Engg. for Industry, Trans. ASME (in press).

69. Hati, S.K. and Rao, S.S., "Determination of Optimum Machining Conditions: Deterministic and Probabilistic Approaches", J. of Engg. for Industry, Trans. ASME, Vol. 98, 1976, p. 354.

70. Hati, S.K. and Rao, S.S., "Computerized Selection of Optimum Machining Conditions for a Job Requiring Multiple Operations", J. of Engg. for Industry, Trans. ASME (in press).

71. Rao, S.S., "Optimum Design of Bridge Girders for Electric Overhead Travelling Cranes", J. of Engg. for Industry, Trans. ASME (in press).

72. George, B.B., "Rocket Engine Turbine Optimization", Aerojet-General Corporation, TM 4901: 66-401, April 1966.

73. Balje, O.E., "Axial Turbine Performance Evaluation: Part A – Loss Geometry Relationship, Part B – Optimization with and without Constraints", J. of Engg. for Power, Trans. ASME, 1968, pp. 341-360.

74. Swift, W.L., "Optimizing Turbine and Pump-Turbine Design by Use of Computers", Water Power, Sept. 1971.

75. Kar, S. and Reddy, Y.R., "Optimum Vane Number and Angle of Centrifugal Pumps with Logarithmic Vanes", J. of Basic Engg., Trans. ASME, Vol. 93, 1971, p. 411.

76. Gupta, R.S., "Optimum Design of Radial Impeller Having Logarithmic Vanes", All India Symposium on System Engineering, H.B.T.I. Kanpur, Aug. 1973.

77. Saravanamuttoo, H.I.H., MacIsaac, B.D., "The Use of Hybrid Computer in the Optimization of Gas Turbine Control Parameters", J. of Engg. for Power, Trans. ASME, Vol. 95, 1973, p. 257.

78. Yadav, R. and Gupta, B.K., "Analytical Method of Optimizing Number of Blades and Blade Angles of Centrifugal Compressor Impellers", J. of Instn. of Engrs. (India), Mech. Engg. Division, Vol. 55, No. ME 3, 1975, pp. 103-107.

79. Blaho, M., "Optimum Design of Axial Flow Fans with Cambered Blades of Constant Thickness", Periodica Polytechnica, Mechanical Engineering, Mashinostoenie, Vol. 19, 1975, pp. 79-89.

80. Paranjpe, P.A. and Murthy, M.V.A., "Optimization and Standardization of Steam Turbine Blade Profiles", Symposium on Blade Design and Development, BHEL Hyderabad, Sept. 1975.

81. Bathe, K.J. and Wilson, E.L., "Large Eigen Value Problems in Dynamic Analysis", J. of Engg. Mech. Div., Proceedings of Am. Soc. of Civil Engrs., Vol. 98, No. 6, 1972, p. 1471.

82. Horlock, J.H., "Losses and Efficiency in Axial Flow Turbines", Int. J. Mech. Science, Vol. 2, 1960, p. 48.

83. Yahya, S.M., "Aerodynamic Losses in Axial Flow Turbines with Partial Admission", Ph.D. Thesis, Liverpool University, 1960.

84. Benson, R.S., "A Review of Methods for Assessing Loss Coefficients in Radial Gas Turbine", Int. J. of Mech. Science, Vol. 12, Oct. 1970, p. 905.

85. Brown, L.E., "Axial Flow Compressor and Turbine Loss Coefficients: A Comparison of Several Parameters", J. of Engg. for Power, Trans. ASME, Paper No. 72-GT-18, 1972.

86. Carter, A.D.S. and Hughes, H.P., "A Theoretical Investigation into the Effect of Profile Shape on the Performance of Aerofoils in Cascade", Aeronautical Research Council, R & M 2384, 1950.

87. Dunavant, J.C. and Erwin, J.R., "Investigation of a Related Series of Turbine Blade Profiles in Cascades", NACA Tech. Note 3802, 1956.

88. Ainley, D.G. and Mathieson, G.C.R., "A Method of Performance Estimation for Axial-Flow Turbines", H.M.S.O., A.R.C., R & M 2974, 1957.

89. Dunham, J. and Came, P.M., "Improvements to the Ainley-Mathieson Method of Turbine Performance Prediction", ASME Paper No. 70-GT-2, 1970.

90. "Symposium on the Effects of Reynolds Number", American Society of Mechanical Engineers, 1963.

91. Holeski, D.E. and Stewart, W.L., "Study of NASA and NACA Single Stage Axial Flow Turbine Performance as Related to Reynolds Number and Geometry", J. of Engg. for Power, Trans. ASME, Vol. 86, 1964, pp. 296-298.

92. Keenan, J.H. and Kaye, J., "Gas Tables", John Wiley, New York, 1961.

93. Cohen, H., Rogers, G.F.C. and Saravanamuttoo, H.I.H., "Gas Turbine Theory", Longman, London, 1972.

94. Rosen, J.B., "The Gradient Projection Method for Nonlinear Programming: Part I: Linear Constraints", SIAM Journal, Vol. 9, 1961, pp. 514-532.

95. Goldfarb, D., "Extension of Davidon's Variable Metric Algorithm to Maximization under Linear Inequality and Equality Constraints", SIAM Journal of Applied Mathematics, Vol. 17, 1966, pp. 739-764.

96. Zoutendijk, G., "Method of Feasible Directions", Elsevier, Amsterdam, 1960.

97. Fiacco, A. and McCormick, G.P., "The Sequential Unconstrained Minimization Technique for Nonlinear Programming, A Primal-Dual Method", Journal of Management Science, Vol. 10, No. 2, January 1964.

98. Box, M.J., "A Comparison of Several Current Optimization Methods and the Use of Transformations in Constrained Problems", Computer Journal (British), Vol. 9, 1966.

99. Fox, R.L., "Optimization Methods for Engineering Design", Addison-Wesley Publishing Co., Reading, Massachussets, 1971.

100. Reddy, C.P., "Automated Optimum Design and Reliability Analysis of Machine Tool Structures", Ph.D. Thesis, I.I.T. Kanpur, Dec. 1975.

APPENDIX A

POLYNOMIAL EXPRESSIONS FOR PROFILE LOSS COEFFICIENTS USED IN SECTION 3.5.4

The profile loss coefficient $Y_p(i,j)$ is expressed as a polynomial function of the spacing to chord ratio, x, as follows:

$$Y_p(i,j) = \sum_{k=0}^{4} c_k x^k \qquad (A.1)$$

where i = 1 for nozzle blades with $\beta_2 = 0$

= 2 for impulse blades with $\beta_2 = \beta_3$,

and j = blade angle in degrees.

The following equations were used for evaluating Y_p in the present work.

$$Y_p(1,80) = -1.0236312\,x^4 + 2.5686004\,x^3 - 2.1936137\,x^2 + 0.74141858\,x - 0.021356594 \qquad (A.2)$$

$$Y_p(1,75) = 1.1784926\,x^4 - 3.2665715\,x^3 + 3.4585936\,x^2 - 1.6462663\,x + 0.34334468 \qquad (A.3)$$

$$Y_p(1,70) = -0.26502239\,x^4 + 0.70910158\,x^3 - 0.49822962\,x^2 + 0.0090238\,x + 0.09513364 \qquad (A.4)$$

$$Y_p(1,65) = 7.1051656\,x^4 - 24.956305\,x^3 + 32.491226\,x^2 - 18.53773\,x + 3.9333972 \qquad (A.5)$$

$$Y_p(1,60) = 6.9573477\ x^4 - 24.391842\ x^3 + 31.685563\ x^2 - 18.048353\ x + 3.8250498 \quad (A.6)$$

$$Y_p(1,50) = 7.1509773\ x^4 - 24.834378\ x^3 + 31.946036\ x^2 - 18.029084\ x + 3.7862075 \quad (A.7)$$

$$Y_p(1,40) = 6.9582213\ x^4 - 24.177738\ x^3 + 31.093230\ x^2 - 17.537165\ x + 3.6792156 \quad (A.8)$$

$$Y_p(2,70) = 0.46636044\ x^4 - 1.6216202\ x^3 + 2.1681230\ x^2 - 1.1824825\ x + 0.35962101 \quad (A.9)$$

$$Y_p(2,65) = -0.7677269\ x^4 + 1.7245656\ x^3 - 1.0102869\ x^2 - 0.00304808\ x + 0.20849764 \quad (A.10)$$

$$Y_p(2,60) = 0.94616804\ x^4 - 2.8471011\ x^3 + 3.3114753\ x^2 - 1.726889\ x + 0.44034477 \quad (A.11)$$

$$Y_p(2,55) = -0.06295425\ x^4 - 0.02127604\ x^3 + 0.50723384\ x^2 - 0.59957593\ x + 0.27957267 \quad (A.12)$$

$$Y_p(2,50) = -0.32384541\ x^4 + 0.87772575\ x^3 - 0.56541410\ x^2 - 0.09070201\ x + 0.19223416 \quad (A.13)$$

$$Y_p(2,40) = -0.04099546\ x^4 - 0.14282837\ x^3 + 0.72273100\ x^2 - 0.78531104\ x + 0.32239876 \quad (A.14)$$

Each of the equations (A.2) to (A.14) was obtained from five data points taken from the profile loss curves. The data points used in obtaining the polynomials are given in Tables A.1 and A.2.

TABLE A.1

Profile Loss Data for Nozzle Blades ($\beta_2 = 0$)

$\beta_3 \rightarrow$	80°		75°		70°		65°		60°		50°		40°	
S.N.	x	Y_p	x	Y_p	x	Y_p	x	Y_p	x	Y_p	x	Y_p	x	Y_p
1	0.41	0.062	0.41	0.058	0.3	0.070	0.3	0.068	0.3	0.066	0.3	0.064	0.3	0.062
2	0.50	0.058	0.50	0.050	0.6	0.040	0.6	0.038	0.6	0.036	0.6	0.032	0.6	0.030
3	0.60	0.056	0.60	0.048	0.8	0.038	0.8	0.030	0.8	0.026	0.8	0.022	0.8	0.020
4	0.70	0.058	0.80	0.050	1.0	0.050	1.0	0.036	1.0	0.028	1.0	0.020	1.0	0.016
5	0.90	0.070	0.95	0.060	1.1	0.058	1.1	0.042	1.1	0.032	1.1	0.024	1.1	0.018

TABLE A.2

Profile Loss Data for Impulse Blades ($\beta_2 = \beta_3$)

$\beta_3 \rightarrow$	70°		65°		60°		55°		50°		40°	
S.N.	x	Y_p	x	Y_p	x	Y_p	x	Y_p	x	Y_p	x	Y_p
1	0.30	0.160	0.30	0.157	0.33	0.140	0.35	0.130	0.35	0.124	0.32	0.140
2	0.55	0.138	0.50	0.122	0.50	0.108	0.50	0.100	0.50	0.095	0.50	0.090
3	0.70	0.150	0.64	0.116	0.65	0.104	0.70	0.086	0.70	0.075	0.70	0.068
4	0.80	0.162	0.80	0.128	0.80	0.108	0.90	0.094	0.90	0.080	0.90	0.070
5	1.00	0.192	1.00	0.152	1.00	0.124	1.00	0.103	1.00	0.090	1.00	0.076

APPENDIX B

AIR PROPERTY RELATIONS

If x and y denote, respectively, the independent and the dependent variables, the n^{th} degree polynomial relation between the two can be expressed as:

$$y = y(x) = p_o + p_1 x + p_2 x^2 + \ldots + p_n x^n \ .$$

By transforming the independent variable as: $x_c = x_c(x)$, the above polynomial relation can be rewritten as:

$$y = y(x_c) = a_o + a_1 x_c + a_2 x_c^2 + \ldots + a_n x_c^n$$

In the present work, a_i, b_i, c_i, d_i, (i = 0, 1, 2 ... n) indicate the various polynomial coefficients in different temperature ranges. The various air property relations are summarized below:

(1) Temperature in terms of enthalpy ($x_c = 0.01\ x$)

$$y = \sum_{i=o}^{5} a_i x_c^i \ , \qquad 100^oR \leq T \leq 1000^oR \qquad \text{(B.1a)}$$

where a_o = 0.6665893 E 00, a_1 = 0.4189995 E 03,**
a_2 = -0.3435174 E 01, a_3 = 0.4291952 E 01,
a_4 = -0.2118072 E 01, a_5 = 0.2575576 E 00,

$$y = \sum_{i=o}^{4} b_i x_c^i \ , \qquad 1000^oR \leq T \leq 3000^oR \qquad \text{(B.1b)}$$

** 0.4189995 E 03 = 0.4189995×10^3

where $b_o = -0.4048060\ E\ 02$, $b_1 = 0.4655783\ E\ 03$,
$b_2 = -0.1588451\ E\ 02$, $b_3 = 0.7941960\ E\ 00$,
$b_4 = -0.1018477\ E\ -01$,

$$y = \sum_{i=o}^{3} c_i x_c^i , \qquad 3000^oR \leq T \leq 6500^oR \tag{B.1c}$$

where $c_o = 0.1628055\ E\ 03$, $c_1 = 0.3799953\ E\ 03$,
$c_2 = -0.3107125\ E\ 01$, $c_3 = 0.5445013\ E\ -01$

(2) Temperature in terms of relative pressure

$$x_c = \ln (10\ x)$$

$$y = \sum_{i=o}^{6} a_i x_c^i , \qquad 100^oR \leq T \leq 1000^oR \tag{B.2a}$$

where $a_o = 0.2543419\ E\ 03$, $a_1 = 0.7281138\ E\ 02$,
$a_2 = 0.1041926\ E\ 02$, $a_3 = 0.1013960\ E\ 01$,
$a_4 = 0.7763628\ E-01$, $a_5 = 0.2131233\ E-02$,
$a_6 = -0.4833005\ E-03$,

$$y = \sum_{i=o}^{6} b_i x_c^i , \qquad 1000^oR \leq T \leq 3000^oR \tag{B.2b}$$

where $b_o = 0.3367258\ E\ 02$, $b_1 = 0.1873639\ E\ 03$,
$b_2 = -0.1345989\ E\ 01$, $b_3 = -0.2795454\ E\ 01$,
$b_4 = 0.1234340\ E\ 01$, $b_5 = -0.1190855\ E\ 00$,
$b_6 = 0.4245929\ E-02$,

$$y = \sum_{i=o}^{5} c_i x_c^i , \qquad 3000^oR \leq T \leq 6500^oR \qquad (B.2c)$$

where c_o = 0.5368253 E 03, c_1 = -0.1870057 E 02,
c_2 = 0.2573325 E 02, c_3 = -0.1423321 E 00,
c_4 = 0.5124743 E-01, c_5 = 0.3583317 E-02,

(3) Temperature in terms of internal energy (x_c = 0.01 x)

$$y = \sum_{i=o}^{5} a_i x_c^i , \qquad 100^oR \leq T \leq 1000^oR \qquad (B.3a)$$

where a_o = 0.1058974 E 01, a_1 = 0.5870682 E 03,
a_2 = -0.7926372 E 01, a_3 = 0.1550686 E 02,
a_4 = -0.1135502 E 02, a_5 = 0.2040550 E 01,

$$y = \sum_{i=o}^{5} b_i x_c^i , \qquad 1000^oR \leq T \leq 3000^oR \qquad (B.3b)$$

where b_o = -0.5067941 E 02, b_1 = 0.6665731 E 03,
b_2 = -0.3422699 E 02, b_3 = -0.2883410 E 00,
b_4 = 0.5878343 E 00, b_5 = -0.4505020 E-01,

$$y = \sum_{i=o}^{5} c_i x_c^i , \qquad 3000^oR \leq T \leq 6500^oR \qquad (B.3c)$$

where c_o = 0.3549173 E 02, c_1 = 0.6147055 E 03,
c_2 = -0.2961354 E 02, c_3 = 0.2515192 E 01,
c_4 = -0.1171622 E 00, c_5 = 0.2249486 E-02

(4) Temperature in terms of relative volume

$$x_c = \ln (100/x)$$

$$y = \sum_{i=o}^{4} a_i x_c^i , \qquad 100^oR \leq T \leq 1000^oR \tag{B.4a}$$

where $a_o = 0.6253480\ E\ 03$, $a_1 = 0.2485310\ E\ 03$,
$a_2 = 0.4707777\ E\ 02$, $a_3 = 0.5013478\ E\ 01$,
$a_4 = 0.2423038\ E\ 00$,

$$y = \sum_{i=o}^{4} b_i x_c^i , \qquad 1000^oR \leq T \leq 3000^oR \tag{B.4b}$$

where $b_o = 0.6352536\ E\ 03$, $b_1 = 0.2254187\ E\ 03$,
$b_2 = 0.6870292\ E\ 02$, $b_3 = -0.3726730\ E\ 01$,
$b_4 = 0.8656939\ E\ 00$,

$$y = \sum_{i=o}^{4} c_i x_c^i , \qquad 3000^oR \leq T \leq 6500^oR \tag{B.4c}$$

where $c_o = 0.7072512\ E\ 03$, $c_1 = 0.1925400\ E\ 03$,
$c_2 = 0.6989422\ E\ 02$, $c_3 = -0.2417352\ E\ 01$,
$c_4 = 0.7004906\ E\ 00$,

(5) Temperature in terms of entropy ($x_c = e^{2x}$)

$$y = \sum_{i=o}^{6} a_i x_c^i , \qquad 100^oR \leq T \leq 1000^oR \tag{B.5a}$$

where $a_o = -0.5001787\ E\ 01$, $a_1 = 0.8689595\ E\ 01$,
$a_2 = 0.3395702\ E\ 02$, $a_3 = 0.7477182\ E\ 01$,

$a_4 = -0.1858278\ E\ 01, \quad a_5 = 0.3150205\ E\ 00,$

$a_6 = -0.2599161\ E\text{-}01,$

$$y = \sum_{i=o}^{6} b_i x_c^i , \qquad 1000^oR \leq T \leq 3000^oR \qquad (B.5b)$$

where $b_o = -0.1702268\ E\ 03, \quad b_1 = 0.8584996\ E\ 02,$

$b_2 = 0.2114853\ E\ 02, \quad b_3 = 0.8462060\ E\ 01,$

$b_4 = -0.1273866\ E\ 01, \quad b_5 = 0.6457035\ E\text{-}01,$

$b_6 = -0.6959124\ E\text{-}03,$

$$y = \sum_{i=o}^{4} c_i x_c^i , \qquad 3000^oR \leq T \leq 6500^oR \qquad (B.5c)$$

where $c_o = -0.1293062\ E\ 04, \quad c_1 = 0.4627224\ E\ 03,$

$c_2 = 0.1436791\ E\ 01, \quad c_3 = 0.9997245\ E\ 00,$

$c_4 = -0.2324186\ E\text{-}01$

(6) Enthalpy in terms of temperature ($x_c = .01\ x$)

$$y = \sum_{i=o}^{4} a_i x_c^i , \qquad 100^oR \leq T \leq 1000^oR \qquad (B.6a)$$

where $a_o = -0.1896111\ E\ 00, \quad a_1 = 0.2392554\ E\ 02,$

$a_2 = 0.8177288\ E\text{-}02, \quad a_3 = -0.3637402\ E\text{-}02,$

$a_4 = 0.4739440\ E\text{-}03,$

$$y = \sum_{i=o}^{3} b_i x_c^i , \qquad 1000^oR \leq T \leq 3000^oR \qquad (B.6b)$$

where $b_o = 0.1380925\ E\ 02$, $b_1 = 0.2042364\ E\ 02$,
$b_2 = 0.2533055\ E\ 00$, $b_3 = -0.2364187\ E\text{-}02$,

$$y = \sum_{i=o}^{3} c_i x_c^i \ , \qquad 3000^oR \leq T \leq 6500^oR \qquad \text{(B.6c)}$$

where $c_o = -0.3553479\ E\ 02$, $c_1 = 0.2542318\ E\ 02$,
$c_2 = 0.8214479\ E\text{-}01$, $c_3 = -0.3846921\ E\text{-}03$

(7) Relative pressure in terms of temperature ($x_c = 0.015\ x$)

$$y = \sum_{i=o}^{6} a_i x_c^i \ , \qquad 100^oR \leq T \leq 400^oR \qquad \text{(B.7a)}$$

where $a_o = 0.1537417\ E\text{-}02$, $a_1 = -0.2998780\ E\text{-}02$,
$a_2 = 0.2099430\ E\text{-}02$, $a_3 = -0.9920470\ E\text{-}04$,
$a_4 = 0.5367652\ E\text{-}03$, $a_5 = -0.4252450\ E\text{-}04$,
$a_6 = 0.1781536\ E\text{-}05$,

$$y = \sum_{i=o}^{6} b_i x_c^i \ , \qquad 400^oR \leq T \leq 1400 \qquad \text{(B.7b)}$$

where $b_o = 0.1704886\ E\ 00$, $b_1 = -0.6836948\ E\text{-}01$,
$b_2 = 0.6571773\ E\text{-}02$, $b_3 = 0.1621208\ E\text{-}02$,
$b_4 = 0.9983916\ E\text{-}04$, $b_5 = 0.1127265\ E\text{-}05$,
$b_6 = 0.2577276\ E\text{-}07$,

$$y = \sum_{i=o}^{5} c_i x_c^i \ , \qquad 1500^oR \leq T \leq 3000^oR \qquad \text{(B.7c)}$$

where $c_o = 0.2833894\ E\ 01$, $c_1 = 0.1159899\ E\ 00$,
$c_2 = -0.3264126\ E\text{-}01$, $c_3 = 0.3273487\ E\text{-}02$,
$c_4 = 0.6062104\ E\text{-}04$, $c_5 = 0.2453331\ E\text{-}05$,

$$y = \sum_{i=o}^{6} d_i x_c^i , \qquad 3000^oR \leq T \leq 6500^oR \tag{B.7d}$$

where $d_o = -0.1474357\ E\ 03$, $d_1 = 0.1026554\ E\ 02$,
$d_2 = -0.2287566\ E\ 00$, $d_3 = 0.2089396\ E\text{-}02$,
$d_4 = 0.1446234\ E\text{-}03$, $d_5 = 0.1600547\ E\text{-}05$,
$d_6 = 0.1381830\ E\text{-}08$

(8) Internal energy in terms of temperature ($x_c = 0.05\ x$)

$$y = \sum_{i=o}^{5} a_i x_c^i , \qquad 100^oR \leq T \leq 1000^oR \tag{B.8a}$$

where $a_o = -0.1879993\ E\ 00$, $a_1 = 0.3408698\ E\ 01$,
$a_2 = 0.1413006\ E\text{-}02$, $a_3 = -0.9960654\ E\text{-}04$,
$a_4 = 0.2502025\ E\text{-}05$, $a_5 = -0.1451709\ E\text{-}07$,

$$y = \sum_{i=o}^{6} b_i x_c^i , \qquad 1000^oR \leq T \leq 3000^oR \tag{B.8b}$$

where $b_o = 0.1340142\ E\ 02$, $b_1 = 0.2697001\ E\ 01$,
$b_2 = 0.1166697\ E\text{-}01$, $b_3 = -0.5392805\ E\text{-}04$,
$b_4 = 0.3659680\ E\text{-}06$, $b_5 = -0.1849987\ E\text{-}08$,
$b_6 = 0.3669679\ E\text{-}11$

$$y = \sum_{i=o}^{5} c_i x_c^i , \qquad 3000^oR \leq T \leq 6500^oR \tag{B.8c}$$

where $c_o = 0.2527138\ E\ 02$, $c_1 = 0.2539249\ E\ 01$,
$c_2 = 0.1174141\ E\text{-}01$, $c_3 = -0.3073682\ E\text{-}04$,
$c_4 = 0.3878235\ E\text{-}07$, $c_5 = -0.1526544\ E\text{-}10$

(9) Relative volume in terms of temperature ($x_c = 80{,}000/x$)

$$y = \sum_{i=o}^{4} a_i x_c^i , \qquad 100^oR \leq T \leq 400^oR \qquad (B.9a)$$

where $a_o = 0.5282485\ E\ 02$, $a_1 = -0.8309882\ E\ 00$,
$a_2 = 0.8322977\ E\text{-}02$, $a_3 = 0.1109702\ E\text{-}04$,
$a_4 = -0.1839174\ E\text{-}08$,

$$y = \sum_{i=o}^{6} b_i x_c^i , \qquad 400^oR \leq T \leq 1300^oR \qquad (B.9b)$$

where $b_o = 0.1825952\ E\ 01$, $b_1 = -0.2004256\ E\ 00$,
$b_2 = 0.6083203\ E\text{-}02$, $b_3 = 0.8056071\ E\text{-}05$,
$b_4 = 0.3655806\ E\text{-}07$, $b_5 = 0.7191527\ E\text{-}10$,

$$y = \sum_{i=o}^{6} c_i x_c^i , \qquad 1300^oR \leq T \leq 3000^oR \qquad (B.9c)$$

where $c_o = 0.4826241\ E\ 00$, $c_1 = -0.4728824\ E\text{-}01$,
$c_2 = 0.9295711\ E\text{-}03$, $c_3 = 0.7207075\ E\text{-}04$,
$c_4 = -0.5315893\ E\text{-}07$, $c_5 = -0.3531268\ E\text{-}08$,
$c_6 = 0.1579739\ E\text{-}10$

$$y = \sum_{i=o}^{6} d_i x_c^i , \qquad 3000^oR \leq T \leq 6500^oR \qquad (B.9d)$$

where $d_o = 0.1891114\ E\text{-}01$, $d_1 = -0.3385984\ E\text{-}02$,
$d_2 = -0.3200193\ E\text{-}04$, $d_3 = 0.5159768\ E\text{-}04$,
$d_4 = 0.5339627\ E\text{-}06$, $d_5 = 0.1317653\ E\text{-}07$,
$d_6 = -0.4221174\ E\text{-}09$

(10) Entropy in terms of temperature

$$x_c = \ln (0.1\ x)$$

$$y = \sum_{i=o}^{4} a_i x_c^i , \qquad 100^\circ R \leq T \leq 500^\circ R \qquad \text{(B.10a)}$$

where $a_o = -0.29292898\ E\ 00$, $a_1 = 0.15769787\ E\ 00$,
$a_2 = 0.40449134\ E\text{-}01$, $a_3 = -0.87987516\ E\text{-}02$,
$a_4 = 0.70923293\ E\text{-}03$,

$$y = \sum_{i=o}^{4} b_i x_c^i , \qquad 500^\circ R \leq T \leq 2000^\circ R \qquad \text{(B.10b)}$$

where $b_o = -0.67293304\ E\ 00$, $b_1 = 0.41571832\ E\ 00$,
$b_2 = -0.15920750\ E\text{-}01$, $b_3 = -0.52829841\ E\text{-}02$,
$b_4 = 0.80601767\ E\text{-}03$

$$\mathbf{y} = \sum_{i=o}^{4} c_i x_c^i , \qquad 2000^\circ R \leq T \leq 6500^\circ R \qquad \text{(B.10c)}$$

where $c_o = 0.24348077\ E\ 00$, $c_1 = -0.29914621\ E\text{-}01$,
$c_2 = 0.26780947\ E\text{-}01$, $c_3 = 0.17085150\ E\text{-}02$,
$c_4 = -0.20158477\ E\text{-}03$

(11) Specific heat at constant pressure in terms of temperature

($x_c = 0.1\ x$)

$$y = \sum_{i=o}^{6} a_i x_c^i , \qquad 100^oR \leq T \leq 1000^oR \qquad \text{(B.11a)}$$

where $a_o = 0.23956114\ E\ 00$, $a_1 = -0.77241925\ E\text{-}04$,
$a_2 = 0.58395085\ E\text{-}05$, $a_3 = -0.20386447\ E\text{-}06$,
$a_4 = 0.34366968\ E\text{-}08$, $a_5 = -0.24666058\ E\text{-}10$,
$a_6 = 0.65225817\ E\text{-}13$,

$$y = \sum_{i=o}^{6} b_i x_c^i , \qquad 1000^oR \leq T \leq 3000^oR \qquad \text{(B.11b)}$$

where $b_o = 0.25720694\ E\ 00$, $b_1 = -0.89639173\ E\text{-}03$,
$b_2 = 0.14075657\ E\text{-}04$, $b_3 = -0.80044782\ E\text{-}07$,
$b_4 = 0.23861391\ E\text{-}09$, $b_5 = -0.38169716\ E\text{-}12$,
$b_6 = 0.26582135\ E\text{-}15$,

$$y = \sum_{i=o}^{5} c_i x_c^i , \qquad 3000^oR \leq T \leq 6000^oR \qquad \text{(B.11c)}$$

where $c_o = 0.23471488\ E\ 00$, $c_1 = 0.26026914\ E\text{-}03$,
$c_2 = -0.41468497\ E\text{-}07$, $c_3 = -0.10828877\ E\text{-}08$,
$c_4 = 0.19215360\ E\text{-}11$, $c_5 = -0.10247290\ E\text{-}14$

(12) Specific heat at constant volume in terms of temperature

($x_c = 0.001\ x$)

$$y = \sum_{i=o}^{3} a_i x_c^i , \qquad 100^oR \leq T \leq 500^oR \qquad \text{(B.12a)}$$

where $a_o = 0.17014188\ E\ 00$, $a_1 = 0.91932141\ E\text{-}02$,

$a_2 = -0.42341176\ E\text{-}01$, $a_3 = 0.57386568\ E\text{-}01$,

$$y = \sum_{i=o}^{3} b_i x_c^i , \qquad 500^oR \leq T \leq 1500^oR \tag{B.12b}$$

where $b_o = 0.18501782\ E\ 00$, $b_1 = -0.59566059\ E\text{-}01$,

$b_2 = 0.74697853\ E\text{-}01$, $b_3 = -0.20197244\ E\text{-}01$,

$$y = \sum_{i=o}^{3} c_i x_c^i , \qquad 1500^oR \leq T \leq 3000^oR \tag{B.12c}$$

where $c_o = 0.11932987\ E\ 00$, $c_1 = 0.74511450\ E\text{-}01$,

$c_2 = -0.18387187\ E\text{-}01$, $c_3 = 0.17363686\ E\text{-}02$,

$$y = \sum_{i=o}^{3} d_i x_c^i , \qquad 3000^oR \leq T \leq 6000 \tag{B.12d}$$

where $d_o = 0.16704180\ E\ 00$, $d_1 = 0.29563507\ E\text{-}01$,

$d_2 = -0.41591628\ E\text{-}02$, $d_3 = -0.22257059\ E\text{-}03$.

The number of data points used in deriving the above relations, the maximum error involved at the data points, and the sum of squared errors at the data points in the various cases are given in Table B.1. Though these relations are obtained for foot-pound-second system of units, these can be used for M.K.S. and S.I. units by using suitable multiplication factors.

TABLE B.1*

Error Involved in the Polynomial Approximation of Air Property Relation

Serial No.	Relation	Equation No.	Temperature range in °R	Degree of polynomial	% Max. error	No. of data points	Sum of squared error
1	2	3	4	5	6	7	8
1	Temperature T Vs Enthalpy	B.1a	100 - 1000	5	0.0058	46	0.1633986 E-01
		B.1b	1000 - 3000	4	0.0139	101	0.2640502 E 01
		B.1c	3000 - 6500	3	0.0164	176	0.2144471 E 02
2	Temperature Vs Relative pressure	B.2a	100 - 1000	6	0.0141	46	0.5287192 E-01
		B.2b	1000 - 3000	6	0.0306	101	0.5261211 E 01
		B.2c	3000 - 6500	5	0.0246	176	0.6941417 E 02
3	Temperature Vs Internal energy	B.3a	100 - 1000	5	0.0081	46	0.2819083 E-01
		B.3b	1000 - 3000	5	0.0049	101	0.4311998 E 00
		B.3c	3000 - 6500	5	0.0076	176	0.3553566 E 01
4	Temperature Vs Relative volume	B.4a	100 - 1000	4	0.0535	46	0.1658011 E 01
		B.4b	1000 - 3000	4	0.0086	101	0.7134934 E 00
		B.4c	3000 - 6500	4	0.0121	176	0.9803763 E 01
5	Temperature Vs Entropy	B.5a	100 - 1000	6	0.0102	46	0.3653213 E-01
		B.5b	1000 - 3000	6	0.0198	101	0.2868459 E 01
		B.5c	3000 - 6500	4	0.0414	176	0.3989530 E 03
6	Enthalpy Vs Temperature	B.6a	100 - 1000	4	0.0146	46	0.5721900 E-02
		B.6b	1000 - 3000	3	0.0133	101	0.4256361 E-01
		B.6c	3000 - 6500	4	0.0122	176	0.1734621 E 01
7	Relative pressure Vs Temperature	B.7a	100 - 400	6	0.0493	16	0.1962360 E-08
		B.7b	400 - 1000	6	0.0478	31	0.1771755 E-03
		B.7c	1000 - 3000	5	0.0532	101	0.1920853 E 00
		B.7d	3000 - 6500	6	0.0153	176	0.2239882 E 02

(Table continued)

*Units used: Temperature T (°R), Enthalpy (Btu/lbm), Internal energy (Btu/lbm), Specific heat at constant pressure and at constant volume (Btu/lbm - °R)

Table B.1 (Continued)

1	2	3	4	5	6	7	8
8	Internal energy Vs Temperature	B.8a	100 - 1000	5	0.0093	46	0.1496723 E-02
		B.8b	1000 - 3000	6	0.0177	101	0.8153742 E-01
		B.8c	3000 - 6500	5	0.0176	176	0.1146354 E-01
9	Relative volume Vs Temperature	B.9a	100 - 400	4	0.0424	16	0.8185626 E 00
		B.9b	400 - 1300	5	0.0644	46	0.8078389 E-02
		B.9c	1300 - 3000	6	0.0376	86	0.3750538 E-04
		B.9d	3000 - 6500	6	0.0318	176	0.2460736 E-06
10	Entropy Vs Temperature	B.10a	100 - 500	4	0.0110	21	0.1295913 E-07
		B.10b	500 - 2000	4	0.0396	76	0.2880954 E-05
		B.10c	2000 - 6500	4	0.0044	226	0.1092946 E-05
11	Specific heat at constant pressure Vs Temperature	B.11a	100 - 1000	6	0.0112	17	0.6424807 E-08
		B.11b	1000 - 3000	6	0.0341	17	0.3466188 E-07
		B.11c	3000 - 6000	5	0.0187	17	0.1982651 E-07
12	Specific heat at constant volume Vs Temperature	B.12a	100 - 500	3	0.0429	9	0.3797442 E-07
		B.12b	500 - 1500	3	0.0265	13	0.4751305 E-07
		B.12c	1500 - 3000	3	0.0453	12	0.6461354 E-07
		B.12d	3000 - 6000	3	0.0325	17	0.3632993 E-07

APPENDIX C

EXPRESSIONS FOR [AK], [BK], ..., [DM]

The following notation is used for convenience:

$$U_i = \int_0^1 z^{i-1}\, dz \; ; \quad i = 1, 2, \ldots, n \tag{C.1}$$

$$L_i = 1^{i-1} \; ; \quad i = 1, 2, \ldots, n \tag{C.2}$$

$$V_i = \int_0^1 z^{i-1} \cos^2\left[(\theta_2 - \theta_1) \frac{z}{1} + \theta_1 \right] dz \; ;$$

$$i = 1, 2, \ldots, n \tag{C.3}$$

$$S_i = \int_0^1 z^{i-1} \sin 2\left[(\theta_2 - \theta_1) \frac{z}{1} + \theta_1 \right] dz \; ;$$

$$i = 1, 2, \ldots, n \tag{C.4}$$

where θ_1 and θ_2 denote the values of pretwist at nodes 1 and 2 respectively of the element.

As the nature of w_b, w_s, v_b and v_s is same except for their positions in the stiffness and mass matrices, one can use $\bar{w}$ to denote any one of the quantities w_b, w_s, v_b or v_s and in a similar manner the set $(\bar{u}_1, \bar{u}_2, \bar{u}_3, \bar{u}_4)$ can be used to represent anyone of the sets (u_1, u_2, u_3, u_4), (u_5, u_6, u_7, u_8), $(u_9, u_{10}, u_{11}, u_{12})$ or $(u_{13}, u_{14}, u_{15}, u_{16})$. Thus

$$\bar{w}(z) = \frac{\bar{u}_1}{l^3}(2z^3 - 3lz^2 + l^3) - \frac{\bar{u}_3}{l^2}(z^3 - 2lz^2 + l^2z)$$

$$+ \frac{\bar{u}_2}{l^3}(3lz^2 - 2z^3) - \frac{\bar{u}_4}{l^2}(z^3 - lz^2) \qquad (C.5)$$

$$\frac{d\bar{w}}{dz} = \frac{\bar{u}_1}{l^3}(6z^2 - 6lz) - \frac{\bar{u}_3}{l^2}(3z^2 - 4lz + l^2) + \frac{\bar{u}_2}{l^3}$$

$$(6lz - 6z^2) - \frac{\bar{u}_4}{l^2}(3z^2 - 2lz) \qquad (C.6)$$

$$\frac{d^2\bar{w}}{dz^2} = \frac{u_1}{l^3}(12z - 6l) - \frac{\bar{u}_3}{l^2}(6z - 4l) + \frac{\bar{u}_2}{l^3}(6l - 12z)$$

$$- \frac{\bar{u}_4}{l^2}(6z - 2l) \qquad (C.7)$$

By letting $P_{i,j,k}$ $(i = 1,\ldots,4;\ j = i,\ldots,4;\ k = 1,\ldots,7)$ denote the coefficient of $z^{k-1}\, l^{7-k}$ for $\bar{u}_i\, \bar{u}_j$ term in the expression of $\bar{w}^2$,

$Q_{i,j,k}$ $(i = 1,\ldots,4;\ j = i,\ldots,4;\ k = 1,\ldots,5)$

the coefficient of $z^{k-1}\, l^{5-k}$ for $\bar{u}_i\, \bar{u}_j$ term in the expression of $(\frac{d\bar{w}}{dz})^2$,

$R_{i,j,k}$ $(i = 1,\ldots,4;\ j = i,\ldots,4;\ k = 1,\ldots,3)$

the coefficient of $z^{k-1}\, l^{3-k}$ for $\bar{u}_i\, \bar{u}_j$ term in the expression of $(\frac{d^2\bar{w}}{dz^2})^2$,

$H_{i,j}$ $(i = 1,\ldots,4;\ j = i,\ldots,4)$ the index coefficient of 1 to account for the difference in index of 1 due to multiplication of rotational degrees of freedom $\bar{u}_1$ and $\bar{u}_2$ and the displacement degrees of freedom $\bar{u}_3$ and $\bar{u}_4$, the values of $P_{i,j,k}$, $Q_{i,j,k}$, $R_{i,j,k}$ and $H_{i,j}$ can be obtained as shown in Tables C.1 and C.2.

Evaluation of [BK] :

As the procedure for the derivation of [AK], [BK], ... [DM] is same the expression for [BK] is derived here as an illustration.

$$[u_o\ u_{10}\ u_{11}\ u_{12}]^T\,[BK][u_9\ u_{10}\ u_{11}\ u_{12}] = \int_o^1 EI_{yy}\left(\frac{\partial^2 v_b}{\partial z^2}\right)^2 dz$$

$$= \int_o^1 EI_{yy}\left(\frac{\partial^2 \bar{w}}{\partial z^2}\right)^2 dz \qquad (C.8)$$

where $\bar{w} = v_b$ and $\begin{Bmatrix} \bar{u}_1 \\ \bar{u}_2 \\ \bar{u}_3 \\ \bar{u}_4 \end{Bmatrix} \equiv \begin{Bmatrix} u_9 \\ u_{10} \\ u_{11} \\ u_{12} \end{Bmatrix}$

Putting the value of I_{yy} and $\bar{w}$ in the Eq. (C.8),

$$\int_0^l EI_{yy}\left(\frac{\partial^2 \bar{w}}{\partial z^2}\right)^2 dz = \int_0^l E[I_{X'X'} + (I_{y'y'} - I_{x'x'})$$

$$\cos^2\{(\theta_2 - \theta_1)\frac{z}{l} + \theta_1\}]\left[\frac{\bar{u}_1}{l^3}(12z - 6l) - \frac{\bar{u}_3}{l^2}(6z - 4l)\right.$$

$$\left. + \frac{\bar{u}_2}{l^3}(6l - 12z) - \frac{\bar{u}_4}{l^2}(6z - 2l)\right]^2 dz \qquad (C.9)$$

with

$$BK_{1,1} = \text{Coefficient of } \bar{u}_1\,\bar{u}_1 \equiv \text{Coefficient of } u_9\,u_9$$

$$= \frac{E}{12l^{10}} l^{H_{i,j}} \int_0^l [< (a_1 z^4 + a_2 l z^3 + a_3 l^2 z^2 + a_4 l^3 z + a_5 l^4)$$

$$+ \{(d_1 z^4 + d_2 l z^3 + d_3 l^2 z^2 + d_4 l^3 z + d_5 l^4)$$

$$- (a_1 z^4 + a_2 l z^3 + a_3 l^2 z^2 + a_4 l^3 z + a_5 l^4)\}$$

$$\cos^2\{(\theta_2 - \theta_1)\frac{z}{l} + \theta_1\} >$$

$$\{R_{1,1,1}\, z^2 + R_{1,1,2}\, lz + R_{1,1,3}\, l^2\}] dz$$

$$= \frac{E}{12l^{10}} L^{(H_{1,1}+1)} \sum_{i=1}^{5} a_i [R_{1,1,1}\, U_{8-i} + L_{i+1} R_{1,1,2} U_{7-i}$$

$$+ L_{i+2}\, R_{1,1,3} V_{6-i}] + (d_i - a_i)[L_i R_{1,1,1} V_{8-i} +$$

$$L_{i+1} R_{1,1,2} V_{7-i} + L_{i+2} R_{1,1,3} V_{6-i}]$$

$$= \frac{E}{121^{10}} L_{(H_{1,1}+1)} \sum_{i=1}^{5} \sum_{j=1}^{3} \{a_i L_{i+j-1} U_{9-i-j} R_{1,1,j}\}$$

$$+ (d_i - a_i) \{L_{i+j-1} V_{9-i-j} R_{1,1,j}\} \qquad (C.10)$$

This relation can be generalized as:

$$BK_{I,J} = \frac{E}{121^{10}} L_{(H_{I,J}+1)} \sum_{i=1}^{5} \sum_{j=1}^{3} \{a_i L_{(i+j-1)} U_{(9-i-j)} R_{I,J,j}\}$$

$$+ (d_i - a_i) \{L_{(i+j-1)} V_{(9-i-j)} R_{I,J,j}\};$$

$$I = 1,\ldots,4; \quad J = I,\ldots,4$$

$$= \frac{E}{101^{10}} \sum_{i=1}^{5} \sum_{j=1}^{3} [\{a_i L_{(i+j+H_{I,J})} U_{9-i-j} R_{I,J,j}\} + (d_i - a_i)$$

$$\{L_{(i+j+H_{I,J})} V_{(9-i-j)} R_{I,J,j}\}] \; ; \quad I = 1,\ldots,4; \; J = I,\ldots,4$$

(C.11)

Similarly

$$AK_{I,J} = \frac{E}{121^{10}} \sum_{i=1}^{5} \sum_{j=1}^{3} [\{d_i L_{(i+j+H_{I,J})} U_{(9-i-j)} R_{I,J,j}\}$$

$$+ (a_i - d_i) \{L_{(i+j+H_{I,J})} V_{9-i-j} R_{I,J,j}\}] \; ;$$

$$I = 1,\ldots,4; \; J = I,\ldots,4 \qquad (C.12)$$

$$CK_{I,J} = \frac{\mu G}{l^8} \sum_{i=1}^{3} \sum_{j=1}^{5} [\, c_i L_{(i+j+H_{I,J})} U_{(9-i-j)} Q_{I,J,j}];$$

$$I = 1,\ldots,4;\ J = I,\ldots,4 \qquad (C.13)$$

$$DK_{I,J} = \frac{E}{12l^{10}} \sum_{i=1}^{5} \sum_{j=1}^{3} [(a_i - d_i)\, L_{(i+j+H_{I,J})} S_{(9-i-j)} R_{I,J,j}];$$

$$I = 1,\ldots,4;\ J = I,\ldots,4 \qquad (C.14)$$

$$AM_{I,J} = \frac{\rho_m}{l^8} \sum_{i=1}^{3} \sum_{j=1}^{7} [\, c_i L_{(i,j+H_{I,J})} U_{(11-i-j)} P_{I,J,j}] ;$$

$$I = 1,\ldots,4;\ J = I,\ldots,4 \qquad (C.15)$$

$$BM_{I,J} = \frac{\rho_m}{12l^{10}} \sum_{i=1}^{5} \sum_{j=1}^{5} [\, \{ d_i L_{(i+j+H_{I,J})} U_{(11-i-j)} Q_{I,J,j} \}$$

$$+ (a_i - d_i)\, \{ L_{(i+j+H_{I,J})} V_{(11-i-j)} Q_{I,J,j} \}] ;$$

$$I = 1,\ldots,4;\ J = I,\ldots,4 \qquad (C.16)$$

$$CM_{I,J} = \frac{\rho_m}{12l^{10}} \sum_{i=1}^{5} \sum_{j=1}^{5} [\, \{ a_i L_{(i+j+H_{I,J})} U_{(11-i-j)} Q_{I,J,j} \}$$

$$+ (d_i - a_i)\, \{ L_{(i+j+H_{I,J})} V_{(11-i-j)} Q_{I,J,j} \}] ;$$

$$I = 1,\ldots,4;\ J = I,\ldots,4 \qquad (C.17)$$

$$DM_{I,J} = \frac{\rho_m}{121^{10}} \sum_{i=1}^{5} \sum_{j=1}^{5} [(a_i - d_i)L_{(i+j+H_{I,J})} S_{(11-i-j)} Q_{I,J,j}];$$

$$I = 1,\ldots,4;\ J = I,\ldots,4 \qquad (C.18)$$

Evaluation of [EK] and [FK]:

$$[u_1\ u_2\ u_3\ u_4]^T [EK][u_1\ u_2\ u_3\ u_4] = \int_0^1 P(z)\left(\frac{\partial w_b}{\partial z}\right)^2 dz$$

$$= \int_0^1 \rho_m A\ \Omega^2 [(eL + \tfrac{1}{2}L^2 - ez_e - z_e^2) - (e + z_e)z - \tfrac{1}{2}z^2]$$

$$\left(\frac{\partial w_b}{\partial z}\right)^2 dz$$

$$= \int_0^1 \rho_m A\ \Omega^2\ (eL + \tfrac{1}{2}L^2 - ez_e - z_e^2)\left(\frac{\partial w_b}{\partial z}\right)^2 dz$$

$$- \int_0^1 \rho_m A\ \Omega^2\ (e + z_e)z\ \left(\frac{\partial w_b}{\partial z}\right)^2 dz - \int_0^1 \frac{1}{2}\rho_m A\ \Omega^2 z^2\ \left(\frac{\partial w_b}{\partial z}\right)^2 dz$$

(C.19)

Thus

$$EK_{I,J} = \{\frac{\rho_m\ \Omega^2}{1^8}(eL + \tfrac{1}{2}L^2 - ez_e - z_e^2) \sum_{i=1}^{3} \sum_{j=1}^{5} [c_i L_{(i+j+H_{I,J})} \cdot$$

$$U_{(9-i-j)} Q_{I,J,j}]$$

$$- \frac{\rho_m\ \Omega^2}{1^8}(e + z_e) \sum_{i=1}^{3} \sum_{j=1}^{5} [c_i L_{(i+j+H_{I,J})} U_{(10-i-j)} Q_{I,J,j}]$$

$$- \frac{\rho_m \Omega^2}{21^8} \sum_{i=1}^{3} \sum_{j=1}^{5} [c_i L_{(i+j+H_{I,J})} U_{(11-i-j)} Q_{I,J,j}] \};$$

$$I = 1,\ldots,4; \; J = I,\ldots,4 \qquad (C.20)$$

Similarly

$$FK_{I,J} = \frac{2 \rho_m \Omega^2}{1^8} \sum_{i=1}^{3} \sum_{j=1}^{7} [c_i L_{(i+j+H_{I,J})} U_{(11-i-j)} P_{I,J,j}] ;$$

$$I = 1,\ldots,4; \; J = I,\ldots,4 \qquad (C.21)$$

TABLE C.1

Values of $H_{i,j}$, $R_{i,j,k}$, $Q_{i,j,k}$

i	j	$H_{i,j}$	$R_{i,j,k}$ for k = 1	2	3	$Q_{i,j,k}$ for k = 1	2	3	4	5
1	1	0	144.0	-144.0	36.0	36.0	-72.0	36.0	0.0	0.0
1	2	0	-144.0	144.0	-36.0	-36.0	72.0	-36.0	0.0	0.0
1	3	1	-72.0	84.0	-24.0	-18.0	42.0	-30.0	6.0	0.0
1	4	1	-72.0	60.0	-12.0	-18.0	30.0	-12.0	0.0	0.0
2	2	0	144.0	-144.0	36.0	36.0	-72.0	36.0	0.0	0.0
2	3	1	72.0	-84.0	24.0	18.0	-42.0	30.0	-6.0	0.0
2	4	1	72.0	-60.0	12.0	18.0	-30.0	12.0	0.0	0.0
3	3	2	36.0	-48.0	16.0	9.0	-24.0	22.0	-8.0	1.0
3	4	2	36.0	-36.0	8.0	9.0	-18.0	11.0	-2.0	0.0
4	4	2	36.0	-24.0	4.0	9.0	-12.0	4.0	0.0	0.0

TABLE C.2

Values of $P_{i,j,k}$

i	j	$P_{i,j,k}$ for k = 1	2	3	4	5	6	7
1	1	4.0	-12.0	9.0	4.0	-6.0	0.0	1.0
1	2	-4.0	12.0	-9.0	-2.0	3.0	0.0	0.0
1	3	-2.0	7.0	-8.0	2.0	2.0	-1.0	0.0
1	4	-2.0	5.0	-3.0	-1.0	1.0	0.0	0.0
2	2	4.0	-12.0	9.0	0.0	0.0	0.0	0.0
2	3	2.0	-7.0	8.0	-3.0	0.0	0.0	0.0
2	4	2.0	-5.0	3.0	0.0	0.0	0.0	0.0
3	3	1.0	-4.0	6.0	-4.0	1.0	0.0	0.0
3	4	1.0	-3.0	3.0	-1.0	0.0	0.0	0.0
4	4	1.0	-2.0	1.0	0.0	0.0	0.0	0.0

APPENDIX D

ELEMENTS OF MATRICES [A], [B], [C] AND [D]

Elements of the Matrix [A]:

$$[A] = \frac{E}{1200} \begin{bmatrix} a_{11} & a_{12} & a_{13} & a_{14} \\ & a_{22} & a_{23} & a_{24} \\ & & a_{33} & a_{34} \\ \text{Symmetric} & & & a_{44} \end{bmatrix} \qquad (D.1)$$

where

$$a_{11} = \frac{1}{l^3} (396\, a_1 + 441\, a_2 + 504\, a_3 + 630\, a_4 + 1260\, a_5)$$

$$a_{12} = - a_{11}$$

$$a_{13} = - \frac{1}{l^2} (114\, a_1 + 126\, a_2 + 147\, a_3 + 210\, a_4 + 630\, a_5)$$

$$a_{14} = - \frac{1}{l^2} (282\, a_1 + 315\, a_2 + 357\, a_3 + 420\, a_4 + 630\, a_5)$$

$$a_{22} = a_{11}$$

$$a_{23} = - a_{13}$$

$$a_{24} = - a_{14}$$

$$a_{33} = \frac{1}{l} (36\, a_1 + 42\, a_2 + 56\, a_3 + 105\, a_4 + 420\, a_5)$$

$$a_{34} = \frac{1}{L}(78\ a_1 + 84\ a_2 + 91\ a_3 + 105\ a_4 + 210\ a_5)$$

$$a_{44} = \frac{1}{l}(204\ a_1 + 231\ a_2 + 266\ a_3 + 315\ a_4 + 420\ a_5)$$

Elements of Matrix [B]:

$$[B] = \frac{\mu G}{1260}\begin{bmatrix} b_{11} & b_{12} & b_{13} & b_{14} \\ & b_{22} & b_{23} & b_{24} \\ & & b_{33} & b_{34} \\ \text{Symmetric} & & & b_{44} \end{bmatrix} \qquad (D.2)$$

$$b_{11} = \frac{1}{l}(432\ c_1 + 756\ c_2 + 1512\ c_3)$$

$$b_{12} = -\ b_{11}$$

$$b_{13} = -\ (90\ c_1 + 126\ c_2 + 126\ c_3)$$

$$b_{14} = -\ (36\ c_1 + 0 + 126\ c_3)$$

$$b_{22} = b_{11}$$

$$b_{23} = -\ b_{13}$$

$$b_{24} = -\ b_{14}$$

$$b_{33} = l(24\ c_1 + 42\ c_2 + 168\ c_3)$$

$$b_{34} = -\ l(18\ c_1 + 21\ c_2 + 42\ c_3)$$

$$b_{44} = l(108\ c_1 + 126\ c_2 + 168\ c_3)$$

Elements of Matrix [C]:

$$[C] = \frac{\rho_m}{1260} \begin{bmatrix} c_{11} & c_{12} & c_{13} & c_{14} \\ & c_{22} & c_{23} & c_{24} \\ & & c_{33} & c_{34} \\ \text{Symmetric} & & & c_{44} \end{bmatrix} \qquad (D.3)$$

$$c_{11} = l(38\, c_1 + 108\, c_2 + 468\, c_3)$$

$$c_{12} = l(46\, c_1 + 81\, c_2 + 162\, c_3)$$

$$c_{13} = -l^2\left(\frac{17}{2} c_1 + 21\, c_2 + 66\, c_3\right)$$

$$c_{14} = l^2\left(\frac{19}{2} c_1 + 19\, c_2 + 39\, c_3\right)$$

$$c_{22} = l(290\, c_1 + 360\, c_2 + 468\, c_3)$$

$$c_{23} = -l^2\left(\frac{25}{2} c_1 + 21\, c_2 + 39\, c_3\right)$$

$$c_{24} = l^2\left(\frac{65}{2} c_1 + 45\, c_2 + 66\, c_3\right)$$

$$c_{33} = l^3\left(2\, c_1 + \frac{9}{2} c_2 + 12\, c_3\right)$$

$$c_{34} = -l^3\left(\frac{5}{2} c_1 + \frac{9}{2} c_2 + 9\, c_3\right)$$

$$c_{44} = l^3\left(5\, c_1 + \frac{15}{2} c_2 + 12\, c_3\right)$$

Elements of Matrix [D]:

$$[D] = \frac{\rho_m}{1260} \begin{bmatrix} d_{11} & d_{12} & d_{13} & d_{14} \\ & d_{22} & d_{23} & d_{24} \\ & & d_{33} & d_{34} \\ & & & d_{44} \end{bmatrix} \qquad (D.4)$$

$$d_{11} = \frac{1}{1}\left(15\, a_1 + \frac{45}{2}\, a_2 + 36\, a_3 + 63\, a_4 + 126\, a_5\right)$$

$$d_{12} = -\, d_{11}$$

$$d_{13} = -\left(\frac{15}{4}\, a_1 + \frac{21}{4}\, a_2 + \frac{15}{2}\, a_3 + \frac{21}{2}\, a_4 + \frac{21}{2}\, a_5\right)$$

$$d_{14} = \left(\frac{15}{4}\, a_1 + \frac{15}{4}\, a_2 + 3\, a_3 + 0 - \frac{21}{2}\, a_5\right)$$

$$d_{22} = d_{11}$$

$$d_{23} = -\, d_{13}$$

$$d_{24} = -\, d_{14}$$

$$d_{33} = 1\left(a_1 + \frac{11}{8}\, a_2 + 2\, a_3 + \frac{7}{2}\, a_4 + 14\, a_5\right)$$

$$d_{34} = -\, 1\left(\frac{5}{4}\, a_1 + \frac{11}{8}\, a_2 + \frac{3}{2}\, a_3 + \frac{7}{4}\, a_4 + \frac{7}{2}\, a_5\right)$$

$$d_{44} = 1\left(\frac{15}{2}\, a_1 + \frac{65}{8}\, a_2 + 9\, a_3 + \frac{21}{2}\, a_4 + 14\, a_5\right)$$

APPENDIX E

DESCRIPTION OF THE COMPUTER PROGRAMME

The computer programme for the automated optimum design of axial flow gas turbine stage is written in FORTRAN IV language and it consists of 21 subroutines. Most of the computations are made on IBM 7044 at Indian Institute of Technology, Kanpur, but some of the computations are also done on IBM 360 of Delhi University. The purpose of the various subroutines is given below:

(1) ALOAD: To formulate the load vectors due to pressure and gas bending forces in the directions of the degrees of freedom of a turbine blade.

(2) CBAND: To perform the Cholesky decomposition of symmetric banded matrices. This routine stores only the upper triangular band of the decomposed matrix and the diagonal of the matrix is stored in the first column.

(3) ZOLF: To solve the equilibrium equations from the upper triangular band of the decomposed stiffness matrix.

(4) MATINV: To find the inverse of a real square matrix.

(5) EIGEN: To compute the eigen values and eigen vectors of the generalized Ritz problem by power method.

(6) BASIC: To obtain the partial eigen solution of a structure by Rayleigh-Ritz sub-space iteration technique. It calls ZOLF, MATINV and EIGEN for solving the generalized Ritz problem.

(7) STRESS : To find stresses, deflections and eigen values of rotating, tapered and twisted beams of rectangular cross-section. It calls the subroutines ALOAD, CBAND, ZOLF and BASIC.

(8) ELU: To perform the Cholesky decomposition of symmetric matrices. This will not take advantage of the banded nature of the matrices.

(9) SOLVEB: To solve a set of simultaneous equations using the lower and upper triangular matrices obtained from the subroutine ELU. This will not take advantage of the banded nature of the original coefficient matrix.

(10) CAMUL: To obtain the coefficients of the square and cube of a fourth order polynomial.

(11) CAPOL: To evaluate the value of a n^{th} order polynomial when the values of the coefficients and the variable are given.

(12) POLFIT: To fit a polynomial for a set of data points using least squares method. It calls ELU and SOLVEB routines.

(13) VINT: To evaluate the integral of a general n^{th} order polynomial in terms of the coefficients of the polynomial and the limits of integration.

(14) SECT: To obtain an equivalent rectangular cross-section of an airfoil section.

(15) YPLOSS: To calculate the profile loss coefficients for the given blading.

(16) CPT: To obtain the value of specific heat at constant pressure for a given temperature range.

(17) FTN: To evaluate the objective function penalty function and the constraints of the optimization problem for any given design vector. It calls STRESS, SECT, YPLOSS and CPT subroutines.

(18) GRADN: To calculate the gradients of objective function, penalty function and constraints using backward difference method. It calls the subroutine FTN as many times as there are design variables.

(19) SLOPE2: To evaluate the slope of the penalty function. It calls GRADN subroutine.

(20) STEPX3: To implement the one dimensional search method by cubic interpolation. It calls the subroutines FTN and SLOPE2.

(21) MINIM4: To implement the Davidon-Fletcher-Powell variable metric method of unconstrained minimization. It calls FTN, GRADN and STEPX3.

The interrelation between the various subroutines is shown in the following chart.

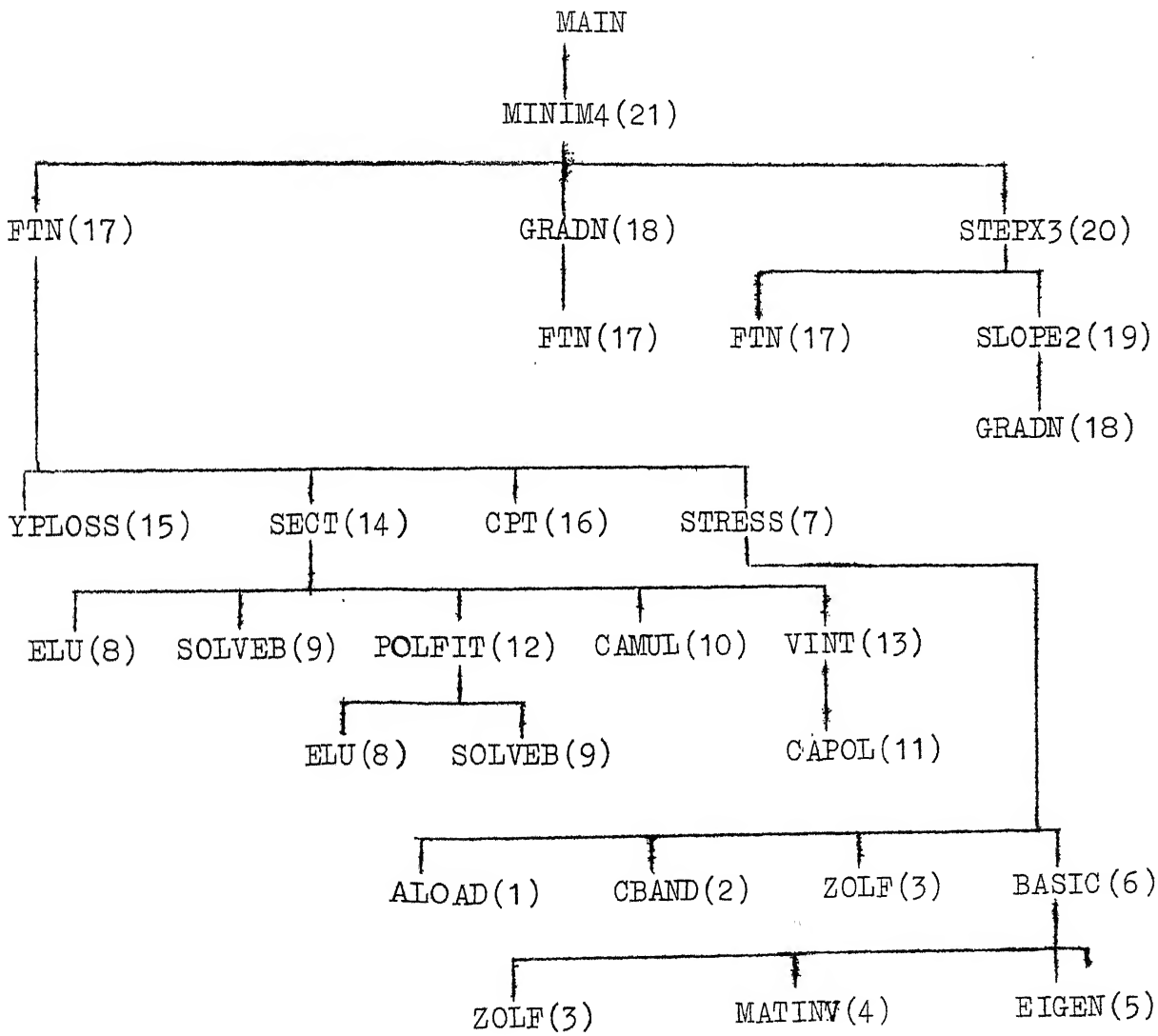

$[\underset{\sim}{K}]$ = generalised stiffness matrix

$[\underset{\sim}{M}]$ = generalised mass matrix

$[X]$ = initial approximate vectors

n_D = degree of freedom

p = number of required first few modes

$ITER_{max}$ = maximum number of subspace iterations allowed

$[Q]$ = eigen vectors of the projected operators

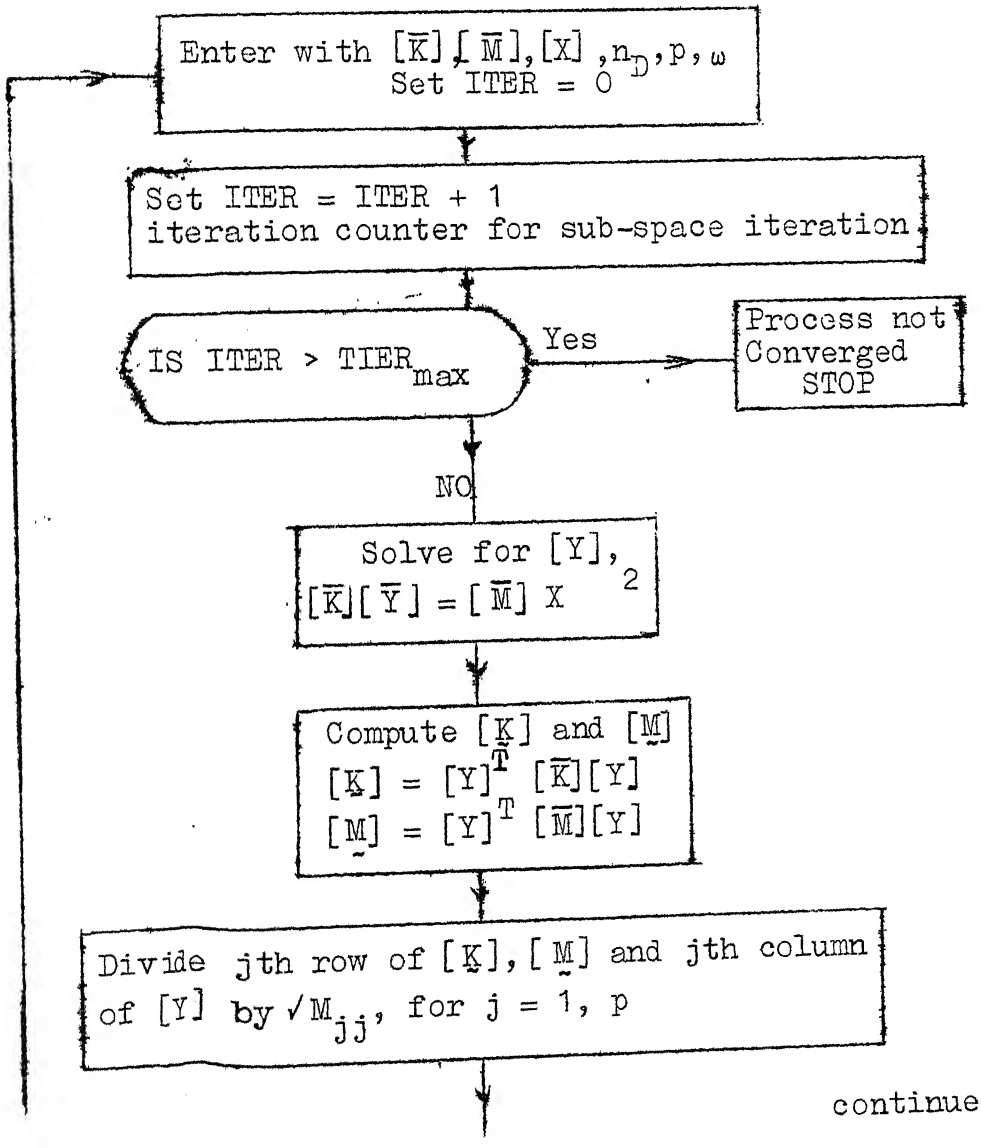

continued...

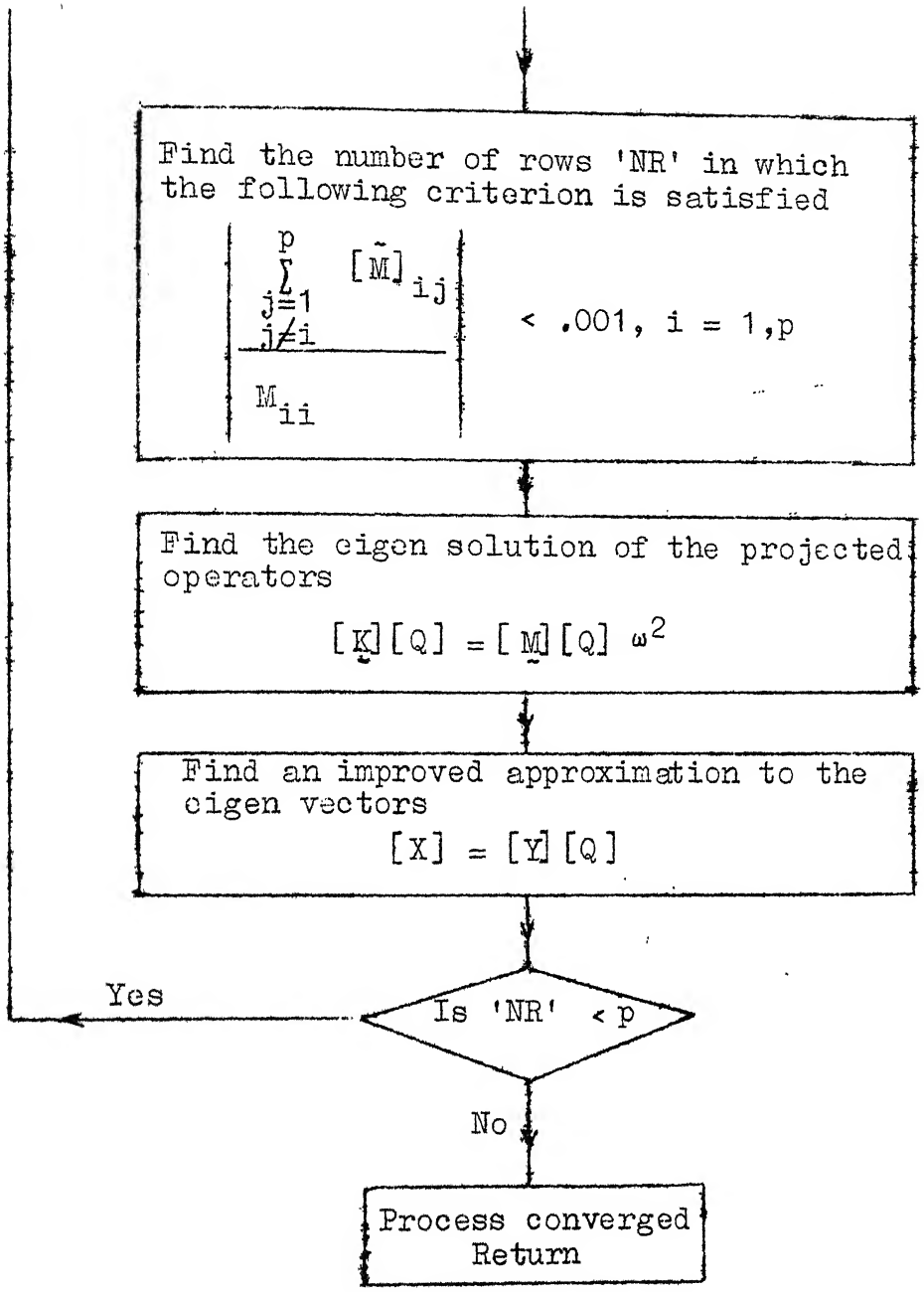

Fig. E.1 Rayleigh-Ritz Sub-space Iteration Algorithm for Determining Eigen Solutions